

ISSN: 2349-6495(P) | 2456-1908 (O)



International Journal of Advanced Engineering Research and Science

(IJAERS)

An Open Access Peer Reviewed International Journal



Journal DOI: [10.22161/ijaers](https://doi.org/10.22161/ijaers)

Issue DOI: [10.22161/ijaers.4.7](https://doi.org/10.22161/ijaers.4.7)

AI PUBLICATIONS

Vol.- 4 | Issue - 7 | July, 2017

editor@ijaers.com | <http://www.ijaers.com/>

FOREWORD

I am pleased to put into the hands of readers Volume-4; Issue-7: 2017 (July, 2017) of “**International Journal of Advanced Engineering Research and Science (IJAERS)** (ISSN: 2349-6495(P)| 2456-1908(O)” , an international journal which publishes peer reviewed quality research papers on a wide variety of topics related to Science, Technology, Management and Humanities. Looking to the keen interest shown by the authors and readers, the editorial board has decided to release print issue also, but this decision the journal issue will be available in various library also in print and online version. This will motivate authors for quick publication of their research papers. Even with these changes our objective remains the same, that is, to encourage young researchers and academicians to think innovatively and share their research findings with others for the betterment of mankind. This journal has DOI (Digital Object Identifier) also, this will improve citation of research papers.

I thank all the authors of the research papers for contributing their scholarly articles. Despite many challenges, the entire editorial board has worked tirelessly and helped me to bring out this issue of the journal well in time. They all deserve my heartfelt thanks.

Finally, I hope the readers will make good use of this valuable research material and continue to contribute their research finding for publication in this journal. Constructive comments and suggestions from our readers are welcome for further improvement of the quality and usefulness of the journal.

With warm regards.

Dr. Swapnesh Taterh

Editor-in-Chief

Date:5th , Aug, 2017

Editorial Board

Dr. C.M. Singh

*BE., MS(USA), PhD(USA), Post-Doctoral fellow at NASA (USA)
Professor, Department of Electrical & Electronics Engineering, INDIA*

Dr. Ram Karan Singh

*BE.(Civil Engineering), M.Tech.(Hydraulics Engineering), PhD(Hydraulics & Water Resources Engineering),BITS- Pilani
Professor, Department of Civil Engineering, King Khalid University, Saudi Arabia.*

Dr. Asheesh Kumar Shah

*IIM Calcutta, Wharton School of Business, DAVV INDORE, SGSITS, Indore
Country Head at CrafsOL Technology Pvt.Ltd, Country Coordinator at French Embassy, Project Coordinator at IIT Delhi, INDIA*

Dr. Swapnesh Taterh

*Ph.d with Specialization in Information System Security
Associate Professor, Department of Computer Science Engineering
Amity University, INDIA*

Dr. Ebrahim Nohani

Ph.D.(hydraulic Structures), Department of hydraulic Structures, Islamic Azad University, Dezful, IRAN.

Dr. Dinh Tran Ngoc Huy

*Specialization Banking and Finance, Professor, Department Banking and Finance
Viet Nam*

Dr. Sameh El-Sayed Mohamed Yehia

*Assistant Professor, Civil Engineering (Structural), Higher Institute of Engineering -El-Shorouk Academy,
Cairo, Egypt*

Dr. Ahmad Nabih Zaki Rashed

*Specialization Optical Communication System, Professor, Department of Electronic Engineering,
Menoufia University*

Dr. Alok Kumar Bharadwaj

BE(AMU), ME(IIT, Roorkee), Ph.D (AMU), Professor, Department of Electrical Engineering, INDIA

Dr. M. Kannan

*Specialization in Software Engineering and Data mining
Ph.D, Professor, Computer Science, SCSVMV University, Kanchipuram, India*

Dr. Sambit Kumar Mishra

*Specialization Database Management Systems
BE, ME, Ph.D, Professor, Computer Science Engineering
Gandhi Institute for Education and Technology, Baniatangi, Khordha, India*

Dr. M. VenkataRamana

*Specialization in Nano Crystal Technology
Ph.D,Professor, Physics,Andhara Pradesh, INDIA*

DR. C. M. Velu

Prof. & HOD, CSE, Datta Kala Group of Institutions, Pune, India

Dr.RabindraKayastha

*Associate Professor, Department of Natural Sciences
School of Science, Kathmandu University, Nepal*

Dr. P. Suresh

Specialization in Grid Computing and Networking, Associate Professor, Department of Information Technology, Engineering College, Erode,Tamil Nadu ,INDIA

Dr. Uma Choudhary

Specialization in Software Engineering Associate Professor, Department of Computer Science Mody University, Lakshmanagarh, India

Dr.Varun Gupta

Network Engineer,National Informatics Center , Delhi ,India

Dr. Hanuman Prasad Agrawal

Specialization in Power Systems Engineering Department of Electrical Engineering, JK Lakshmi Pat University, Jaipur, India

Dr.Hou, Cheng-I

Specialization in Software Engineering, Artificial Intelligence, Wisdom Tourism, Leisure Agriculture and Farm Planning, Associate Professor, Department of Tourism and MICE, Chung Hua University, Hsinchu Taiwan

Dr. Anil Trimbakrao Gaikwad

Associate Professor at Bharati Vidyapeeth University, Institute of Management , Kolhapur, India

Dr. Ahmed Kadhim Hussein

Department of Mechanical Engineering, College of Engineering, University of Babylon, Republic of Iraq

Dr.GamalAbd El-Nasser Ahmed Mohamed Said

Computer Lecturer, Department of Computer and Information Technology, Port Training Institute (PTI), Arab Academy For Science, Technology and Maritime Transport, Egypt

Mr. T. Rajkiran Reddy

*Specialization in Networking and Telecom
Research Database Specialist, Quantile Analytics, India*

M. HadiAmini

Carnegie Mellon University, USA

Vol-4, Issue-7, July 2017

Sr No.	Detail
1	<p><u>Assessment of contamination of soil by pesticides in Djidja's cotton area in Benin</u> <i>Firmin H. Aikpo, Miriac Dimitri S. Ahouanse, Lucien Agbandji, Patrick A. Edorh, Christophe S. Houssou</i>  DOI: 10.22161/ijaers.4.7.1 Page No: 001-005</p>
2	<p><u>Iron and Nickel -ligand bonding in metallocene: Differentiation between bond Stability and reactivity</u> <i>Tesfalem Belay Woldeamanuale</i>  DOI: 10.22161/ijaers.4.7.2 Page No: 006-019</p>
3	<p><u>Design and Analysis of 8x8 Wallace Tree Multiplier using GDI and CMOS Technology</u> <i>Pradeep Kumar Kumawat, Gajendra Sujediya</i>  DOI: 10.22161/ijaers.4.7.3 Page No: 020-024</p>
4	<p><u>Prevalence of Musculoskeletal Problems among Sugarcane Workers in Uttar Pradesh</u> <i>Sushma Gangwar, Seema Kwatra</i>  DOI: 10.22161/ijaers.4.7.4 Page No: 025-028</p>
5	<p><u>Microcontroller Based Wireless Controlled Pick & Place Robot</u> <i>Md. Faiz Akram</i>  DOI: 10.22161/ijaers.4.7.5 Page No: 029-033</p>
6	<p><u>Information and Communication Technologies for Veterinary Sciences and Animal Husbandry in Jammu and Kashmir</u> <i>T. A. Raja, Azmat Alam Khan, N A Ganai and Imtiyaz Ahmad Najar</i>  DOI: 10.22161/ijaers.4.7.6 Page No: 034-038</p>
7	<p><u>Design, Buckling and Fatigue Failure Analysis of Connecting Rod: A Review</u> <i>Manish Kumar, Shiv N Prajapati</i>  DOI: 10.22161/ijaers.4.7.7 Page No: 039-044</p>
8	<p><u>The Effect of Ketapang Leaf Extracts (<i>Terminalia catappa</i> L.) on the Cholesterol Levels of Male Mice (<i>Mus musculus</i> L.) Hypercholesterolemia</u> <i>Joko Waluyo, Dwi Wahyuni</i>  DOI: 10.22161/ijaers.4.7.8 Page No: 045-049</p>

9	<u>Construction Productivity Estimation Model Using Artificial Neural Network for Foundations Works in Gaza Strip Construction Sites</u> <i>Dr. Eyad Haddad</i>  DOI: 10.22161/ijaers.4.7.9	Page No: 050-062
10	<u>Implementation of Invisible Digital Watermarking Technique for Copyright Protection using DWT-SVD and DCT</u> <i>Devasis Pradhan</i>  DOI: 10.22161/ijaers.4.7.10	Page No: 063-069
11	<u>Climate Variability and Its implication on Wheat Productivity; Farmers' Adaptation strategies: in Robe Town and Surrounding Area, Oromia Regional State, Ethiopia</u> <i>Aliyi Mama Gasu</i>  DOI: 10.22161/ijaers.4.7.11	Page No: 070-081
12	<u>Structural and Electronic Properties of Cis-platin Metal Complex: B3LYP-SDD/DFT Calculations</u> <i>Faeq A. Mohammed, Hamid I. Abbood</i>  DOI: 10.22161/ijaers.4.7.12	Page No: 082-086
13	<u>Energy and Exergy Analysis of a CI engine fuelled with biodiesel fuel from palm kernel oil and its blends with petroleum diesel</u> <i>Iortyer H. A, Likita Bwonsi</i>  DOI: 10.22161/ijaers.4.7.13	Page No: 087-097
14	<u>The Effect of various Sterilization Procedure on Number of Colony-Forming units of isolated endophytic bacteria from Cosmos caudatus Kunth. leaf</u> <i>Fiqih Ramadhan, Fikri Ainur Risma Hardianti Oktavia, Luluk Mukarramah, Ria Yulian, Nurul Hilyatun, Iis Nur Asyiah</i>  DOI: 10.22161/ijaers.4.7.14	Page No: 098-100
15	<u>Studies on Preparation of Custard Apple Vinegar</u> <i>S. J. Raichurkar, R. A. Dadagkhair</i>  DOI: 10.22161/ijaers.4.7.15	Page No: 101-106
16	<u>Health benefits of Green and Black Tea: A Review</u> <i>K.H.G.K. Kodagoda, I. Wickramasinghe</i>  DOI: 10.22161/ijaers.4.7.16	Page No: 107-112
17	<u>Removal of Zinc Metal Ions from Electroplating Industrial Waste Water by Using Bio-Sorbent</u>	

	<i>Mr. Vivek S. Damal, Mrs. V. U. Khanapure</i>  DOI: 10.22161/ijaers.4.7.17	Page No: 113-117
18	<u>Antioxidants and antioxidant activity common eight banana varieties in Kerala</u> <i>Siji .S, Nandini. P.V</i>  DOI: 10.22161/ijaers.4.7.18	Page No: 118-123
19	<u>Theoretical Study of Electronic and Electrical Properties of Pure and Doped Graphene Sheets</u> <i>Hamid I. Abbood, Hakiema S. Jabour</i>  DOI: 10.22161/ijaers.4.7.19	Page No: 124-127
20	<u>Nutritional Evaluation of Different Mango Varieties available in Sri Lanka</u> <i>Kothalawala S.G., Jayasinghe J.M.J.K.</i>  DOI: 10.22161/ijaers.4.7.20	Page No: 128-131
21	<u>Five New Ways to Prove a Pythagorean Theorem</u> <i>Nurul Laily, Hobri, Dafik</i>  DOI: 10.22161/ijaers.4.7.21	Page No: 132-137
22	<u>Survival Analysis in Patients with Dengue Hemorrhagic Fever (DHF) Using Cox Proportional Hazard Regression</u> <i>Luluk Handayani, Mohamat Fatekurohman, Dian Anggraeni</i>  DOI: 10.22161/ijaers.4.7.22	Page No: 138-145
23	<u>An Efficient Energy Savings Schemes using Adjacent Lossless Entropy Compression for WSN</u> <i>Cisil Baby, Dr .H. N. Suresh</i>  DOI: 10.22161/ijaers.4.7.23	Page No: 146-150
24	<u>Reactive Power Control in Power System using Modified UPFC</u> <i>Engr. M. Bilal, Engr. Dr. Ejaz Hassan, Engr. Hamza Zafar</i>  DOI: 10.22161/ijaers.4.7.24	Page No: 151-155
25	<u>Revolutionary Automatic Traffic Controller</u> <i>Satyendra Pratap Singh, Rajan Tiwari</i>  DOI: 10.22161/ijaers.4.7.25	Page No: 156-163
26	<u>Short-term rhGH increases PIIINP, a biomarker of endothelial dysfunction</u> <i>Graham M. R., Gu Y., Evans P. J., Cooper S. M., Davies B., Baker J. S.</i>	

	 DOI: 10.22161/ijaers.4.7.26	Page No: 164-173
27	<p><u>Data modeling diagnostics for share price performance of Islamic Bank in Malaysia using Computational Islamic Finance approach</u></p> <p><i>Nashirah Abu Bakar, Sofian Rosbi</i></p>  DOI: 10.22161/ijaers.4.7.27	Page No: 174-179
28	<p><u>Characterization of alpha-Amylase Produced by the Endophytic Strain of Penicillium digitatum in Solid State Fermentation (SSF) and Submerged Fermentation (SmF)</u></p> <p><i>Sideney Becker Onofre, Ivan Carlos Bertoldo, Dirceu Abatti, Amarildo Antonio Tessaro, Douglas Refosco</i></p>  DOI: 10.22161/ijaers.4.7.28	Page No: 180-187

Assessment of contamination of soil by pesticides in Djidja's cotton area in Benin

Firmin H. Aïkpo^{1*}, Miriac Dimitri S. Ahouansè², Lucien Agbandji¹, Patrick A. Eдорh¹,
Christophe S. Houssou²

¹Research Laboratory in Biochemistry and Environmental Toxicology (LaRBITE), University of Abomey-Calvi (UAC), 03
PO BOX 0994, Cotonou, Benin.

²Laboratory Pierre Pagney "Climat, Water, Ecosystem and Development" (LACEEDE), University of Abomey-Calavi
(UAC), PO BOX 922, Cotonou, Benin

Abstract— The aim of the research is to assess the level of soil contamination by pesticides in Djidja's cotton area in Benin. Soil samples have been collected in nine (09) cotton fields from 15th to 19th March, 2014. The analysis has been done by gas chromatography after extraction and purification. The results show a soil contamination by glyphosate varying from 0.271 to 0.317 µg/kg, by profenofos varying from 0.109 to 0.130 µg/kg, by acetamiprid varying from 0.088 to 0.153 µg/kg and by cypermethrin varying from 0.165 to 0.190 µg/kg. A regular supervision program must be planned to limit as possible the soil contamination by pesticides in this township.

Keywords— Agriculture, pesticides, cotton, contamination, soil.

I. INTRODUCTION

In Benin, the agricultural sector employs 70% of the workforce and contributes 39% to the Gross Domestic Product (GDP), provides 90% of the country's export revenues and contributes about 15% to the revenue of the State (MAEP, 2010). Therefore, it has an important place in Benin's economy. The main cash crop is cotton, whose current production level is largely insufficient to satisfy national and international market high needs. The main food crops (maize, cassava, yam, cowpea, rice, etc.) overcome food needs, but are still below the potential of the ecological conditions of the country (MAEP, 2008). Cultures are submitted to animals attacks and harmful plants. Such situations cause defoliation and destruction of the plants, thus causing huge losses to farmers. To reach the end of such situations pesticides are used (Gbaguidi et al., 2004). Pesticides used for cotton production and pest control in the growing of food crops such as beans, maize and vegetables eventually may not only end up on the crops, but also contaminate soil and surface water (Pazou et al., 2014). The use of insecticides in agriculture has been incriminated in the emergence of insecticide in insect vectors (Akogbéto et al., 2005). Glyphosate can bind to soil particles under certain

conditions (Shushkova et al., 2009), especially in clay soils. It can be quickly leached in sandy soil, while it may persist for over a year in soils which contain clay (Bergström et al., 2011). Even when bound to soil particles, it can be dissolved later in the ground water, in the presence of phosphates (Simonsen et al., 2008). Glyphosate has the ability to form chemical complexes with metal ions (Eker et al., 2006), that may influence the availability of soil nutrients. It has been proven that glyphosate can change the absorption of agricultural plants, minerals (Zobiolo et al., 2011). Pesticides can therefore stay in the ground or be washed by rain into groundwater or rivers or transferred to plants, animals and humans. The aim of the research is to assess the level of soil contamination by pesticides in Djidja's cotton area in Benin.

II. MATERIALS AND METHODS

2.1 STUDY AREA

Located between 7° 10' and 7° 40' north latitude, 1° 40' and 2° 10' west longitude, the township of Djidja covers 41.66% of the total area of the department (Zou). With a total area of 2.184 km², it has a sub-equatorial climate next to Sudan Guinea in the northern parts (Akomagni, 2006). This township has a variety of soil types (ferrallitic, ferruginous, vertisols, hydromorphic) and floodplains (SDS, 2004). The township is 145 km² watered by streams where Zou and Couffo are the most important. The vegetation consists of several formations (palm groves, wooded savannah, savannah, forest islands, galleries). The township of Djidja is located in the cotton area of the Centre of Benin. This area is dominated by cereals, tubers and legumes. The population is 80% invested in agricultural activities.

2.2 METHODS

2.2.1- Selection of sampling sites

Three main villages were chosen in the township. The selected villages correspond to experimental areas where phytosanitary treatments are followed. These villages are

Zakan Kossossa (district of Djidja), Fonpkodji (district of Monsourou) and Aklinmè (borough Agouna). In each village, three sampling areas were selected. The number of samples taken per area is a sample so that three samples were taken from the village.

2.2.2 Soil Sampling protocol

Soil samples were taken from the cotton fields from 15th to 19th of March 2014. The IRGIB-AFRICA laboratory was committed. To do this, the procedure is as follows. Geographic identification of plots was carried out and each plot was defined, that means, an area that has the same historical phytosanitary treatment and even the same vegetative aspect of crop (cotton). Areas (10 m x 10 m) have been delineated in the middle of the field. Before sampling, the surface is cleaned herbs, organic residues and other residues for surface clean soil. Using a spade which has been previously washed with detergent and rinsed with water and acetone, elementary 5 samples were taken at the horizon 0-15 cm along the diagonals and the sides of the square. To take the sample, a hole the depth of the spade was dug with enough space to remove the earth in it. Earth volumes of each sample is important, each sample was mixed in a bucket forming the average sample plot. The samples contained in the bucket were crushed, stones and plant materials were removed and the bucket contents were thoroughly mixed. The equivalent of 1 kg of soil was recovered. The latter was then wrapped in aluminum foil, then put in a plastic bag bearing the words in indelible ink the sample code. Collection sheets stating the place, date of collection and the identity of sampler accompany samples. These were sent to the laboratory in a cool cooler where the conversation was conducted in a refrigerator at 4°C.

2.2.3 Sample Preparation

The preparation of soil samples and pesticide residue analysis were done by the laboratory of IRGIB-AFRICA and included the active ingredients namely glyphosate, profenofos, acetamiprid and cypermethrin. These active materials were selected based on the frequency of their use. All chemicals (reagents and solvents) used were of analytical grade. Solvents of a residue grade purity as acetone, dichloromethane, hexane, cyclohexane and the anhydrous sodium sulfate were obtained from Merck Co. (Darmstadt Germany). The water used in the detergent-

free distilled water. A standard stock solution (between 75 and 550 pg/mL) was prepared by accurately weighing and dissolving was performed in acetone and stored in a freezer at -30°C without exposure to light. Working standard solutions (5 µg/mL) were prepared by appropriate dilution of the stock standard solution with cyclohexane and stored in a refrigerator (4°C).

Extraction (method soxhlet) of 10 g of pesticide residues from a soil sample is carried out with 50 mL of a mixture of acetone (1/1, v/v) and stirred on a horizontal shaker for 12 hours. Then the extract was filtered and concentrated to 1 mL using exactly to the flow of the rotary evaporator and nitrogen, respectively (Tor et al., 2006; Aydin et al., 2006). The concentrated extraction was transferred to the traditional cleaning column and the elution was performed with 100 mL of n-hexane/ethyl acetate (1/1, v/v), then the extract was concentrated to exactly 1 mL using a rotary evaporator and the nitrogen released before analysis.

2.2.4 Pesticide Analysis

The determination of pesticides was performed by gas chromatography. A mass spectrometer with high resolution DSQII Thermo was used. The chromatograph used for analysis is a gas chromatograph equipped with a Thermo Scientific split/splitless injector and a temperature controlled GC-MS interface. A smuggler AS 3000 sample was used. 10ul aliquots were injected into the gas chromatograph (GC) operating using a syringe with an injection rate of 20 µL. The initial injection temperature at the nozzle was maintained at 70°C for 5 minutes, and increased and maintained for 10 minutes at 310°C and at 100°C/minute. The initial temperature at the oven was maintained at 70°C during 4 minutes, then increased to 150°C at 50°C/minute, then to 235°C with 3°C/minute at last maintained for 3 minutes at 300°C with 50°C/minute. It has been operating the mass spectrometer and the vacuum pump to achieve a different level of "Vacuum" stable injection. The transfer line temperatures, the flow of gas (helium) were settled. The analysis was done with a multiplier filament delay of 5 minutes to prevent the shock ionization filament level.

III. RESULTS

The results of the analysis of the active materials for soils collected are mentioned in figures 1, 2 and 3 as follow.

Kossossa area

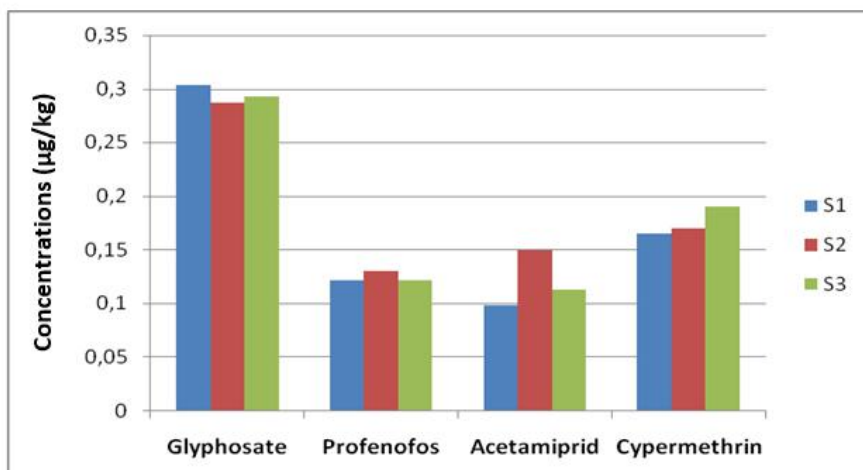


Fig.1: Level of soil contamination of Kossossa area

In the village of kossossa, the glyphosate was chosen in average concentrations of 0.303 µg/kg (S1), of 0.287 µg/kg (S2) and of 0.293 µg/kg (S3); the profenofos was chosen in average concentrations of 0.121 µg/kg (S1), of 0.130 µg/kg (S2) and of 0.121 µg/kg (S3); the

acetamiprid was found in average concentrations of 0.098 µg/kg (S1), of 0.149 µg/kg (S2) and of 0.112 µg/kg (S3); the cypermethrin is found in average concentrations of 0.165 µg/kg (S1), of 0.170 µg/kg (S2) and 0.190 µg/kg (S3) for the collected soil samples.

Fonkpodji area

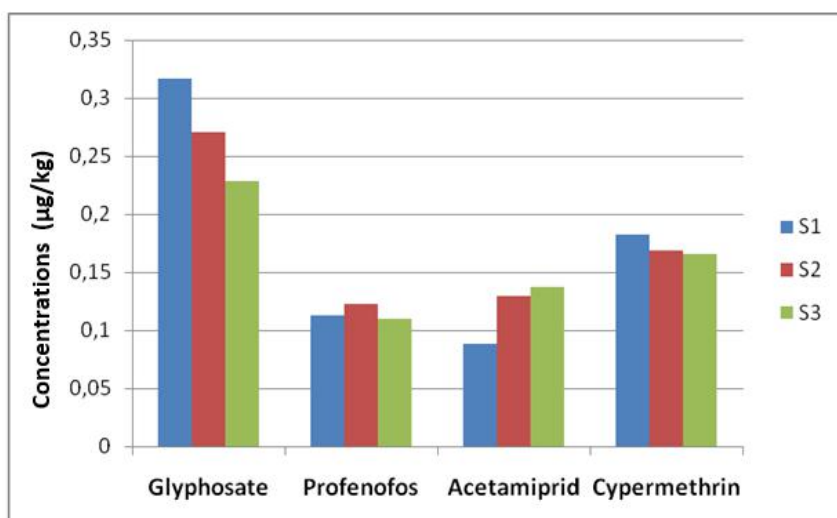


Fig.2: Level of soil contamination of Fonkpodji area

For the collected samples of Fonkpodji area, the glyphosate was chosen in average concentrations of 0.317 µg/kg (S1), of 0.271 µg/kg (S2) and of 0.228 µg/kg (S3); the profenofos was chosen in average concentrations of 0.113 µg/kg (S1), of 0.123 µg/kg (S2) and of 0.110

µg/kg (S3); the acetamiprid was found in average concentrations of 0.088 µg/kg (S1), of 0.129 µg/kg (S2) and of 0.137 µg/kg (S3); the cypermethrin is found in average concentrations of 0.182 µg/kg (S1), of 0.169 µg/kg (S2) and of 0.166 µg/kg (S3).

Aklinmè area

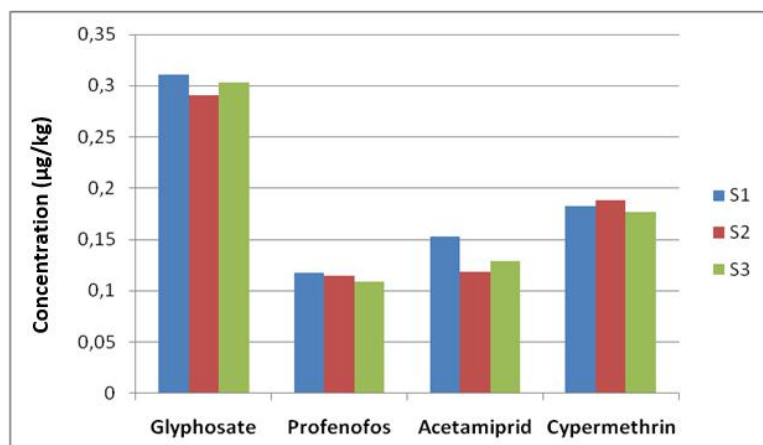


Fig.3: Level of soil contamination of Aklinmè area

In the collected soil samples at Aklinmè, the glyphosate is found in average concentrations of 0.311 µg/kg (S1), of 0.291 µg/kg (S2) and of 0.303 µg/kg; the profenofos is found in average concentrations of 0.118 µg/kg (S1), of 0.115 µg/kg (S2) and of 0.109 µg/kg (S3); the acetamiprid was chosen in average concentrations of 0.153 µg/kg (S1), of 0.119 µg/kg (S2) and of 0.129 µg/kg (S3); the cypermethrin was chosen in average concentrations of 0.183 µg/kg (S1), of 0.188 µg/kg (S2) and of 0.177 µg/kg (S3).

The average concentrations in profenofos and in acetamiprid in the three villages soils are relatively low compared to glyphosate and cypermethrin.

IV. DISCUSSION

Soil samples analyzed showed the presence of glyphosate at average concentrations more than those of the other active materials. These concentrations vary between 0.271 to 0.317 µg/kg in all soil samples. One of glyphosate features is its strong ability to bind to soil particles, that's why its particularly high Koc index (24 000mL/g) (Delabays and Bohren, 2007). Average levels of cypermethrin in all samples vary between 0.165 to 0.190 µg/kg and are superior to those of profenofos which vary between 0.109 and 0.130 µg/kg, but lower than those found by Nafees and Jan (2009) in the valley of Swat. The average concentrations of acetamiprid vary between 0.088 and 0.153 µg/kg in soil samples. The average levels of profenofos and acetamiprid found are lower than those found by Adam et al. (2010) in Gogounou, Kandi and Banikoara and also lower than those found by Ngan et al. (2005) in Cameroun. The total use of herbicides, insecticides and land pressure with the abandonment of the fallow are potential risks to lower fertility and contaminate soil. However, soils are constitute of ecosystems and the biodiversity of these ecosystems can not be compared both in terms of wealth and biomass and

many functions provided by the soil fauna are harmful to agricultural production (Aubertot et al., 2005). Some invertebrates living on earth involved in maintaining the structure of soil and greatly improve the quality of these areas and others involved in the decomposition process that leads to nutrient recycling. Pesticides can, for example, cause among microbial communities in the emergence of populations, including bacterial, could degrade, with consequences increasing the dose or frequency of application and therefore deleterious effects on wildlife and flora (Le Roux et al., 2008). It is clear that the pesticides that have been used for many years in the township have probably destroyed the soil or at least modified living organisms that are present. Therefore, due to the destruction of soil ecosystems, it is highly likely that these pesticides have seriously damaged their fertility.

V. CONCLUSION

Soil analyzes showed the presence of pesticides in the areas. The average levels of glyphosate and cypermethrin are highest. The mean levels of other active materials are generally low. The future of its active materials in the soil varies according to their nature and their chemical composition and environmental risks are even greater than these toxic products are used on surfaces and in doses/high frequencies. Thanks to the results of the analyzes of residues of pesticides involved in the work, to produce more without pesticides is no longer a utopia because these chemicals are very badly used in Djidja. A regular supervision program must be planned to limit as possible the soil contamination by pesticides in this township.

ACKNOWLEDGEMENTS

We sincerely thank the laboratory IRGIB-AFRICA and the Professors Patrick A. Edoth and Christophe S.

Houssou for their contribution to the realization of this article.

REFERENCES

- [1] Adam S., Edoh P., Totin H., Koumolou L., Amoussou E., Aklikokou K. et Boko M. (2010). Pesticides et métaux lourds dans l'eau de boisson, les sols et les sédiments dans la ceinture cotonnière de Gogounou, Kandi et Banikoara. *International Journal of Biological and Chemical Sciences*, 4 : 1170-1179.
- [2] Akogbéto M.C., Djouaka R. et Noukpo H. (2005). Utilisation des insecticides agricoles au Bénin. *Bull. Soc. Pathol. Exot.*, 98 (5) : 400-405.
- [3] Akomagni L.A. (2006). Monographie de la commune de Djidja. Programme d'Appui au Démarrage des Communes, Afrique Conseil, 44 p.
- [4] Aubertot S.N., Barbier J.M. et Carpentier A. (2005). Pesticides, agriculture et environnement, réduire l'utilisation des pesticides et limiter leurs impacts environnementaux. Rapport d'expertise scientifique collective, INRAB et CEMAGREF, France, 86 p.
- [5] Aydin M.E., Tor A. and Ozcan S. (2006). Determination of selected polychlorinated biphenyls in soil by miniaturized ultrasonic solvent extraction and gas chromatography-mass selective detection. *Analytica chimica Acta*, 577 : 232-237.
- [6] Bergström L., Borjesson E. and Stenström J. (2011). Laboratory and Lysimeter Studies of Glyphosate and Aminomethylphosphonic Acid in a Sand and Clay Soil. *Journal of Environmental Quality*, 40 : 98-108.
- [7] Delabays N. et Bohren C. (2007). Le glyphosate: bilan de la situation mondiale et analyse de quelques conséquences malherbologiques pour la Suisse. *Revue Suisse Vitic. Arboric. Hortic.*, 39 (5) : 333-339.
- [8] Eker S. Ozturk L., Yazici A., Erenogly B., Römheld V. and Cakmak I. (2006). Foliarapplied Glyphosate substantially reduced uptake and transport of iron and manganese in sunflower (*Helianthus annuus* L.) plants. *J. Agric. Food chem.*, 54 : 10019-10025.
- [9] Gbaguidi B., Allagbé C., Bani G., Dohoué E., Gbèboutin E. et Houndékon R. (2004). Analyse des aspects socio-économiques de l'utilisation des POP. Rapport final, MEHU, Cotonou, Bénin, 34 p.
- [10] Le Roux X., Barbault R., Baudry J., Burel F., Doussan I., Garnier E., Herzog F., Lavorel S., Lifranc R., Roger-Estrade J., Sarthou J.P. and Trommetter M. (2008). Agriculture et Biodiversité. Valoriser les synergies. Expertise scientifique collective, synthèse du rapport. INRA, France, 116 p.
- [11] MAEP (Ministère de l'Agriculture, de l'Elevage et de la Pêche) (2008). Plan Stratégique de Relance du Secteur Agricole au Bénin. Orientations stratégiques et Plan d'action, Cotonou, Bénin, 70 p.
- [12] MAEP (Ministère de l'Agriculture, de l'Elevage et de la Pêche) (2010). Analyse de l'insécurité alimentaire et des inégalités d'accès à l'alimentation au Bénin. Rapport, Cotonou, Bénin, 27 p.
- [13] Nafees M. et Jan M. (2009). Les résidus de cyperméthrine et de l'endosulfan dans les sols de la vallée de Swat. *Sol et Environnement*, 28 (2) : 113-118.
- [14] Ngan C.K., Cheat U.B., Wan Abdullah W.Y., Lim K.P. et Ismail B.S. (2005). Sort de chlorthaloniel, Chlorpyrifos et Profénofos dans une ferme de légumes à Highlands de Cameroun, la Malaisie. *Focus*, 5 (1-2) : 125-136.
- [15] Pazou E., Glin L.C., Vodouhè D.S., Fanou J., Babadankpodji A.P., Dassou S., Vodouhè S., van Hattum B., Swart K. and van Gestel C.A.M. (2014). Pesticides contamination of the Dridji cotton plantation area in the Republic of Benin. *African Journal of Food, Agriculture, Nutrition and Development*, 14 (3) : 8885-8902.
- [16] SDS (Schéma de Développement Sectoriel) (2004). Document de synthèse, Diagnostic, Vision et Planification des projets sur 2004-2008 du secteur de l'agriculture, de l'élevage et de l'exploitation des ressources naturelles de la commune de Djidja, PADeCoM/Zou, 159 p.
- [17] Shushkova T., Ermakova I. and Leontievsky A. (2009). Glyphosate bioavailability in the soil. *Biodegradation*, 21 : 403-410.
- [18] Simonsen L. Fomsgard I.S., Svensmark B. and Splid N.H. (2008). Fate and availability of glyphosate and AMPA in agricultural soil. *Journal of Environmental Science and Health, Part B*, 43 : 365-375.
- [19] Tor A., Aydin M.E. and Ozcan S. (2006). Determination of selected of polychlorinated biphenyls in soil by miniaturised ultrasonic solvent extraction and gas chromatography-mass selective detection. *Analytica Chemical Acta*. 577 (2) : 232-237
- [20] Zobiole L.H.S., Kremer R.J., Oliveira R.S.jr and Constantin J. (2011). Glyphosate affects chlorophyll, nodulation and nutrient accumulation of "second generation" glyphosate-resistant soybean (*Glycine max* L.). *Pesticide Biochemistry and Physiology*, 99 : 53-60.



Iron and Nickel -ligand bonding in metallocene: Differentiation between bond Stability and reactivity

Tesfalem Belay Woldeamanuale

Central Ethiopia Environment and forest research Center, Ethiopia

Email Id: tesbel23@gmail.com

Abstract— The electronic structure and geometry optimization of ferrocene and nickelocene molecules are calculated using DFT/B3LYP with the basis set of 6-31G (d). The Eigen values, Eigen vector and population analysis of the molecules show that the first 13 molecular orbitals in ferrocene and 14 in nickelocene have contribution from 2p orbitals of carbon of $(C_5H_5)^-$ and 4s, 4p and 3d orbitals of iron and nickel respectively. We found that the extent of involvement of metal orbitals in the two cases is different. In ferrocene the maximum involvement out of 4s and 4p orbital is in the order $4p_z > 4p_y > 4s > 4p_x$ and out of 3d orbitals the order of involvement is $3d_{yz} > 3d_{xz} > 3d^2_z > 3d^2_x - y^2 > 3d_{xy}$. The involvement of corresponding orbital in nickelocene with respect to the 4s and 4p orbitals is in the order of $4p_y > 4p_x > 4s > 4p_z$ and in 3d orbitals the order is $3d_{yz} > 3d^2_x - y^2 > 3d_{xy} > 3d_{xz} > 3d^2_z$ molecules. The total involvement of 3d, 4s and 4p orbitals of metal and 2p orbitals of the ten carbon atoms of both ligands of $(C_5H_5)^-$ in ferrocene and nickelocene respectively are 42.2528 and 38.3776 hence we can conclude that ferrocene is more stable than nickelocene. Similar results are found from calculation of parameters like dipole moment, HOMO-LUMO gap and Mulliken charge distribution. The population analysis shows that only 2p orbitals of carbon of $(C_5H_5)^-$ and 3d orbitals of metal provide electrons to MOs of ferrocene and nickelocene.

Keywords— Ferrocene, Nickelocene, Eigen vector, population analysis, Eigen values, atomic and molecular orbitals.

I. INTRODUCTION

In the last decade, there has been a phenomenal advancement in theoretical inorganic chemistry [1, 2], much faster computers are available and commercial programs incorporating the latest methods have become widely available and are capable of providing more information about molecular orbitals (MOs), with a simple input of chemical formula. The focus of attention has been on computational transition-metal chemistry [3, 4]. This is largely due to the successful employment of gradient corrected density functional theory in calculating molecules, particularly of the heavier atoms [5-8] and in the use of small-core relativistic effective core potential [9-11] which set the stage for calculation of geometries, bond energies, and chemical reaction and other important properties of transition metal compounds with impressive accuracy [8, 12]. Application of density functional calculation to organometallic [13,14] and transition metal compounds is growing [15]. density functional parameters such as eigenvectors, eigenvalues and population analysis are well calculated with this method. In this paper present the calculations of eigenvectors, Eigen values and population analysis of ferrocene and nickelocene in order to study the extent of contribution of 3d, 4s and 4p orbital in the formation of MOs. The significant of Ferrocene and nickelocene are contribute of atomic orbitals in the formation of molecular orbital, chemical stability, mediator, asymmetric catalysis and more reactive material such as Ferrocene and

Nickelocene as the commercially important for production of various metallocene, polymers and co-polymers. Such a quantitative study will provide correct information about the involvement of $3d$, $4s$ and $4p$ orbital of Iron and nickel in bonding will help to resolve the controversy raised by other workers [16-20].

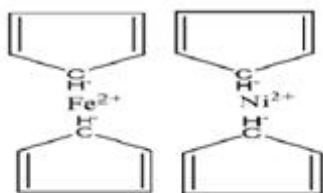


Fig.1: Structure of Ferrocene, and nickelocene molecules

II. MATERIALS AND METHODS

In computational chemistry tools the DFT offers the fundamentals for interpreting multiple chemical concepts used in different branches of chemistry. In modern computational chemistry, quantum chemical calculations are typically performed with in a finite set of basic functions. When molecular calculations are performed, it is common to use a basis sets composed of a finite number of atomic orbitals, centered at each atomic nucleus with in the molecule, for example linear combination of atomic orbitals. The methods most commonly used for this research are DFT/B3LYP a combination of Beck's three-parameter exchange functional and Lee-Yang-Parr correlation functional with 6-31G (d) basis set.

These methods are found in Gaussian 03W program. B3LYP is a DFT method with hybrid functional that provides qualitative results at a lower cost than abinitio methods with a comparable accuracy [21]. By using these methods we have optimized the energy, eigenvalues, eigenvector, population analysis, HOMO-LUMO energy gap, hardness, softness, electronegativity, visualize the

HOMO and LUMO orbitals' of ferrocene and nickelocene molecules. The coefficients in linear combination for each molecular orbital being found by solution of the Roothaan-equation. A widely used method to analyze SCF wave function is population analysis, introduced by Mullikan population methods [22]

III. RESULT AND DISCUSSION

This research is aimed to study the electronic structure and optimized geometry of ferrocene and nickelocene molecules. Geometry optimization is used to find minima on the potential energy surface representing equilibrium structure and used to obtain structure for a single-point quantum mechanical calculation, which provides a large set of structural and electronic properties. The electronic structure and geometry of ferrocene and nickelocene molecules are found through DFT/B3LYP with a basis set of 6-31G (d) calculations. The optimized structures of these two compounds are shown in Fig 1, A and B respectively for ferrocene and nickelocene. The significant computed parameters are available in Tables 1 and 2 including the bond lengths, bond angles and dihedral angles of these two compounds. The optimized bond length of C-C double and single bonds in ferrocene rings fall in the range 1.36-1.83 Å, and nickelocene 1.392-1.98 Å at DFT/ B3LYP, level through 6-31G (d) basis set.

There are two types of C-C bonds involved in these species. These are C-C single bonds and C-C double bonds of ferrocene and nickelocene and according to its bond length are in the order of C=C < C-C. From Tables 1 and 2 we observe a slight difference in the bond lengths, bond angles and dihedral angles throughout the molecules of ferrocene and nickelocene. This indicates that the aromatic iron atom in ferrocene and nickel atom in nickelocene are relatively stable metabolically.

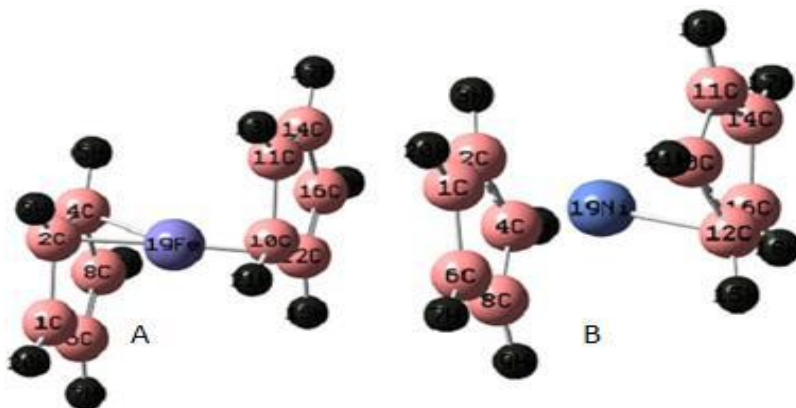


Fig.2: The optimized structures of (A) ferrocene, (B) nickelocene molecules

Table.1: The selected bond lengths in Å, some bond angles and Dihedral angles of the optimized structure of ferrocene using DFT levels with B3LYP / 6-31G (d) basis set.

Entry	Bond length(°Å)	Entry	Bond angle (°Å)	Entry	Dihedral angle (o)
C1-C2	1.509	C6-C1-C2	109.511	C6-C1-C2-C4	0.027
C1-C6	1.509	C8-C6-C1	109.560	C8-C6-C1-C4	-0.027
C8-C6	3.359	C12-C10-C11	92.513	C10-C11-C14-C16	-85.951
C10-C11	1.509	C14-C10-C12	92.513	C16-C12-C10-C11	91.533
C10-C12	1.509	C10-C11-C14	85.520	Fe-C2-C1-C6	-67.604
C11-C14	1.359	C10-C12-C16	109.510		
C12-C16	1.359	Fe-C2-C1	88.83		
C2-C4	1.359				
C4-C8	1.47				
Fe-C2	1.825				

As shown in Fig 2. (A) and Table 1. due to the effect of the partial charge distribution of iron atom in ferrocene molecule, the bond connectivity of Fe-(C₅H₅)₂ of the two ligands are asymmetrical. The iron atom in ferrocene is bonded with C₁₂ atom with bond length of 1.954 (°Å) in one side of the ligand and C₄ with bond length of 1.856(°Å) and with C₂ atom of bond length 1.856 (°Å) on the opposite side. The Fe-C bond length on the two sides of the ligand have small variations due to the double bond of C₂-C₄ which possess more energy to attract iron atom towards itself than the single bond on the other side, hence Fe-C₂ and Fe-C₄

bonds measure shorter distance than the bond in Fe-C₁₂. In the ferrocene molecule the iron atom is located between the two ligands but inclined by -67.604° from the plane of the cyclopentadienyl and the two ligands are almost parallel but with a slide of one from the other by a center of mass separation of 1.67°Å. Table.2: The selected bond length Å, bond angles and Dihedral angles of the optimized Structure of nickelocene using DFT levels with B3LYP / 6-31G (d) basis set.

Entry	Bond length(°Å)	Entry	Bond angle (o)	Entry	Dihedral angle (o)
C1-C2	1.424	C1-C2-C4	106.850	C6-C1-C2-C4	-174.834
C2-C4	1.419	C2-C1-C6	108.850	C2-C1-C6-C8	-8.963
C1-C6	1.448	C1-C6-C8	107.560	C1-C2-C4-C8	6.050
C6-C8	1.391	C10-C11-C14	93.450	C10-C11-C14-C16	-85.112
C10-C11	1.471	C12-C10-C11	97.468	C12-C10-C11-C14	87.862
C10-C12	1.427	C10-C12-C16	105.110	C10-C11-C14-C16	82.950
C11-C14	1.366	Ni-C12-C10	72.433	C14-C16-C12-Ni	-67.377
C12-C16	1.427				
Ni-C2	1.976				

As shown in Figure 2, B and Table 2. The bond connectivity of Ni-(C₅H₅)₂ of the two ligands are asymmetrical. The nickel atom in nickelocene is bonded with C₁₂ atom of bond length 1.976 (°Å) only from one side of the ligand. This is due to the weak ligand fields of nickelocene having high spin arrangement with two d electrons and low spin arrangement with six d electrons of nickel atom which resulted in more reactivity of nickelocene molecule with respect to the other two molecules. In the nickelocene molecule the nickel atom is

located between the two ligands but inclined by -67.377° as measured from the plane of the cyclopentadienyl and the two ligands are almost parallel but with a slide of one from the other by a center of mass separation of only 0.22°Å.

Generally comparing the bond length and bond angles between metal atom and carbon in ferrocene and nickelocene molecules the former molecule possesses higher bond angles and the later molecule possesses larger bond length. The larger the bond length the less stability but

more reactivity, hence nickelocene is more reactive and less stable than the ferrocene. In the calculations of Mulliken charge distributions of ferrocene and nickelocene molecules, given in Figure 2, the red color indicates for excess of negative charges (-Ve) while the green color

indicates for excess of positive charges (+Ve) among the bonded atoms, where electrons can flow from positions of excess of negative charges (-Ve) to the positions of excess of positive charges (+Ve).

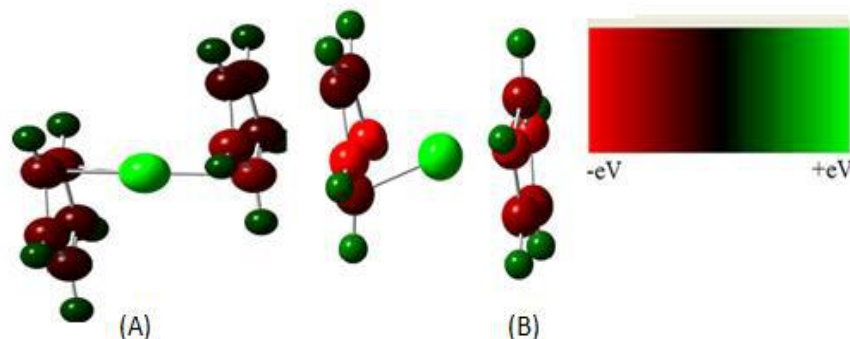


Fig.3: The Milliken charge distributions of (A) ferrocene, (B) nickelocene Molecules.

Energies of molecular orbitals are called Eigen values. The main focus has been on the molecular structure and the properties that will be evaluated can be used to determine the molecular reactivity as well as the molecular stability. The HOMO (Highest Occupied Molecular Orbital) and LUMO (Lowest Unoccupied Molecular Orbital) are very important aspects to consider for these types of observations. This is because the HOMO and LUMO are the most likely locations where reaction will occur. The reaction is likely to occur there because the electrons in the

HOMO have the highest energy and therefore the electrons are most willing to react. The LUMO is likely the location for a bond to occur as well because any invading electrons for another molecule will fill in to the LUMO, that is why comparing the energies of these orbitals create an idea of how reactive a molecule is important parametric properties of the molecules at the DFT/B3LYP levels in 6-31G (d) basis set has been calculated and are given in Table 3

Table.3: Important parametric properties of the molecules calculated at the DFT/B3LYP levels in 6-31G (d) basis set.

Molecular properties	ferrocene	nickelocene
RB-HF-LYP (eV)	-1896.275	-1650.740
ϵ HOMO(eV)	-0.6491	-0.6427
ϵ LUMO(eV)	-0.5628	-0.5614
ϵ LUMO- ϵ HOMO energy gap (eV)	0.0863	0.0813
Ionization potential (I in eV)	0.6491	0.6427
Electron affinity (A in eV)	0.5628	0.5614
Global hardness (η in eV)	0.0431	0.04065
Global softness (S in eV)	23.1803	24.6030
Electro negativity (χ in eV)	0.60591	0.6021
Chemical potential (μ in eV)	-0.6059	-0.6021
Dipole moment (μ in Debye)	1.464	1.931
Mulliken charge distributions (M.C.D in e)	± 1.093	± 1.692

At the DFT/B3LYP level the HOMO energy of ferrocene is -0.6491 eV which is slightly more negative than the and nickelocene of -0.6427 eV and the LUMO energy of ferrocene is -0.5628 eV, and nickelocene -0.5614 eV. The HOMO-LUMO gap of ferrocene and nickelocene are

0.0863 and 0.0813 eV respectively. These prove that the positions of HOMO, LUMO and the HOMO-LUMO gap can predict the stability and reactivity of the molecules, and the ferrocene molecule shows relatively high energy gap value and the data here suggested that ferrocene is relatively

less reactive and more stable than nickelocene molecule. The most stable MO energy of ferrocene and nickelocene are respectively -254.0054, and -295.6703 eV. In general the HOMO and LUMO energy gap reveals the chemical activity of the molecules. LUMO as an electron acceptor represents the ability to obtain an electron (i.e. the electron affinity) and HOMO as an electron donor represents the ability to donate an electron from its orbital (i.e. the Ionization Potential). The less values in the HOMO-LUMO energy gap explains eventually charge transfer interaction taking place within the molecules. Hard molecules have large HOMO-LUMO energy gaps and soft molecule have small HOMO-LUMO energy gaps. So soft molecules (molecules with small energy gap) are favorable for easy reactions. This description also supports for ferrocene and nickelocene molecule, ferrocene is harder than nickelocene. In Table 3, the HOMO-LUMO gap, as a characteristic of reactivity, shows ferrocene has lower chemical reactivity comparing to nickelocene molecule. Absolute hardness and softness are important properties to measure the molecular stability and reactivity. It is apparent

that the chemical hardness fundamentally signifies the resistance towards the deformation or polarization of the electron cloud of the atoms, ions or molecules under small perturbation of chemical reaction. A hard molecule has a large energy gap and a soft molecule has a small energy gap. So for more energetically stable and less reactive ferrocene molecule, the HOMO-LUMO energy gap and hardness, is larger comparing to nickelocene molecules.

The dipole moments and Mulliken charge ranges as displayed in Table 3, Nickelocene would have more charge than the ferrocene molecule. This is due to higher dipole moment and lower HOMO-LUMO energy gap indicated that the molecule is better reactive. This indicates that nickelocene is more polar so that it will react with polar solvents like water. Since the separation between mass centers of the two ligands is small. The higher the dipole moment, the more polar a molecule is. This could mean that the receptor is more likely to accept polar molecules into its active site. The receptor's active sites may serve as home to atoms that have very high electron affinities that attract the negatively charged end of a polar molecule

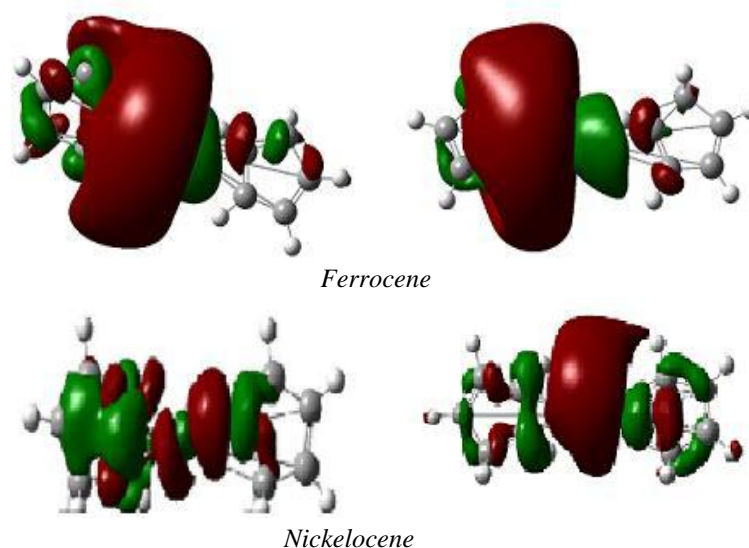


Fig.4: The left side of HOMO and the right side of LUMO surfaces of ferrocene and nickelocene compounds, down of the column respectively.

The above Figure shows the visualized structures of ferrocene and nickelocene show the population of electrons on their orbitals. The HOMO orbitals represented by green color, whereas for LUMO is represented by red color. The red color represents the negatively charged areas of surface (i.e. those areas where accepting the electrophiles is most favorable) while the green color represents the positively charged areas of surface (i.e. those areas where accepting the nucleophiles is more favorable). The electron density of HOMO and LUMO of ferrocene and nickelocene molecule

are concentrated throughout the compound except at the right and left terminals whereas some of the π^* orbitals may be empty.

Eigen vector values of atomic orbitals have been evaluated for the study of linear combination of atomic orbitals (LCAO). The MOs of ferrocene and nickelocene are formed by linear combination of fifty AOs of two $(C_5H_5)^-$ and nine orbital of iron and nickel. These fifty-nine AOs χ_1 to χ_{59} on LCAO approximation form same number of MOs, Φ_1 to Φ_{59} . The AOs χ_1 to χ_{40} for 2s, 2p_x, 2p_y,

2pz of 1C to 10C, χ_{41} to χ_{49} for 4s, 4px, 4py, 4pz, $3dx^2-y^2$, $3d^2z$, 3dxy, 3dxz, 3dyz of 11M and χ_{50} to χ_{59} for 1s of 12H to 21H respectively, where M = Fe and Ni, for ferrocene and nickelocene, respectively. The 2s, 2px and 2py orbitals of each carbon atom of $(C_5H_5)^-$ are involved in the formation of σ bond between C-C and C-H. The orbitals involved in σ bond hence shall remain out of discussion. The 2pz orbitals of ten carbons and nine orbitals of iron or nickel i.e. in total nineteen orbitals are relevant to our discussion in respect of bonding between iron or nickel orbitals and 2pz orbital of $(C_5H_5)^-$. These atomic orbitals are $\chi_4, \chi_8, \chi_{12}, \chi_{16}, \chi_{20}, \chi_{24}, \chi_{28}, \chi_{32}, \chi_{36}$ and χ_{40} of carbon and χ_{41} to χ_{49} of iron and nickel. The coefficients of these orbitals are the eigenvector values of χ [21]. They express the forms of MOs i.e. the extent of involvement of χ in the formation of Φ . In order to examine the contribution of various atomic orbitals in the formation of molecular orbitals. The Eigen vector analysis has been made and studied and data are given tables 1 to 11 respectively. The coefficients of these orbitals are the Eigen vector values of χ which have been evaluated by density functional method using Gaussian-03 software. They express the form of molecular orbital that is the extent of involvement of χ in the formation of Φ . The calculated Eigen vector values of

atomic orbitals of Fe and Ni in the formation of molecular orbitals in ferrocene and nickelocene in Table 4, 5, 8, and 9 respectively and the calculated Eigen vector values of 2pz orbital of carbon are given in Table 6, 7, 10 and 11. Table 5, 7, 9 and 11 are summation of Eigen vector values of ferrocene and nickelocene. Negative, Zero and near zero coefficient values are negligible contributions [21, 23] of electrons and have been excluded from the Tables.

Out of the 59 molecular orbitals of ferrocene molecule only 22 molecular orbitals shall be discussed as described in Table 4 for Iron orbital and Table 6 for Carbon orbital. In ferrocene the first 13 molecular orbitals $\Phi_{18}, \Phi_{20}, \Phi_{22}, \Phi_{23}-\Phi_{31}$ and Φ_{35} are formed by only two atomic orbitals, 3d orbital of iron and 2pz orbital of $(C_5H_5)^-$. These orbitals are the most stable molecular orbital and have their energies in the range -2.03849 to -0.54008 eV. The next nine molecular orbitals $\Phi_{36}-\Phi_{37}, \Phi_{40}-\Phi_{41}, \Phi_{43}, \Phi_{50}-\Phi_{51}, \Phi_{54}-\Phi_{55}$ have formed from contribution of vacant 4s, 4px, 4py and 4pz orbital of the iron and 2pz orbital of carbon. These MOs are comparatively less stable and have their energies between -0.53616 and -0.107076 eV. To examine the extent of involvement of 3d, 4s and 4p orbital in the formation of molecular orbitals the values of coefficient of each orbital have been added as shown in Table 5.

Table.4: Contributions of orbitals of iron and their summation values in the formation of molecular orbitals of ferrocene. $.S =$ summation $SS =$ sum of summation, SS of 3d orbitals = 10.4655 and SS of 4s and 4p orbitals = 12.0732. N.B; orbitals having coefficient values above 0.1 have only been considered.

MOs	4s	4p x	4py	4pz	$3dx^2-y^2$	$3dz^2$	3dxy	3dxz	3dyz
	χ_{41}	χ_{42}	χ_{43}	χ_{44}	χ_{45}	χ_{46}	χ_{47}	χ_{48}	χ_{49}
Φ_{18}	-	-	-	-	0.2947	0.2991	-	-	-
Φ_{20}	-	-	-	-	-	-	-	-	0.2361
Φ_{22}	-	-	-	-	-	-	-	0.2728	-
Φ_{23}	-	-	-	-	0.4708	0.1156	-	0.2893	0.2288
Φ_{24}	-	-	-	-	0.1041	-	0.2847	0.4762	0.2718
Φ_{25}	-	-	-	-	0.6472	-	-	-	0.3147
Φ_{26}	-	-	-	-	-	0.2269	0.8185	-	0.1004
Φ_{27}	-	-	-	-	0.1063	0.5776	0.2565	-	0.4672
Φ_{28}	-	-	-	-	0.3760	-	-	-	0.1352
Φ_{29}	0.1452	-	-	-	0.1367	0.5383	-	-	-
Φ_{30}	-	-	-	-	-	0.3496	-	0.5271	0.3891
Φ_{31}	-	-	-	-	-	-	-	0.4573	0.4577
Φ_{35}	-	-	-	-	0.2392	-	-	-	-
Φ_{36}	-	0.7335	0.6722	0.4698	-	-	-	-	-
Φ_{37}	0.5031	0.7533	0.6888	-	-	-	-	-	-
Φ_{40}	0.7981	-	0.2865	-	-	-	-	-	-
Φ_{41}	-	-	0.2780	0.7412	-	-	-	-	-
Φ_{43}	-	-	-	0.3154	-	-	-	-	-

Φ50	0.9232	-	-	0.7275	-	-	-	-	-
Φ51	-	-	0.3489	0.9974	-	-	-	-	-
Φ54	-	0.2810	0.3923	0.6228	-	-	-	-	-
Φ55	0.5802	0.3805	0.4346	-	-	-	-	-	-

Table.5: Sum of contributions and reactivity of atomic orbital's of iron in the formation of molecular orbitals of ferrocene

Atomic orbital's of Fe	Sum of contributions of orbital's of Fe	Sum of reactivity
4s	2.9498	0.3390
4p _x	2.1483	0.4655
4p _y	3.101	0.3225
4p _z	3.8741	0.2581
3d _{x²-y²}	2.375	0.4215
3d _{z²}	2.1071	0.4746
3d _{xy}	1.3597	0.7356
3d _{xz}	2.0227	0.4944
3d _{yz}	2.601	0.3845

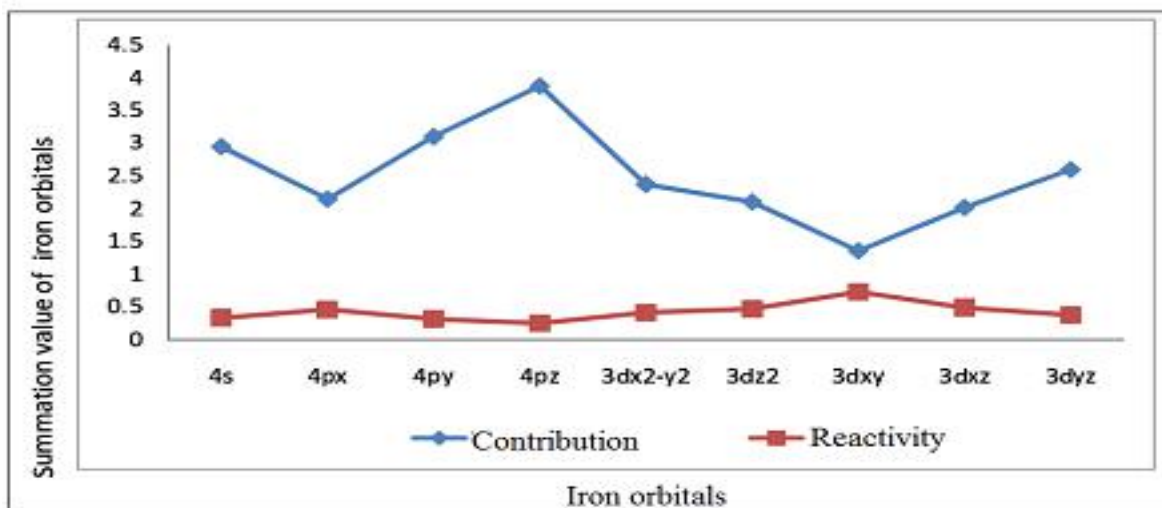


Fig.5: Sum of contributions and reactivity of atomic orbitals of, iron in the formation of molecular orbitals of ferrocene.

The summation of contributions of iron orbitals are placed in Table 5 and the total contribution from each atomic orbital is shown in Figure 5. It is clearly indicated that 4p_zorbital has the maximum involvement out of 4s and 4p orbitals, and 3d_{yz} orbital has the maximum involvement out of the 3d orbital. The exact order of availability of atomicorbital of Fe in ferrocene for contributions of atomic orbitals for the formation of molecular orbital is given below;

$$4p_z > 4p_y > 4s > 4p_x \text{ And}$$

$$3d_{yz} > 3d_{x^2-y^2} > 3d_{z^2} > 3d_{xz} > 3d_{xy} \text{ Eq (1)}$$

Sum of contributions of atomic orbitals of iron in the formation of molecular orbitals of ferrocene is shown in Table 5, in here the sum of contributions of 3d_{xy}orbital in the formation of molecular orbitals is least out of the 3d orbitals and 4p_xorbital in the formation of molecular orbitals is least out of 4s and 4p orbitals. Hence 3d_{xy} and 4p_x are comparatively free for complex formations. The exact order of availability of atomic orbital of Fe in ferrocene for complex formation is given below;

$$4p_x > 4s > 4p_y > 4p_z \text{ and } 3d_{xy} > 3d_{xz} > 3d_{z^2} > 3d_{x^2-y^2} > 3d_{yz} \text{ Eq (2)}$$

Table.6: Contributions of 2p orbitals of carbon atoms in $(C_5H_5)^-$ and their summation values in the formation of molecular orbitals of ferrocene. SS of 2p orbitals are 19.869. N.B; orbitals having coefficient values above 0.1 have only been considered

MOs	1C	2C	4C	6C	8C	10C	11C	12C	14C	16C
	χ^4	χ^8	χ^{12}	χ^{16}	χ^{20}	χ^{24}	χ^{28}	χ^{32}	χ^{36}	χ^{40}
Φ18	-	-	-	-	0.2872	-	-	-	-	-
Φ20	0.3559	-	-	-	-	-	-	-	-	0.2361
Φ22	-	0.2261	-	-	-	-	-	0.3794	-	-
Φ23	-	0.2151	-	0.2796	-	-	0.2336	-	-	0.2841
Φ24	0.2133	-	-	0.1005	0.1385	0.1852	-	0.2312	0.1199	0.1272
Φ25	0.2062	-	0.2511	-	-	0.1770	-	0.1981	-	0.1486
Φ26	-	-	0.1668	0.1949	0.1218	0.1761	-	-	-	0.1848
Φ27	-	0.2685	-	-	-	-	0.2273	-	-	-
Φ28	-	0.2347	0.2169	0.1190	0.1844	0.3799	0.2591	0.2011	0.3185	-
Φ29	-	0.3310	0.1780	0.1828	0.2399	-	0.2523	-	0.1163	0.2543
Φ30	0.2886	-	0.3015	-	-	0.2907	-	0.2767	-	-
Φ31	0.2644	0.3474	-	-	0.3104	-	0.3409	0.2797	0.3116	-
Φ35	0.4567	0.4381	-	-	0.3623	-	0.4564	0.4820	0.3912	0.2243
Φ36	0.2629	-	-	-	-	-	-	-	-	0.2243
Φ37	-	0.2973	-	-	-	-	0.2673	0.2552	-	-
Φ40	-	-	0.3089	-	-	-	-	-	-	0.3653
Φ41	0.2114	-	0.2234	-	-	-	-	-	-	0.2387
Φ43	-	-	-	0.2661	-	-	-	-	-	-
Φ50	-	-	-	0.4338	-	-	-	-	-	0.3828
Φ51	-	-	-	0.3149	-	-	-	-	-	0.3416
Φ54	-	-	-	-	0.1856	-	-	-	-	-
Φ55	-	-	-	-	-	-	0.3004	-	-	-

Table.7: Sum of contribution values and reactivity of atomic orbitals of carbon in the formation of molecular orbitals of ferrocene

Atomic orbital's of carbon	Sum of contribution of carbon orbital's	Sum of reactivity
1C	2.2594	0.4426
2C	2.3582	0.4241
4C	1.6466	0.6073
6C	1.8916	0.04589
8C	1.8301	0.5465
10C	1.2089	0.8274
11C	2.3373	0.4278
12C	2.3034	0.4341
14C	1.2575	0.7955

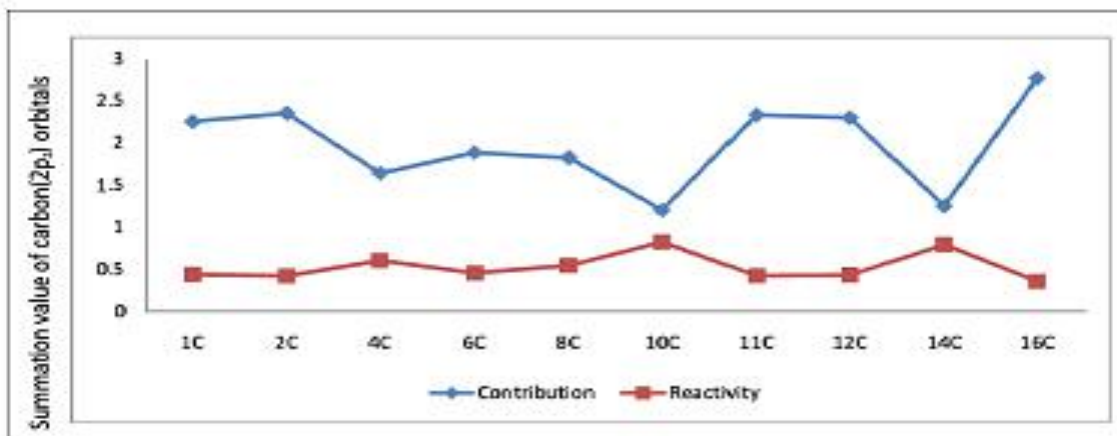


Fig.6: Sum of contributions and reactivity of atomic orbitals of carbon in the formation of molecular orbitals of ferrocene.

Table 7 and Figure 6 show the summation values where the total contributions from each atomic orbital of carbon clearly indicates that eigenvector value of $2p_z$ orbital of 16C has the maximum involvement out of the ten carbon atoms in both $(C_5H_5)^-$ ligands. The sequences from the series are as below:

$$16C > 2C > 11C > 12C > 1C > 6C > 8C > 4C > 14C > 10C. \quad \text{Eq (3)}$$

Sum of contributions of atomic orbitals of carbon ($2p_z$) in the formation of molecular orbitals of ferrocene is shown in Table 7 and Figure 6 where the 10C contributions in the formation of molecular orbitals are least out of the ten carbon atoms. Hence 10C is comparatively free for complex formation. The sequence from the series is shown below:

$$10C > 14C > 4C > 8C > 6C > 1C > 12C > 11C > 2C > 16C. \quad \text{Eq (4)}$$

Out of 59 molecular orbital Eigen values of nickelocene we shall discuss only 25 of them described in Table 8, for nickel orbitals and Table 10 for carbon orbitals. The first 14 MOs are $\Phi_{15}-\Phi_{16}$, $\Phi_{18}-\Phi_{20}$, Φ_{21} and $\Phi_{23}-\Phi_{30}$, are formed by various $3d$ and $2p_z$ orbitals of $(C_5H_5)^-$. These orbitals with energies in the range of -9.9338 to -0.64271 eV are the most stable molecular orbital between nickel and $2p_z$ orbital of $(C_5H_5)^-$. The next eleven MOs i.e. $\Phi_{36}-\Phi_{40}$, $\Phi_{42}-\Phi_{43}$, Φ_{50} , Φ_{53} , Φ_{54} and Φ_{59} are formed by interaction of $4s$, $4p_x$, $4p_y$ and $4p_z$ orbital of metal and $2p_z$ orbital of carbon of $(C_5H_5)^-$. These MOs with energies in the range -0.56142 to -0.10622 eV are comparatively less stable. To examine the extent of involvement of $3d$, $4s$, $4p$ and $2p_z$ orbitals in the formation of molecular orbitals the values of coefficient of each orbital are tabulated in Table 9.

Table.8: Contributions of orbitals of nickel and their summation values in the formation of molecular orbitals of nickelocene. SS of $4s$ and $4p$ orbitals = 13.0598. And $3d$ orbitals = 9.3888.

N.B; Orbitals having coefficient values above 0.10 have only been considered.

MOs	$4s$	$4p_x$	$4p_y$	$4p_z$	$3d_{x^2-y^2}$	$3d_{z^2}$	$3d_{xy}$	$3d_{xz}$	$3d_{yz}$
	χ_{41}	χ_{42}	χ_{43}	χ_{44}	χ_{45}	χ_{46}	χ_{47}	χ_{48}	χ_{49}
Φ_{15}	-	-	-	-	-	-	-	0.3209	0.3365
Φ_{16}	-	-	-	-	-	-	-	0.2294	0.1991
Φ_{18}	-	-	-	-	-	-	0.3605	-	-
Φ_{19}	-	-	-	-	-	-	0.3125	-	-
Φ_{20}	-	-	-	-	0.5297	-	-	-	-
Φ_{21}	-	-	-	-	0.3029	-	-	-	-
Φ_{23}	-	-	-	-	0.3279	-	-	-	0.1838
Φ_{24}	-	-	-	-	-	-	0.3849	0.4986	0.2011
Φ_{25}	-	-	-	-	0.5232	0.3369	-	0.2396	0.2782
Φ_{26}	-	-	-	-	-	0.7408	-	-	0.4949
Φ_{27}	-	-	-	-	-	-	0.6697	-	0.2358
Φ_{28}	-	-	-	-	0.1702	-	-	-	-

Φ29	-	-	-	-	-	0.2012	-	-	-
Φ30	-	-	-	-	-	0.2979	0.1819	0.4786	0.3521
Φ36	-	0.5037	0.5563	0.2729	-	-	-	-	-
Φ37	0.4088	0.3254	0.2960	-	-	-	-	-	-
Φ38	0.6732	0.2423	0.3695	-	-	-	-	-	-
Φ39	-	0.7569	0.3868	0.3261	-	-	-	-	-
Φ40	-	0.2201	0.3706	-	-	-	-	-	-
Φ42	-	0.3487	0.3318	-	-	-	-	-	-
Φ43	-	0.6971	0.7470	-	-	-	-	-	-
Φ50	0.7225	-	-	-	-	-	-	-	-
Φ53	-	0.3020	-	0.2283	-	-	-	-	-
Φ54	0.6421	0.4372	0.5633	-	-	-	-	-	-
Φ59	-	0.4436	0.7620	1.1256	-	-	-	-	-

Table.9: Sum of contributions and reactivity of atomic orbital's of nickel in the formation of molecular orbitals of nickelocene.

Atomic orbital's of Ni	Sum of contributions of orbital's of Ni	Sum of reactivity
4s	2.4466	0.4087
4p _x	4.277	0.2338
4p _y	4.3833	0.2281
4p _z	1.9529	0.5121
3d _{x²-y²}	1.9439	0.5144
3d ² _z	1.5768	0.6342
3d _{xy}	1.9095	0.5237
3d _{xz}	1.7671	0.5657
3d _{yz}	2.2815	0.4383

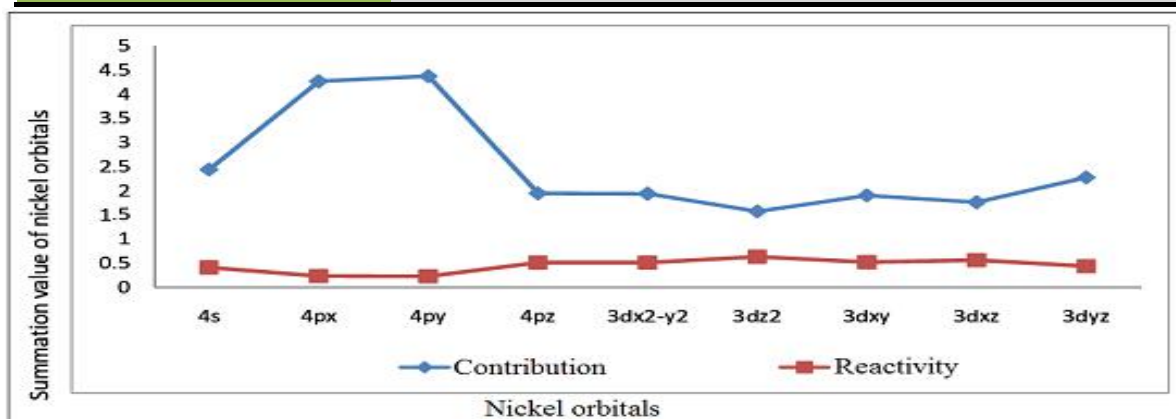


Fig.7: Sum of contributions and reactivity of atomic orbital's of nickel in the formation of molecular orbitals of nickelocene.

The summation values given in Table 9 and plotted in Fig. 7 show the total contributions from each atomic orbital. It is clearly indicated that 4pyorbital has the maximum involvement out of 4sand 4porbital and 3dyzorbital has the maximum involvement out of 3dorbitals. The sequence from the two series is given below:

$$4py > 4px > 4s > 4pz \text{ and } 3dyz > 3dx^2-y^2 > 3dxy > 3dxz > 3d^2_z \tag{5}$$

Sum of contributions of atomic orbitals of nickel in the formation of molecular orbitals of nickelocene is shown in

Table 9 and Figure 7 that the sum of contributions of 3d²zorbital in the formation of molecular orbitals is least out of the 3dorbitals and 4pzorbital is least out of 4sand 4porbitals. Hence 3d²zand 4pz are comparatively free for complex formations. The exact order of availability of atomic orbitals of Ni in nickelocene for complex formation is given below;

$$4pz > 4s > 4px > 4py \text{ and } 3dyz > 3dxz > 3dxy > 3dx^2-y^2 > 3dyz \tag{6}$$

Table.10: Contributions of 2pz orbitals of carbon atoms in $(C_5H_5)^-$ and their summation values in the formation of molecular orbitals of nickelocene. SS of, 2pz orbitals are, 11.8502. N.B; orbital having coefficient value above, 0.10 have only been considered

MOs	1C	2C	4C	6C	8C	10C	11C	12C	14C	16C
	χ^4	χ^8	χ^{12}	χ^{16}	χ^{20}	χ^{24}	χ^{28}	χ^{32}	χ^{36}	χ^{40}
Φ15	-	-	-	-	-	-	-	-	0.1678	-
Φ16	-	-	-	-	-	-	-	-	-	-
Φ18	-	-	-	-	-	-	-	-	-	-
Φ19	-	-	-	-	-	-	-	-	-	-
Φ20	-	-	-	-	-	-	-	-	-	-
Φ21	-	-	-	0.2019	-	-	-	-	-	0.1986
Φ23	-	-	-	0.2182	-	-	0.1815	-	-	-
Φ24	-	-	-	-	0.1692	-	-	0.1544	-	0.1707
Φ25	-	-	-	-	-	-	-	-	-	0.2018
Φ26	-	-	-	-	-	-	-	-	-	-
Φ27	-	-	0.2142	-	-	0.1666	-	-	-	-
Φ28	0.2818	-	0.3050	-	0.2252	0.4088	0.2304	-	0.3089	-
Φ29	-	0.4189	0.2037	0.2561	0.2707	-	0.3600	-	0.2006	0.3209
Φ30	0.3293	-	0.3232	0.1812	0.1505	0.3096	-	0.3219	0.1864	0.2300
Φ36	-	-	0.2106	-	-	0.2172	-	-	0.3003	-
Φ37	0.2124	0.2023	-	-	-	0.2123	-	-	-	-
Φ38	-	-	-	-	-	-	-	-	-	-
Φ39	-	-	-	-	-	-	0.2029	0.2264	-	-
Φ40	-	-	-	-	0.4239	-	-	-	-	-
Φ42	-	-	-	-	0.2725	-	-	-	-	-
Φ43	-	-	-	-	-	-	-	-	-	-
Φ50	-	-	-	-	0.4095	-	-	-	-	0.3640
Φ53	-	-	-	0.2129	-	-	-	-	-	-
Φ54	-	-	-	-	-	0.2723	-	-	-	-
Φ59	-	-	-	-	0.2227	-	-	-	-	-

Table.11: Sum of contributions and reactivity of atomic orbitals of carbon (2pz) in the formation of molecular orbitals in nickelocene.

Atomic orbital's of carbon	Sum of contribution of carbon orbital's	Sum of reactivity
1C	0.8235	1.2143
2C	0.6212	1.6098
4C	1.2567	0.7957
6C	1.0703	0.9344
8C	2.1442	0.4667
10C	1.5868	0.6302
11C	0.9748	1.0259
12C	0.7027	1.4231
14C	1.164	0.8591
16C	1.486	0.6729

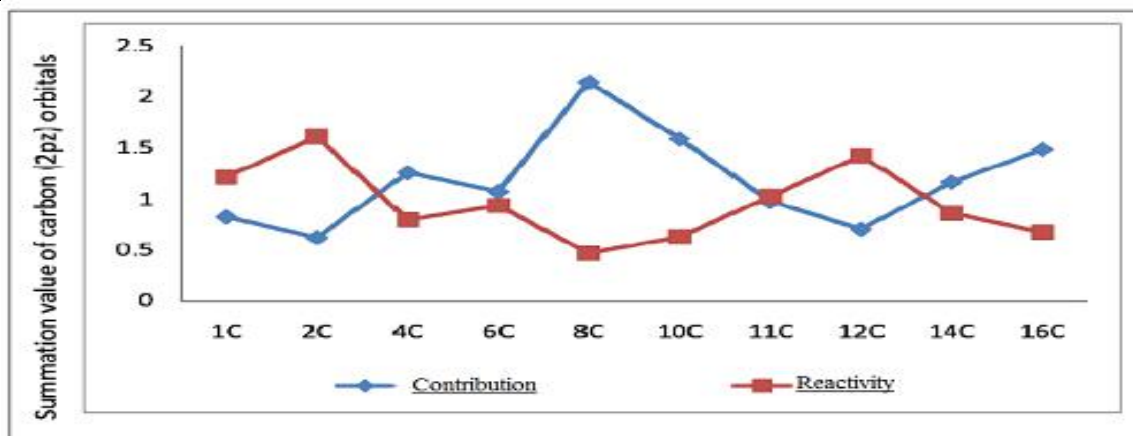


Fig.8: Sum of contributions and reactivity of atomic orbital's of, Ni in the formation of molecular orbitals of nickelocene.

The summation values shown in Table 11 and Figure 8 clearly indicates that contribution of $2p_z$ orbital of 8C has the maximum involvement out of the ten carbon atoms in $(C_5H_5)^-$. The sequence from the series are given below:

$$8C > 10C > 16C > 4C > 14C > 6C > 11C > 1C > 12C > 2C.$$

Eq (7)

Sum of contributions of atomic orbitals of carbon ($2p_z$) in the formation of molecular orbitals of nickelocene is shown in Table 11 and Figure 8 where the sum of contribution of 2C of $2p_z$ orbital's in the formation of molecular orbital's are least out of the ten carbon atoms. Hence 2C are comparatively free for complex formations. The exact order of availability of carbon atom for complex formation is given below:

$$2C > 12C > 1C > 11C > 6C > 14C > 4C > 16C > 10C > 8C.$$

Eq (8)

The total involvement in relation to the bonding between metal orbital derived from coefficient values are 22.6107 in ferrocene, and 22.8486 in nickelocene hence nickelocene is more stable than ferrocene. The total involvement in relation to the bonding between $2p_z$ orbital of the ten carbon atoms of both ligands of $(C_5H_5)^-$ 19.889 and 15.529 in ferrocene and nickelocene respectively, hence ferrocene is more stable than nickelocene. The total involvement of $3d$, $4s$ and $4p$ orbitals of metal and $2p_z$ orbitals of the ten carbon atoms of both ligands of $(C_5H_5)^-$ in ferrocene and nickelocene respectively are 42.2528, and 38.3776 hence we can conclude that ferrocene is more stable than nickelocene.

Population analysis

The contribution of electrons in each occupied MO is calculated by using the population analysis method

introduced by Mullikan [24, 25, and 26]. This method apportions the electrons of n -electron molecule into net population n_i in the basis function $\chi(r)$. Let there be n_i electrons in the MO Φ_i ($n_i = 0, 1, 2$) and let n_{ri} symbolize the contribution of electrons in the MO Φ_i to the net population in χ_r , we have:

$$n_{ri} = n_i c_{ri}^2 \quad \text{Eq (9)}$$

Where, c_{ri} is the coefficient of atomic orbital for the i^{th} MO $r = 1-29$ in ferrocene and $r = 1-30$ in nickelocene. Eq(9) has been solved for, 58 electrons of 29 molecular orbitals in ferrocene and 60 electrons of 30 molecular orbitals in nickelocene. Each MOs has two electrons in ferrocene and nickelocene but (the 30th MOs of nickelocene has only one electron). The coefficient of atomic orbital c_{ri} is treated as Eigen vector value [24, 25, and 26]. Values less than 0.1 have negligible contributions and are omitted in the calculations. Only $3d$ orbitals of metal and $2p_z$ orbitals of carbon are considered in the calculation.

The summation value of population analysis of these orbitals is shown in Table 12 of ferrocene, and 13 of nickelocene. It is indicated that in MOs 1-17 of ferrocene, in MOs 1-14 of nickelocene only $2s$, $2p_y$ and $2p_x$ electrons of carbon have contributions in the formation of molecular orbital of ferrocene and nickelocene hence are out of discussion.

The summation value of population analysis of these orbitals to contribute electrons in the formation of molecular orbital is shown Tables 12 and 13 the result of the population analysis shows that only $2p_z$ orbitals of carbon of $(C_5H_5)^-$ and $3d$ orbitals of metal provide electrons to MOs of ferrocene, and nickelocene.

Table.12: The Sum of contribution of electrons 3d orbitals of iron and 2pz orbitals of carbon in the formation of molecular orbitals of ferrocene.

MOs	No. of atomic orbitals	Eigenvector (c_{ri})	No. of electrons (n_i)	Net population (n_{ri})
Φ18	3	0.8811	6	0.5176
Φ20	3	0.8256	6	0.4850
Φ22	3	0.8783	6	0.5161
Φ23	8	2.1169	16	1.2437
Φ24	11	2.2446	22	1.3187
Φ25	7	1.9429	14	1.1414
Φ26	8	1.9902	16	1.1692
Φ27	6	1.9034	12	1.1182
Φ28	10	2.4248	20	1.4246
Φ29	10	2.3758	20	1.3958

Sum of summation value of population analysis, (n_{ri}) of occupied molecular orbital of ferrocene is, 10.3302.

Table.13: The Sum of contribution of electrons, 3d orbitals of nickel and, 2pz orbitals of carbon in the formation of molecular orbitals of nickelocene.

MOs	No. of atomic orbitals	Eigenvector (c_{ri})	No. of electrons (n_i)	Net population (n_{ri})
Φ15	3	0.8252	6	0.4884
Φ16	2	0.4285	4	0.2537
Φ18	1	0.3605	2	0.2134
Φ19	1	0.4718	2	0.2793
Φ20	1	0.5297	2	0.4163
Φ21	3	0.7034	6	0.5529
Φ23	4	1.1606	8	0.9122
Φ24	6	1.5789	12	1.2410
Φ25	5	1.7438	10	1.0979
Φ26	2	1.2357	4	0.7780
Φ27	4	0.9055	8	0.5701
Φ28	7	1.9303	14	1.1425
Φ29	8	2.2311	16	1.3206
Φ30	12	1.3426	24	0.7947

Sum of Summation value of population analysis, (n_{ri}) of occupied molecular orbital of nickelocene is, 10.0609

IV. CONCLUSION

We studied the electronic structure and geometry optimization of ferrocene and nickelocene molecules using DFT/B3LYP with the basis set of 6-31G (d) calculations. We found that orbitals corresponding to the Eigen values (energy ranges -2.03849 to -0.54008 eV in ferrocene and -9.90743 to -0.64271 eV in nickelocene) formed between 3d orbitals and 2pz orbitals are the most stable molecular orbitals. The less stable orbitals are in the energy ranges of -0.53616 to -0.10707 eV in ferrocene and in -0.56142 to -0.10622 eV nickelocene. Eigenvectors of ferrocene and nickelocene show that the first 13 MOs in ferrocene 14 MOs nickelocene are formed by various 3d orbitals of metal and 2pz orbital of carbon of (C_5H_5)⁻ and the most stable

MOs. The next 9 MOs in ferrocene and 11 MOs of nickelocene are formed by the interaction of 4s and 4p orbitals of metal and 2pz orbital of carbon of (C_5H_5)⁻ and these MOs are comparatively less stable orbitals. Out of the 3d orbitals of ferrocene and nickelocene molecules the 3dyz orbitals have maximum involvement in the formation of molecular orbitals, whereas the 4pz orbital out of 4s and 4p orbital of iron and 4py orbital out of 4s and 4p orbital of nickel show maximum involvement, in the order of 4pz > 4py > 4s > 4px and 3dyz > 3dx²-y² > 3dz² > 3dxz in ferrocene, and 4py > 4px > 4s > 4pz and 3dyz > 3dx²-y² > 3dxz > 3dz² in nickelocene. The total involvement in relation to the bonding between metal orbital derived from coefficient values are 22.6107 in

ferrocene and 22.8486 in nickelocene hence nickelocene is more stable than ferrocene. The total involvement in relation to the bonding between $2p_z$ orbital of the ten carbon atoms of both ligands of $(C_5H_5)^-$ 19.889, and 15.529 in ferrocene and nickelocene respectively, hence ferrocene is more stable than nickelocene. As a summary, the total involvement of $3d, 4s$ and $4p$ orbitals of metal and $2p_z$ orbitals of the ten carbon atoms of both ligands of $(C_5H_5)^-$ in ferrocene and nickelocene respectively are 42.2528 and 38.3776 hence we can conclude that ferrocene is more stable than nickelocene. This is in support of the results shown in terms of the parameters like dipole moment, HOMO-LUMO gap, Ionization potential etc discussed in the above. The population analysis shows that only $2p_z$ orbitals of carbon of $(C_5H_5)^-$ and $3d$ orbitals of metal provide electrons to MOs of ferrocene and nickelocene. We recommend to simulate bigger molecules using higher basis sets and to study more properties of the molecules. Larger basis sets provide approximations more accurately by imposing fewer restrictions on the interaction of electrons in space.

ACKNOWLEDGMENT

The author acknowledges Dr. Hagos Woldegebriel for his advising, ideas, guidance, enjoyable discussion and unforgettable support throughout my study.

REFERENCES

- [1] FA Cotton, G Wilkinson, PL Gaus. Basic Inorganic Chemistry, 3rd ed., Wiley and Sons, Asia, 2001, pp 667.
- [2] S Girolami, TB Rauchfuss, RJ Angelici. Synthesis and Technique in Inorganic Chemistry, CA: University Science Books- Mill Valley, 1999.
- [3] ER Davidson. Chem. Rev. 2000, 100, 351.
- [4] ER Davidson. Chem. Rev. 1991, 91, 649.
- [5] RF Nalewajski. Topics in current chemistry, Ed., Heidelberg: Berlin: Springer-Verlag, 1996, pp 180.
- [6] RG Parr, W Yang. Density Functional Theory of atoms and molecules, Eds., New York: Oxford University Press, 1989.
- [7] J Labanowski, J and elm. Density Functional Methods in Chemistry, Eds., Heidelberg: Springer-Verlag, 1991.
- [8] T Ziegler, Chem. Rev. 1991, 91, 651.
- [9] L Szasz. Pseudopotential Theory of Atoms and Molecules, New York: J. Wiley & Sons, 1986.
- [10] M Krauss; WJ Stevens. Ann. Rev. Phys. Chem. 1984, 35, 357.
- [11] P Durand; JP Malrieu, Adv. Chem. Phys. 1987, 67, 321.
- [12] TR Cundari, MT Benson, ML Lutj, SO Sommerer, Reviews in Computational Chemistry, KB Lipkowitz, DB Boyd, Eds.; VCH: New York, 1996, 8, pp145.
- [13] RC Mehrotra, A Singh. Organometallic Chemistry, Wiley Eastern Ltd. 1992, pp 247.
- [14] IN Levine Quantum Chemistry, 5th edn., New Jersey: Prentice Hall, 2000, pp 664.
- [15] DA Cleary; AH Francis, J. Phys. Chem. 1985, 89, pp 97.
- [16] PK Byszewski; E Antonova; J Kowalska; Radomska; J Baran, Chem. Phys. Lett. 2000, 323, pp 522.
- [17] C Elschenbroich, ASalzer. Organometallics, VCH: Weinheim, 1991.
- [18] G Wilkinson; PL Pauson, FA Cotton, J Am. Chem. Soc. 1954, 76, pp 1970.
- [19] JH Schachtschneider; R Prins; P Ros, Inorg.Chim. Act. 1967, 1, pp 462.
- [20] ER David. Chem. Rev. 2000, 100, pp 351
- [21] G. K.; Ra, N. V. and P. P. S. Molecular mechanics and Quantum Chemistry Study of Cobaltocene and Nickelocene, Archives of Physics Research, Vol.3, No. 2, PP. 297-310, 2011.
- [22] V. Kahn. S. G. Kahn., R. N. V. and Pashupati .P. S. Complexes of Cobaltocene: and Effective Atomic Softness and Fukui Function Based Study, Journal of Pharmaceutical, Biological and Chemical Sciences, Vol.5, No. 12, PP. 211-326, 2010.
- [23] Khan. Molecular Mechanics Based Study on Molecular and Atomic Orbital of Nickelocene, Journal of Applied Chemical Research, Vol.10, No. 19, PP.66-84, 2011.
- [24] G. Kahn. And Rajendra, P. T. Study of Molecular Orbitals of Ruthenium (II) Bromide Based on Molecular Mechanics, K. S. Saket Post Graduate College, Ayodhya, Faizabad, U. P. INDIA, Applied Science Research, Vol.3, No. 2, pp. 483-492, 2011.
- [25] G. Kahn. Comparative Study of Molecular Orbitals of Cobaltocene and Nickelocene Based on Molecular Mechanics, K. S. Saket Post Graduate College, Ayodhya, Faizabad, U. P. INDIA, Applied Science Research, Vol.3, No. 2, pp. 297-310, 2011.
- [26] P. P. Singh, P. Mishra and J. P. Singh. Molecular mechanics and quantum chemistry based study of cobalt-thiazolidinedione complexes, Bareilly College, Bareilly, U.P. Vol.34, No. 3, pp. 215-224, (2006).

Design and Analysis of 8x8 Wallace Tree Multiplier using GDI and CMOS Technology

Pradeep Kumar Kumawat¹, Gajendra Sujediya²

¹Research Scholar, Department of ECE, Rajasthan Institute of Engineering and Technology, Jaipur, India

²Assistant Professor, Department of ECE, Rajasthan Institute of Engineering and Technology, Jaipur, India

Abstract— Multiplier is a small unit of an arithmetic circuit that is widely used in Digital filters, Digital Signal Processing, microprocessors and communication applications etc. In today's scenario compact and small digital devices are critical concern in the field of VLSI design, which should perform fast as well as low power consumption. Optimizing the delay, area and power of a multiplier is a major design issues, as area and speed are usually conflicting constraints. A Wallace tree multiplier is an improved version of tree base multiplier.

The main aim of this paper is a reconfigurable 8x8 Wallace Tree multiplier using CMOS and GDI technology. This is efficient in power and regularity without increase in delay and area. The generation of partial products in parallel using AND gates. The addition of partial products is reducing using Wallace Tree which is divided into levels. Therefore there will be a certain reduction in the power consumption, since power is provided only to the level that is involved in computation and the remaining two levels remain off.

Keywords— Multiplier, GDI, CMOS, Wallace tree .

I. INTRODUCTION

Arithmetic operations are penetrating into more and more applications with the advances in VLSI technology. The root operation found in most arithmetic components are binary addition and multiplication and division, which improves the performance using low-power, area efficient circuits operating at higher speed[1].

Multiplication is an operation that uses frequently in DSP and much other application. It occupies more area that it consumes large delay when compared to adder. Therefore it is imperative that special techniques be used to speed up the calculation of the product while maintaining a reasonable area. Addition is the most basic arithmetic operation and adder is the most fundamental arithmetic component of the processor. In addition, each resulting bits are depending on its corresponding In case of addition each of resulting output bits are depending on its inputs. It is important operation because it involves a carry ripple step i.e. the carry from the previous bits addition should propagates to next bit of addition.

II. PROCESS OF MULTIPLICATION

In digital electronics the multiplication operation is very simple and easy to access. The multiplier uses addition and shift left operations for calculating the product of two binary numbers. Techniques involve in computing a set of the partial products, thereafter summation of partial products together.

2.1 Multiplication involves two steps:

Partial Product Generation

2.1.2 Their Summation

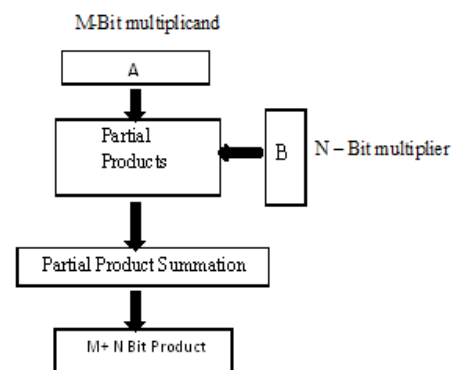


Fig 2.1: Multiplier Block Diagram

The figure 2.1 shows the multiplication process of two unsigned binary digits. In the multiplication process the first digit is called Multiplicand and the second digit is called multiplier and the first step in the multiplication is called partial product. In the partial product row if the multiplier bit is "1" then partial product row is same as multiplicand digit, if the multiplier bit is "0" then the partial product row is zero.

An example of multiplication that is consisting product of the two unsigned (positive) binary numbers radix 2 given below,

1011 (this binary number represents 11)
X 1010 (this binary number represents 10)
0000 (1011 x 0)
1010 (1010 x 1, shifted one position to left)
0000 (1010 x 0, shifted two position to left)
+1010 (1010 x 1, shifted three position to left)
01101110 (This binary number represents 110)

III. WALLACE MULTIPLIER

Scientist Chris Wallace in 1964 introduced an easy and simple way of summing the partial product bits in the parallel using the tree of the Carry Save Adders which is known as “Wallace Tree”[2]. A typical Wallace tree architecture is shown in figure 3.1.

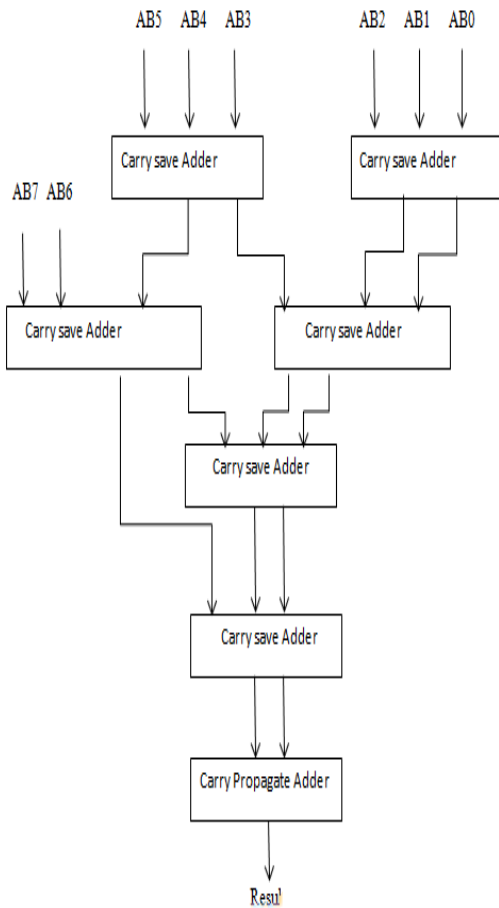


Fig.3.1: Wallace Multiplier

Wallace multiplier includes steps to multiply two numbers. The first step is formation of the bit products. Then carry save adder reduces bit product matrix into two row matrix. After that the remaining two rows are summed by using the fast carry propagate adder to produce the final result. However the process become complex, the multiplier with delay proportional to logarithm of operand size n [3]. This algorithm reduced the partial product at a rate of $\log_3/2 N/2$. By using carry-save adder the need of carry propagation in the adder is avoided and latency of one addition is equal to gate delay of adder.

IV. CIRCUIT DESIGN

4.1 OR Gate:

Schematic diagram of GDI based OR gate is shown in figure 4.1. The OR gate is one of the basic digital logic gate. Basically, the function of the OR effectively finds

the maximum digit between two binary digits. In OR gate one out of three inputs is fixed, connected to Vdd, While other two inputs are variable can be logic High (logic 1) or logic Low (logic 0). The output of the OR Gate gives logic high when one or both of the input to the gate are logic High, if both input to the gate are logic low then the result will be logic low.

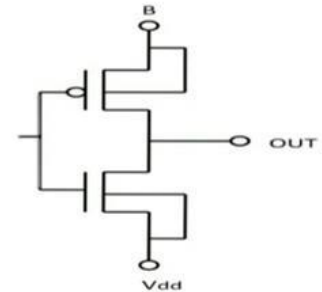


Fig.4.1: GDI based OR gate

4.2 AND Gate:

Schematic diagram of GDI based AND gate is shown in figure 4.2. The AND gate is used for the product of two binary digits. Basically, the function of the AND effectively finds the minimum digit between two binary digits. It gives high output (logic 1) only if both inputs to AND gate are logic high (logic 1). And if none or only one input to AND gate is high, than a low output is generated. Therefore, the output is always low ('0') except when all inputs are high ('1's)

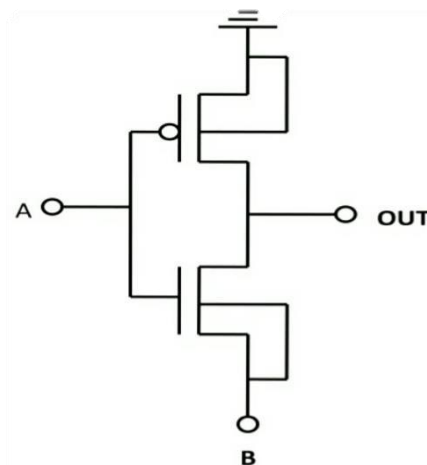


Fig.4.2: GDI based AND gate

4.3 XOR Gate:

Schematic diagram of GDI based XOR gate is shown in figure 4.3. When inputs are different then output is logic high and both inputs are same either logic high or logic low then output will become logic low (logic 0).

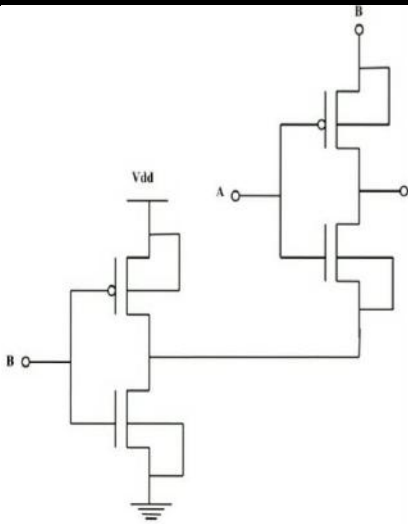


Fig.4.3: GDI based XOR gate

4.4. Half Adder:

Half adder has two inputs, generally denoted A and B, and two outputs, the sum (S) and carry (C). Essentially the output of a half adder is the sum of two one-bit numbers, XOR operation of the two inputs A and B produces output Sum, AND operation of the input produces Carry as a output. Although by itself, a half adder is not such useful, it can be used as a building block for larger adding circuits (Full Adder) [4]. In fig a logic & block diagram of half adder (HA) is shown in figure 4.4.

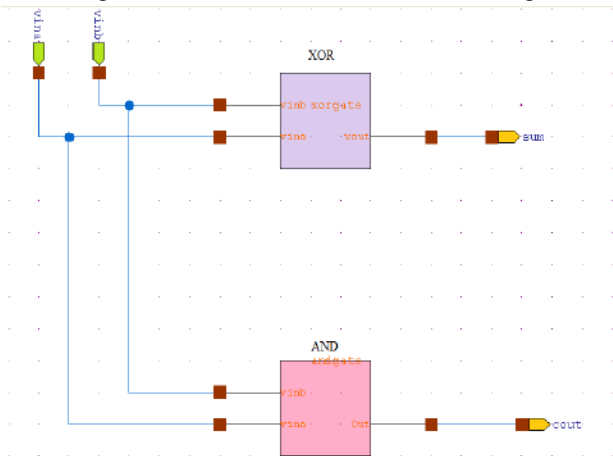


Fig.4.4:GDI based Half Adder

4.5 Full Adder:

Full Adder is used to add three inputs Vina, Vinb and Vinc to produce sum and carry out (Cout). Vinc input is the carry generated from previous stage[4]. Schematic diagram of GDI based full adder circuit is shown in figure4.5.

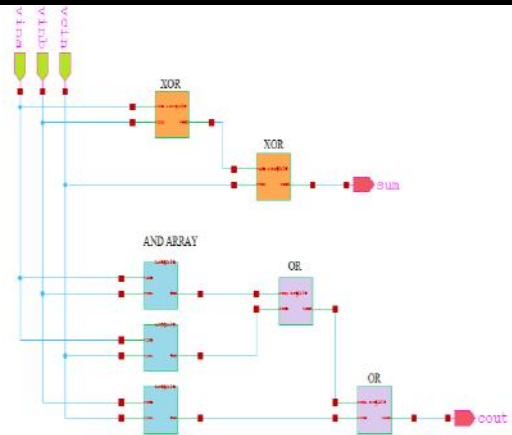


Fig.4.5: GDI based Full Adder

4.6 Compressor:

For three inputs full adder can be used to summation, but for more than three input other types of adder are used which is called compressor circuit. Compressor circuit is used to add four or five input. Compressor circuit is used for addition of more than three inputs. The 4:2 Compressor has 5 inputs to generate 3 outputs Sum, Carry and Cout. The input Vcin is the output from a previous lower significant compressor and the Cout output is for the compressor in the next significant stage [3]. Circuit diagram of 4:2 compressor is shown in figure 4.6 and Circuit diagram of 5:2 compressor is also shown in figure 4.7.

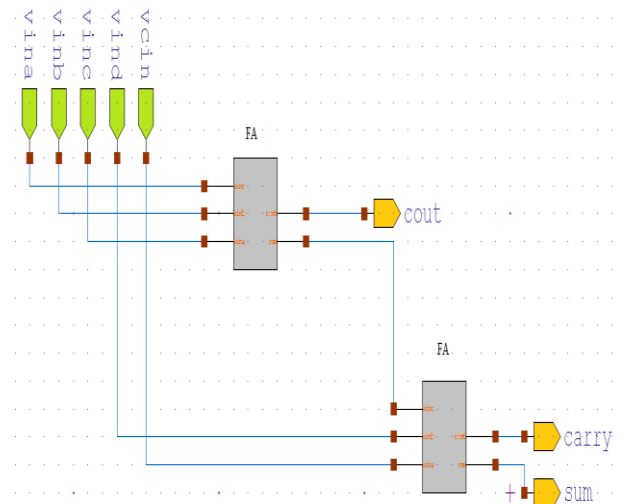


Fig.4.6: GDI based 4:2 Compressor

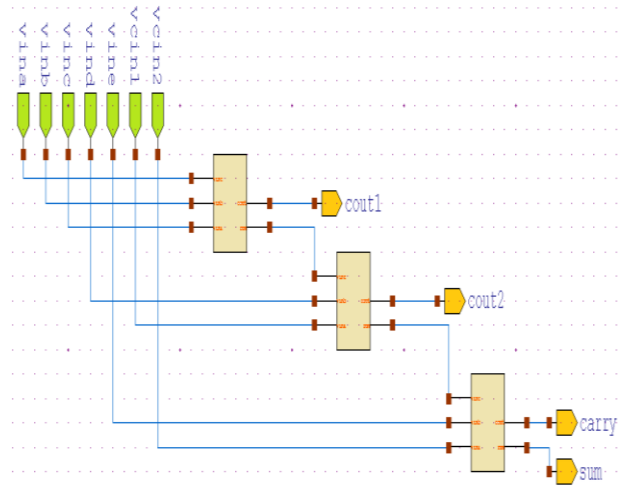


Fig.4.7: GDI based 5:2 Compressor

4.8 8-Bit Multiplier:

8x8 bit multiplier based on Wallace Tree is efficient in terms of the power and the regularity without increase in the delay as well as in the area. The idea involves generation of partial products in the parallel using the AND gates. Furthermore, the addition of the partial products is done using the Wallace tree, which is hierarchal, divided into levels. There will be a reduction in power consumption, since the power is provided only to level that is involved in the computation [5].

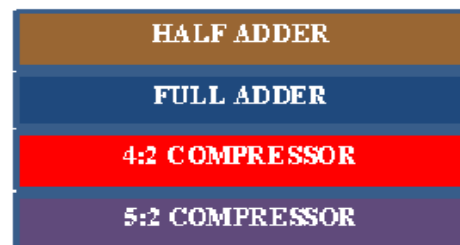
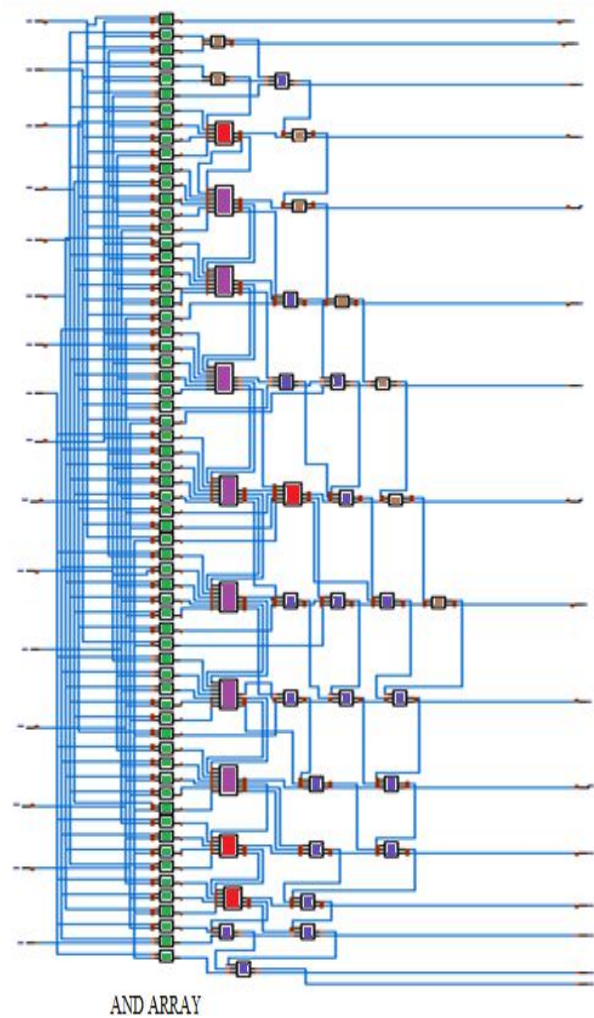


Fig.4.8: GDI based 8-Bit Multiplier Schematic

V. RESULT AND ANALYSIS

This paper shows comparison of power calculation, Delay calculation and area in terms of transistor and the design has been implemented and simulated using Tanner Tool in 180nm technology with operating voltage of approximately 1.8V. Comparison of delay at different power supply voltage of different bit multiplier is shown in figure 5.1.

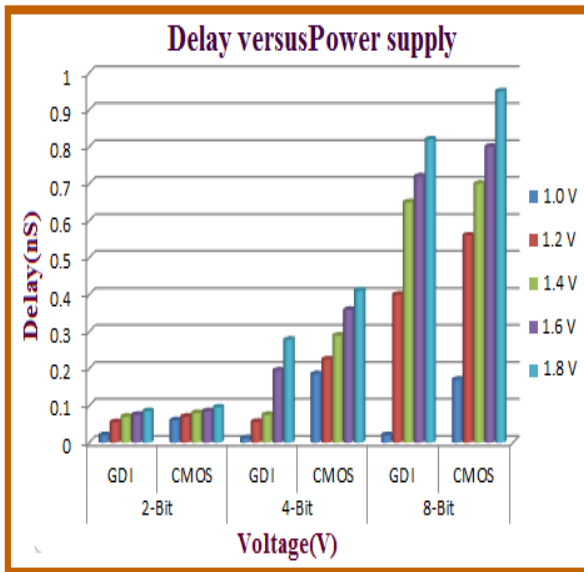


Fig.5.1: Comparison of Delay at different supply

VI. CONCLUSION

Multiplier is one of the important units for most of digital circuits. Low power dissipation, minimum propagation delay and area minimization of the circuit are major concern. Wallace tree multiplier based on GDI technology occupies smaller silicon area than the conventional Wallace tree multiplier. At different power supply, propagation delay are calculated and shown in the graph 5.1. The comparison at 1.8V power supply shows the delay of Wallace tree 8-Bit multiplier GDI based and CMOS based are 0.02nS and 0.17nS respectively. Thus GDI based circuit helps us to reduce propagation delay, power dissipation compare to CMOS based circuits.

REFERENCES

- [1] P.V. Rao, C. P. R. Prasanna, and S. Ravi, VLSI Design and Analysis of Multipliers for Low Power, IEEE Fifth International Conference on Intelligent Information Hiding and Multimedia Signal Processing, Kyoto,2009,pp.1354-1357.
- [2] C. S. Wallace, A Suggestion for a Fast Multiplier, IEEE Transactions on Computers, 13, 1964, pp.14-17
- [3] Ron S. Waters and Earl E. Swartzlander, "A reduced Complexity Wallace Multiplier Reduction. IEEE Transactions On Computers, Vol. 59, No. 8, August 2010. Published by the IEEE computer Society.
- [4] Puneet Bhardwaj Dhammi, "Analysis and Implementation of various Adders and Multipliers with Power and Performance Perspectives", Thapper University Patiala.
- [5] K. G. Krishna, B. Santhosh, and V. Sridhar, "Design of Wallace Tree Multiplier using Compressors",

Prevalence of Musculoskeletal Problems among Sugarcane Workers in Uttar Pradesh

Sushma Gangwar*, Seema Kwatra

Department of Family Resource Management, College of Home Science, G.B.P.U.A. & T. Pantnagar, Uttarakhand, India

Abstract— Agricultural work in both developed and in developing countries continues to be one of the most hazardous occupations. India is primarily an agrarian economy as farming is one of the most important occupations in the country. Many risk factors are associated with the development of musculoskeletal disorders are common in agricultural tasks. Thus in the present study an attempt has been made to analyze the prevalence of MSDs among sugarcane workers of Bareilly District, UP. A total sample size of 60 farm workers was taken for data using purposive and random sampling without replacement. Due to long working hours, awkward body postures, repetitive work and physical load there exist a high prevalence of physiological discomforts among sugarcane workers engaged in sugarcane sowing and harvesting both the activities are associated with MSD most dominated in neck, upper arm and low back. The above investigation revealed that the workers suffered from pain and discomforts more in neck, upper arm, and low back.

Keywords— Musculoskeletal disorders, posture, discomfort, pain.

I. INTRODUCTION

Agricultural work in both developed and in developing countries continues to be one of the most hazardous occupations. India is primarily an agrarian economy as farming is one of the most important occupations in the country. It is generally perceived as a healthy outdoor occupation. However number of studies have classified farming as a risky and hazardous job. Because of the nature of farm work, farm workers are at particular risk of developing musculoskeletal disorder, besides a large number of other health problems. Agriculture ranks among the most hazardous industries. Farmers are at very high risk for fatal and non-fatal injuries; and farming is one of the few industries in which family members (who often share the work and live on the premises) are also at risk for fatal and non-fatal injuries (NIOSH 2013).

Most of the sugarcane production activities describe a wide range of inflammatory and degenerative diseases and disorders that result in pain and functional impairment and may affect the body's soft tissues, including damage to tendons, tendon sheaths, muscles

and nerves of the hands, arms, wrists, elbows, shoulders, neck, back, knee and legs which are produced due to awkward posture of farm workers.

OSHA (Occupational Safety and Health Administration) define ergonomics as “the science of fitting the task to the worker. When there is a mismatch between the physical requirements of the job and physical capacity of the worker, work related Musculoskeletal Disorders (MSDs) result. Workers who repeat the same motion throughout their workday, who do their work in an awkward position, who use a great deal of force to perform their jobs, who repeatedly lift heavy objects or who feel a combination of these risk factors are most likely to develop work related musculoskeletal Disorders (WMSDs).”

The musculoskeletal problems are considered to be the most prevalent and pricey of all work related injuries. Musculoskeletal problems start as minor aches and pain, but when left unaddressed can result in serious injuries that can be permanently disabling. In addition, these painful injuries take long recovery periods and chances are that severely injured worker may never be able to return to their jobs. The present study was planned with the following objectives-

- To assess the physical characteristics of the workers engaged in sugarcane production system.
- To assess the prevalence of MSD among workers.

II. MATERIAL AND METHOD

The present study was carried out in four villages of Bareilly district of Uttar Pradesh to assess work postures. A total sample size of 60 farm workers (40 from harvesting and 20 from sowing) was taken for experimental data using Purposive and Random sampling without replacement. To assess MSDs of farm workers questionnaire developed by FRM component of AICRIP Homescience was used. Postural discomfort analysis questionnaire was used to assess musculoskeletal disorders among farm workers.

Postural Discomfort Analysis Questionnaire

The postural discomfort analysis questionnaire was used to find out the discomforts of different body parts. The questionnaire was given to each subject and was asked to put the mark on the line, ranging from 0-10 (known as VAS scale), with 0 meaning ‘no discomfort’ and 10 meaning ‘severe discomfort’. This data was then being analyzed. Mean and SD values were determined, validated by Corlett and Bishop (1976) and Huskisson (1983).

III. RESULTS AND DISCUSSION

Work related musculoskeletal discomforts of the workers were assessed using Postural discomfort analysis questionnaire. Responses of 60 workers were analyzed. Table 1. depicts the physical characteristics of the respondents selected for ergonomic experiments to carryout the identified drudgery prone activity of sugarcane production system i.e sowing. The mean age and SD values of the respondents was 33.35 ± 7.70 years and height 166.75 ± 5.03 cms. The mean body weight was 58.75 ± 6.24 kgs. The computation of Body Mass Index (BMI) revealed that the average BMI was 21.10 ± 1.66 per cent and almost all the respondents fell in the normal range.

Table.1: Physical characteristics of the subjects involved in sowing activity of sugarcane.

n=20

S.No.	Physical characteristics	Mean ± S. D.
1	Age (yrs)	33.35 ± 7.70
2	Height (cm)	166.75 ± 5.03
3	Weight (kg)	58.75 ± 6.24
4	BMI	21.10 ± 1.66

Table.2: Physical characteristics of the subjects involved in harvesting activity of sugarcane.

N=40

S.No.	Physical characteristics	Mean ± S. D.
1	Age (yrs)	36.08 ± 7.86
2	Height (cm)	168.5 ± 5.10
3	Weight (kg)	58.06 ± 8.44
4	BMI	20.43 ± 2.64

The mean age and SD values of the respondents who were involved in harvesting activity was 36.08 ± 7.86 years and height 168.5 ± 5.10 cms. The mean body weight was 58.06 ± 8.45 kgs. The computation of Body Mass Index (BMI) revealed that the average BMI was 20.43 ± 2.64 per cent and almost all the respondents fell in the normal range.

Table.3: specific pain symptoms in different body parts of the respondents in sowing of sugarcane by traditional method.

Body parts	Frequency(%)
Neck	17(85)
Shoulder	16(80)
Upper arm	18(90)
Elbow	-
Lower arm	16(80)
Wrist	17(85)
Palm	6(30)
Fingers	7(35)
Chest	5(25)
Abdomen	-
Upper back	2(10)
Lower back	17(85)
Hips	-
Upper legs	18(90)
Lower legs	18(90)
Ankles	6(30)
Feet	11(55)

In sowing activity most farm workers reported pain in upper leg, lower leg, upper arm ,neck, shoulder and low back.

Table.4: specific pain symptoms in different body parts of the respondents in Harvesting of Sugarcane

Body parts	frequency	percentage
Neck	30	75
Shoulder	34	85
Upper arm	35	87.5
Elbow	11	27.5
Lower arm	23	57.5
Wrist	34	85
Palm	19	47.5
Fingers	21	52.5
Chest	6	15
Abdomen	-	-
Upper back	17	42.5
Lower back	36	90
Hips	5	12.5
Upper legs	37	92.5
Lower legs	28	70
Ankles	21	52.5
Feet	9	22.5

In harvesting activity pain in upper leg, neck, shoulder ,low back ,upper arm,and wrist was reported from more than 80 percent workers.

Postural Discomfort Analysis (VAS scale)

The postural discomfort analysis questionnaire was used to find out the discomforts of different body parts during the vegetable pre-harvesting activities. The questionnaire was given to each subject and was asked to put the mark on the line, which was then being analyzed. The descriptive (mean and SD values) were determined for VAS (Visual Analogue Scale) validated by **Corlett and Bishop (1976) and Huskisson (1983)**. Similar work was reported by **Newel (2003)**. She conducted studies to find out the comparison of instantaneous and cumulative loads of the low, back and neck in orthodontists. She applied the VAS scale ranging from 0-10, with 0 meaning 'no discomfort' and 10 meaning 'severe discomfort'. Her individual values ranged between 0.6-9. The neck had the highest mean value 2.6, with shoulder and lower back closest behind at the 2.3 and 1.6 respectively. The mean and SD results of the postural discomfort questionnaire were analyzed and found among respondents.

The results depict (table 5) that the mean value was highest during sowing in the neck i.e. 7.11 followed by legs (7.0), thighs (6.75), lower back (6.75), shoulder(6.66),upper arm(6.60), lower arms(5.37) , mid back (5.25)and upper back(5). The pain and discomfort in neck was highest due to lifting and forceful action. They work in standing and bending position for 8 hours per day with a rest in between for 1 hour. This is the reason for pain in legs ,thighs ,lower back and other body parts.

Table.5: Postural Discomfort among the respondents engaged in sowing of sugarcane (VAS Scale)

Body parts	Traditional method (n=20) (Mean±SD)
Neck	7.11±0.92
Shoulder	6.66±0.84
Upper back	5±1.53
Upper arm	6.61±0.68
Mid back	5.25±0.5
Lower arms	5.37±1.58
Low back	6.75±3.02
Buttocks	-
Thighs	6.75±1.01
Legs	7.0±0.85

Table.6 depicts) that the mean value was highest during harvesting in the upper arm i.e. 6.74 followed by low back (6.63), leg (6.37), thighs (6.01), lower arm (6.0), shoulder (5.81), mid back (5.45), upper back(5.16),and neck(5.1). In harvesting activity pain and discomfort in was highest in upper arm and low back because hands are most active organs while working thus overwork by these

lead to pain and low back pain may be due to the frequent standing and bending while doing harvesting for 8 hours a day. Lower part of the back bears the weight of the upper body plus any weight that is carried and it also twists and bends more than the upper back causes low back pain.

Table.6: Postural Discomfort among the respondents engaged in Harvesting of sugarcane (VAS Scale)

Body parts	(Mean±SD)
Neck	5.1±1.18
Shoulder	5.81±1.10
Upper back	5.16±0.61
Upper arm	6.74±1.01
Mid back	5.45±0.82
Lower arms	6±0.90
Low back	6.63±1.07
Buttocks	-
Thighs	6.01±1.10
Legs	6.37±0.86

Hence the above investigation revealed that the workers suffered from pain and discomforts more in neck ,upper arm, low back, mid back, upper back, etc. These discomforts were due to bending and standing postures adopted by them at work place. Finally it can be concluded that the continuous maintaining of static posture and repetitive movements were the main reason for discomfort in these parts. **Toomingas et al. (2002)** conducted a study which revealed that eighty six per cent female and sixty eight per cent male reported for musculoskeletal problems, especially pain in neck and shoulder regions. **Tripathi and Kwatra (2016)** found that Due to long working hours, awkward body postures, repetitive work and physical load there exist a high prevalence of physiological discomforts among farm workers. Highest Postural load factor was reported during manual transplanting and land preparation activities for which workers have adopted Bending and Semi Bending postures respectively.

IV. CONCLUSION

Farm workers suffer from multiple musculoskeletal problems that are caused by over use or misuse of muscles, bones and nerves and significantly impair their activities of daily living. High incidence of pain as reported by farm workers in various body parts viz. neck, shoulder, elbow, wrist, mid back and low back, knee and calf muscles in overburdened rural workers indicates that farm workers are at continuous health risk. The erroneous habit of not mentioning about musculoskeletal problems at the right time, or "having learned to live with pain"

makes them susceptible to high health risks, as left unaddressed, musculoskeletal disorders that comprise of over many diseases and syndromes and are usually progressive and associated with pain, result in lifelong pain and permanent disability giving rise to enormous health care expenditure and loss of work. The fact that is required to be ascertained before the farm workers is that when they suffer from musculoskeletal problems although their physical health is principally impinged on, but their mental, economic and social functions are also impaired, thus affecting the quality of life of not only the farm workers themselves, but their families as well.

REFERENCES

- [1] **Corlett, E.N. and Bishop, R.P. 1976.** A technique for assessing postural discomfort. *Journal of Ergonomics*, 19: 175-182.
- [2] **Huskisson E C. (1983).** Visual analogue scales. In Ronald Melzak (ed.), *Pain Measurement and Assessment*. New York, Accessed <http://www.farabloc.com/mUBC.html> on 9th May 2010 at 12.05 pm.
- [3] **National Institute for Occupational Safety and Health. 1999.** Stress at work. Centers for Disease Control and Prevention.
- [4] **National Research Council and Institute of Medicine. 2001.** Musculoskeletal disorders and the workplace: low back and upper extremities. National Academy Press: Washington, D.C.
- [5] **Newell T. (2003).** Comparison of instantaneous and cumulative loads of the low back and neck in orthodontists. MSc Programmes in Engineering Industrial Ergonomics. Lulea University of Technology. Accessed <<http://epubl.ltu.se/14021617/2003/053/index-en.html> on 5th March 2010 at 3.00 pm.
- [6] **NIOSH 2013.** Agricultural Safety. Official Home Page of Centre for Disease Control and Prevention. From <<http://www.cdc.gov/niosh/topics/aginjury/>> (Retrieved on 15 July 2013).
- [7] **Tripathi,N and Kwatra,S .2016.** Musculoskeletal Disorder:A Potential Risk factor Amongst Farm Workers Engaged In Vegetable Transplanting in Uttarakhand , *Paripex- Indian Journal of Research* ,Vol.5(6) ,pp.343.

Microcontroller Based Wireless Controlled Pick & Place Robot

Md. Faiz Akram

Bachelor of Science in Instrumentation, Department of Physics, Jamia Millia Islamia, New Delhi, India.

Abstract— This thesis focuses on implementation and control of a pick & place robot using radio frequency transmitter and receiver system. The control of this robot is achieved by PIC16f877A microcontroller. The main duty of microcontroller is to generate pulse which are applied to the DC motors for completing the desired task. In this study three DC motors are used in which two are utilized to control the movement of robot and one is used to control the gripper.

The operation of designed pick & place robot has been experimentally verified. Simulation and experimental results are presented and discussed.

Keywords— DC motor , PIC 16F877A, pick and place robot , RF-434.

I. INTRODUCTION

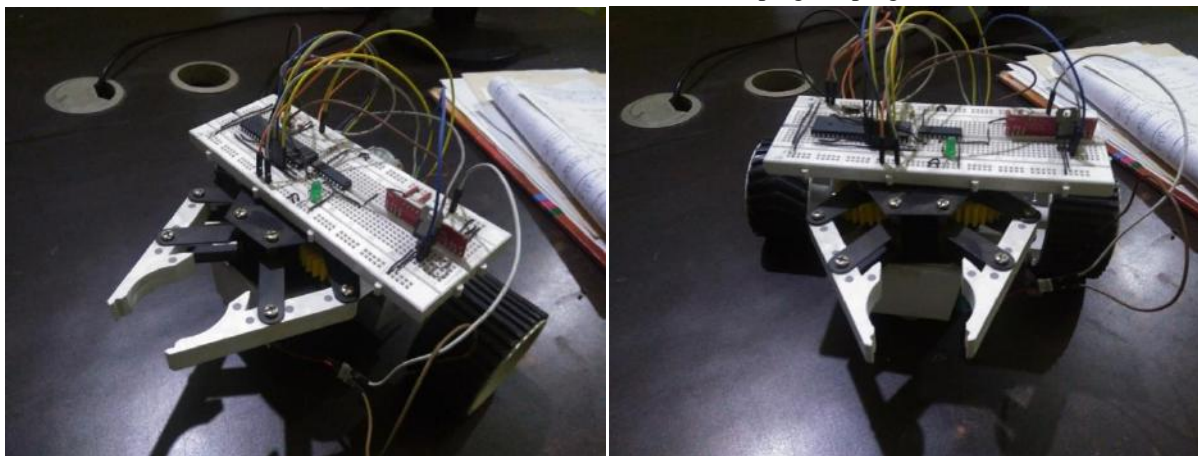
The field of robotics and machine learning originated in science fictions movies and novels. The word robot comes from the Czech word "robota" means forced labor in 1920. In 21st century, robotics is the field where machines are automated by the use of electronics , mechanical and electrical devices and controlled by different ways of communications but basically by computers and specifically

designed softwares. Robots are especially designed and build for a specific task to do some specific job.

There are three laws of robotics

1. A robot may not injure a human being or, through inaction, allow a human being to come to harm.
2. A robot must obey orders given it by human beings except where such orders would conflict with the First Law.
3. A robot must protect its own existence as long as such protection does not conflict with the First or Second Law.

In this work, The pick and place processes are the primary requisite for many of the industrial and house hold application where there is a need to automate the pick and place process basically comprising of picking the intended objects , possibly performing certain tasks and placing them to desired location . The automated pick and place robot mainly uses sensors and robotic arms. in this prototype robotic arm pick and place system utilizes dc motor, gripper , PIC16f877a microcontroller and software's such as Micro C for programming , PROTEUS for simulation, and PICKit 2 for dumping the program.

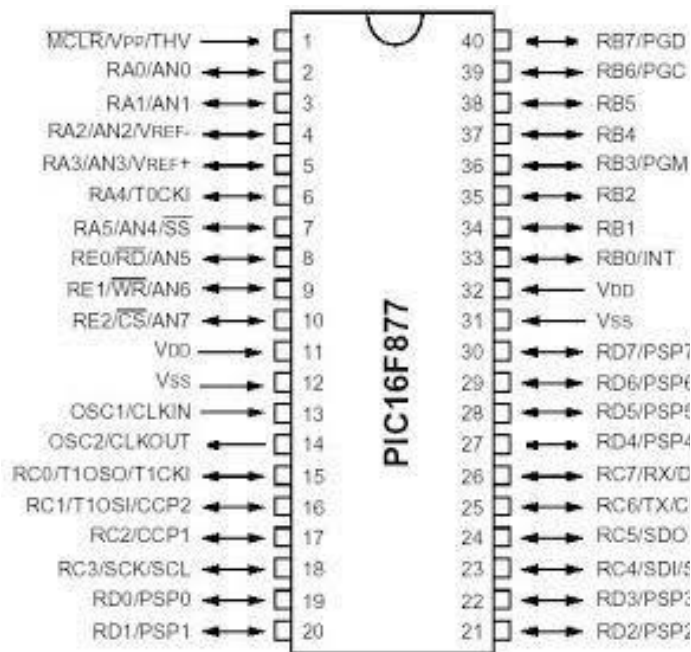


Prototype of pick & place robot.

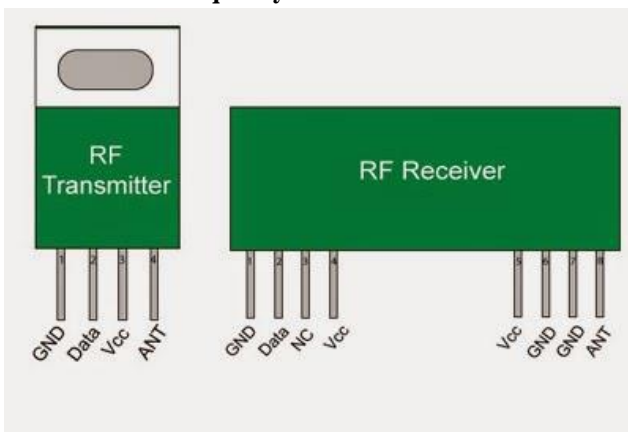
II. HARDWARE

2.1 PIC 16F877A Microcontroller

PIC 16F877A microcontroller has 40 pins and is a popular microcontroller capable of doing complex tasks. This microcontroller has 8192×14 flash program memory which consists of 368 bytes of RAM and 256 bytes of non-volatile EEPROM memory. 33 pins are dedicated for input/output pins and 8 multiplexed analog/digital converters with 10 bits resolution. This microcontroller also has specifications such as PWM generator, 3 timers, analog capture and comparator circuit, universal synchronous receiver transmitter (USART), internal and external interrupt capabilities. Figure shows the pin configuration of the PIC 16F877A microcontroller.



2.2 Radio frequency : RF- 434

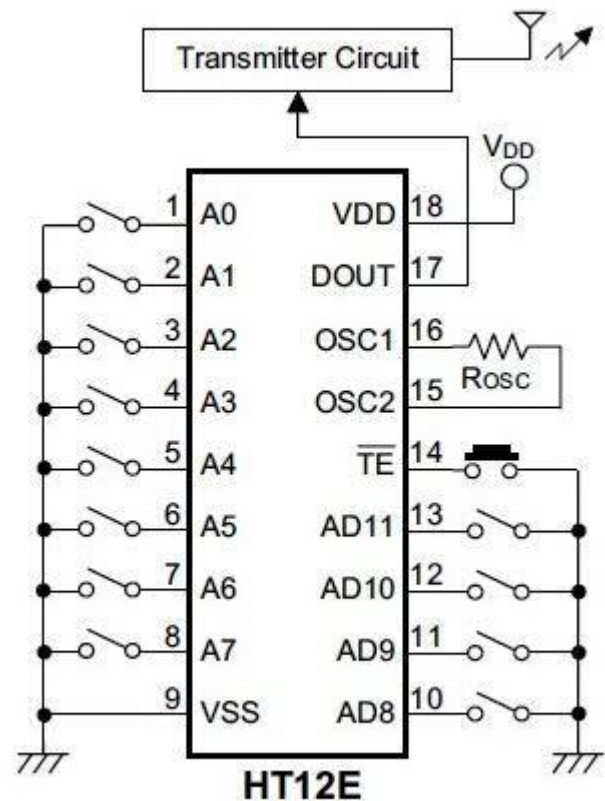


In this RF system , the digital data is represented as variations in the amplitude of carrier wave. This kind of modulation is known as ‘amplitude shift keying’(ASK).

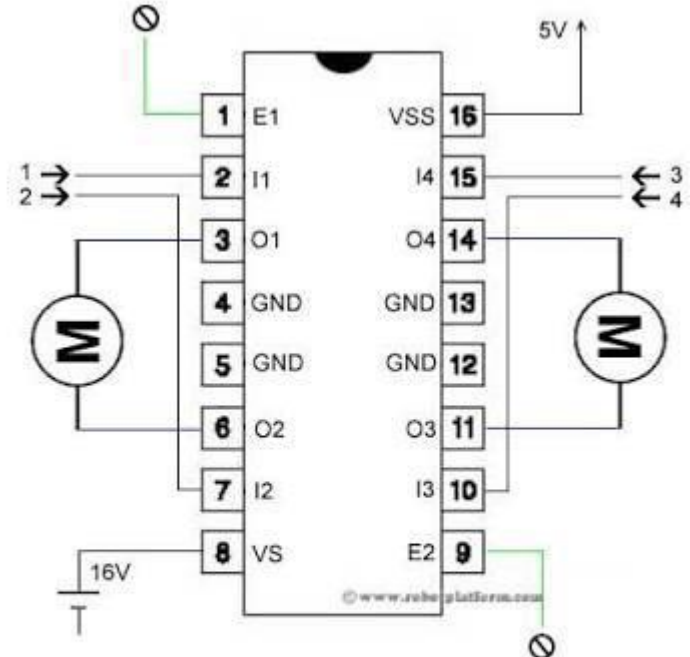
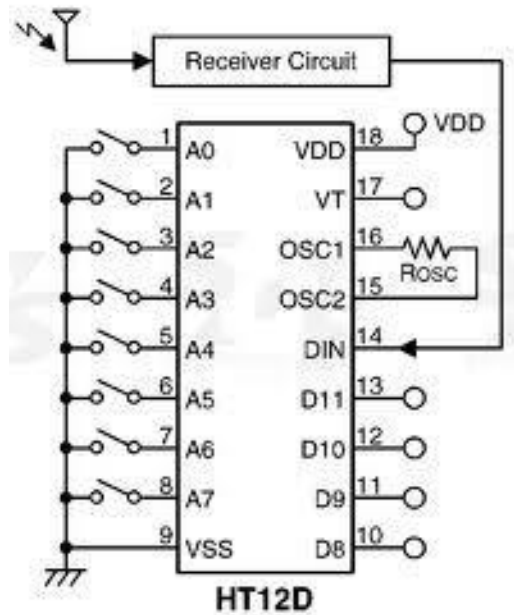
The Tx/Rx pair operates at a frequency of 434Mhz. An RF transmitter receives serial data and transmits it wirelessly through antenna connected at pin4 . The transmission occurs at the rate of 1kbps-10kbps. The transmitted data is received by the RF Rx operating at the same frequency as that of the Tx.

2.3 Encoder & decoder : HT12E & HT12D

HT12E is an encoder of 2^{12} series which converts parallel inputs into serial outputs. It encodes 12 bits parallel data into serial. These 12 bits are divided into 8 address bits and 4 data bits.



HT12D is a decoder that converts serial data into parallel. The input data code is decoded when no error or unmatched codes are found. A valid transmission is indicated by a high signal at VT pin. HT12D is capable of decoding 12 bits of which 8 are address bits and 4 are data bits.

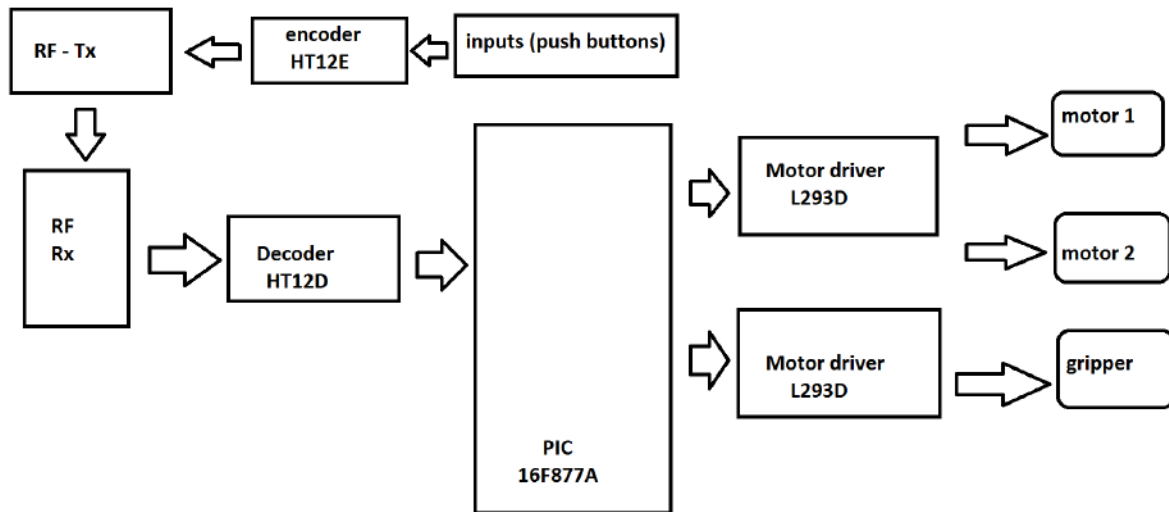


- Input from Microcontroller : 4 Inputs - I1, I2, I3, I4
- ⊖ Enable Pins : E1 & E2
- M Output to 2 Motors : O1, O2 & O3, O4
- GND Connect to microcontroller ground

2.4 Motor driver : L293D

L293D is a dual H-bridge motor driver IC that can drive two DC motors simultaneously and is available in 16 pin DIP. L293D has a current capacity of 600mA per channel and a wide supply voltage range of 4.5V to 36V DC.

III. WORKING LOGIC

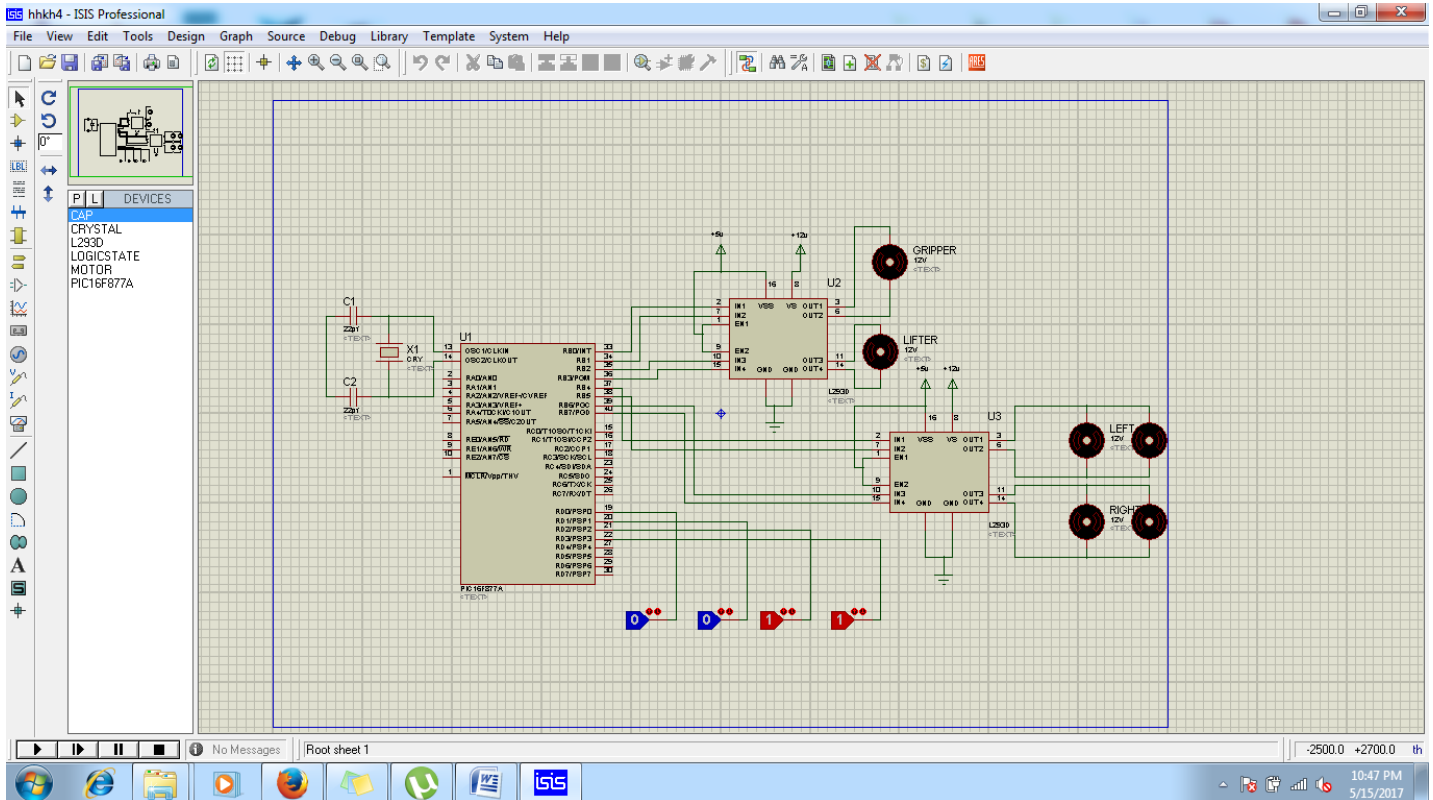


IV. SIMULATION

The Proteus Design Suite is an Electronic Design Automation (EDA) tool including schematic capture, simulation and PCB Layout modules. The micro-controller simulation in Proteus works by applying either a hex file or

a debug file to the microcontroller part on the schematic. It is then co-simulated along with any analog and digital electronics connected to it. This enables it's used in a broad spectrum of project prototyping in areas such as motor control temperature control and user interface design.

The desired circuit is designed on a simulator software proteus and microcontroller is programmed in microC.



Proteus is used for the simulation of receiver section of the robot and logic state on PORT D of PIC16f877a work as the output from the decoder HT12D.

V. MICRO C

The mikroC PRO for PIC is a full-featured ANSI C compiler for PIC devices from Microchip®. It is the best solution for developing code for PIC devices. It features intuitive IDE, powerful compiler with advanced optimizations, lots of hardware and software libraries. The mikroC PRO for PIC is a powerful, feature-rich

development tool for PIC microcontrollers. It is designed to provide the programmer with the easiest possible solution to developing applications for embedded systems, without compromising performance or control.

The code to use the robot as PICK & PLACE:

```

void main() {
    trisd=0xff; // D port is used as inputs
    trieb=0x00; // B port as outputs
    while(1)
    {
        if( portd.f0 ==0 && portd.f1 == 1 && portd.f2==1 && portd.f3==1 ){
            portb=0x01; // gripper opens
        }
        else if( portd.f0 == 1 && portd.f1 == 0 && portd.f2==1 && portd.f3==1 ){
            portb=0x02; // gripper closes
        }
        else if( portd.f0 ==1 && portd.f1 == 0 && portd.f2==1 && portd.f3==0 )
        {
            portb=0xA0; // ROBOT MOVES FORWARD
        }
        else if( portd.f0 == 0 && portd.f1 == 1 && portd.f2==0 && portd.f3==1 )
        {
            portb=0x50; // ROBOT MOVES BACKWARD
        }
        else if( portd.f0 == 1 && portd.f1 == 1 && portd.f2==0 && portd.f3==0 )
        {
            portb=0x90; // ROBOT MOVES LEFT
        }
        else if( portd.f0 == 0 && portd.f1 == 0 && portd.f2==1 && portd.f3==1 )
        {
            portb=0x60; // ROBOT MOVES RIGHT
        }
        else{
            portb=0x00; }
    }
}

```

VI. CONCLUSION

This pick and place robot is successfully build which can be controlled with wireless technology using radio frequency RF434 from the remote and this robot follows the command and move to the desired location and perform pick and place operation of item .This types of Robots can be deployed in industries , laboratories and also used for military.

REFERENCES

- [1] Balakrishna Annapureddy, G.V.Ramana Reddy, L.Srinivas Reddy “Robotic Revolution With Smart Remote Cotrol For Pick And Place Applications ”.
- [2] Muhammad Jabir.N.K, Neetha John, Muhammad Fayas,MidhunMohan , Mithun Sajeev , Safwan.C.N “Wireless Control of Pick and Place Robotic Arm Using an Android Application“ Vol. 4, Issue 4, April 2015
- [3] Leon Bodenhagen and Andreas R.Fugl. [2014] “An Adaptable Robot Vision System Performing Manipulation Actions With Flexible Objects” IEEE transactions on automation science and engineering, vol. 11,no. 3.
- [4] B.O. Omijeh, R. Uhumwangho, M. Ehikhamenle, “Design Analysis of a Remote Controlled Pick and Place Robotic Vehicle”, International Journal of Engineering Research and Development, Volume 10, PP.57-68, May 2014.
- [5] Sanjay Lakshminarayan, Shweta Patil, “Position Control of Pick and Place Robotic Arm”, Department of Electrical Engineering MS Ramaiah Technology, Bangalore, India.
- [6] Ankit Gupta, Mridul Gupta, NeelakshiBajpai, Pooja Gupta, Prashant Singh, “Efficient Design and Implementation of 4-Degree of Freedom Robotic Arm”, International Journal of Engineering and Advanced Technology (IJEAT) ISSN: 2249 – 8958, Volume-2, June 2013.
- [7] Currie, Adam (1999). "The History of Robotics" Retrieved 10 September 2007.
- [8] Pic16F877A and Data Sheet : <http://www.microchip.com/>
- [9] Douglas, V.H; “Microprocessor and Interfacing”. TataMcGraw-Hill, New Delhi; 2nd Edition, 1999.
- [10] Kensuke Harada “An object placement planner for robotic pick-and-place tasks”, National institute of advanced industrial science and technology ASIT, Volume 4, Issue May 2014.

Information and Communication Technologies for Veterinary Sciences and Animal Husbandry in Jammu and Kashmir

T. A. Raja, Azmat Alam Khan*, N A Ganai and Imtiyaz Ahmad Najar

Central Computer Laboratory, Faculty of Veterinary Sciences and Animal Husbandry, Sher-e-Kashmir University of Agricultural Science and Technology of Kashmir, Shuhama, Alusteng, Srinagar 190006 J&K, India

*Division of Livestock Production and Management, Sher-e-Kashmir University of Agricultural Science and Technology of Kashmir, Shuhama, Alusteng, Srinagar 190006 J&K, India

Abstract— *Use of Information and Communication Technology (ICT) is growing in all spheres of activity. Veterinary Sciences and Animal Husbandry should therefore be no exception. Efforts are needed to incorporate ICT in all endeavours related to livestock development in Jammu and Kashmir. All organizations and departments concerned with Veterinary Sciences and Animal Husbandry need to realize the potential of ICT for the speedy and timely dissemination of information modules to the livestock rearers. The awareness among livestock rearers about the information and availability of ICT services is the first step to be taken to increase livestock rearers' participation in ICT initiatives. Access to information and communication is essential to the stakeholders at all levels in the process of development. Various information and communication technology tools in knowledge and information dissemination needed for livestock rearers and possible IT application tools in realizing their needs in Jammu and Kashmir are discussed.*

Keywords— *Information and Communication Technology (ICT), Veterinary Science and Animal Husbandry, Information needs, ICT tools, Livestock rearers.*

I. INTRODUCTION

Organized data into meaningful form within a specific time interval is termed as information and information is the basic need of every society. Communication is the exchange of thoughts, knowledge or information in the form of audio, video, signals, gestures, behaviour etc. Technology is the development, modification, usage and knowledge of tools, machines, techniques, traits, systems, modules in order to solve problems related to any discipline. Information and Communication Technology (ICT) for Veterinary Science and Animal Husbandry refers to the application of

information and communication technologies within the field of Veterinary Sciences. Mostly the number of changes that we see occurring in every sphere of life is the result of application of ICT and Animal Husbandry is not an exception. ICT in Veterinary Research, Development and Extension are becoming an indispensable part of our society in Jammu and Kashmir as well. The ICT advances in last few years have created new opportunities and challenges for Veterinary professionals like Veterinary students, Veterinary technicians, Livestock farm managers, Livestock assistants and above all Livestock rearers.

Veterinary Sciences and Animal husbandry occupies an important place in the economy of our state. The share of Veterinary and allied sectors in the Gross state domestic product for the year 2013-2014 (preliminary) stands at 38% on the other hand nearly 70% of the population in the state derives its livelihood directly or indirectly from the agriculture and animal husbandry sectors (Anonymous 2014).

II. ICT IN VETERINARY SCIENCES AND ANIMAL HUSBANDRY

Livestock census actually covers the census of livestock, poultry, implements and machinery used for livestock rearing. It is the only source for providing various kind of detailed information for these groups. India has largest livestock numbers in the world. Sound and timely available database are the basic requirement for any planning and policymaking purposes. The conduct of livestock census is thus essential for making plans and policies for growth of livestock sector and also for overall growth of the economy. Livestock Census in our country started in the year 1919 and since then the process has been continuing on five year basis. Large body of data generated as a result of census

needs to be tabulated analysed and interpreted. Use of ICT not only eases the mammoth exercise but helps in its better tabulation, analysis, interpretation and presentation.

Teaching and Learning of Veterinary Sciences is greatly enhanced by use of ICT technology. With growing animal welfare concerns more of videos, animations and simulations are being used in teaching and learning process in place of animal experimentation. The ICT provides new pedagogical models for Veterinary professionals. Similarly Veterinary and Animal Science Research that is gaining importance day by day is greatly benefited through use of bioinformatics tools and statistical programs.

Veterinary and Animal Husbandry extension system is playing an important role in disseminating technology to stakeholders of the State. ICT will strengthen our extension system manifold by use of various information technology(IT) tools in technology dissemination and empowering Veterinarians with the desired information. Their use with right perspective will provide information services to the Veterinarians timely, logistically and effectively. Shaiket *al.*(2004), Griffin *et al.*(2008) and Rajaet *al.* (2013) have worked on applications of ICT in Agriculture.

The present paper discusses various techniques of information simulation and dissemination needed for livestock rearers of the Jammu and Kashmir for the upliftment of Veterinary and Animal husbandry sector.

Information Needed

The focus of ICT in Veterinary Science and Animal Husbandry is to meet the modern advances in research and extension technologies. A Veterinary practice at a Veterinary centre or a Veterinary clinic or an Animal hospital is in most cases a small business offering a range of services to clients and livestock owners. Many people are involved in delivering the service and ensuring that you as the client get the best care for your animal, in the most efficient manner. The delivering of services and efficiency is taken care by use of ICT. Information on cost, quality of treatment, availability of medicines and inputs like history of animals, species, breed, are required by veterinary professionals at various levels of practice. imilarly for more remunerative production of farms (dairy, sheep, goat, poultry etc.)accurate, reliable, timely and precise information should reach to the investors at proper time as and when required. The information needed by the investors in veterinary field can be broadly categorized into following.

- Input Procurement

- Package of practices
- Disease forecasting and forewarning
- Pre and Post harvest information
- Past trends
- Marketing Information
- Farm Business and Management Information
- Policy Decisions

Input Procurement

Information relating to availability of various inputs and their cost is the first priority. Livestock rearers frequently require the information regarding various inputs such as germplasm, feed, medicine etc in terms of cost, quality, availability and possible sources.

Business Project Planning

Proper planning of an enterprise goes a long way in running a successful enterprise. Entrepreneurs desirous of taking up livestock rearing require expert advice in drafting viable project proposals. Livestock business proposals tailored to specific conditions, specific areas and specific regions are required.

Package of Practices

The area specific package of practices for various livestock species is pre-requisite. Preparation of package of practices its continuous updating with changing times and its timely dissemination among livestock rearers is essential. The package of practices includes breeding, feeding, housing and management practices.

Disease forecasting and fore-warning

Diseases take a heavy toll of livestock enterprise on account of morbidity and mortality. Availability of timely disease forecast can help farmer to take prophylactic measures well in advance and prevent losses.

Preservation and Value addition

Livestock products being of perishable nature their preservation is very essential. Methods that enhance shelf life of various livestock products are required by the livestock owners. At the same time methods of value addition and product development are also required.

Past trends

Information on past trends regarding production, consumption, utilization, environmental factors and climatic conditions are of immense use in decision making regarding rearing of livestock.

Marketing Information and Intelligence

After the harvest, the most important query is about its marketing, so that the farmer may not fall prey to middle man and hoarders. At this very time, information related to processing and grading, any government interventions like

support price, identified central markets and legal agencies involved is must which may help livestock rearers in making right decisions in selling their produce.

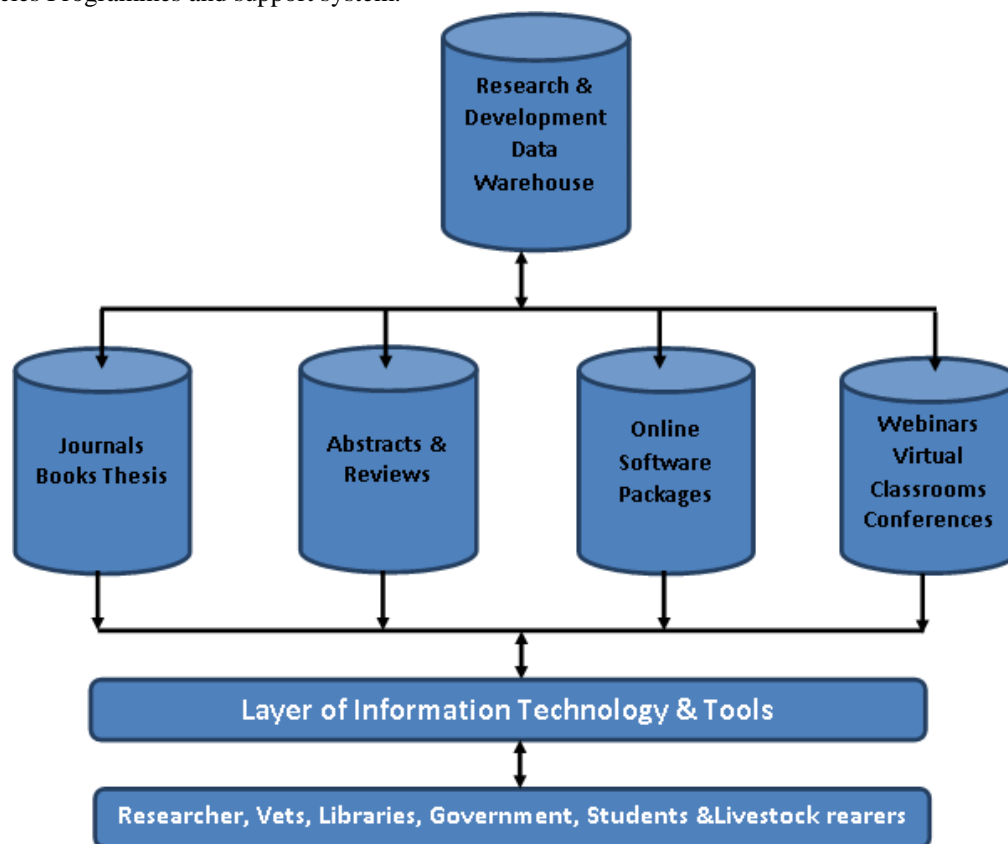
Policy Decisions

News about various Animal Husbandry events and decisions related to livestock and its products, labour laws, rural development programmes, government schemes etc are also important in decision making, All such information, must be available to the farmer to take right decision and get maximum returns.

Many communication tools, Such as radio, television, mobile phones, video chatting etc. are used in information dissemination and making livestock rearers aware about government policies Programmes and support system.

IT tools

A variety of IT tools are available for development and implementation of information technology and decision support systems. Recent development in Electronics and communication technology has made it possible to gather data, process, transmit and disseminate information in meaningful order with click of a button. This helps to analyse and interpret the data using sophisticated computational tools and techniques such as artificial intelligence, machine learning, image processing, pattern recognition, Probabilistic modelling, large scale simulation, data mining, text mining and graph algorithms and decision support system.



The support of information technology required for Veterinary Research of the State is as under:-

- Database management system
- Information Retrieval system
- Decision Support System
- Expert Support System
- Trend Analysis and Forecasting
- Electronic Network and Messaging System
- Helpline.
- Geographical Information System

Database System (DBS)

Database Management System or DBMS in short refers to the technology of storing and retrieving data with utmost efficiency along with security measures. Aim of building database is to convert traditional knowledge into electronic knowledge base, so that the data can be filtered along x and y axis which means rows and columns respectively. Huge and metadata is generated in Veterinary research related to animal breeding, genetic disorders and disease, their characters, and control. Database technologies play an important role in storing data in electronic form. Database

operations like Insert, Append, Update and Delete are used to quickly manage data for addition, alteration and modification. Information from Database can be harnessed by Information Retrieval System, Expert System and Forecasting System, to produce information in desirable way. Database system is a group of hardware and software for addition, modification, compilation, processing and reporting of data.

Information Retrieval System

Store and retrieval of information in user friendly manner is ultimate objective of an information system. Such systems uses search engines, user friendly interface and other controls to mine the data from database and present the same in the form of reports, graphs, images, tables, etc. On the same line information retrieval system is developed to retrieve information as and when required.

Decision Support System

A veterinary meteorological decision-support system, VetMet developed by Danish Meteorological and Veterinary Research Institutes and authorities firstly implemented it at the Danish Meteorological Institute and it was used by the Danish Veterinary and Food Administration, which has the responsibility for prevention and control of animal diseases. By estimating the risk of atmospheric spread of airborne animal diseases, including first of all foot-and-mouth disease, VetMet improved the preparedness and the disease eradication. The Internet-based system is being used for decision support regarding establishment of surveillance and eradication zones. VetMet can describe both local spread of infectious airborne diseases between neighbouring farms and long-range dispersion, including disease spread to or from other countries.

Expert Support System

An Expert system is a computer program with artificial intelligence, knowledge base and inference engine to solve problems that are difficult enough to require significant human expertise for their solution. A knowledge base is the repository of facts and rules about the specific problem. An inference engine is the software for solving the particular problem using the knowledge base. It is an efficient IT tool and is referred as a tool for Transfer of Technology (TOT) from scientist to farmer. This disables dilution of contents by reducing the number of agencies involved in technology transfer process.

Such IT system can provide instant solution to problems faced by livestock rearers. Expert system can be developed to help and guide the veterinarian under various situations such as feed and fodder, health check-ups, disease control

and vaccine scheduling. It can also suggest control measures on the basis of symptoms.

Trend Analysis and Forecasting

Forecasting and trend analysis are purely statistical techniques. Study of statistical trends regarding live stock, weather data, utilization, consumption patterns, disease attacks, fertilization, etc. may be executed with IT tools. Trend analysis assists livestock rearers in decision making during entire process of livestock production and marketing. Graphical or pictorial trends may be generated using the database of specific parameters.

Analysis of trends enables the forecasting and prediction in live stock production system. For example, forecasting weather is a useful endeavour in deciding the various Livestock operations. IT has many tools to develop such forecasting system.

Electronic Network and Messaging System

Internet has made the world in a global community and enables information transfer and exchange quickly. Ready available online modules are available to livestock rearers for quick disposal of their problems. Websites can be developed to provide information to livestock rearers in their own regional languages. E-mails, Chatting and conferencing will help livestock rearers in getting discussions with experts and other livestock rearers to exchange views and information and find solutions to problems. Mobile phones are widely being used and have facilitated in addressing the day to day issues of the livestock rearers. Internet and its application are highly involved in planning, weather forecast, post-harvest management, marketing, disaster management, extension management and thus a very powerful source to disseminate knowledge to the livestock rearers. It provides a gamut of information through online sources of information regarding different crops and thus in turn will shape the future of veterinary and animal husbandry development in the State.

Kisan Call Centre

The Purpose of Kisan Call Centre is to respond to issues raised by livestock rearers instantly in the farm of local language. Queries related to Veterinary and allied sectors are being addressed through these centres. A Kisan Call Centre is a combination of ICT and agricultural technology. It uses a backend data support system, which is inbuilt in Management Information System (MIS). It consists of a complex telecommunication infrastructure, computer support and human resources organized to manage effectively and efficiently the queries raised by livestock rearers instantly in the local language. Mainly, Scientists,

Experts and Subject Matter Specialists (SMSs) using telephone and computer, interact with livestock rearers to understand the problem effectively and provide the solution directly.

Kisan Call Centres are functional in areas like Agricultural Technology Information Centre (ATIC), Krishi Vigyan Kendra (KVK), Agricultural Consultation Cell (ACC), or any outsourced Wing, where separate facilities exist solely to answer inbound calls or make outbound telephone calls or to resolve the queries of pending calls of information needy livestock rearers. Usually it refers to a sophisticated voice operations centre that provides a full range of inbound or outbound call handling services including customer support, direct assistance, multi-lingual customer support and other services.

This is important and vital existing extension mechanisms, which find it otherwise difficult to reach the livestock rearers quickly. This enables close and quick linkages and communication mechanism among the veterinary scientists, subject matter specialists, extension activists, communication centres, consultancy agencies, Livestock rears and other development departments involved in the process.

Geographical Information System

One of the key characteristics of Livestock is that it is a user of land and other natural resources, particularly water, fodder and pastures. Monitoring and policy evaluation in the key areas of land use and the environmental effects of livestock require information that is location specific. Advances in technology, particularly remote sensing using satellites, have made it technically feasible and increasingly cost effective to obtain and process geo-referenced data for policy analysis. A major application is the preparation of spatial inventories of land use. Through the use of geographical information systems (GIS) technology changes in land use patterns can be examined. Geo-referenced data can also be an important management tool for livestock rearers in dealing with environmental issues.

III. CONCLUSION

Information Technology can offer solutions in order to improve the livestock production in J&K state. Latest IT tools for information dissemination offer enormous potential in transfer technology. Systematic and coordinated approach is required to identify, organize make available information on time to the livestock rearers when it is required by them and in a user friendly manner. Use of IT techniques using regional languages in dissemination of livestock rearing technologies will certainly enhance the

decision-making capabilities of livestock rearers. This will further improve economic status of the livestock rearers involved in live stock production in J&K. For sustainable live stock production, it is must to understand the information need of livestock rearers and develop such information systems that supports the operational aspects of livestock rearers. All organizations including concerned departments need to realize the potential of ICT for speedy dissemination of information to livestock rearers. Government at State and central level has to reorient veterinary and a animal husbandry policies so that a strategy is farmed to harness ICT's potential for over all live stock development.

REFERENCES

- [1] Anonymous (2014) Digest of Statistics 2013-2014, Directorate of economics & statistics, government of J&K(India).
- [2] Griffin C, Dennis G. Watson and Tony V. H. (2008) Integrated information system for group collaboration. *Journal of Information Technology in Agriculture* 3(1)
- [3] Jens Havskov, Soren Alexandersen, Poul Astrup, Knud Erik Christensen, Torben Mikkelsen, Stenortensen, Torben Strunge Pedersen, Soren Thykier-Nielsen (2008) The VetMet Veterinary Decision Support System for Airborne Animal Diseases, Part of the series [NATO Science for Peace and Security Series Series C: Environmental Security](#) pp 199-207
- [4] Raja, T. A and Ahmad Bashir (2013) Information and communication technologies for agricultural system in Jammu and Kashmir. *International Journal of Science, Technology and Management*, 3: 65-7
- [5] Babbu, S. C., Glendening, C. J., Seno-Okyere K. A. and Govindrajana, S. K. 2012 Farmer's information needs and search behaviours: Case study in Tamil Nadu, India. (IFPRI, Discussion paper 01165)
- [6] Shaik N. Meera, Jhamtani Anita and Rao, D.U.M. (2004) Information and communication technology in agricultural development: A comparative analysis of three projects from India. Network Paper No:-135

Design, Buckling and Fatigue Failure Analysis of Connecting Rod: A Review

Manish Kumar¹, Shiv N Prajapati²

¹Department of MT, CIPET Lucknow, India

²Department of ME, NIET Greater Noida, India

Abstract— A connecting rod works in variably complicated conditions, and is subjected to not only the pressure due to the connecting rod mechanism, but also due to the inertia forces. Its behavior is affected by the fatigue phenomenon due to the reversible cyclic loadings. When the repetitive stresses are developed in the connecting rod it leads to fatigue phenomenon which can cause dangerous ruptures and damage. Yield, fatigue and buckling characteristics are often used as evaluation indexes for the performance of engine connecting rods in mass reduction design to optimize vibration. Various rod cross-section like I section, + section, Rectangular section, Circular section and H section have important role in design and application. In this paper the design methodology is covered and FEA results for stresses have been presented and strain life theories studied.

Keywords— Buckling, Connecting rod Shank, Design, Fatigue, Finite element method, Stress

I. INTRODUCTION

Connecting rods are widely used in variety of engines such as, oppose-piston engines, V-engines, opposed-cylinder engines, radial engines and In-line engines to transmit the thrust of the piston to the crankshaft, and results into conversion of the reciprocating motion of piston to the rotational motion of crankshaft. It consists of a pin-end, a shank section, and a crank-end as shown in Fig. 1. Pin-end and crank-end pin holes are machined to permit accurate fitting of bearings. One end of the connecting rod is connected to the piston with the help of a piston pin. The other end revolves with the crankshaft and is split to permit it to be clamped around the crankshaft. Connecting rods are subjected to forces generated by mass and fuel combustion. These two forces results in axial and bending stresses. Bending stresses appear due to eccentricities, crankshaft, case wall deformation, and rotational mass force; therefore, a connecting rod must be capable of transmitting axial tension/compression and bending stresses caused by the thrust and pull on the piston and by the centrifugal force [1]. The connecting rods of the automobile are mostly made of cast iron through the forging or powder

metallurgy. The main reason for applying these methods is to produce the components integrally and to reach high productivity with the lowest cost [2] and optimized shape [3].

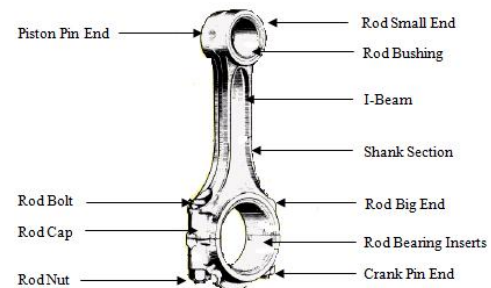


Fig.1: Schematic of a typical connecting rod

II. CONNECTING ROD MATERIALS

A primary design criterion for the connecting rod is endurance limit. The cyclic material properties are used to calculate the elastic-plastic stress-strain response and the rate at which fatigue damage accumulate due to each fatigue cycle [4]. Imahashi et al. [5] discuss the factors which affect the fatigue strength in powder forged (PF) connecting rod, i.e., hardness of the material, depth of decarburized layer, metallurgical structure, density, and surface roughness. Olaniran et al. [4] investigated a new crack able alloy of forged steel (FS) for connecting rod application. The material properties for connecting rod material are given in Table 1 [6].

Table.1: Mechanical Properties for connecting rod materials

Monotonic Properties	Forged Steel (FS)	Powder Metal (PM)	C-70 Alloy Steel
Young's Modulus (E), GPa	201	199	212
Yield Strength, MPa	700	588	574
Ultimate Tensile Strength, MPa	938	866	966
Strength Coefficient (K),	1400	1379	1763

MPa			
Strain Hardening Exponent (n)	0.122	0.152	0.193
Density, kg/m ³	7.806	7.850	7.700
Poisson's Ratio	0.30	0.29	0.30
Fatigue Properties			
Fatigue Strength Coefficient (σ_f'), MPa	1188	1493	1303
Fatigue Strength Exponent (b)	-0.0711	-0.1032	-0.0928
Fatigue Ductility Coefficient (ϵ_f')	0.3576	0.1978	0.5646
Fatigue Ductility Exponent (c)	-0.5663	-0.5304	-0.5861
Cyclic Strength Coefficient (K'), MPa	1397	2005	1739
Cyclic Strain Hardening Exponent (n')	0.1308	0.1917	0.1919

III. FORCES ON ROD AND DESIGN

The various forces acting on the connecting rod are as follows: Force on the piston due to gas pressure and inertia of the reciprocating parts, and Force due to inertia of the connecting rod or inertia bending forces, For all practical purposes, the force in the connecting rod (F_C) is taken equal to the maximum force on the piston due to pressure of gas (F_P),

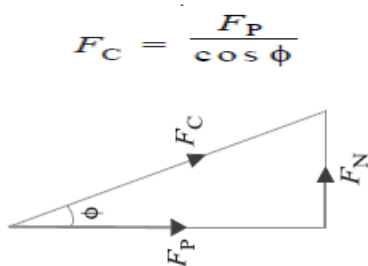


Fig.2: Force in connecting rod

In designing a connecting rod, the following dimensions are required to be determined [7]: Dimensions of cross-section of the connecting rod, Dimensions of the crankpin at the big end and the piston pin at the small end, Size of bolts for securing the big end cap, and Thickness of the big end cap. A connecting rod is which is subjected to alternating direct compressive and tensile forces. Since the compressive forces are much higher than the tensile forces, therefore, the cross-section of the connecting rod is designed as a strut. Hence the design should be

according to buckling phenomenon. As shown in Fig. 3, there are two practical buckling modes of connecting rod. One mode called 'side buckling' occurs in the direction parallel to the rotational axis of the connecting rod. The other mode called 'front-rear buckling' occurs in the direction perpendicular to side buckling.[8]

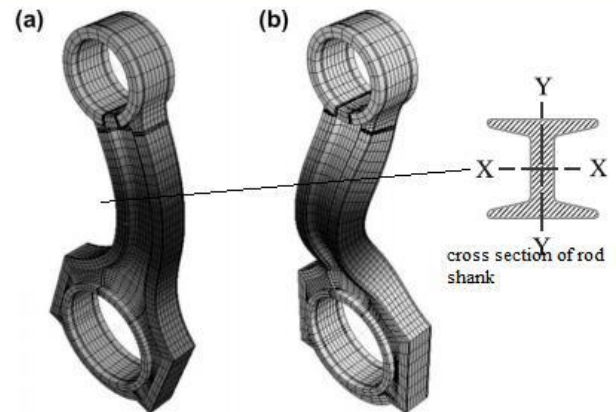


Fig.3: Buckling modes of the connecting rod: (a) side buckling and (b) front-rear buckling.

Rod may buckle with X-axis as neutral axis (i.e. in the plane of motion of the connecting rod) or Y-axis as neutral axis (i.e. in the plane perpendicular to the plane of motion). The connecting rod is considered like both ends hinged for buckling about X-axis and both ends fixed for buckling about Y-axis.

$$\sigma_{cr|x}^e = \frac{\pi^2 E}{(K_x L/r_x)^2} \quad \sigma_{cr|y}^e = \frac{\pi^2 E}{(K_y L/r_y)^2}$$

Where σ_{cr}^e is elastic critical buckling stress (Euler formula), E is the elastic modulus, L is effective length, r is radius of gyration for each axis, K_x is 0.5 for a fixed-fixed joint and K_y is the unity for a pinned-pinned joint. For I section rod $I_{xx} = 4 I_{yy}$ is quite satisfactory.

A connecting rod in a high-performance engine, compressor, or pump is a critical component: if it fails, catastrophe follows. Yet to minimize inertial forces and bearing loads it must weigh as little as possible, implying the use of light, strong materials, stressed near their limits. To design a connecting rod of minimum mass with two constraints: that it must carry a peak load F without failing either by fatigue or by buckling elastically.

The mass of rod shank

$$m = \beta A L \rho$$

Where L is the length of the con-rod, ρ the density of the material of which it is made, A the cross-section of the shaft, and β a constant multiplier to allow for the mass of the bearing housings. The con-rod, to be safe, must meet both constraints. For a given length, L , the active

constraint is the one leading to the largest value of the mass, m out of m_1 and m_2

$$m_1 = \beta FL \left(\frac{\rho}{\sigma_e} \right) \quad m_2 = \beta \left(\frac{12F}{\alpha \pi^2} \right)^{1/2} L^2 \left(\frac{\rho}{E^{1/2}} \right)$$

where α is a dimensionless ‘‘shape-constant’’ and σ_e is endurance limit.

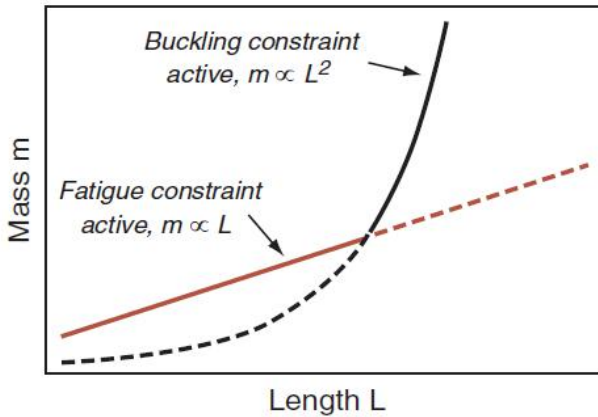


Fig.4: Mass of the rod as a function of L [9]

IV. STRESSES IN CONNECTING ROD

The connecting rod should be designed with high reliability. It must be capable of transmitting axial tension, axial compression, and bending stresses caused by the thrust and pull on the piston, and by centrifugal force without bending or twisting. An explanation of the axial forces acting on connecting rod is provided by Tilbury [2]. The connecting rods are subjected to mass and gas forces due to the fuel combustion resulting into axial and bending stresses [3]. The gas force is determined by the speed of rotation, the masses of the piston, gudgeon pin and oscillating part of the connecting rod consisting of the small end and the shank. Bending moments originate due to eccentricities, crankshaft, case wall deformation, and rotational mass force, which can be determined only by strain analyses in engine [10]. Fig. 5 shows axial loading due to gas pressure and rotational mass forces.

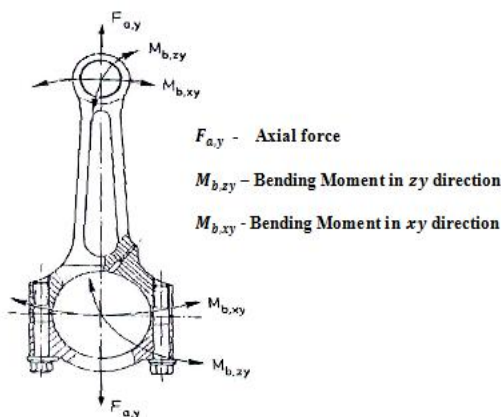


Fig.5: The origin of stresses on a connecting rod [10]

Sugita et al. [11], discussed the static analysis, quasi-dynamic analysis and design of a lightweight CR. Fig. 6 shows the boundary conditions used for static finite element analysis under tensile load. Fig. 7 shows compressions of the maximum principal stress values obtained at the critical locations based on FEA and strain gauge measurements under static loading.

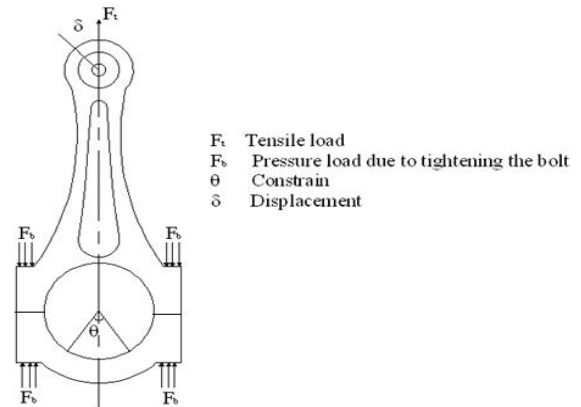


Fig.6: Boundary conditions for static FE analysis [11]

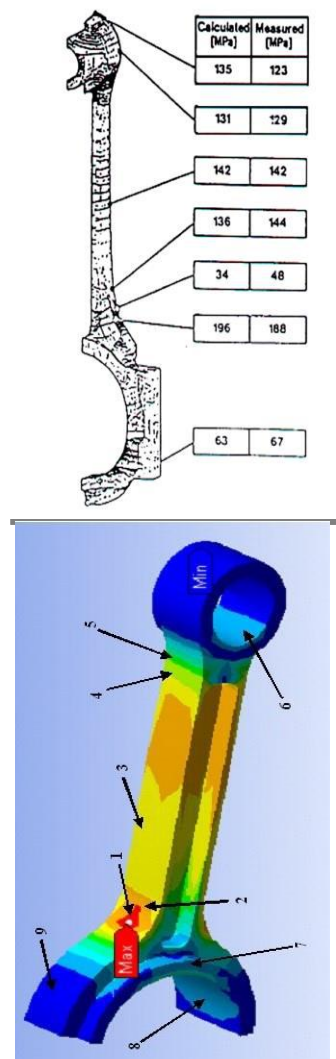
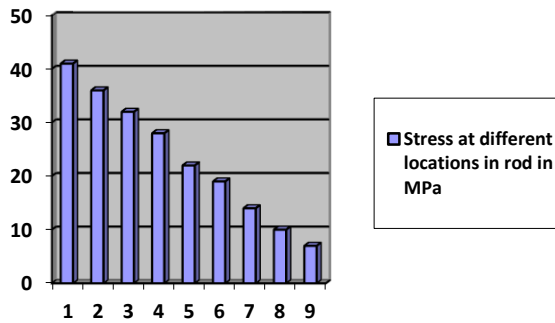


Fig.7: Comparisons between FEA and strain gage measured values



Webster et al., [12] discuss the loading criteria of connecting rod used in an IC engine. For tension loading the crank end and piston ends are found to have a sinusoidal distribution on the contact surface with pins and connecting rod. Fig. 8 shows the load distribution in tension and compression.

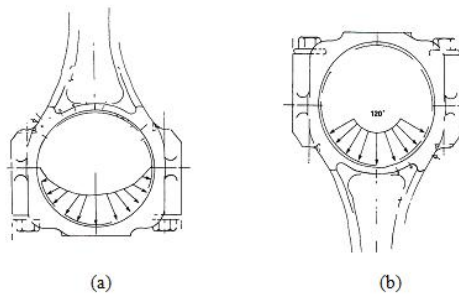


Fig.8: (a) Distribution of tension loading and (b) distribution of compressive loading in the connecting rod [12]

A. Tevatia, et al. discussed the maximum stress calculations in different cross sections connecting rod by FEM method for different materials, stresses were lower in I section rod and for powder metal Fig 9 [13].

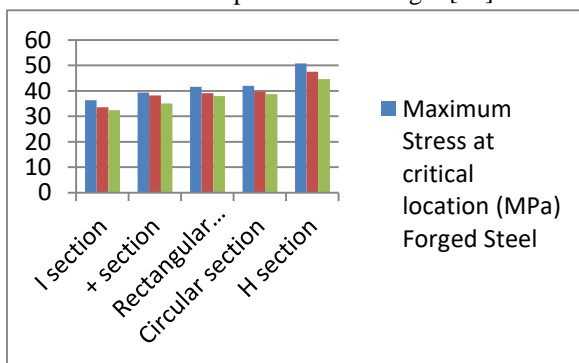


Fig.9: Comparison of max stress for different cross-section connecting rod

V. FATIGUE FAILURE IN CONNECTING ROD

Fatigue is the behaviour of materials under fluctuating and reversing loads. The various FE tools are used for analyzing the fatigue behaviour of connecting rod by the various researchers. Beretta et al. [14] investigated fatigue performance of the connecting rods made of either cast

iron or hot forging carbon steel. They state that if a CR working in a car engine is subjected to bench test loading conditions, the different areas of the CR are subjected to peculiar load spectra with different stress ratios. A study by Sugita et al. [11] used boundary element method to reduce the weight of the connecting rod. The connecting rod is designed by incorporating a thin I section column and adopting the two-rib design to the big end.

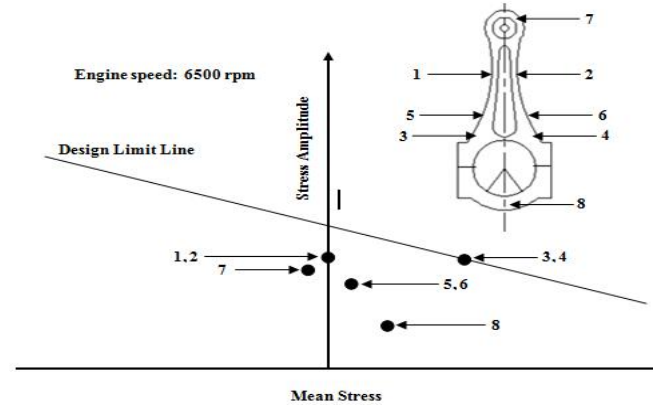
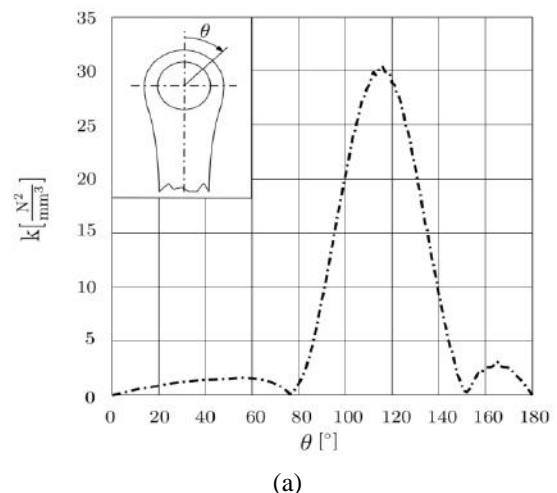


Fig.10: The comparison of FE calculated and strain gage measured stresses [11]

Antonio Strozzi et al. discussed about fretting fatigue in con-rod small end and big end with reference to the titanium con-rod by Rutz parameter k [15]

$$k = \sigma_c \cdot \Delta \cdot p \cdot f$$

where σ_c is circumferential stress, Δ is the relative tangential displacement amplitude displacement, p is the pressure distribution between the con-rod small end and the bush and, f is the friction coefficient assumed to be equal to 0.1



(a)

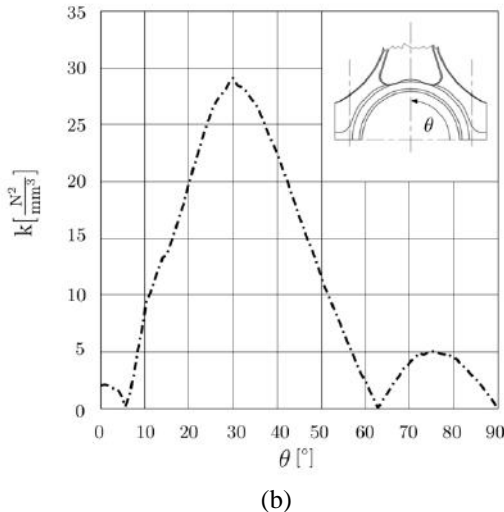


Fig.11: Fretting fatigue distribution in (a) small end, (b) big end [16]

The fatigue resistance of metals can be characterized by a strain-life curve as shown in Figure 12. Coffin [17] and Manson [18] established a mathematical relationship between the total strain amplitude, and the reversals to failure cycles as,

$$\frac{\Delta \epsilon}{2} = \frac{\sigma'_f}{E} (2N_f)^b + \epsilon'_f (2N_f)^c$$

Morrow [19] established a relationship between the mean stress, and fatigue life as,

$$\epsilon_a = \frac{\sigma'_f - \sigma_{mean}}{E} (2N_f)^b + \epsilon'_f (2N_f)^c$$

Smith *et al.* [20] established another relationship, Smith-Watson-Topper (SWT) mean stress correction model, expressed as,

$$\sigma_{max} \epsilon_a E = (\sigma'_f)^2 (2N_f)^{2b} + \sigma'_f \epsilon'_f E (2N_f)^{b+c}$$

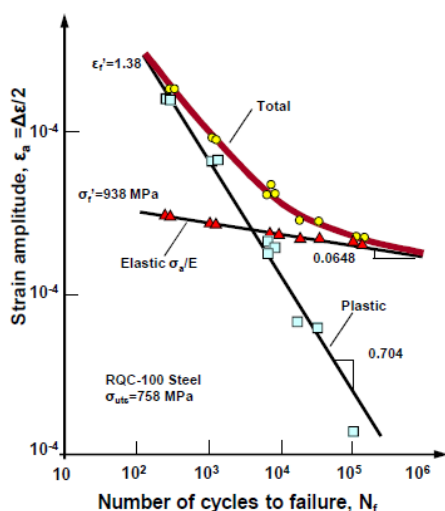


Fig.12: Strain-life curve [21]

Figure 15 shows Fatigue life at critical location for different materials and cross-sections of Connecting rod using strain life theories [22]

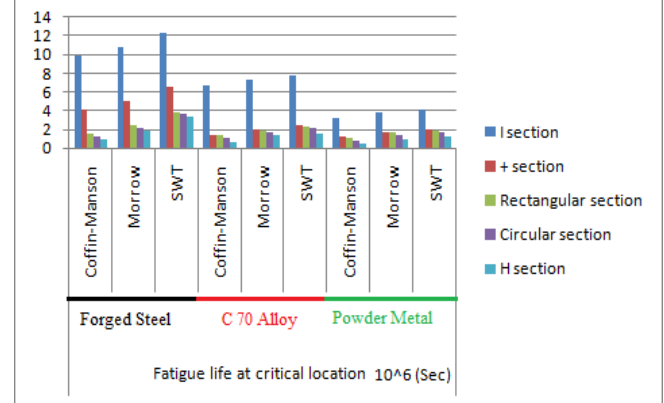


Fig.15: Comparison of fatigue life

VI. CONCLUSION

In the paper, the literature background regarding connecting rod material and their application in different kind of engines has been taken to consideration. The material properties play a vital role to design the rod for a particular application and its durability is studied. The forces in the crankshaft during a cycle and maximum load in a cycle/stroke defines the design of rod based on buckling criteria and optimum mass of rod to avoid the natural vibrations to a lower level are discussed. The stress calculation using FEM is studied for different kind of rod cross-section is viewed and concluded that the Von Mises stress is minimum for a I cross-section of rod. The fatigue failure of piston pin end and crank pin end has been studied under the pressure variation at locations of ends. It is presented that fatigue life is more in I section rod for forged steel rod under various strain life theories.

REFERENCES

- [1] Schreier, L., 1999, "Tension and Compression in Connecting Rods", <http://em-ntserver.unl.edu>, date: 12-02-2011.
- [2] Tilbury, R.J., 1982, "The Prediction and Measurement of Axial Forces, Bending Moments and Accelerations in an Engine Connecting Rod", *Journal of Strain*, Vol. 18, No. 2, pp. 55- 59.
- [3] Norton, R., 1994, "Design of Machinery," McGraw Hill, pp. 583
- [4] Olaniran, M.A. and Stickels, C.A., 1993, "Seperation of Forged Steel Connecting Rods and Caps by Fracture Splitting", *SAE Technical Paper 930033*, pp. 1-6.
- [5] Imahashi, K., Tsumuki, C., and Nagare, I., 1984, "Development of Powder-Forged Connecting Rods", *SAE Technical Paper 841221*, pp. 1-7.
- [6] Afzal, A., and Fatemi, A., 2003, "A Comparative Study of Fatigue Behavior and Life Predictions of Forged Steel and PM Connecting Rods", *SAE Int.*

- [7] Khurmi, R. S. and Gupta, J. K., 2005, "A Text Book of Machine Design", S. Chand & Company Ltd.
- [8] Moon Kyu Lee et al, "Buckling sensitivity of a connecting rod to the shank sectional area reduction", doi:10.1016/j.matdes.2010.01.010
- [9] Michael F. Ashby, "Materials Selection in Mechanical Design" 3rd edition, ISBN 075066168 2
- [10] Sonsino, C.M., 1990, "Fatigue Design of Sintered Connecting Rods", Metal Powder Report, Vol. 45, No. 6, pp. 408-412.
- [11] Sugita, J., Itoh, T., and Abe, T., 1990, "Engine Component Design System Using Boundary Element Method," SAE Technical Paper 905206
- [12] Webster, W.D., Coffell, R., and Alfaro, D., 1983, "A Three Dimensional Finite Element Analysis of A High Speed Diesel Engine Connecting Rod," SAE Technical Paper 831322, pp. 83-96.
- [13] Finite Element Fatigue Analysis of Connecting Rods of Different Cross-Sections, A. Tevatia, S.B. Lal and S.K. Srivastava, International Journal of Mechanics and Solids, ISSN: 0973-1881, pp. 45-53, 2011
- [14] B retta, S., Blarasin, A., Endo, M., Giunti. T., and Murakami, Y., 1997, "Defect Tolerant Design of Automotive Components", International Journal of Fatigue, Vol. 19, No. 4, pp. 319-333.
- [15] Merritt D, Zhu G. "The prediction of connecting rod fretting and fretting initiated fatigue fracture" No. 2004-01-3015. SAE Technical Paper 2004
- [16] Antonio Strozzi et al., "A repertoire of failures in connecting rods for internal combustion engines, and indications on traditional and advanced design", Article in Engineering Failure Analysis • November 2015 DOI: 10.1016/j.engfailanal.2015.11.034
- [17] Coffin, L.F., 1954, "A Study Of The Effects of Cyclic Thermal Stresses on A Ductile Metal", Transactions of American Society for Testing and Materials, 76, pp. 931-950
- [18] Manson, S.S., 1953, "Behavior of Materials Under Conditions of Thermal Stress", Heat Transfer Symposium, pp. 9-75
- [19] Morrow, J., 1968, "Fatigue Design Handbook-Advances in Engineering" Warendale, PA, SAE, pp. 21-29K. Elissa, "Title of paper if known," unpublished.
- [20] Smith, K.N., Watson, P. and Topper, T.H., 1970, "A Stress-Strain Functions for the Fatigue on Materials", J. of Materials. 5(4), pp. 767-78
- [21] Bishop, N., and Sherratt, F., 2000, "Finite Element Based Fatigue Calculations", The Int. Association for the Engg. Analysis Community Netherlands, NAFEMS Ltd.
- [22] Fatigue Life Prediction of Connecting Rod using Strain Life Theories, A. Tevatia and S.K. Srivastava, Global Journal of Engineering.

The Effect of Ketapang Leaf Extracts (*Terminalia catappa* L.) on the Cholesterol Levels of Male Mice (*Mus musculus* L.) Hypercholesterolemia

Joko Waluyo, Dwi Wahyuni

Department of Biology Education, University of Jember, Indonesia

Abstract— Cholesterol is a useful substance for the body to regulate chemical processes such as building cell membranes, producing vitamin D, and forming steroid hormones. Hyper-cholesterol is a condition where cholesterol levels increase over the normal range (>200 mg/dL). One of the herbs which can be used as a cholesterol-lowering substance is Ketapang leaf. The leaf has several compounds which function as antioxidants. Based on Phytochemical test, this leaf contains flavonoid, saponin, triterpen, diterpen, phenolic, and tannin. Those compounds function to inhibit cell damage. This study was aimed to determine the effect of Ketapang leaf extracts (*Terminalia catappa* L.) to decrease cholesterol levels of hypercholesterolemia of male mice (*Mus musculus*) which are induced with lard. The study employed experimental design involving 25 male mice, aged at 2 months old and weighing 20-30 grams. These mice were divided into 5 groups, comprising of treatment 1 (2 mg/ 20 grams of weight), treatment 2 (4 mg/ 20 grams of weight), treatment 3 (8mg/ 20 grams of weight), positive control (simvastatin 0,26 mg/kg of weight), and negative control (CMC Na 1%). The extract was given for 14 days with 1% volume of weight. The measurement of blood cholesterol levels was done on day 8 as the preliminary data, day 14 after hypercholesterolemia of male mice, day 21 and day 28 after giving Ketapang leaf extracts. The dosage of Ketapang leaves extracts which was given during the treatments significantly affected ($p=0,0043$) the average of blood cholesterol levels of male mice. Giving the leaf extracts for two months of treatments was found successful in decreasing blood cholesterol $157,62 \pm 17,54$; $341,55 \pm 12,73$; $196 \pm 16,32$; $196,17 \pm 16,93$ mg/dL.

Keywords— Cholesterol, Hypercholesterolemia, Ketapang Leaf Extracts, Male Mice.

I. INTRODUCTION

Cholesterol is a useful substance for the body to regulate chemical processes such as building cell membranes, producing vitamin D, and forming steroid hormones.

However, for some of cardiovascular cases, such as coronary heart, the blood cholesterol levels are crucial in the emergence of such disease^[1]. Changing of lifestyles in society refers to fast foods, fast services, flavored spice foods, and chosen food varieties has influential bearing on cholesterol-related disease. Those foods actually do not contain high nutrients for the body, but its contents have high cholesterol instead^[2]. Modern dietary habit containing more cholesterol which complemented by high intensity of eatings and stresses pressing during the whole day also cause uncontrolled levels of cholesterol on blood^[3].

Based on the data from The World Health Organization (WHO) in 2002, 16.7 million people died due to cardiovascular cases. The number of cases reached 17.3 million people in 2008, and the estimated number is projected to increase to 23.3 million people in 2030^[4]. The case of cardiovascular and blood-vessel diseases is influenced by many factors, one of which is hypercholesterolemia. It is the condition where blood cholesterol levels rise over normal range (>200 mg/dL)^[5]. The total Cholesterol levels can be affected by nutrient intake, specifically foods containing high fat. Besides the high fat consumption, the hyper-cholesterol condition due to heredity, less exercises, and smoking habit factors^[6]. Accordingly, the availability of herbal alternative medicine for lowering the cholesterol levels is necessary. Baluran National Park, East Java, Indonesia, is a rich natural conservation area of various flora and fauna resources. It has various kinds of forest ecosystems in a same area: season forest, evergreen forest, coastal forest, ecotone, mangrove forest, and grassland. Evergreen forest is rain forest of tropical lowlands which are normally found in such areas as coastal regions to mountainous ones. The plant originating from this kind of area does not possess too high trunk, but very hard wood. Evergreen forest provides various plants having rich substances which are useful in health domains. One of these plants is Ketapang (*Terminalia catappa* L.)^[7].

Ketapang leaves (*Termaliacatappa L.*) contain flavonoid, saponin, tritepen, diterpen, fenolik compound, and tannin. These leaves possess secondary metabolite which has antioxidant compounds^[8]. Flavonoid is one of polyphenol compounds having various effects such as antioxidants, antitumor, anti-inflammatory, antibacterial, and anti-virus^[9]. This study has revealed that Ketapang leaf extracts can decrease cholesterol levels of the hypercholesterolemia male mice^[10].

II. RESEARCH AND METHOD

Mice which were used in the study were male mice, aged 56-70 days old and weighing 20-30 grams. The mice were acclimatized for seven days to adapt to the environment.

The creation of hypercholesterolemia condition on mice was done by inducing lard orally as much as 1% of the mice weight. For example, a mouse weighing 30g was given 0.3ml lard, and it was given for seven days from day 8 to day 14.

In the production of Ketapang leaf extracts (*Termaliacatappa L.*), the samples were taken from Baluran National Park, Situbondo, East Java, Indonesia. The selected leaves were dried, and then they were crushed using a blender to generate Ketapang powder (*Termaliacatappa L.*). The powder was then extracted by using 96% ethanol and further the Ketapang extract was given to the mice for 14 days: from day 14 to 28.

The medications for decreasing cholesterol levels in this study used 10 mg simvastatin. The dosage for adults (70kg) was 10mg/day; hence, the simvastatin dosage for the mice (20 grams) was $10 \times 0.026 = 0.26$ mg/day/20g of weight (0.026 was the conversion factor of human to mice)^[11]. Simvastatin was the positive control which was given for 14 days, especially on day 14-28^[12].

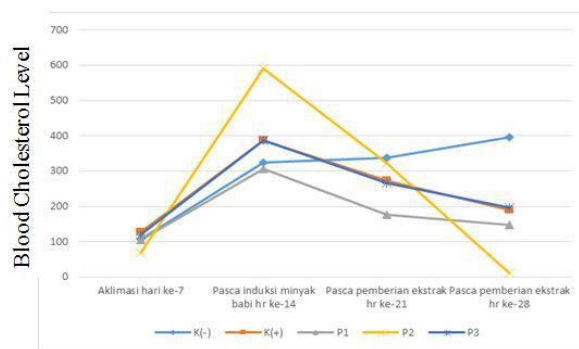
The measurement of cholesterol levels was done by using cholesterol-level measuring device, namely glucometer. The measuring was completed by making an injury on the point of mice's tail, and then the blood was dripped on cholesterol strips and glucometer would show the numeric scale indicating the cholesterol level. This measuring was done on day 8, 14, 21, and 28.

The data analysis was executed by using one-way anova with a credibility level of 95%, and it was followed by duncan test at 5% significant level.

III. RESEARCH RESULT

The Measurement Result of Cholesterol Level of Male Mice (*Termaliacatappa L.*)

The research result revealed that the measurement of cholesterol levels for the all treatments decreased, except cholesterol level for the negative control group increased. The research result is drawn on Picture 1.



Picture 1. The Graph of Average Decrease on Cholesterol Level Note:

C (-) = 1% CMCNA; C (+) 0.26 mg/20 g body weight Simvastatin;

T1 = 2 mg/20 g body weight extract of Ketapang leave; T2 = 4 mg/20 g body weight extract of Ketapang leave; T3 = 8 mg/20 g body weight extract of Ketapang leave.

The research execution indicated an average decrease of the cholesterol levels in each treatment. The various average decrease of cholesterol levels are put in Table 1.

Table.1: The Average and Standard Deviation of Decrease on Cholesterol Level

Treatment	Average \pm Standard Deviation of Decrease (mg/dL)
C (-)	-73.33 ± 05.47
C (+)	196.17 ± 16.93
T1	157.62 ± 17.54
T2	341.55 ± 12.73
T3	196.00 ± 16.32

Note:

C (-) 1% CMCNA

C (+) 0.26 mg/kg body weight Simvastatin

T1 = 2 mg/20 g body weight extract of Ketapang leave

T2 = 4 mg/20 g body weight extract of Ketapang leave

T3 = 8 mg/20 g body weight extract of Ketapang leave.

As seen in Table 1, it is clear that the highest average decrease on cholesterol level is evident in T2 (4 mg / 20 g body weight extract of Ketapang leave), which reaches 341.55 ± 12.73 mg/dL. Treatment group of T3 (8 mg/20 g body weight extract of Ketapang leave) indicates a figure of 196.00 ± 16.32 mg/dL. This result is almost equal with the positive control group's. Treatment group of T1, 2 mg/20 g body weight extract of Ketapang leave, has the lowest average decrease on cholesterol level for about 157.62 ± 17.54 mg/dL. Treatment Group, which indicates an increase in cholesterol level for about -73.33 ± 05.47 mg/dL, is C (-) 1% CMCNA.

The data of normality test evinced extract provision of $p = 0.892$ evident on the decrease of cholesterol level on day 28. A figure of $p = 0.451$ was representative of

homogeneity test. In accordance with the aforementioned data, with the statistical analysis of $p > 0.05$, it indicated that the obtained data could proceed to further analysis by ANOVA test.

Referring to ANOVA test result, the analysis indicated significant value of $p = 0.408$ ($p < 0.05$). Owing to this result, the provision of Ketapang leave extract on high-cholesterol mouse yielded significant influence on the decrease on cholesterol level. The ANOVA test revealed that all treatment groups had significant difference to negative control. As a result, it allows further analysis by means of Duncan test.

Table.2: The Result Test on The Average Influence of Ketapang Leave Extract on The Decrease on Cholesterol Level

Treatment	Average \pm Standard Deviation of Decrease (mg/dL) on day 28
C (-)	-73.33 \pm 05.47a
C (+)	196.17 \pm 16.93b
T1	157.62 \pm 17.54b
T2	341.55 \pm 12.73b
T3	196.00 \pm 16.32b

Based on Table 2 on Duncan Test, Group C (-) has meaningful difference to C (+), T1, T2, and T3. C (+) group shows no meaningful difference to T1, T2, and T3. It proves that C (+), T1, T2, and T3 have nearly similar characteristics in lowering cholesterol level.

IV. DISCUSSION

The research finding indicated that the treatment groups, C (+), T1, T2, and T3 exerted significant influence on the decrease on cholesterol level, except on treatment group C (-). It indicated an opposing result that there was increased cholesterol level in the blood. That increase occurred in as much as there was no provision of cholesterol medicine or Ketapang leave extract.

As regard with the average decrease of sugar level in each treatment, the data indicated the following results: positive control of 196.17 ± 16.93 , negative control of 196.17 ± 16.93 , treatment 1 of 157.62 ± 17.54 , treatment 2 of 341.55 ± 12.73 , and treatment 3 of 196.00 ± 16.32 . Referring to the aforementioned data, the experiment revealed that, on the highest-to-smallest scale, the average decreases comprised of Ketapang leave extract of 4 mg/20 g body weight in treatment 2, positive control, Ketapang leave extract 8 mg/20 g body weight in treatment 3, and Ketapang leave extract 2 mg/20 g body weight in treatment 1.

This research discovered disclosed that treatment 2 possessed the maximum potential in decreasing cholesterol level compared to treatment 1 and treatment 3. Based on the average of cholesterol level measurement, the research indicated that treatment 3 had the optimum result in reducing the sugar level. This feature resembled the

performance of positive control in decreasing the cholesterol level. This showed that the provision of 8 mg/20 g body weight Ketapang leave extract had the same function as Simvastatin 0.26 mg/kg body weight.

On treatment 2, the mice's cholesterol level was easy to fluctuate. This was due to the presence of steroid hormone which was influential in decreasing cholesterol [16]. The different existence of steroid hormone on every individual triggered the physiological sensitivity in receiving suspensions given during the research. This caused significant increase in mice's cholesterol level when the induction of lard was operated, which was also representative of the provision of Simvastatin, resulting in experimental animal undergoing significant decrease. This finding was also corroborated by the physical features of experimental animal 2, marked by the enlargement of prostate. The research indicated that the instability of steroid hormone in the body had significant influence on volatile cholesterol level. Moreover, that volatility was indicated by enlarged prostate, resulting in prostate cancer [17].

Ketapang extract leave had the potential to trigger cholesterol level since the research finding indicated the leave extract could bring down cholesterol level of experimental mice under hypercholesterolemia condition. That was due to the presence of antioxidant compounds preserved in the leave extract. These compounds, which had the potential to reduce cholesterol level, included flavonoid, phenol, tannin, and fenol [8]. In medical realm, sinamaldehyd compound, which was the subordinate from phenol compound, was known to possess platelet anti-aggression feature and function as similar vasodilator [12] via invitro. Flavonoid is one of phytochemical division having the same structure known as polinenol. Abundance of research claimed that flavonoid could reduce the risk of cardiovascular disease since it played essential role in lipid metabolism [13]. Flavonoid mechanism in reducing total cholesterol level was germane to decreasing the activity of HMG-KoA reductase, reducing the activity of *cyl-CoA* enzyme cholesterol acyltransferase (ACAT), and lowering cholesterol abortion in digestion system [14]. Tannin was used as antioxidant in lipid and tanning compound could precipitate protein mucosa existing in the small intestine surface which caused reduction on food absorption. As such, tanning compound could aid in reducing food lipid absorption, which as a corollary reduced the work of liver cell in synthesizing lipid [15]. Under such circumstance, tannin, flavonoid, and phenol possibly worked together in controlling cholesterol level in the blood. Accordingly, in hypercholesterolemia condition the mice's cholesterol level decreased.

The positive control employed in this research was Simvastatin. It is was given orally on daily basis during the

treatments. Simvastatin is a medicine from statin class which has superior in some aspects. First, this medicine is *Generik*-available in Indonesia, meaning it is available and quite cheap. Additionally, the medicine has been reliably consumed in society for more than 20 years. Second, based on researches documented in Cardiovascular Disease Book called Braunwalds, Simvastatin can decrease cholesterol level by 20% and the risk of blood-vein disease by 24% when given at a dose of 40mg/day. The mechanism of Simvastatin is reducing lipid by means of inhibiting 3-hydroxy-3-methyl-glutaryl coenzyme A (HMG-CoA) reductase. HMG-CoA reductase releases the precursor of mevalonic acid cholesterol from coenzyme A. Simvastatin's competitive inhibition affect cellular compensation response such as the escalation of HMG-CoA reductase enzyme and Low Density Lipoprotein (LDL) [16] receptor.

In the Duncan test operation, the negative control group had meaningful difference from positive control group, treatment 1, treatment 2, and treatment 3. That difference was due to the escalated cholesterol level on negative control group, while on the other control groups was found decreased cholesterol level. The extract control groups T1, T2, and T3 had no significant differences as every treatment group had almost same skills and activities to decrease blood cholesterol level. Therefore, it can be concluded that T1, T2, and T3 groups have compounds potential in lowering cholesterol level.

Based on the accomplished research, the effect of *Ketapang* (*Terminalia catappa* L.) leaves extract on cholesterol level was not merely due to the impact of such compounds as tannins, flavonoids and phenols, but also the presence of other compounds which had not been researched. Therefore, a further research is still needed to obtain the other maximum effects of *Ketapang* leaves as one of the effective natural alternative medicines to decrease blood cholesterol level in the hypercholesterolemia condition.

V. CONCLUSION

The provision of *Ketapang* leaves extract with concentrations of 2 mg/20 g weight, 4 mg/20 g body weight, and 8 mg/20 g body weight was influential in decreasing blood cholesterol level in male mice significantly by the negative control.

The extract concentration of 4 mg/20 g body weight had a maximum potential in decreasing blood cholesterol level with an average decrease of $341, 55 \pm 12.73$ mg/dL. The extract concentration of 8 mg/20 g body weight had the optimum potential in decreasing blood cholesterol level with an average decrease of 196 ± 16.32 mg/dL.

It is essential to carry out a further research on the *Ketapang* leave compound which has crucial affects in

decreasing the male mice cholesterol level. The intended research using a rat (*Rattus norvegicus* L.) in the experiments is still called upon.

ACKNOWLEDGEMENTS

We gratefully acknowledge the support from FKIP – University of Jember of year 2017-07-06

REFERENCES

- [1] Nugraha, Agung, M. 2014. LDL and HDL levels in the Blood Model of Periodontitis Mice. *Journal of Health Library*. Vol. 2 (1). Jember: University of Jember.
- [2] Sandi, C, Saryono, Rahmawati, D. 2008. Differences Blood Cholesterol Levels On Office Workers And Rough Workers In Majasari Village, Bukateja Purbalingga District *The Soedirman Journal Of Nursing*. Vol. 3 (3) : 131-137.
- [3] Baraas, F. 1993. Preventing Heart By Pressing Cholesterol . Jakarta : Gramedia Utama.
- [4] World Health Organization (WHO). 2013. *Cardiovascular diseases (CVDs) Fact sheet NO 317*. Available from: <http://www.who.int/mediacentre/factsheets/fs317/en/> [15 Maret 2015].
- [5] Yani, Muhammad. 2015. Controlling Cholesterol Levels On Hypercholesterolemia. *Achievement Sport Journal*. Vol. 11 (2). Yogyakarta: University State of Yogyakarta.
- [6] Pareira, F. M. M. 2010. The Influence of White Dragon Fruit Juice (*Hylocereus undatus* H.) on Total Cholesterol Mice (*Rattus norvegicus*). *Thesis*. Semarang: University of Sebelas Maret.
- [7] Dumalag, Rolito M. 2012. Southeast Asian Ecology of the Indonesian Archipelago . Jakarta: Salemba Kartika.
- [8] Rosnani. 2008. *Terminalia catappa* L. as Alternative In Water Treatment System In Shrimp Pond. Malaysia: Universiti Technology Malaysia.
- [9] Parubak, A, S. 2013. Antibacterial Flavonoid Compounds from Akway. *Chem Prog*. Vol 6 (1).
- [10] Suhailah. 2016. Effect of *Ketapang* Leaf Extract (*Terminalia catappa* L.) on Network Tolerance to Glucose and Island Diamerhans Diamet (*Mus musculus* L.) Diabetik. *Thesis*. Surabaya: Airlangga of University.
- [11] Astuti. 2007. Practical Guidelines for Biological Material Analysis. Yogyakarta: University State of Yogyakarta.
- [12] Vanessa, Rebecca. 2011. Utilization of Instant Wood Powder Drink (*Cinnamomum burmanii* Bl.) To Lower Total Cholesterol Levels In White Rats (*Rattus norvegicus*). *Thesis*. Yogyakarta: University Atma Jaya Yogyakarta.

- [13] Rumanti, Rizna. 2011. Effects of Propolis on Total Cholesterol Levels on High Fat Model Mice. *Journal of Public Health*. Vol. 11 (1) Bandung: University of Kristen Maranatha.
- [14] Prior RL. Phytochemicals. 2006. *Modern Nutrition in Health and Diseases*. USA: Lippincott Williams & Wilkins.
- [15] E, Kurniawaty. 2013. The Effect of Granting Jengkol Seed Extract (*Pithecellobium lobatum* Benth.) to Total Cholesterol Levels in The Blood of Rats Diabetes Induced Alloxan. *Biodiversitas*. Vol. 7 (4). Lampung: University of Lampung.
- [16] Herlina, Eka. 2015. Cassava Flakes Formulation (*Manihot esculenta* Crantz.) As a Potential Antioxidant Breakfast Substitute. *Jurnal Fitofarmaka*. Vol. 5 (1). Bogor: University of Pakuan Bogor.
- [17] Heryansyah, Teuku. 2013. Influence of Duration of Giving a High Fat Diet to White Lipid Lipid Profile (*Rattus Novergicus*) Strain Wistar . *Jurnal Kedokteran Syiah Kuala*. Vol. 13 (3). North Sumatera: Universiti of Syiah Kuala.

Construction Productivity Estimation Model Using Artificial Neural Network for Foundations Works in Gaza Strip Construction Sites

Dr. Eyad Haddad

Assistant Professor, Civil Engineering Department, Faculty of Engineering, University of Palestine. Gaza, Gaza Strip.

Abstract—Estimating the construction labor productivity considering the effect of multiple factors is important for construction planning, scheduling and estimating. In planning and scheduling, it is important to maximize labor productivity and forecast activity durations to achieve lower labor cost and shorter project duration. In estimating, it is important to predict labor costs. The aim of this study is to develop a new technique for estimating labor productivity rate for foundation works in (m³/ day) for building projects in Gaza Strip, through developing a model that is able to help parties involved in construction projects (owner, contractors, and others) especially contracting companies to estimating labor productivity rate for foundation works. This model build based on Artificial Neural Networks. In order to build this model, quantitative and qualitative techniques were utilized to identify the significant parameters for estimating labor productivity rate for foundation works. The data used in model development was collected using questioner survey as a tool to collect actual data from contractors for many projects in Gaza Strip. These questionnaires provided 111 examples. The ANN model considered 16 significant parameters as independent input variables affected on one dependent output variable “labor productivity rate for foundation works in (m³/ day)”. Neurosolution software was used to train the models. Many models were built but GFF model was found the best model, which structured from one input layer, included 16 input neurons, and included one hidden layer with 22 neurons. The accuracy performance of the adopted model recorded 98% where the model performed well and no significant difference was discerned between the estimated output and the actual productivity value. Sensitivity analysis was performed using Neurosolution tool to study the influence of adopted factors on labor productivity. The performed sensitivity analysis was in general logically

where the “Footings Volume” had the highest influence, while the unexpected result was “Payment delay” factor which hadn’t any effect on productivity of foundation works.

Keywords—Artificial Intelligence, Neural Network, Construction Industry, Construction management, Construction projects, Gaza Strip.

I. INTRODUCTION

Many neural network models have been developed to assist the project managers or contractors in their jobs. This study describes the design of an ANNs model for estimating production rate. The most effective factors affect production rate for foundation works were identified from previous studies. These factors were considered as inputs variables for the neural network model, whereas the labor productivity rate for foundation works in (m³/ day) considered as the output variable to this model. The data used in model development was collected using questioner survey as a tool to collect actual data from contractors for many projects in Gaza Strip. These questionnaires provided 111 examples. NeuroSolution, was used as a standalone environment for Neural Networks development and training. Moreover, for verifying this work, a plentiful trial and error process was performed to obtain the best model. A structured methodology for developing the model has been used to solve the problem at hand. This methodology incorporates five main phases: 1) Select application 2) Design structure 3) Model implementation 4) Training and testing 5) Discussion (analysis) of results.

II. METHODOLOGY

The methodology of this study which described below consists of five main phases: 1) Select application 2) Design structure 3) Model implementation 4) Training

and testing 5) Discussion (analysis) of results.

III. SELECTION OF THE NEURAL NETWORK SIMULATION SOFTWARE

Many design software are used for creating neural network models. Like SPSS, MATLAB, etc. in this study, NeuroSolution application was selected, where NeuroSolutions is the premier neural network simulation environment. As mentioned in NeuroDimension, Inc., (2012) NeuroSolutions combines a modular, icon-based network design interface with advanced learning procedures and genetic optimization. Perform cluster analysis, sales forecasting, sports predictions, medical classification, and much more with NeuroSolutions, which is:

- powerful and flexible: neural network software is the perfect tool for solving data modeling problems, so it's flexible to build fully customizable neural networks or choose from numerous pre-built neural network architectures. Modify hidden layers, the number of processing elements and the learning algorithm [1].
- Easy to use: NeuroSolutions is an easy-to-use neural network development tool for Microsoft Windows and intuitive, it does not require any prior knowledge of neural networks and is seamlessly integrated with Microsoft Excel and MATLAB. NeuroSolution also includes neural wizards to ensure both beginners and advanced users can easily get started. [1].
- Many researchers used NeuroSolution application in building their neural networks that it achieved good performance and it has multiple criteria for training and testing the model.

IV. FACTORS AFFECTING CONSTRUCTION PRODUCTIVITY ESTIMATION

In fact, one of the most significant keys in building the neural network model is identifying the factors that have real impact on the productivity estimation for foundation works. Depending on this great importance of selecting these factors, several techniques were adopted carefully to identify these factors in Gaza Strip building projects; as reviewing literature studies, and Delphi technique by conducting expert interviews.

V. DELPHI TECHNIQUE

Different technique has been used to determine the effective factors on the productivity estimation for founda-

tion works. This technique relies on the concept of Delphi technique, which aimed to achieve a convergence of opinion on factors affecting the productivity estimation for foundation works. It provides feedback to experts in the form of distributions of their opinions and reasons. Then, they are asked to revise their opinions in light of the information contained in the feedback. This sequence of questionnaire and revision is repeated until no further significant opinion changes are expected [2]. For Delphi process, several rounds should be conducted where first round begins with an open-ended questionnaire.

The open-ended questionnaire serves as the cornerstone of soliciting specific information about a content area from the Delphi subjects, then after receiving the responses, the researcher converts the collected information into a well structured questionnaire to be used as the survey instrument for the second round of data collection. In the second round, each Delphi participant receives a second questionnaire and is asked to review the items summarized by the investigators based on the information provided in the first round, where in this round areas of disagreement and agreement are identified. However, in third round Delphi panelists are asked to revise his/her judgments or to specify the reasons for remaining outside the consensus. In the fourth and often final round, the list of remaining items, their ratings, minority opinions, and items achieving consensus are distributed to the panelists. This round provides a final opportunity for participants to revise their judgments.

Accordingly, the number of Delphi iterations depends largely on the degree of consensus sought by the investigators and can vary from three to five [3]. Five experts in construction field were selected to reach a consensus about specifying the key parameters. The results with those five experts were significantly close to the questionnaire results, and only three rounds were conducted due to largely degree of consensus, where they proposed to exclude retaining wall and curtain wall from these factors because of their rarity in Gaza's projects.

VI. STRUCTURE DESIGN

The choice of ANN architecture depends on a number of factors such as the nature of the problem, data characteristics and complexity, the numbers of sample data ... etc. [4]. With the 16 inputs readily identified, the outputs describing the estimation of productivity for foundation works (m³/day) can be modeled in different ways. The choice of artificial neural network in this study is based

on prediction using feedforward neural network architectures and backpropagation learning technique. The design of the neural network architecture is a complex and dynamic process that requires the determination of the internal structure and rules (i.e., the number of hidden layers and neurons update weights method, and the type of activation function) [5].

A common recommendation is to start with a single hidden layer. In fact, unless the researcher is sure that the data is not linearly separable, he may want to start without any hidden layers.

The reason is that networks train progressively slower when layers are added [6]. Based on the literature review, the neural network type deemed suitable for productivity estimation has been identified as feed-forward pattern recognition type (Back propagation) to suit the desired interpolative and predictive performance of the model. Two kinds of feed-forward patterns were chosen to build the models multilayer perceptron and general feed forward. ANN architecture was chosen after several trials.

VII. MODEL IMPLEMENTATION

Once there is a clear idea about feasible structures and the information needed to be elicited, the implementation phase starts with knowledge acquisition and data preparation [7].The flow chart for model structure is show in Figure1

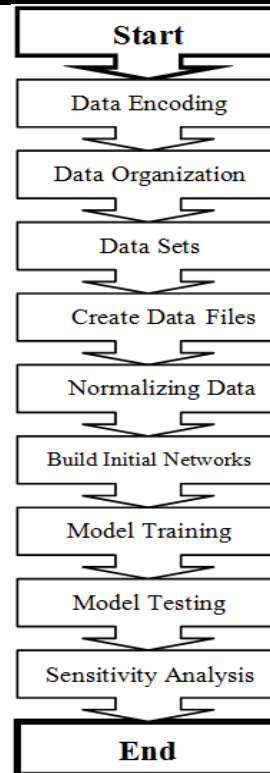


Fig.1: Model implementation steps flowchart

7.1. Data Encoding

Artificial networks only deal with numeric input data. Therefore, the raw data must often be converted from the external environment to numeric form [8]. This may be challenging because there are many ways to do it and unfortunately, some are better than others are for neural network learning [6].

In this research, the data is textual and numeric, so it is encoded to be only numeric or integer according to Table 1.

Table.1: Inputs/Output encoding

No	Input factor	Encode	Code
1	Area of the building(m2)	Number	Number
2	Footings type	Shallow Footings Deep Footings	= 1 = 2
3	Footings Volume	Number	Number
4	Method of casting concrete	Manual mechanical	= 1 = 2
5	Number of Labor	Number	Number
6	Material shortages	Low quantity Medium quantity High quantity	= 1 = 2 = 3
7	Tool and equipment shortages and	Low Efficiency	= 1

No	Input factor	Encode	Code
	Efficiency	Medium Efficiency High Efficiency	= 2 = 3
8	labor experiences	Low experiences Medium experience High experiences	= 1 = 2 = 3
9	Duration of formwork and casting Footings	Number	Number
10	Working hours per day at site	Number	Number
11	Weather	Rain Hot Moderate	= 1 = 2 = 3
12	Complexity due to steel bars	Complex Medium Easy	= 1 = 2 = 3
13	Drawings and specifications alteration during execution	High alteration Medium alteration Low alteration	= 1 = 2 = 3
14	Easy to arrive to the project location	Difficult Medium Easy	= 1 = 2 = 3
15	Lack of labor surveillance	Low surveillance Medium surveillance High surveillance	= 1 = 2 = 3
16	Payment delay	High delay Medium delay Low delay	= 1 = 2 = 3
No.	Output Parameter	Encode	Code
	Labor productivity	Number form	M ³ /day

7.2 Data Organization

Initially, the first step in implementing the neural network model in NeuroSolution application is to organize the Neurosolution excel spreadsheet as shown at Figure 2. Figure 2 shows a snapshot of the Excel program that represents part of the data matrix. Then, specifying the input factors that have been already encoded, which consist of 16 factors; Area of the building(m2), footings type, footings volume, method of casting concrete, number of La-

bor, material shortages, tool and equipment shortages and efficiency, labor experiences, duration of formwork and casting footings, working hours per day at site, weather, complexity due to steel bars, drawings and specifications alteration during execution, easy to arrive to the project location, lack of labor surveillance, and payment delay . The desired parameter (output) is Labor productivity by (M3/day).

	A	B	C	D	E	F	G	H	I	J	K	L	M	N	O	P	Q
1	Area of the building(m ²)	Footings type	Footings Volume	Method of casting concrete	Number of Labor	Material shortages	Tool and equipment shortages and Efficiency	labor experiences	Duration of formwork and castings Footings	Working hours per day: at site	Weather	Complexity due to steel bars	Drawings and spe. Alteration	project location	labor surveillance	Payment delay	Productivity (M3/day)
2	145	1	35	2	6	2	2	2	4	10	3	3	2	3	2	3	9.3
3	500	2	81	2	8	3	2	2	7	8	3	3	2	3	3	3	12.1
4	500	1	85	2	9	3	2	3	7	8	3	3	3	3	3	3	12.6
5	122	2	53	2	5	2	2	2	3	8	3	3	3	3	2	3	18.2
6	110	1	32	1	5	2	2	2	3	9	3	3	3	3	2	3	11.2
7	128	2	43	1	5	2	3	2	3	8	3	3	3	2	2	3	14.8
8	152	2	52.1	2	5	2	3	2	4	8	3	3	3	2	2	3	13.5
9	231	2	78.4	2	7	2	2	2	4	9	3	3	3	2	2	3	20.1
10	176	2	62.6	2	7	3	2	2	4	8	3	3	3	2	2	3	16.2
11	130	2	48.3	2	4	3	2	2	3	8	3	2	3	2	2	3	16.6
12	138	2	52.3	2	5	3	2	2	3	8	2	2	3	2	2	3	17.9
13	145	2	56.1	1	5	2	2	2	4	8	2	2	3	2	2	3	14.5
14	195	1	45.5	2	5	2	3	2	4	8	2	2	3	2	2	3	11.9
15	147	2	50.7	2	5	2	3	2	4	8	2	2	3	3	2	3	13.2
16	155	2	55.4	2	5	3	3	2	3	9	2	2	3	3	2	3	19.0
17	144	2	55.5	1	6	3	3	2	3	8	2	2	3	3	2	3	19.0
18	229	2	89.8	1	7	2	2	3	5	8	3	3	3	3	2	3	18.5
19	159	2	52.8	2	5	2	2	2	4	8	3	3	3	3	2	3	13.7

Fig.2: Snapshot showing the data matrix

7.3 Data Set

The available data were divided into three sets namely; training set, cross-validation set and test set [9]. Training and cross validation sets are used in learning the model through utilizing training set in modifying the network weights to minimize the network error, and monitoring this error by cross validation set during the training process. However, test set does not enter in the training process and it hasn't any effect on the training process, where it is used for measuring the generalization ability of the network, and evaluated network performance [10].

In the present study, the total available data is 111 exemplars that are divided randomly into three sets with the following ratio:

- Training set (includes 83 exemplars ≈ 75%).
- Cross validation set (includes 15exemplars ≈ 14%).
- Test set (includes 13 exemplars ≈ 11%).

See Figure 3 and 4 which explain how the data was distributed into sets and defined each exemplar for the corresponding.

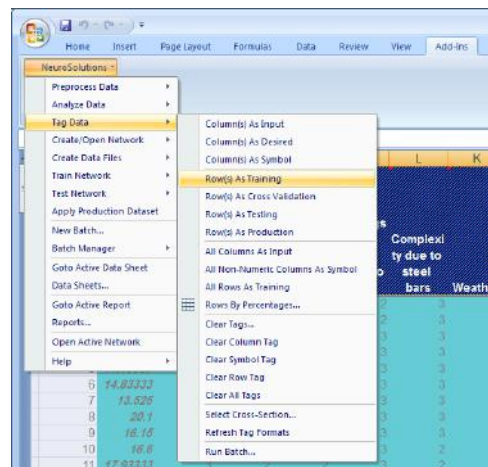


Fig.3: Tag rows of data as a training set

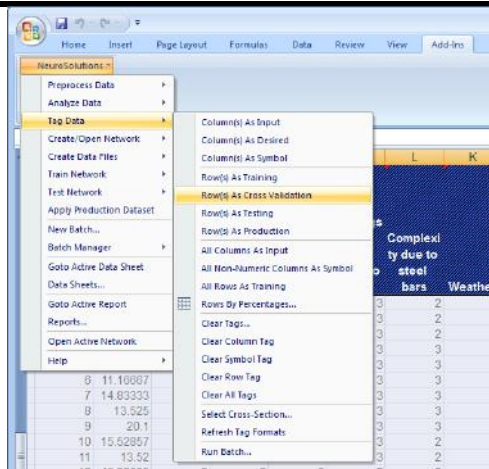


Fig.4: Tag rows of data as a cross-validation set

7.4 Building Network

Once all data were prepared, then the subsequent step is represented in creating the initial network by selecting the network type, number of hidden layer/nodes, transfer function, learning rule, and number of epochs and runs. An initial neural network was built by selecting the type of network, number of hidden layers/nodes, transfer function, and learning rule. However, before the model becomes ready, a supervised learning control was checked to specify the maximum number of epochs and the termination limits, Figure 5 presents the initial network of Multilayer Perception (MLP) network that consists of one input, hidden, and output layer.

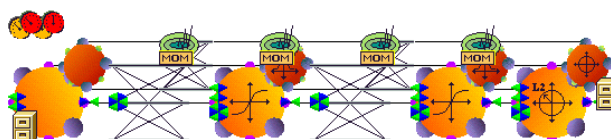


Fig.5: Multilayer Perceptron (MLP) network

Before starting the training phase, the normalization of training data is recognized to improve the performance of trained networks by Neurosolution program which as shown in Figure 6 which ranging from (0 to +0.9).

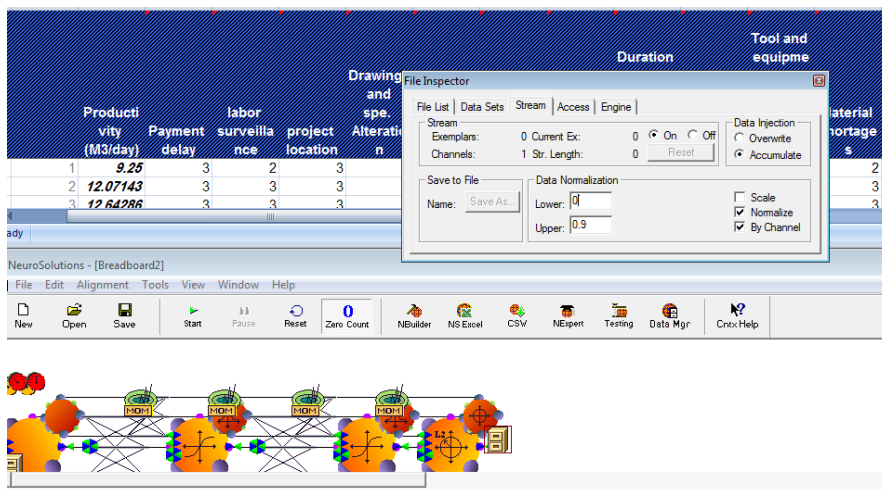


Fig.6: selecting the normalization limits of data

7.5 Model Training

The objective of training neural network is to get a network that performs best on unseen data through training many networks on a training set and comparing the errors of the networks on the validation set [11]. Therefore, several network parameters such as number of hid-

den layers, number of hidden nodes, transfer functions and learning rules were trained multiple times to produce the best weights for the model. As a preliminary step to filter the preferable neural network type, a test process was applied for most of available networks in the application. Two types Multilayer Perceptron (MLP) and

General feed Forward (GFF) networks were chosen to be focused in following training process due to their good initial results. It is worthy to mention that, previous models that have been applied in the field of estimating productivity of foundation works by neural networks used earlier two types of networks because of giving them the best outcome. The following chart illustrates the procedures of training process to obtain the best model having the best weight and minimum error percentage.

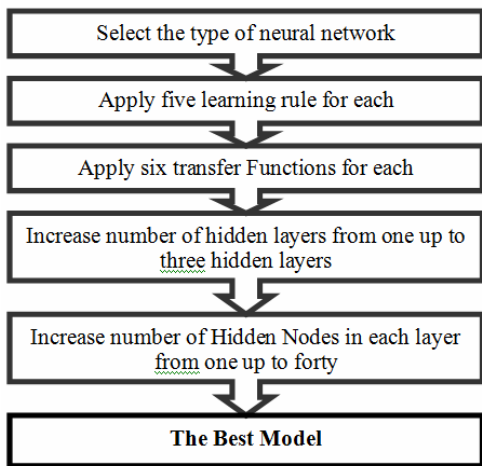


Fig.7: the procedures of training process

The chart shows the procedures of the model training, which starts with selecting the neural network type either MLP or GFF network. For each one, five types of learning rules were used, and with every learning rule six types of transfer functions were applied, and then one separate hidden layers were utilized with increment of hidden nodes from 1 node up to 40 nodes this layer. By another word, thousand trials contain 40 variable hidden nodes for each was executed to obtain the best model of neural network. Figure 8 clarifies training variables for one trial. It comprises of number of epochs, runs, hidden nodes, and other training options. Ten runs in each one 3000 epochs were applied, where a run is a complete presentation of 3000 epochs, each epoch is a one complete presentation of all of the data[6].

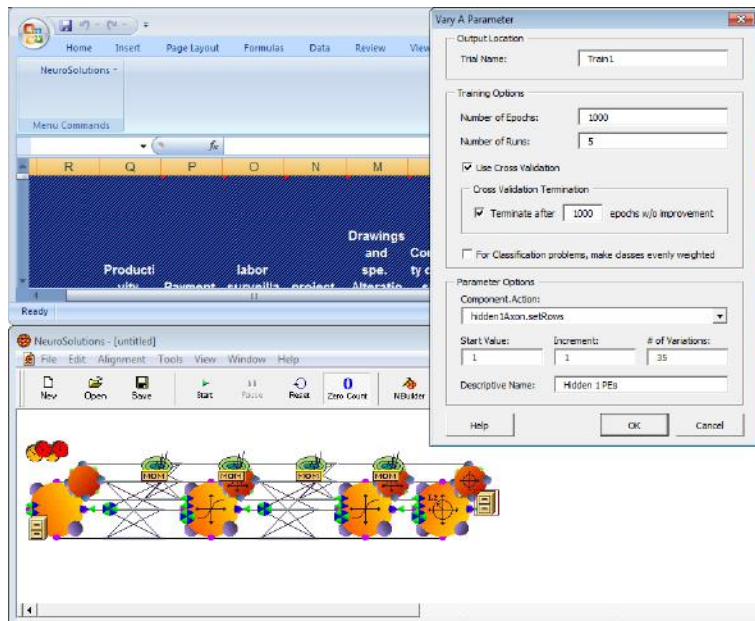


Fig.8: Training options in Neurosolution application

However, in each run, new weights were applied in the first epoch and then the weights were adjusted to minimize the percentage of error in other epochs. To avoid overtraining for the network during the training process,

an option of using cross-validation was selected, which computes the error in a cross validation set at the same time that the network is being trained with the training set. The model was started with one hidden layer and

one hidden node in order to begin the model with simple architecture, and then the number of hidden PEs was growing up by one node up to 40 hidden nodes.

7.6 Model Results

As mentioned above, the purpose of testing phase of ANN model is to ensure that the developed model was successfully trained and generalization is adequately achieved, through a system of trial and error. The best model that provided more accurate productivity estimate without being overly complex was structured of Multi-layer Perception (MLP) includes one input layer with 16 input neurons and one hidden layer with (22 hidden neurons) and finally three output layer with one output neuron (Labor productivity (M3/day)). However, the main downside to using the Multilayer Perception network structure is that it required the use of more nodes and more training epochs to achieve the desired results. Figure 9 summarizes the architecture of the model as number of hidden layer/nodes, type of network and transfer function.

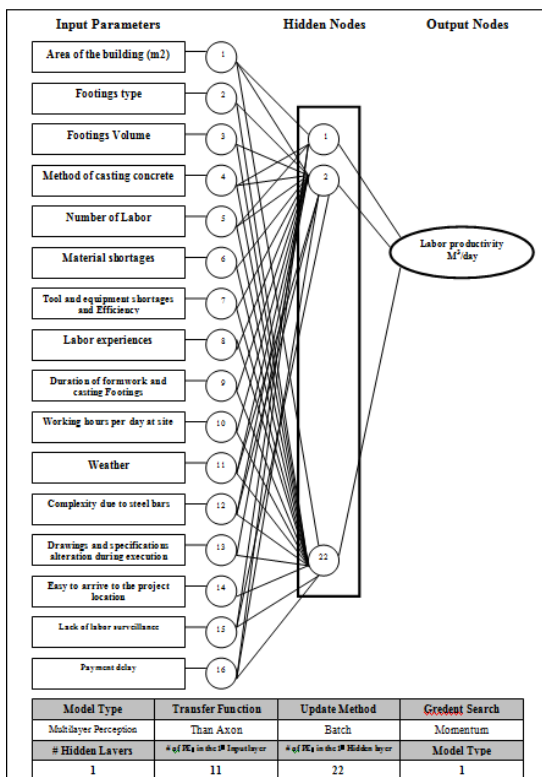


Fig.9: Architecture of the model

7.7 Results Analysis

The testing dataset was used for generalization that is to produce better output for unseen examples. Data from 15

cases were used for testing purposes. A Neuro solution test tool was used for testing the adopted model accordingly to the weights adopted. Table 2 present the results of these 15 cases with comparing the real productivity (M3/day) of tested cases with estimated productivity from neural network model, and an absolute error with an absolute percentage error is also presented.

Table.2: Results of neural network model at testing phase

Case	Actual Productivity (M3/day)	Estimated Productivity (M3/day)	Absolute Error AE	Absolute Percentage Error (%)
1	10.80	10.81	0.01	0%
2	16.60	15.45	1.15	7%
3	10.10	10.57	0.47	5%
4	12.64	12.46	0.18	1%
5	18.16	16.84	1.32	7%
6	11.16	11.12	0.04	0%
7	14.83	14.97	0.14	1%
8	13.53	13.59	0.06	0%
9	20.10	20.18	0.08	0%
10	15.53	15.79	0.26	2%
11	13.52	13.77	0.25	2%
12	45.83	46.05	0.22	0%
13	40.50	40.64	0.14	0%
14	45.16	43.89	1.27	3%
15	39.70	40.52	0.82	2%

Mean Absolute Error

The Mean Absolute error (MAE) for the presented results in Table 3 equals (0.743 M3/day), it is largely acceptable for Gaza Strip construction industry. However, it is not a significant indicator for the model performance because it proceeds in one direction, where the mentioned error may be very simple if the project is large, and in turn; it may be a large margin of error in case the project is small.

Mean Absolute Percentage Error

The mean absolute percentage error of the model is calculated from the test cases as shown in Table 2, which equals 2%; this result can be expressed in another form by accuracy performance (AP) according to Wilmot and Mei, (2005) which is defined as (100-MAPE) %. AP= 100% - 2% = 98%. That means the accuracy of adopted model for estimating productivity. It is a good result especially when the construction industry of Gaza Strip is facing a lot of obstacles [12].

□ Correlation Coefficient (R)

Regression analysis was used to ascertain the relationship between the estimated productivity and the actual productivity. The results of linear regressing are illustrated in table 3. The correlation coefficient (R) is 0.997, indicating that; there is a good linear correlation between the actual value and the estimated neural network productivity

Table.3: Results of performance measurements

Performance	Productivity (M3/day)
MSE	0.9512
NMSE	0.0057
MAE	0.7426
Min Abs Error	0.0085
Max Abs Error	2.4343
r	0.9970

The previous results show that the models have excellent performance. The accuracy of the best model developed by General Feed Forward sounds very favorably with data based from test set. It has been shown from the results that the model performs well and no significant difference could be discerned between the estimated output and the desired value. Results of cross validation set are shown in Figures 10.

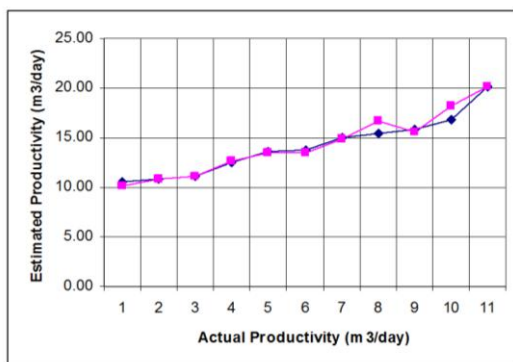


Fig.10: Desired output and actual network output for C.V set exemplar

Figure 11 describes the actual productivity comparing with estimated productivity for cross validation (C.V) dataset. It is noted that there is a slight difference between two quantities lines.

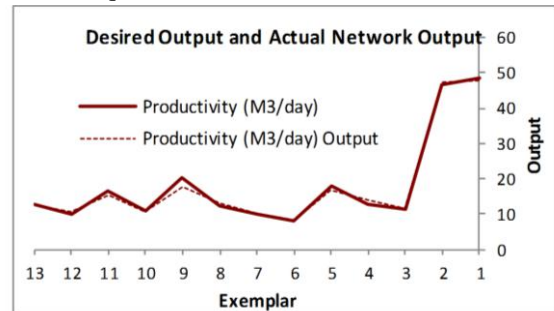


Fig.11: Comparison between desired output and actual network output for Test set

7.7 Sensitivity Analysis

Sensitivity analysis is the method that discovers the cause and effect relationship between input and output variables of the network. The network learning is disabled during this operation so that the network weights are not affected. The basic idea is that the inputs to the network are shifted slightly and the corresponding change in the output is reported either as a percentage or as a raw difference [6]. Table 4 and 5 show the sensitivity analysis of the GFF model which includes 16 graphs each of them represents the relation between one input and the output (productivity m3/day).

Table.4: the sensitivity analysis of the GFF model

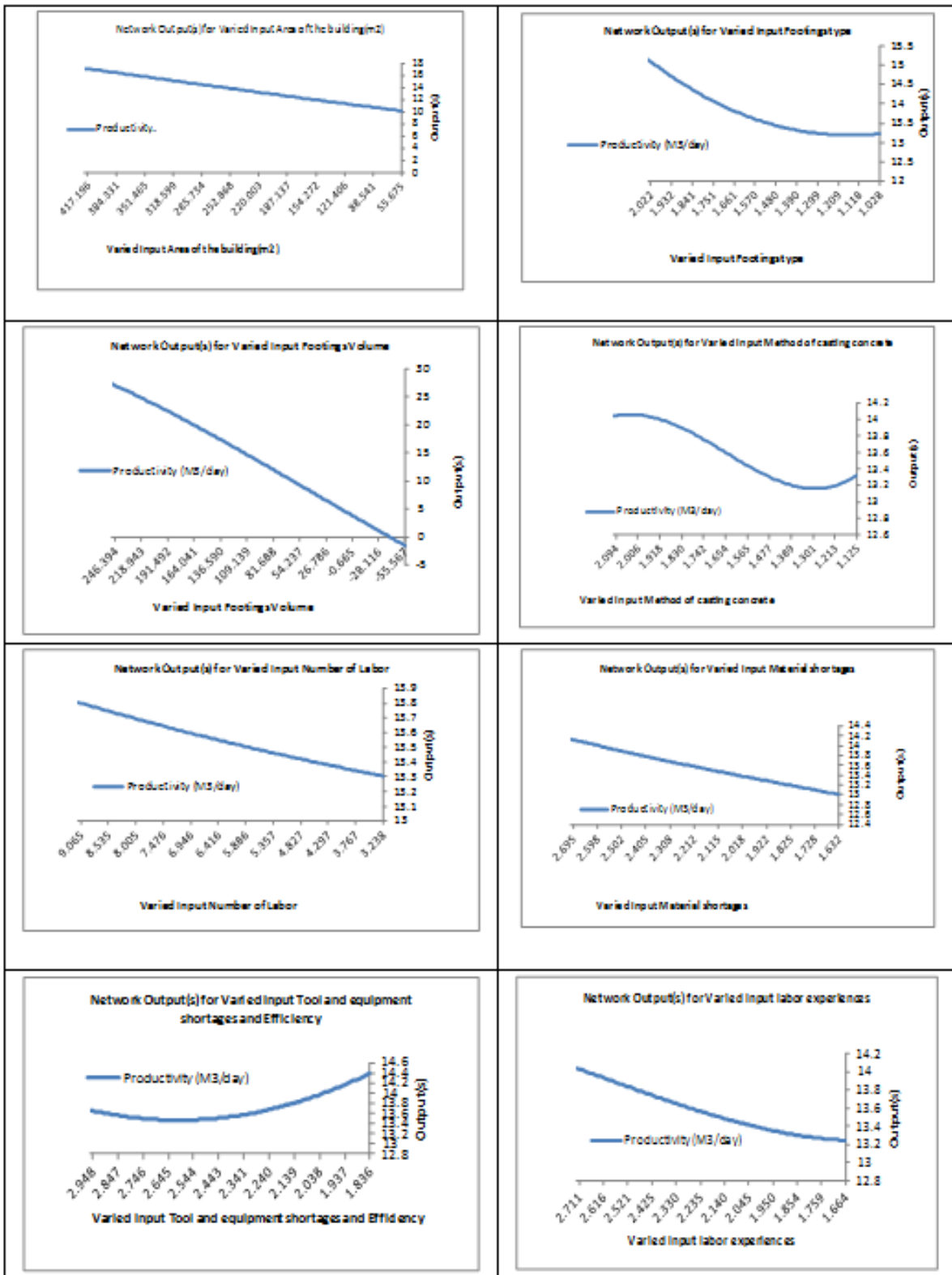
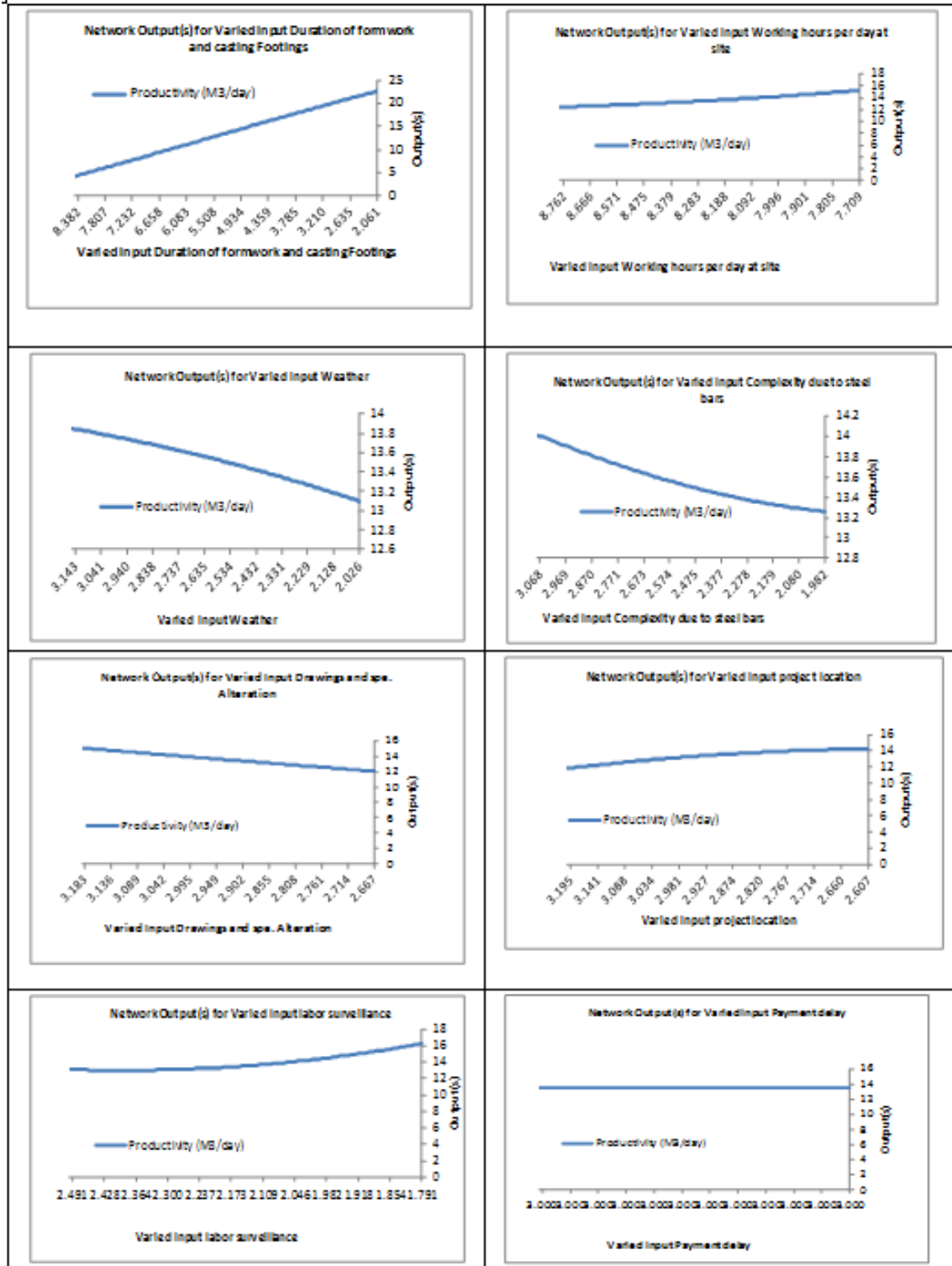


Table.5: the sensitivity analysis of the GFF model



Sensitivity analysis was carried out by Neurosolution tool to evaluate the influence of each input parameter to output variable for understanding the significance effect of input parameters on model output. The sensitivity analysis for the best GFF model was performed and the result is summarized and presented in figure 12.

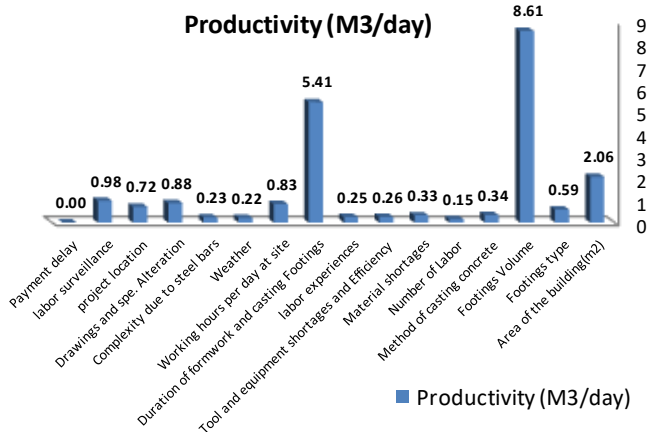


Fig.12: Sensitivity about the mean

Figure 12 shows “Footings Volume” parameter has the greatest effect on the productivity of foundation works output where its influence exceeds the impact of other factors combined. But the result of (Mady M., 2013) showed that number of labor factor had the greatest effect on labor productivity for casting concrete slabs. Mady study was consisting of 11 factors which affect labor productivity for casting concrete slabs [13]. The value 8.61 for the footings volume input parameter is the value of the standard deviation for 111 output values. These output values are recorded after training the model with fixing the best weights on a matrix data. All inputs are fixed on the mean value for each row except the footings volume value which varied between (the mean – standard deviation) to (the mean + standard deviation). The second parameter affecting the total productivity is “Duration of formwork and casting Footings” which has great effect on productivity. While the result shows that parameter “Payment delay” hasn’t any effect on productivity of foundation works. This result is unexpected.

VIII. CONCLUSION

- Historical data of building projects were collected from the questionnaire. The projects were executed between 2012 and 2016 in Gaza Strip. 111 case

studies were divided randomly into three sets as training set (83 projects 75%), cross validation set (15 projects 14%), and testing set (13 projects 11%).

- Developing ANN model passed through several steps started with selecting the application to be used in building the model. The Neurosolution5.07 program was selected for its efficiency in several previous researches in addition to its cease of use and extract results. The data sets were encoded and entered into MS excel spreadsheet to start training process for different models.
- Many models were built but GFF model was found the best model, which structured from one input layer, included 16 input neurons, and included one hidden layer with 22 neurons.
- The accuracy performance of the adopted model recorded 98% where the model performed well and no significant difference was discerned between the estimated output and the actual productivity value.
- In order to ensure the validity of the model in estimating the productivity of new projects, many statistical performance measures were conducted i.e; Mean Absolute Error (MAE), Mean Absolute Percentage Error (MAPE), Total Mean Absolute Percentage Error (Total MAPE), and Correlation Coefficient (r). The results of these performance measures were acceptable and reliable.
- Sensitivity analysis was performed using Neurosolution tool to study the influence of adopted factors on labor productivity. The performed sensitivity analysis was in general logically where the “Footings Volume” had the highest influence, while the unexpected result was “Payment delay” factor which hadn’t any effect on productivity of foundation works.

REFERENCES

- [1] NeuroDimension, Inc., 2012.
- [2] Creedy, G. D., Skitmore, M. & Sidwell, T., 2006. Risk factors leading to cost overrun in the delivery of highway construction projects, Australia: Research Centre: School of Urban Development.
- [3] Hsu, C., 2007. The Delphi Technique: Making Sense Of Consensus. Practical Assessment, Research & Evaluation electronic journal, 12(10).
- [4] Sodikov, J., (2005). Cost estimation of highway

- projects in developing countries Artificial Neural Network Approach. *Journal of the Eastern Asia Society for Transportation Studies*, 6, PP. 1036 - 1047.
- [5] Gunaydin, M. & Dogan, Z., (2004). A neural network approach for early cost estimation of structural systems of buildings. *International Journal of Project Management*, Volume 22, PP. 595–602.
- [6] Principe, J., Lefebvre, C., Lynn, G. & Wooten, D., (2010). *NeuroSolutions - Documentation*. Help. NeuroDimension, Inc.
- [7] Hegazy, T., Moselhi, O. & Fazio, P., (1994). Developing practical neural network applications using back- propagation. *Micro computers in Civil Engineering*, 9, PP. 145- 159.
- [8] Kshirsagar, P. & Rathod, N., 2012. Artificial Neural Network. *International Journal of Computer Applications*
- [9] Ghiassi, M., Saidane, H. & Zimbra, D., (2005). A dynamic artificial neural network model for forecasting time series events. *International Journal of Forecasting*, 21, PP. 341-362.
- [10] Arafa, M. & Alqedra, M., 2011. Early stage cost estimation of buildings construction projects using ANN. *Journal of Artificial Intelligence*, 4(1), pp. 63-75.
- [11] Dindar, Z., 2004. *Artificial Neural Networks Applied To Option Pricing*, s.l.: s.n.
- [12] Willmott, C. & Matsuura, K., 2005. Advantages of the mean absolute error (MAE) over the root mean square error (RMSE) in assessing average model performance. *Climate Research*, Volume 30, p. 79–82.
- [13] Mady M., 2013. *Prediction Model of Construction Labor Production Rates in Gaza Strip using Artificial Neural Networks*. Unpublished Msc Thesis. The Islamic university of Gaza (IUG).

Implementation of Invisible Digital Watermarking Technique for Copyright Protection using DWT-SVD and DCT

Devasis Pradhan

Asst. Prof. Department of Electronics & Communication Engineering, Acharya Institute of Technology, Bangalore, India

Abstract—The digital watermarking is a process of hiding an information in multimedia for copyright protection. Where, one data is hidden inside another data. We implement the watermarking algorithm in frequency domain by using a combination of DWT (Discrete Wavelet Transform) and SVD (Singular Value Decomposition) with DCT (Discrete Cosine Transform) algorithms. In which the performance analysis of an invisible watermarking can be measured with comparison of MSE (Mean Square Error) and PSNR (Peak Signal to Noise Ratio) with respect to the embedded and extracted images respectively. Here, the invisible watermarking is used to protect copyrights of multimedia contents. The invisible watermarks are the technologies which could solve the problem of copyright protection. Which is required for ownership identification as well as the hidden information can also be identified.

Keywords— DWT(Discrete Wavelet Transform) and SVD (Singular Value Decomposition) based transform, DCT (Discrete Cosine Transform), MSE (Mean Square Error), PSNR (Peak Signal Noise Ratio).

I. INTRODUCTION

Digital watermarking is a technique of hiding one data with other data. Where, the method of hiding data is invisible. In case of DWT (Discrete Wavelet Transform) watermarking technique, decomposition of the original image is done to embed the watermark and in case of DWT-SVD watermarking technique, firstly original image is decomposed according to DWT and then watermark is embedded in singular values obtained by applying SVD (Singular Value Decomposition). Where, the DCT (Discrete Cosine Transform) helps to separate the image into parts (or spectral sub-bands) of differing importance (with respect to the image's visual quality). Here, the frequency domain analysis is used for invisible watermarking. Where, the watermark is embedded after taking image transforms, because the frequency domain methods are more robust than the spatial domain techniques.

II. COPYRIGHT PROTECTION

Copyright protection is used to claim the ownership of an designed data, which may be image, audio or video. The copyright protection plays necessary role for protection of data. Hence, the concept of invisible watermarking is used for copyright protection. The digital watermarking technique is one of the process to avoid illegal copying of multimedia data. The protection of multimedia information becomes more and more important. So, the digital watermarking is mostly used for copyright/piracy protection [1].

III. INVISIBLE WATERMARKING TECHNIQUE

The watermark which is invisible i.e. known as invisible watermarking. Such watermarking is very much secure for copyright protection. The digital watermark is embedded in to an image just like a code. To protect illegal access basically such invisible digital watermark technique is used. The invisible watermark is used to maintain the ownership, authenticity of the original data like audio, images, video or even text. Where, the digital watermarking provides copyright protection of data [5]. The invisible watermarking is a process of embedding information into a digital data (Such as; Image, audio and video) which is difficult to remove. In the transform domain (DWT, DCT, and DWT-SVD etc.) are more robust to various attacks while the computational complexity is greater than the spatial domain transform [6].

DWT-SVD based transform:

IV. PROPOSED SCHEME

Here, the proposed scheme can be explained as follows;
DWT-SVD based transform: A hybrid image watermarking technique based on DWT and SVD has been presented where the watermark is embedded on the singular values of the cover image’s DWT sub bands [2]. Such a technique is known as hybrid watermarking algorithm.

DWT (Discrete Wavelet)transform:The DWT based transform-domain watermarking techniques are generally more effective in terms of the imperceptibility and robustness of digital watermarking algorithms . The DWT technique is proposed which performs greater robustness to common signal distortions. The advantage of the wavelet-based technique lies in the method used to insert the watermark in low frequency band using blending(Invisible) technique. In case of DWT the Performance could be obtained by increasing the level of DWT [7].The DWT in one dimensional signal is divided in two parts one is low frequency part and another is high frequency part. Next the low frequency part is split into two parts and the similar process will continue until the desired level. The high frequency part of the signal is contained by the edge components information of the signal. The decomposition in DWT (Discrete Wavelet Transform) on an image divides into four parts of approximation image such as; (LL) as well as horizontal (HL), vertical (LH) and diagonal (HH) for detail components [9].

Singular Value Decomposition: The singular value decomposition (SVD) is a factorization of a real or complex matrix, with many useful applications in signal processing and statistics. The fundamental properties of SVD from the viewpoint in the field of image processing applications are: the singular values(SVs) of an image have very good stability, i.e. when a small perturbation is added to an image whose SVs do not change significantly; and ii) SVs represent intrinsic algebraic image properties [4].Here, an image can be represented as a matrix of positive scalar values. The SVD for any image let, A of size $m \times m$ is a factorization of the form given by $A=USVT$, where U and V are orthogonal matrices in which columns of U are left singular vectors of image A. S is a diagonal matrix of singular values in decreasing order. The basic idea behind SVD technique of watermarking is to find SVD of image and the altering the singular value to embed the watermark. In digital watermarking schemes, SVD is used due to its main properties: 1) A small agitation added in the image, doesn't cause large variation in its singular values 2) The

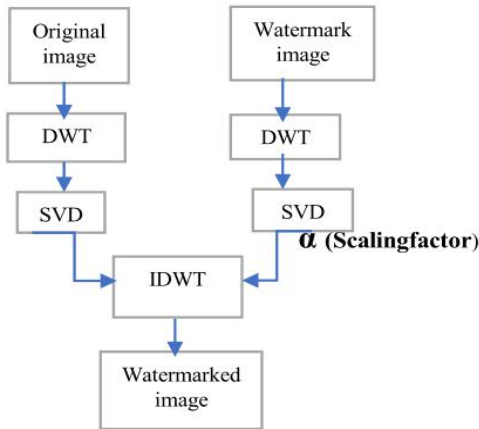


Fig.1: Watermark Embedding Process

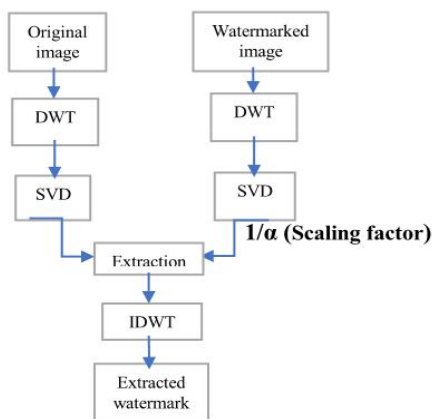


Fig.2: Watermark Extracted Process

DCT based transform:

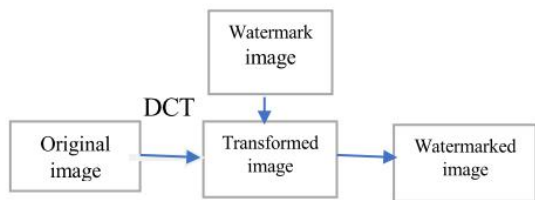


Fig.3. Watermark Embedding Process

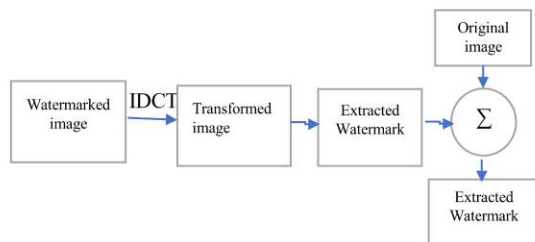


Fig.4: Watermark Extracted Process

singular value represents intrinsic algebraic image properties [5].

DCT (Discrete Cosine Transform): The discrete cosine transform (DCT) helps separate the image into parts (or spectral sub-bands) of differing importance (with respect to the image's visual quality). The DCT is like the discrete Fourier transform: it transforms a signal or image from the spatial domain to the frequency domain. The DCT is performed on an $N \times N$ square matrix of pixel values and it yields an $N \times N$ matrix of frequency coefficients. Here, N most often equals 8 because a larger block, though would probably give better compression, often takes a great deal of time to perform DCT calculations; creating an unreasonable tradeoff. As, a result, DCT implementations typically break the image down in to more manageable 8×8 blocks. -Here, an image into non-overlapping blocks where (8×8) blocks are commonly used and applies DCT to each block. This will divide an image into three main regions such as; low frequencies sub-band (FL), middle frequencies sub-band (FM) and high frequencies sub-band (FH) which makes it easier to select the band in which the watermark is to be inserted. Many studies indicate that the middle frequency bands are commonly chosen, because embedding the watermark in a middle frequency band does not scatter the watermark information to most visual important parts of the image. The remaining steps involves embedding the watermark by modifying the selected coefficients and finally applying inverse DCT transform on each watermark image, original image, transformed image,watermarked Image, extracted watermark, Original Image.Watermark is embedded into an image by modifying the coefficients of the middle frequency sub-band, this is done so that the visibility of the image will not be affected, and the watermark will not be removed by compression [3].

V. EXPERIMENTAL RESULTS AND ANALYSIS

The above procedure has been implemented using the DWT-SVD on two color images and DCT transform on two gray scale images in MATLAB and the results are tested respectively. Where, one is the original image and another one is the watermark image. For DWT-SVD based transform the original color image (5), watermark color image (6),watermarked image (7), extracted watermark image (8) and similarly, for DCT based transform the original color image and watermark color image both are converted in to gray scale image then the watermark image can be embedded and extracted. So, for DCT original color image(9), original watermark image (10), Gray scale

watermark image(11), Gray scale watermarked image (12), Extracted watermark image(13). **Results:**

i) DWT-SVD on color image



Fig.5: Original image



Fig.6. Watermark image



Fig.7: Watermarked image



Fig.8: Extracted image

ii) DCT on gray scale image



Fig.9: Original image



Fig.10: Watermark image



Fig.11: Gray scale watermark image



Fig.12: Gray scale watermarked image



Fig.13: Extracted watermark

VI. COMPARISONS (Comparing of different % of embedding watermark)

After embedding the watermark image in to an original image there is a variation of characteristics of the final watermarked image. According to the addition of % of watermark we obtain different values of PSNR (Peak signal to noise ratio) and MSE (Mean square error). For the restoration result that requires a measurement of image quality.

Here, different value of watermark can be embedded and extracted in both the DWT-SVD and DCT based transforms. Hence, there are two methods which are commonly used for this purpose. Such as; Mean-squared error and Peak signal to noise ratio.

MSE (Mean square error): The mean square error (MSE) is the error or difference between the original image and watermarked image. Let us, consider that the original image is $g(x, y)$ and the watermarked image is $g^w(x,y)$ then the MSE can be calculated as;

$$eMSE = \frac{1}{MN} \sum_{n=1}^M \sum_{m=1}^N [g^{n,m} - g(n, m)]^2$$

But, one problem in Mean square error is that it depends strongly on the image intensity scaling.

PSNR (Peak signal to noise ratio): The PSNR is a good measure for comparing restoration results for the same

image, but between image comparison of PSNR are meaningless. For example, if one image with 15 dB PSNR may look much better than another image with 30 dB PSNR. The PSNR is measured in decibels (dB). But, PSNR avoids the problem of MSE by scaling the MSE according to the image range.

$$PSNR = -\log(eMSE/S^2) \text{ in dB}$$

The DWT-SVD based transform has good imperceptibility on the watermarked image and superior in terms of Peak Signal to Noise Ratio (PSNR) [4].

MSE Extraction: The difference between the error between final watermarked image and extracted watermark image.

PSNR Extraction: The difference between the Peak signal to noise ratio between final watermarked image and extracted watermark image.

Comparison Table:

Table.1: For DWT-SVD based transform

SL.N O.	% of watermark	MSE for embedded	PSNR for embedded (In dB)	MSE for extraction	PSNR for extraction (In dB)
1.	0.089	0.0341	62.837	0.0018	74.1073
2.	0.0008	0.0381	62.355	0.0020	73.2433
3.	0.0689	0.0348	62.749	0.0022	72.3376
4.	0.7	0.0370	62.482	0.0024	71.4064
5.	0.0342	0.0356	62.650	0.002	70.4632

Graphs:

(For DWT-SVD based transform)

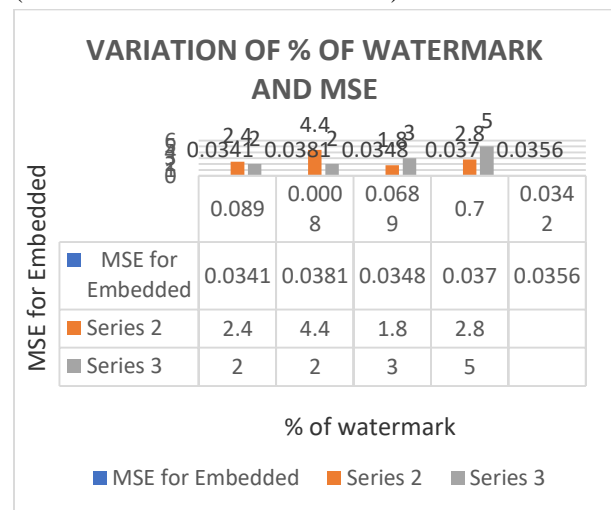
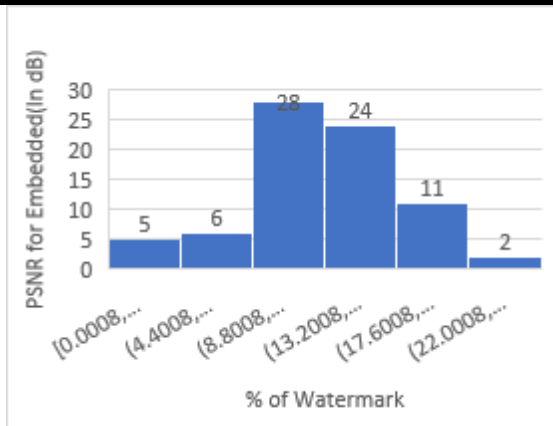
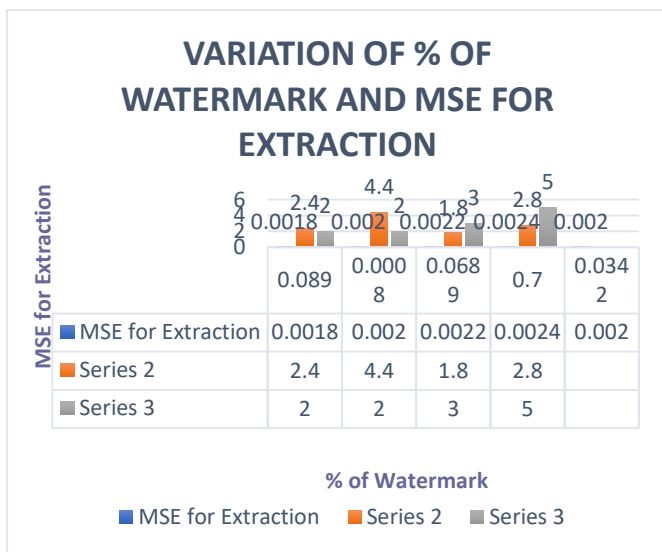


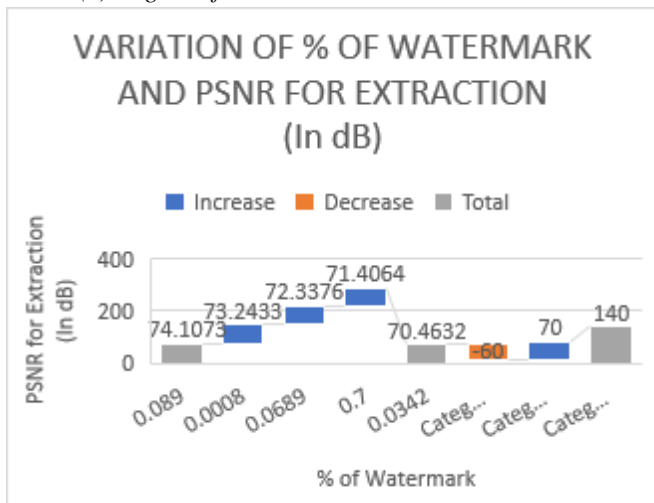
Fig.14: (a) Variation % of watermark and MSE



(b) Fig. % of watermark and PSNR (in dB)



(c) Fig. % of watermark and MSE Extraction



(d) Fig. % of watermark and PSNR Extraction (in dB)

Table.2: For DCT based transform (Values from [8])

SL.N O.	% of waterm ark	MSE for embed ded	PSNR for embed ded (In dB)	MSE for extracti on	PSNR for extract ion (In dB)
1.	0.089	0.0437	29.6702	1.9998e+003	77.6418
2.	0.0008	0.0452	29.3405	0.0103	44.0937
3.	0.0689	0.0439	29.6145	1.1906e+003	72.4558
4.	0.7	0.0491	28.5111	1.2618e+005	119.0881
5.	0.0342	0.0449	29.3947	284.6479	58.146

Graphs:

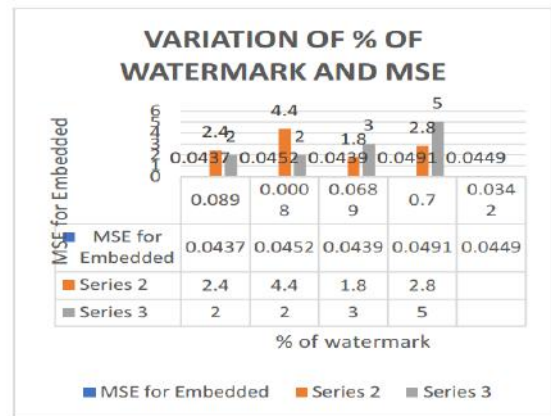
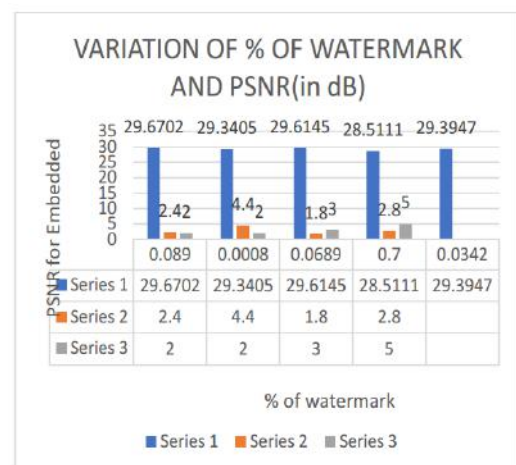
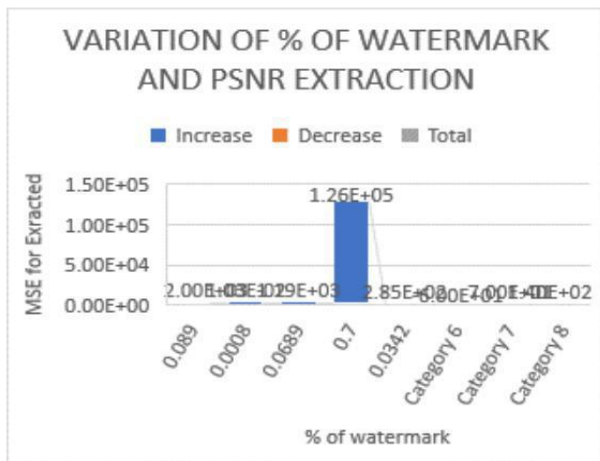


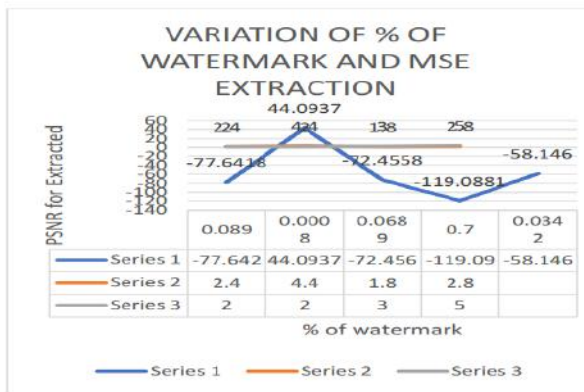
Fig.15 (a) Variation % of watermark and MSE



(b) Fig. % of watermark and PSNR (in dB)



(c). Fig. % of watermark and MSE Extraction



(d). Fig. % of watermark and PSNR Extraction (in dB)

The result what we have got shown in table 1 and 2 related to MSE and PSNR for embedded and extraction in DWT-SVD is improved as compared to DCT. The algorithm DWT-SVD is better than DCT for invisible watermarking.

VII. APPLICATION OF WATERMARKING IN VARIOUS FIELDS

-Television Broadcasting: Broadcast monitoring also watermarking technique is able to track when a specific video is being broadcast by a TV station. Where, information used to identify individual videos which could be embedded in the videos themselves using watermarking, making broadcast monitoring easier.

-Copy control is a very promising application for watermarking. In this application, the watermarking can be used to prevent the illegal copying of songs, images, movies by embedding a watermark in them, that would instruct a watermarking in a compatible DVD or CD writer to not write the song or more because it is an illegal copy.

- The producer of a movie could identify which recipient of the movie was the source of leak. Because the

watermarking could be used to reach recipient of every legal copy of a movie by embedding a different watermark.
 -Medical applications: For providing authentication and Confidentiality without affecting the medical for secure purpose.

VIII. CONCLUSION

The DWT-SVD based transform get better quality of the invisible watermarking. By combining DWT-SVD approaches for watermarking so that their fusion makes very much secure watermarking technique [10]. From the above comparison we found that the DWT-SVD based transform is much better than the DCT based transform. Also, the MSE and PSNR value of DWT-SVD is better than the DCT based transform. Digital watermarking provides owner authentication, Copyright Protection. Digital watermarking tries to hide a message related to the actual content of the digital signal. The simulation results also showing that the watermarking transform method having image quality as well as robust against many common image processing operations by using DWT-SVD based transform in comparison to DCT based transform.

IX. FUTUREWORK

The future work can be implemented on DWT-SVD and DCT based transform on invisible audio and video watermark with comparison of MSE (Mean Square Error) and PSNR (peak Signal to Noise Ratio) with addition of secret key in both audio and video. Using invisible watermarking FFT and LWT will be performed. This work can be extended to watermark an image, audio, video and also use other transform domain techniques individually and measure the various performance parameters. The future watermarking techniques will be equipped with intelligence that reveals the content of image, audio and video.

REFERENCES

- [1] M. Prajapati, "Transform based digital image watermarking technique for image authentication", International Journal of Emerging Technology and Advanced Engineering, ISSN 2250-2459, ISO 9001:2008 Certified Journal, Volume 4, Issue 5, May 2014).
- [2] N .Narula¹, D. Sethi² and ParthaPratim Bhattacharya³, "Comparative Analysis of DWT and DWT-SVD Watermarking Techniques in RGB Images ", International Journal of Signal Processing, Image Processing and Pattern Recognition Vol. 8, No. 4 (2015), pp. 339-348.

- [3] S.A. Mansoori, A. Kunhu, "Robust Watermarking Technique based on DCT to Protect the Ownership of DubaiSat-1 Images against Attacks", IJCSNS International Journal of Computer Science and Network Security, VOL.12 No.6, June 2012.
- [4] MdSaiful Islam and UiPil Chong, "A Digital Image Watermarking Algorithm Based on DWT, DCT and SVD", International Journal of Computer and Communication Engineering, Vol. 3, No. 5, September 2014.
- [5] S. Sirmour, A. Tiwari, "A Hybrid DWT-SVD Based Digital Image Watermarking Algorithm for Copyright Protection", International Journal of P2P Network Trends and Technology (IJPTT) – Volume 6 – March 2014.
- [6] Anjana Gupta, Mukesh Pathela, "Performance Analysis of DWT-SVD-AES Watermarking", International Journal of Electronics & Communication Technology, (IJECT) Vol. 7, Issue2, April - June 2016.
- [7] Asma Ahmad, G.R.Sinha, Nikita Kashyap, "3-Level DWT Image Watermarking Against Frequency and Geometrical Attacks", I.J. Computer Network and Information Security, 2014, 12, 58-63 Published Online November 2014 in MECS (<http://www.mecspress.org/>).
- [8] Rabinarayan Panigrahi, Manini Monalisa Pradhan, Dibyashree Panda, Devasis Pradhan, "Robust Digital Invisible Watermarking for Copyright Protection of Image using DCT (Discrete Cosine Transform)", Journal of Digital Image Processing and Computer Vision Volume 2 Issue 1.
- [9] R. Patel, Prof.A.B.Nandurbarkar, "Implementation of DCT, DWT, SVD based watermarking algorithms for copyright protection", International Research Journal of Engineering and Technology (IRJET), Volume: 02 Issue: 02 | May-2015.
- [10] Y. Pathak, S. Dehariya, "A More Secure transmission of medical images by Two Label DWT and SVD based watermarking technique", IEEE International Conference on Advances in Engineering & Technology Research (ICAETR - 2014), August 01-02, 2014, Dr. VirendraSwarup Group of Institutions, Unnao, India.

Climate Variability and Its implication on Wheat Productivity; Farmers' Adaptation strategies: in Robe Town and Surrounding Area, Oromia Regional State, Ethiopia

Aliyi Mama Gasu

Department of Environment and Climate Change Management, College of urban development and engineering, Ethiopian Civil Service University Addis Ababa, Ethiopia.

Abstract— Climate variability has a drastic impact on wheat output and production. Robe town and its surrounding area, south eastern Ethiopia, is among the highly vulnerable areas. The aim of the study was to analyze climate variability and its implications on wheat productivity in Robe town and the surrounding area. The descriptive experimental and survey research strategy was conducted for this study. ARIMA model was used to forecast medium time scale for mean annual temperature and rainfall. To strengthen the finding of the study primary data on the implication of climate variability on Wheat yields and coping strategies used by the farmers in response to climate variability risk were collected by selecting the sample Households. To select sample Households, first three kebeles were purposively selected based on the numbers of farmers exist in those kebeles. Then probabilistic proportionate to size technique was applied to determine the total sample household size from each kebele. Ultimately, a total of 160 sample household heads were selected by using simple random sampling technique. The results of the study shows that the temperature of the town has increased by 0.04°C and the total annual rainfall shows 0.28mm decrement per year over the years considered. 1mm decrement of spring rainfall would result to 0.014 quintal decrement of wheat yields per hectare per year whereas 1°C increment of annual temperature would result to 1.41 quintal decrement of yield. The current study also found significant variation in the amount of rainfall and temperature. Majority of the coping mechanisms used by the farmers are traditional and destructive. For the future there will be appreciable increase in temperature (0.71 to 1.27°C) and increasing wheat yield fluctuation due to temperature and rainfall instability.

Keywords— Climate variability, Coping strategies, Robe, wheat productivity.

I. INTRODUCTION

Developing countries in general and least developed countries like Ethiopia in particular are more vulnerable to the adverse impacts of climate variability and change. This is due to their low adaptive capacity and high sensitivity of their socio-economic systems to climate variability and change. Climate related hazards in Ethiopia include drought, floods, heavy rains, strong winds, frost, heat waves [NAPA, 2007]. Climate changes over the late part of the 20th century are well documented. Since 1960s, mean temperatures have increased and precipitation has become frequently variable, with extreme drought and flood events occurring with increased frequency. Global models predict future temperatures and precipitation and generally they concluded that many region of the world will become warmer with great precipitation variation and more frequent climatic extremes [UNFCCC, 2006]. For instance, the global average temperature showed a warming of 0.78 (0.72 to 0.85) $^{\circ}\text{C}$ over the period of 1850 to 2012, and current predictions for the end of the 21st century are that global average temperature increase will be between 1.5°C , and 2°C [IPCC, 2013]. Climate changes and variability will directly and significantly affect the current and the future agriculture [Greg et al., 2010]. The changes and variability of fundamental variables; temperature and rainfall, have been profound effects on agriculture in Robe town and its surrounding area [Mekuria, 2015]. Since, wheat production has been significantly affected by climate change and variation in the study area majority of the people in Robe town and surrounding area which in turn depends mainly on the functioning of wheat system as their source of

livelihood and income are highly affected. Therefore, such system may be regarded as more important than a similar system in an isolated area. Moreover, even though climate variability accounts the greatest proportion of agricultural loss in the country as a whole and in Robe in particular, the coping mechanisms are still traditional. Hence, the main objective of the study is to assess major climatic variability and its implications on Wheat production and productivity in Robe town and surrounding area, Oromia Regional State.

Bale administrative zone of Oromia regional state, capital city for Sinana district and Robe city administration. The city is found to the South-eastern part of Addis Ababa at 430kms along the highway through Shashemene or 460kms through Asella. In absolute terms the city is found between the latitude of 7°3'30"N to 7°10'45"N and longitude 39° 57'38"E to 40° 2'38"E. The total proposed area of the city is 8024 hectares according to area measured from the base map of the city surveyed by surveyors of Oromia urban planning institute (Robe Municipality, 2015).

II. METHODOLOGY

The proposed study was carried out in Robe town and its' surrounding Sinana district. Robe city is the capital city of

Table.1.1: Description of study sites

District	Latitude & longitude	Elevation (meters above sea level) (m)	Average temperature (°C)	Average rainfall (mm)	Years of observation	No. of years with no data
Robe	7°7'N 40°0'E	2,492	15	1100	1986-2016	-

Source: Robe Municipality, (2015)

Map of the study area

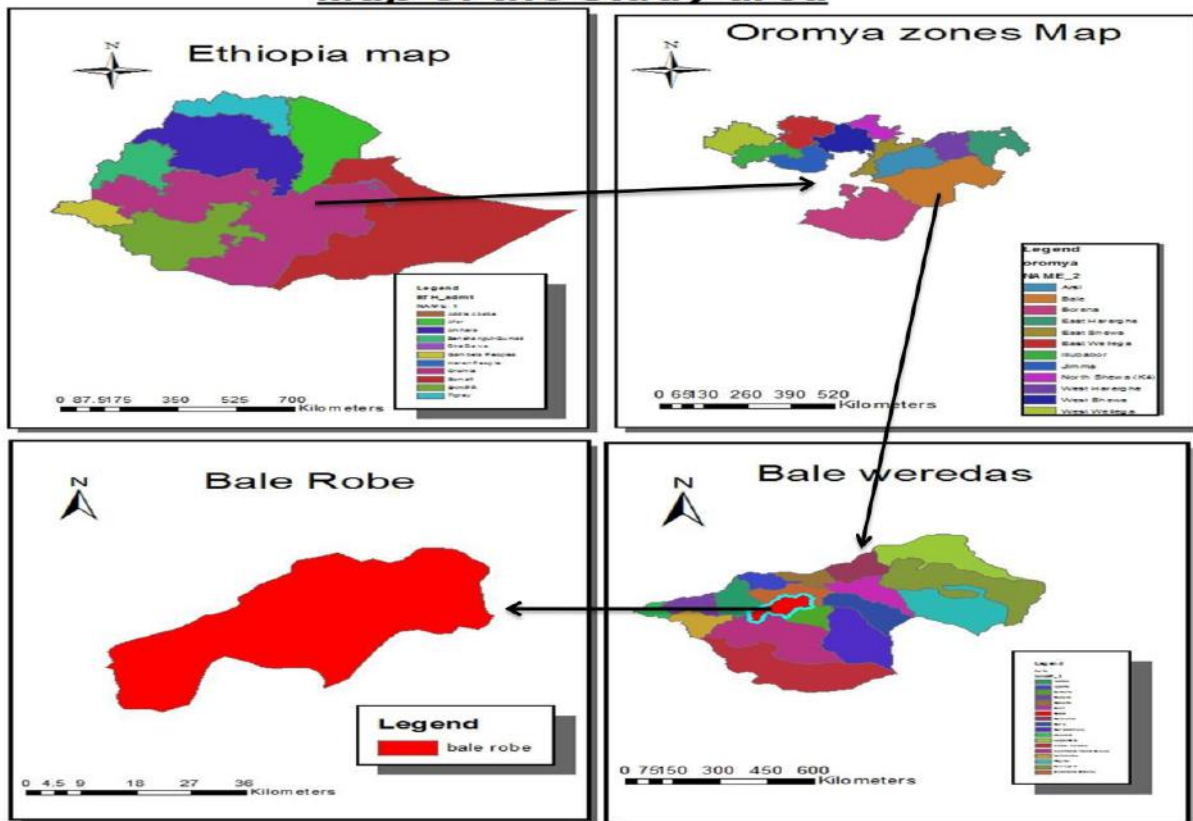


Fig.1.1: Indicator Map of the Study Area

Source: GIS, 2016

2.2. Research Design

A longitudinal research design was used in this study due to its advantage of allowing data to be collected showed long time trends. The design is suitable for descriptive experimental and survey research strategy. The rationale behind employing descriptive type was that it is concerned with describing the characteristics of an event and specific predictions with narration of facts and characteristics about a situation; in this case, the study was analyzed climate variability and its impact on the wheat production and productivity. Moreover, the current study has employed quantitative research approach more dominantly to analyze climate variability and its implications on wheat production and qualitative approach was also employed only to analyze impacts of climate variability on wheat production and farmers' coping measures in the study area using tools like structured questionnaire and key informant Interviews.

To collect secondary data thirty years of climatic data were collected based on IPCC scenario which recommends the thirty years of data for time series analysis of climatic variability and change. Coming to primary data, the two stage sampling design was used to select the sample households. In the first stage, three kebeles (namely Hora Boka, Nano Robe and Kabira Shaya Temo), which were recently expected to be mixed with Robe town and where the large number of farm households are prevalent were purposively selected by the help of land use and administration office workers. In the second stage, according to the number of total Households in each kebele, probabilistic proportionate to size technique was applied to determine the total sample household size from each kebele. Ultimately, a total of 160 sample household heads were selected by using simple random sampling technique.

To analyze the data, both descriptive and inferential statistics were used. The data was edited, coded, and tabulated based on the nature and type of the obtained data on the assessment of climate variability trends, its implications on wheat production and productivity and its coping mechanisms. Hence, descriptive and inferential data analyses were conducted using excel, Origin software and Statistical Package for Social Sciences (SPSS) version 20.

One of the objectives of this research was to determine the medium range forecast of rainfall and temperature from the past observation in the study area. Modern time series forecasting methods was essentially rooted in the idea that the past tells us something about the future. For this purpose, linear time series ARIMA model was used to forecast from 10 to 20 years of time series. ARIMA model and its variations were based on famous Box-Jenkins

principles. The ARIMA (p, d, q) forecasting equation was used where: p, d and q are integers greater than or equal to zero & refers to the order of the autoregressive integrated and moving average (ARIMA) parts of the model respectively.

2.3. Model selection and Approach

The current research was employed quantitative research techniques to analyze the data. Quantitative data analysis was carried out using both ARIMA and inferential statistical tools such as multiple regressions and time series trend analysis as necessary. In the multiple regression dependent variable (wheat yield) and independent variables (annual mean temperature, mean spring temperature, total annual rainfall and total spring rainfall) were calculated and entered in the software. Hence, the functional relationship between wheat productions and some climatic variables namely annual rainfall and number of rain days in a given years were analyzed by using Auto Regressive Integrated Moving Average (ARIMA) approach which is commonly used in time series data for prediction and determining the relationship between variables [Bosello, F. and Zhang, J. 2005]. The ARIMA models work under the basic assumption that some aspects of the past pattern will continue to remain in the future; that is current data have some effect from the previous data which leads to autocorrelation. Main advantages of ARIMA model is its ability to account for autocorrelation problem which OLS linear regression model does not, ARIMA models discover the patterns in the variation not explained by a regression model and incorporate those patterns into its model, according to, Hanke and Wichern [2009]. ARIMA model is suitable for both short term and long term forecast, besides the said advantages the ARIMA model has some weaknesses; ARIMA model needs large amount of historical data and it is not easy to update the parameters of ARIMA model as new data becomes available. In addition to these model summary was considered to check what percent the predictors explain the dependent variable. Moreover, first moments of variation (minimum, maximum, mean, and standard deviation) was obtained using descriptive analysis. Besides, inter annual fluctuation of rainfall, standardized rainfall anomalies, was also calculated. Thus, R square and adjusted R square was interpreted.

The information gathered through interviews was reported through narrative descriptions to complement those that were generalized through software. Finally, conclusions and recommendations were based on research findings and

preceding facts. The regression equations that were used for trend analysis is:

$$Y = \beta_0 + \beta_1 X_{i1} + \beta_2 X_{i2} + \varepsilon \dots\dots\dots \text{Equation-1}$$

Where Y = Wheat yields in Quintals' per hectare of i^{th} year

X_{i1} = Average annual millimeters of rainfall of the i^{th} year

X_{i2} = Average annual degree Celsius of

temperature of the i^{th} year

β_0 = Regression constant.

β_1 = Regression slope

ε = random disturbance term/error term in the observed value for the i^{th} year

The magnitudes of the trend was calculated and estimated by global model ordinary least squares (OLS) linear regression method. That is;

$$\hat{Y} = a +$$

$$bX \dots\dots\dots \text{Equation-2}$$

Where a is a constant which gives the value of Y when $X=0$. It is called the Y -intercept. b is a constant indicating the slope of the regression line, and it gives a measure of the change in Y for a unit change in X . It is also regression coefficient of Y on X .

a and b are found by minimizing

$$SSE = \sum \varepsilon^2 = \sum (Y_i - \hat{Y}_i)^2 \dots\dots\dots \text{Equation-3}$$

Where: Y_i = observed value, SSE - Sum Square of Error

\hat{Y}_i = estimated value = $a +$

$$bX_i \dots\dots\dots \text{Equation-4}$$

Minimizing $SSE = \sum \varepsilon^2$ gives

$$b = \frac{\sum (X_i - \bar{X})(Y_i - \bar{Y})}{\sum (X_i - \bar{X})^2} =$$

$$\frac{\sum XY - n\bar{X}\bar{Y}}{\sum X^2 - n\bar{X}^2} \dots\dots\dots \text{Equation-5}$$

$$a = \bar{Y} -$$

$$b\bar{X} \dots\dots\dots \text{Equation-6}$$

In this case $\beta_0 = a$ and $\beta_1 = b$

It was hypothesized that there is no trend in the amount of rainfall or temperature over time. Thus the null hypothesis was stated as; $H_0: \beta_1 = 0$. Variability of annual and seasonal rainfall was assessed using Coefficient of Variation (CV), techniques. It was calculated as the ratio of standard deviation to the mean. In addition, first moments of variation (minimum, maximum, mean, and standard

deviation) were obtained using descriptive analysis. Besides, the Inter annual fluctuation of rainfall, standardized rainfall anomalies, was calculated as follows:

$$SRA = (P_t - P_m) / \sigma$$

where:.....Equation-7

SRA: is standardized rainfall anomaly,

P_t : is annual rainfall in year t ,

P_m : is long-term mean annual rainfall over a period of observation and σ : is standard deviation of annual rainfall over the period of observation. Standard rainfall anomalies and mean annual temperature were plotted against time (in years) to visualize the time series variation of annual and seasonal rainfall as well as temperature about the mean. The t -test was used to evaluate statistical significance of the trend at 95% confidence level [Time Series Research Staff, 2016].

2.4. Calibration of prediction model

Real-time seasonal forecasts need to be complemented by an extensive set of retrospective forecasts. Calibration depends on the comparison of past observations against the corresponding retrospective forecasts, so that, long-year data can be arranged accordingly in the format of seasonal climate prediction model. Half of the total year, available rainfall data was used for model construction and the rest data have been used for verification.

Therefore, more years were available for producing retroactive forecasts. Model calibration perform as follows; first, check seasonal forecasts required an estimate of skill and reliability of the forecast system or model is necessary to provide such skill assessments. Secondly, values generated from the model were then calibrated against the observations and remove biases that are often part of the dynamical prediction systems. Hence, the observed data in the past years was taken by assuming that it is going to be predicted then after interring the data in to the model some of the techniques were used in order to compare pairs of predicted and the observed data to which they pertain to proportional correction was also checked. when the difference between the actual and the predicted one is -0.5 to 0.5 then it is the most direct measure of the accuracy of categorical forecasts but when it is beyond this value it was rejected [David, 2002].

III. RESULTS AND DISCUSSION

3.1. Trends of Climate

3.1.1. Total annual rainfall Trend of the Robe town from 1986-2016

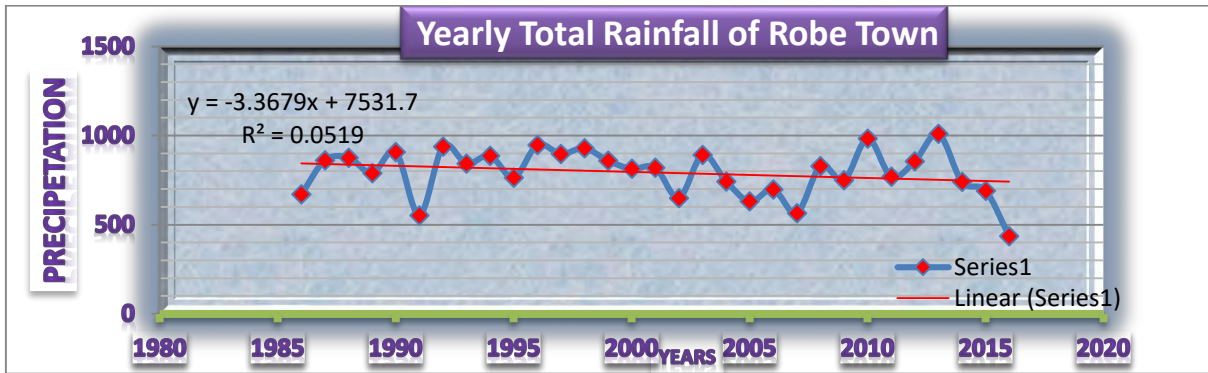


Fig.3.1: Total Annual rainfalls of Robe Town from 1986 to 2016

Source: computed from NMA, 1986-2016

As clearly drawn in Figure 3.1, the total annual rainfall pattern over 30 years for Robe station has been decreased by 3.37mm per year. The average annual rainfall for 30 years (1986 to 2016) was 792.65 mm. The variability is very high that the annual rainfall for these years ranged from 434.7mm (2016) to 1009.5mm (2013), with high variation over the year 1986 to 2016. In general, the total annual rainfall of Robe station has decreasing by 3.37mm per year.

Table.3.1: Total mean, maximum and minimum rainfalls of Robe Town from 1986 to 2016.

District	Variable	Minimum	Max	Mean	CV%	Std. Deviation
Robe	Precipitation	434.70 in 2016	1009.50 in 2013	792.65	20.7	134.43743

Source: Computed from NMA, 1986-2016

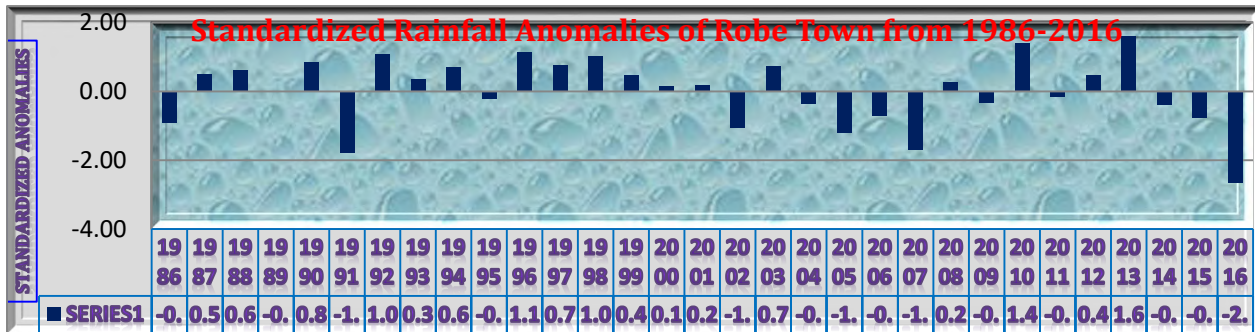


Fig.3.2: Standardized anomalies of annual rainfall in Robe town from 1986-2016.

Source: Computed from NMA, 1986-2016

As clearly evident from Figure 3.2, the standardized anomalies of annual rainfall was calculated for the station, during the periods between 1986 and 2016 noticed the proportion of negative anomalies ranged from 41.9% to 61.3% in Robe from the total observation. In all the years annual rainfall has shown negative anomalies for much of the years.

Based on the result of Coefficient of Variation in Robe over the last three decades it is considered as drought area and that is why currently it is affected by climate variability impact. Because, area with Coefficient of Variation >30, are classified as drought [Australian, 2010]. The year 2016 was

come up with the lowest rainfall record from all the years and showed the worst drought year (SRA <-2.66). The other drought year include 1991, 2002, 2005 and 2007. According to the research reported by Dereje et al, [2004], the drought severity classes are extreme drought (SRA < -1.65), severe drought (-1.28 > SRA > -1.65), moderate drought (-0.84 > SRA > -1.28), and no drought (SRA > -0.84). The best cause of variability of rain fall is the El Niño-southern Oscillation (ENSO). The warm phases of ENSO (El Niño) have been associated to reduced rainfall in the main rainy season in north, central, and southern Ethiopia causing severe drought and famine [Woldeamlak et al, 2007;

Australian, 2010]. Besides, the result of the current study stated that some of the period mentioned was coincide with previous research in Ethiopia. According to different literatures 1994, 1995 and 2002 years were drought years in many part of Ethiopia [Woldeamlak et al., 2007; Getenet, 2013].

This means that the decline in precipitation in this period indicates the finding of the study support previously investigated research reports. Therefore from the result, the distribution of the current research rainfall is not the same in Robe town from time to time. Hence, even though positive anomalies were observed in some of the years under the study period, Robe station noted proportion of negative anomalies ranged from 41.9% to 61.3% from the

total observation (Table 3.1). All in all Rainfall is the major climate parameter with the highest degree of temporal variability in the station shows year to year variability or fluctuation within the year. Such variation of rainfall between the years is due to changes in space-time patterns of one or more of the climate-controlling systems movement of the ITCZ.

3.1.2. Seasonal precipitation Trend of Robe Town from 1986 to 2016

Periodic linear trend models were fitted on mean precipitation of seasons of different months to determine if there is significant trend in mean precipitation of the past consecutive 30 years of winter, spring, summer and autumn.

Table.3.3: Seasonal mean rainfall and coefficient of variation over 30 years in Robe town.

Stations	Winter		Spring		Summer		Autumn	
	mean (mm)	CV%						
Robe	56.1	69	244.8	36	277.7	35	220.8	26

Source: Computed from NMA, 1986-2016

Hence, the seasonal precipitation in Robe in the study period matches with the previous finding which means rainfall is the major climate parameter with the highest degree of temporal variability in all the time scale in months, years, and in seasonal scales shows variations in Robe town in general.

3.1.3. Mean Annual Temperature trends of Robe town from 1986-2016.

The results in Figure (3.3) show that there is statistical significant change (0.04°C) per year. The yearly maximum temperature of the past 30 years of Robe town was 22.22°C with the average minimum value of 8.5°C.

According to Getenet [2013] the coldest temperatures generally occur in December or January and the hottest in February, March, April, or May. However, in many localities July has the coldest temperatures because of the

moderating influence of rainfall. May is a hot and dry month, preceding the long rainy season in June, July, and August [NMA, 2007]. Hence, over the past three decades in Robe town the result of temperature indicates that its pattern of is not uniform from month to month. Such temperature variation is due to the climate-controlling systems, movement of the ITCZ. The minimum temperature is more variable since its moving average is (0.0430c) than the maximum temperature (0.0380c). The trend shows that both the maximum and minimum temperature of the Robe town will continue to raise in the future. Trends in mean annual temperature variations in the Robe town, from 1986-2016, shows an appreciably rising trend of 0.40c per decades. This result is greater as other scientific literature conducted at national and international on assessing temperature variability indicated.

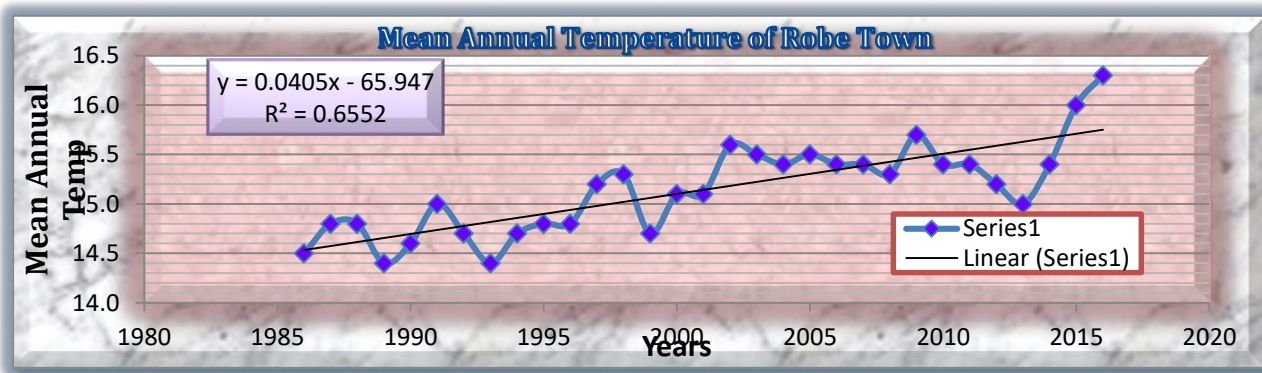


Fig.4.5: Trends in mean annual temperature variations in Robe town from 1986-2016.

Source: Computed from NMA, 1986-2016

3.1.4. Analysis of seasonal mean temperature from 1986-2016

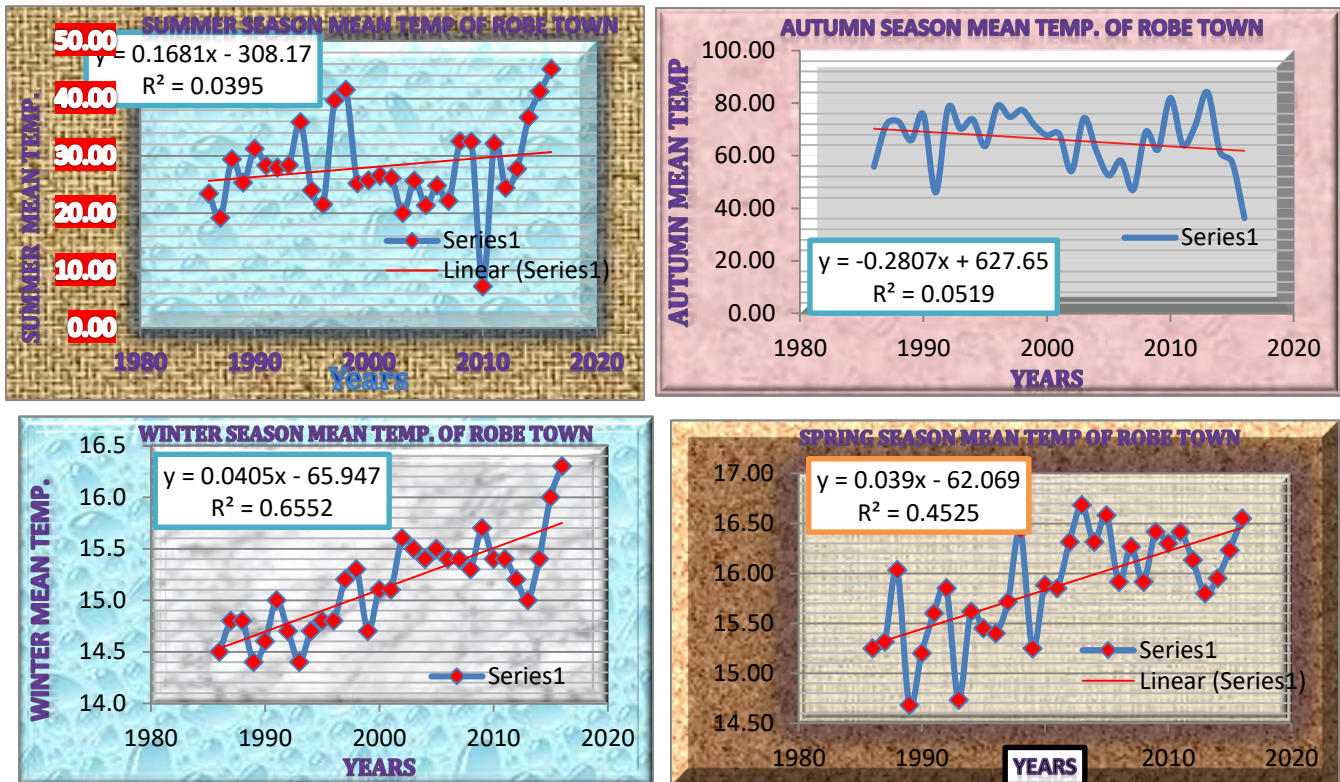


Fig.3.4: Analysis of seasonal mean temperature from 1986-2016

Source: Computed from NMA, 1986-2016

As presented in Figure (3.4), seasonal average temperature was increased over all seasons but the magnitude of the trend varies from season to season. The mean temperature of spring and summer had increased by 0.04°C/year or 0.4°C per decade in Robe. In the autumn season the maximum increase was (0.05°C/year or 0.5°C per decade) and that of the winter season had increased by 0.03°C/year or 0.3°C per decade in Robe.

3.2. Forecasting mean annual temperature and precipitation with the ARIMA Model

For climate variability trends and wheat production prediction purpose ARIMA model is developed using Equation $Y(t) = 0.0372 + 0.9749\varepsilon(t-1)$ and $Y = \beta_0 + \beta_1 X_{i1} + \beta_2 X_{i2} + \varepsilon$. In Equation, $Y(t)$ is the forecasted temperature or rainfall at time t . In the AR part, p is the order of the AR process (lingering effects of previous observations) and I is the AR coefficient (trends). In the MA part, q is the order of the MA or error term of the MA coefficient and $\varepsilon(t)$ is the white noise that produces random uncorrelated variables with zero mean and constant variance. The second Equation is for wheat production prediction.

Hence, as the temperature predicted in the study area showed the town will see further warming in the next

twenty years at different rates. Which means as the number of years increases the change in degree Celsius increases to the observed time (mean temperature of 1986-2016). For example the temperature will increase by 0.730c, 0.910c, 1.10c and 1.270c by 2020, 2025, 2030 and 2036 respectively in Robe which is consistent with the result of Getenet, [2013] who implied that the mean annual temperature will increase in the range of 0.9 -1.1 °c by 2030; in the range of 1.7 - 2.1 °c by 2050 and in the range of 2.7-3.4 °c by 2080 over Ethiopia compared to the 1961-1990 normal. In addition to this a small increase in annual precipitation is also expected over the study area. Unlike temperature in case of rainfall, Robe station shows different result. As observed from the (Table 3.4) the precipitations will decrease at different millimeter from the observed amount of rainfall (mean of 1986-2016). However, the output of the model also shows neither increasing nor decreasing for in the next few years in Robe town. This shows variations of rain fall will also continue not only in the past but also in the future between years. Regarding wheat yield per hectare per year of the study period in Robe town and surrounding area it is forecasted that as it will be sharply decreased per hectare per year from 2025 onward

even though for the next 10 years there will be an increment. This is due to the fact that currently existing temperature in Robe town is at the lowest boundary of

temperature requirement for wheat production which in turn gives some guarantee for wheat production.

Table.3.4: Data summary for mean temperature, precipitation & Wheat yield forecast for 20 years computed by ARIMA model and data for hypothesis tested. Source: Computed from NMA, 1986-2016.

Station	Mean annual temperature (°C) From 1986-2016	projected change by 2020 (change in°C)	projected change by 2025 (change in°C)	projected change by 2030 (change in °C)	projected change by 2036 (change in°C)			
Robe	15.09	+0.71	+0.9	+1.1	+1.27			
	Mean annual precipitation (mm) From 1986-2016	projected change by 2020 (change in mm)	projected change by 2025 (change in mm)	projected change by 2030 (change in mm)	projected change by 2036 (change in mm)			
	865	0	-32	-15	-12.1			
	Annual Wheat yield in quintals per hectore From 1995-2016	projected change by 2020 (change in mm)	projected change by 2025 (change in mm)	projected change by 2030 (change in mm)	projected change by 203 6 (change in mm)			
	26	+4.43	+13.34	+8.6	+7.8			
Hypothesis Tested								
	t	df	Mean	Std.	Sig. (2 tailed)	Std. Error Mean	95% Confidence Interval	
							Lower	Upper
Mean monthly rainfall	.000	30	68.36	38.79	1.00	11.19890	-24.6503	24.6470
Mean seasonal rainfall	-.020	30	199.9	37.35	1.00	6.70741	-13.8306	13.5661
Mean Annual Rainfall	-47.84	30	233.5	65.074	0.986	11.688	-583.04	-535.30
Medium term future pattern of rainfall	-.003	20	826.7	44.6	.998	9.97	-20.90	20.84
Mean Annual Temperature	.036	30	15.36	.74078	.971	.13305	-.2669	.2766
Medium term future pattern of temperature	12.999	20	16.45	.377	1.00	.08422	.9185	1.2711

3.3. Impacts of climate variability on wheat productivity

There have been changes due to climate variability over the last three decades. Hence, the impacts of this climate variability on wheat productivity in the study area are presented in detail as follows:

3.3.1 Impacts of climate variability on wheat productivity by multiple regressions

Under this subsection the actual impacts of climate parameters (mean annual temperature, mean spring temperature, total annual rainfall and total spring rainfall) on wheat were analyzed by using multiple regression models. The model also revealed to what extent the independent variables explains productivity. So the following table indicates the impacts of climate variability on wheat productivity in the study area.

Table.3.5: Regression analysis

Model Summary								
Model	R	R Square	Adjusted R Square	Std. Error of the Estimate	Mean Square	F	Sig.	df
1	.537 ^a	.288	.169	4.40056	46.962	2.425	.099 ^b	3
Dependent Variable: Yearly Wheat product per Hectore								
Predictors: (Constant), Total spring season rainfall, Total Annual Rainfall, Average Temperature								

Coefficients ^a						
Model		Unstandardized Coefficients		Standardized Coefficients	t	Sig.
		B	Std. Error	Beta		
1	(Constant)	36.998	32.945		1.123	.276
	Mean Annual Temperature	-1.409	1.770	-.205	-.796	.437
	Total Annual Rainfall	.010	.009	.281	1.124	.004
	Total spring season rainfall	.014	.015	.201	.949	.355

a. Dependent Variable: Yearly Wheat product per Hector

Source: Computed from SARD and NMA

As presented in Table 3.5, wheat productivity is significantly associated with spring rainfall and mean annual temperature. This means an increment of 1 mm of spring rainfall is likely to result in an increment of 0.014 quintal of wheat yields per hectare per year and 1^oc increment of temperature is likely to result in a decrease of 1.41 quintal of wheat yields per hectare per year (see Table 3.5).

As indicated by Walther, et.al, [2000] indicated, the effects of rainfall and temperature on wheat yield depend on certain threshold. If a variability beyond or below the threshold happened, wheat yields will be negatively affected. On the other hand, as FAO, (2015), indicated wheat yield shows some correlation (R= 0.47) with El Niño sea surface temperature anomalies which is highly predictable factors of cereal and crop production and productivity. In agreement to this but far from it, the problems in Robe town for 2015 and 2016 might agreed with this conclusion for wheat production and productivity. In fact, 2015 and 2016 was characterized by rather unfavorable weather over the whole of the country except for some parts, which experienced an exceptional drought (lasting until the winter 2016). As a matter of fact, the impact is delicated due to the complex Ethiopian topography and climate patterns are contrasted between the influence of the Alps in the north and the hot and dry Indian Ocean in the south. Hence, the outcome of this study states that through regression analysis of climatic parameters in Robe town; 1mm decrement of spring rainfall would result to 0.014 quintal decrement of wheat yields per hectare per year whereas 1mm increment of annual temperature would result to 1.41 quintal decrement of productivity in the study period in Robe town.

So the researcher observed that temperature and spring rainfall are responsible for the decline and fluctuation of wheat over the years because one can see two things in wheat productivity trends. That means there is decreasing trends and within decreasing again there is fluctuation. On the other hand the impacts of total annual rainfall and spring temperature are also observed in the regression result. Even though, no significant impact of total annual rainfall are observed in Table 3.4, both spring rainfall and mean annual temperature are the most key factors for the fluctuation and decline of wheat productivity in the study area. Because both spring rainfall and mean annual temperatures are significantly influence the yields of wheat per year since p value is <0.05 at 5 % level of confidence. Furthermore, the independent variables (predictors) can explained about only 28.8 % by R square or 16.9 % by adjusted R of the dependent variable (productivity). Hence for total annual rainfall, the p value is <0.05 that indicates as there is significant impact for the fluctuation or wheat productivity decline over the years considered. However, the p value of mean spring temperature and Mean annual temperature is > 0.05 which indicates that there is no significant impact for the fluctuation or wheat productivity decline over the years considered. Therefore, the finding of this research agreed with Curtis, [2009] that strengthen the climate variability can affect wheat production through the direct effects on yield via physiological processes, through changes in sowing dates or increased rainfall, and through changes in the areas under production and as regions become more or less unsuitable for wheat due to climate variability.

3.4. Farmers' coping strategies

3.4.1 Farmers' response on the methods to cope with the basic commodities and services in Robe town

Table.3.6: Farmers’ response on the Methods to cope with the Basic commodities and Services in Robe town

Variable	Frequency	Percent
eat less	6	3.8
selling/rent the wheat farming itself and others asset	5	3.1
Asking credit from relatives or rural financial institutions	13	8.1
Depend on relatives and NGOs Support	11	6.9
Exposed to Hunger, illness in home, withdrawal of children from school	2	1.3
Engaged in off farm activity	123	76.9

Source: field survey, 2016

Based on the sample survey results in (Table 3.6) 76.9 % of Farmers who were asked to mention how they are surviving since income did not enough all-round the year; reported that they engaged in off farm activity and 8.1% of them said that they request credit from relatives or rural financial

institutions. Meanwhile the others 6.9%, 3.8%, 3.1 and 1.3% elaborated as they depend on relatives, NGOs support;eat less; selling/rent the farm itself and others asset and exposed to hunger, illness in home, withdrawal their children from school and etc.

3.4.1.1 Alternative options to reduce the problem used by local farmers

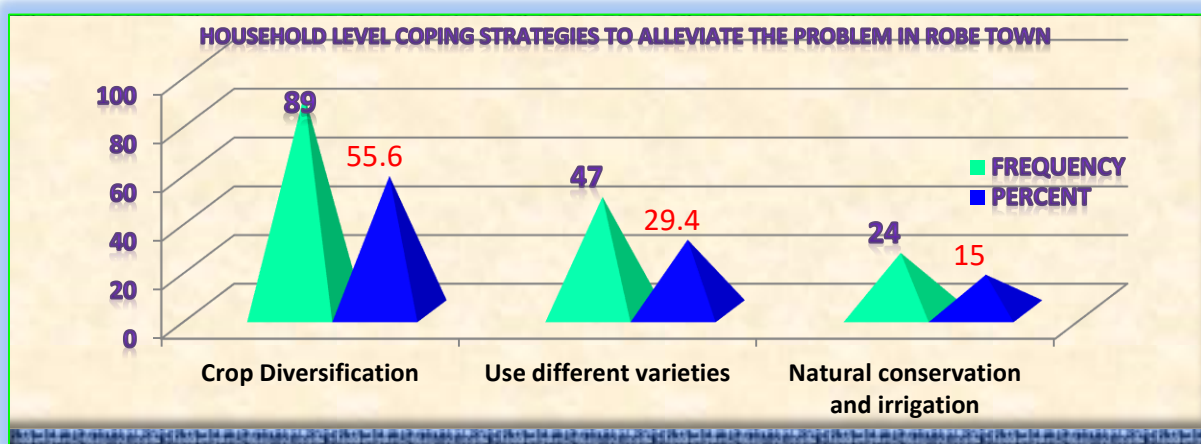


Fig.3.5: Farmers’ response on what they do at the household level to alleviate the problem in Robe town

Source: field survey, 2016

As presented in the (Figure 3.5), 55.6 % of the respondents’ do crop diversification at the household level to alleviate the problem in the area, 29.4% of them use different varieties and 15% are said they conserve nature, use irrigation at household level to alleviate the problem.

The result of this study revealed that, Effective coping initiative is a multistage process and a careful understanding on traditional and institutional coping strategies. Hence, regarding possible coping strategies to combat climatic variability in the study area, respondents suggest that coping mechanism to climate change are by crop diversification, use different varieties and natural conservation and irrigation, Households in these Kebeles tend to allocate their fixed land (by village and Households) from their customarily farming practice to new [Figure,3.5]. For instance, the midland wheat based area is shifting their land

from growing maize and wheat to teff and barley. Similarly, some of the Households shift their time, labor and land resource from crop plantation to livestock production etc. Moreover, some of the respondents sustain all year round by using the previous saving in various forms. On the other hand, about quarter of them used diversification of their income and small scale irrigation systems like horticulture and near river banks during dry seasons [3.6]. Majority of them reported as they engaged in off farm activity and others suggest that “selling their Wheat farm and other assets, renting their land and selling labor. On the other hand, some of them used credit from rural financial institutions and private money lenders. However, the private rural money lenders system exacerbates their problem since rating system is illegal (locally areta system). Because “we pay at the rate of 50 % at the end of Wheat harvesting

season” they said. So in the subsequent year “we also remain suffering due to the expense of previous year” they said. About few of them are coping by minimizing their daily consumption [Table 3.6].

IV. CONCLUSIONS

Contrary to the expected direction of trends and variability, this study found significant variation in the amount and distribution of monthly, annual and seasonal rainfall as well as temperature. The calculated standardized rainfall anomalies and coefficient of variation showed good agreement indicating there was high variation of rainfall in the area. As a result of rainfall variations the districts become vulnerable to recurrent drought. El-nino and topographical setting may be the main factor for its variation. Concurrently, at 5% level of significance, by the coefficient of regression line the mean monthly temperature, annual mean temperature and seasonal average temperature has increased for Robe town from time to time. Statistical models, based on indicators of climate have been developed to anticipate shifts in Rainfall, temperature and crop yield in Robe town. Thus, a medium term future pattern of mean annual temperature is found significantly greater in the amount for future than the previous monthly, annual and seasonal temperature. Hence, prediction by ARIMA model showed in the next twenty years; Robe station will see more warming at different rates as the time increases (0.71 to 1.270c). But, from other years 2036 will see more warming. On the Other side, rainfall and wheat yield showed mixed result in the next 20 years for the district. For instance, 2025 will see more decline of rainfall than any other years.

Regarding the implications of climate variability on wheat yields in the study area there is significant linear relationship between Wheat yields and climate variability. Hence, Wheat yields are significantly declined and fluctuation of productivity is associated with mean annual temperature, spring rainfall and mean annual temperature. Therefore, increasing climatic trends and seasonal variations led to a conclusion that the productivity of Wheat in the study area has been negatively affected by rising mean temperatures and seasonal precipitation variation rather than annual rainfall. The observed climate change patterns and impacts which were diverse temporally and impose their impacts on crop development and production have become significant in Robe town. The most important conclusions to be drawn from the study are that most of the farmers have been using traditional coping strategies such as selling their Wheat farms and other assets, credit from

rural money lenders; even though some of them suggested that crop diversification, use different varieties and natural conservation and irrigation are some of their coping strategies. In addition to this, they have been coping by, engaging in off-farm activities such as charcoal selling and temporal and permanent migration and minimizing of their daily consumptions. Thus, most of the coping strategies farmers have been using are destructive rather than constructive and depletive ones.

Therefore, it is recommended that, The office of agriculture in collaboration with Oromia agricultural enterprise Robe branch should encourage farmers to better adapt to future climate condition, by providing new breeds that can stand with climatic change, genetic improvements to identify more drought resistant wheat varieties in addition to link farmers to relevant research institutions to promote access to certified seeds of these varieties. Again government institutional coping strategies should be incorporated for the sustainability of farmers coping strategies; in addition to integration and effective collaboration of all sectors of stakeholders for conservation of water and natural resources. Last but not list, for more confidence further studies by including additional climate models, farmers’ perception and additional stations is recommended.

V. ACKNOWLEDGEMENTS

The authors would like to express their sincere thanks to Civil Service University which helped us in buying Model that is used to made prediction, informants who work under the various offices of Ethiopian National Meteorological Agency, Robe town administration, Sinana Woreda Agricultural office, Oromia agricultural enterprise Bale Branch office, and Bale Zone agricultural office. Our special thanks also extend to three kebeles farmers and DAs of Sinana Woreda (Kabira Shayatemo, Hora Boka and Nano Robe) for giving us relevant information and for their kind cooperation.

REFERENCES

- [1] Australian Bureau of Metrology, (2010). Rainfall variability in Australia. <http://www.bom.gov.au/climate/data/index.shtml>. Accessed on 23/12/2015.
- [2] Bosello, F. and Zhang, J. 2005, *Assessing Climate Change Impacts: Agriculture*. Venice, Italy: CCMP – Climate Change Modelling and Policy.
- [3] Curtis B.C., H. Gómez Macpherson, S. Rajaram, 2009, *FAO Plant Production and Protection Series bread*

- wheat improvement and production, Food and agriculture organization of the united nations, Rome.
- [4] David D. Houghton, 2002, *Introduction to climate change: lecture notes for meteorologists* Prepared by WMO-No.926 Secretariat of the World Meteorological Organization Geneva Switzerland.
- [5] Dereje T. Kinde,T. and Mulugeta, 2004, *Climate Change, Variability and vulnerability in Ethiopia. Journal of African Agriculture and development*, Addis Ababa, Ethiopia.
- [6] FAO, 2015, *The State of Food and Agriculture (SOFA) report*, retrieved in Jan 2016: <http://www.fao.org/docrep/013/i2050e/i2050e.pdf>.
- [7] Getenet K., 2013, *Spatial and Temporal Uncertainty of Rainfall in Arid and Semi-Arid Areas of Ethiopia*, Department of Geography and Environmental Studies, College of Social Science and Education, Wollega University, Post Box No: 395, Nekemte, Ethiopia.
- [8] Greg,P.,Ingram, J., and Brklacich, M., 2010, *Climate Variability and food security, Philosophical Transaction of the Royal Society B*, 2139 - 2148.
- [9] Hanke, J. E. and Wichern, D. W., 2009, *Business Forecasting*, (9th Edition.), Pearson International, London, 512 pp.
- [10] IPCC, 2013, *Summary for Policymakers*, In Climate Change 2013: The Physical Science Basis. Contribution of Working Group I to the Fifth Assessment Report of the Intergovernmental Panel on Climate Change.
- [11] MekuriaTefera, 2015, *Wind Resource Assessment in Bale Zone*, South Eastern Ethiopia, A Thesis Submitted to a School of Natural Science, Maddawalabu University. Unpublished.
- [12] NAPA, 2007, *Climate Change National Adaptation Programme of Action Ethiopia*, Addis Ababa.
- [13] NMA, 2007, National Meteorology Agency: *Final Report on Evaluation Criteria for Identifying High Priority Adaptation Activities*; prepared by B and M Development Consultants for NMA, Addis Ababa, Ethiopia.
- [14] Robe town municipality, 2015, Municipality annual report unpublished data.
- [15] Time Series Research Staff (2016). *Center for Statistical Research and Methodology*; U.S. Census Bureau Washington, DC; <http://www.census.gov/srd/www/x13as/>
- [16] UNFCCC, 2006, *Climate change: impacts, vulnerabilities and adaptation in developing countries*.
- [17] Walther G., Post E., Convey P., 2002, *Ecological responses to recent climate change*. Nature, 416:389–395.
- [18] Woldeamlak B. and Conway D., 2007, *A note on the temporal and spatial variability of rainfall in the drought-prone Amhara region of Ethiopia. International journal of climatology*, 27:1467– 1477.

Structural and Electronic Properties of Cis-platin Metal Complex: B3LYP-SDD/DFT Calculations

Faeq A. Mohammed, Hamid I. Abbood

Babylon University-College of Science, Najaf road, Babil, Iraq

Abstract—Current work deals with the structural and electronic properties of the cis-platin by employing the B3LYP density functional theory with SDD basis sets at the Gaussian 09 package of programs. We showed a good relax was obtained for the cis-platin. The great contribution for constructing the molecular orbitals is due to the outer electrons in the platinum metal with few contributions from the p-orbitals of the ligands, cis-platin has insulating behavior. Also, the cis-platin has low electronic softness and it needs high excitation energy to electron transfer or to accepting an electron from the surrounding species.

Keywords: cis-platin, SDD basis sets, ionization energy, softness and electrophilic index.

I. INTRODUCTION

Since the discovery of the activity of one of the most effective anticancer compound [cis-(NH₃)₂PtCl₂], cis-iaminedichloroplatinum(II), where clinically named cis-platin thousands of platinum complexes have been synthesized and evaluated for their anticancer activity. Cis-platin was first discovered and synthesized by Peyrone in 1844 but, unfortunately, its biological activity was discovered much late by Rosenberg and et al., its represented the first inorganic metal complex compound introduced in clinical using for the treatment of the cancer [1-5]. Cis-platin remains in the middle of the most widely used platin chemotherapeutics, with particular effectiveness in the treatment of cancer. The pharmacodynamics properties of Cis-platin can also be modified in a markedly diverse way by targeting biological substrates distinct from DNA. Cisplatin is a prototype of several thousand platinum [6-12]. Quantum chemical studies of the molecular and electronic structure, and prediction of spectroscopic characteristics of pharmacologically active compounds,

have always been challenging for computational chemists. Moreover, such data are quite useful for better understanding the reactivity of the drugs with physiological target molecules [2,5].

II. COMPUTATIONAL DETAILS

The calculations in present work are carried out theoretically by employing three parameters B3LYP(Becke's three parameter exchange with Lee, Yang, and Parr correlation functional) density functional theory and SDD (Stuttgart Dresden triple zeta ECPs (Effective-Core Potential)) basis sets. The SDD basis sets possible quality for the system of interest for heavy metals use relativistic ECPs, it is powerfully recommended for the heavy metals [14,15].

III. RESULTS AND DISCUSSION RESULTS

Fig. 1 represents the relax structure of cis-platin compound. The standard orientations as Cartesian coordinates in Angstroms for all atoms in the studied compound were listed in Table 1. Table 2 illustrated the resultant theoretical optimized parameters for the studied structure involve the bond length in Angstrom A° and bond angle in degree. As shown, the calculated values of bonds and the angles using SDD basis sets in present study are in good agreement with the experimental data [16].

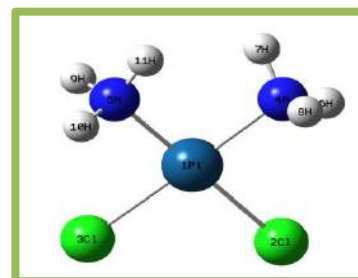


Fig.1: The relax structure of cis-platin.

Table.1: The standard orientations for all atoms in the cis-platin.

Atom	X	Y	Z
Pt	-0.000007	0.195450	-0.000010
Cl	1.781581	-1.402826	0.000049

Cl	-1.781643	-1.402763	-0.000028
N	1.599444	1.570299	-0.000040
N	-1.599310	1.570413	0.000083
H	2.407470	0.928257	0.000079
H	1.618117	2.151830	-0.841352
H	1.618001	2.152118	0.841063
H	-1.617473	2.152503	-0.840847
H	-2.407492	0.928601	-0.000437
H	-1.617949	2.151639	0.841599

Table.2: The optimize parameters of the cis-platin.

Geometric parameter	Present work	Experimental[16]	Theoretical [6]	
			method A	method B
R(N-H)	1.022-1.032) A°(1.00	1.04	1.04
R(Pt-N)	2.049 A°	2.054	2.088	2.094
R(Pt-Cl)	2.393 A°	2.318	2.374	2.323
A(N-Pt-N)	89.671 deg.	90.2	100.2	99.8
A(N-Pt-Cl)	(90.234-90.429) deg.	88.9	81.7	82.1
A(Cl-Pt-Cl)	89.703 deg.	91.9	96.4	96.1
A(H-N-H)	(109.248-109.487) deg.	107	110	110
A(H-N-Pt)	(112.607-109.882) deg.	111	109	109

Table 3 illustrates the calculated values of the high occupied molecular orbital energy E_{HOMO} , the low unoccupied molecular orbital E_{LUMO} energy and the energy gap E_{gap} in eV of the cis-platin. We showed a good agreement in a comparison with ref.[17] and this an indication to a suitable method was used in present work, where a wide separation was obtained between the valence and conduction bands as noted in fig.2. Fig.3 illustrated the 3-D distribution of the HOMO and LUMO energies due to the linear combination of atomic orbitals for all atoms in the compound to construct the

molecular orbitals, where the great contribution is from outer electrons in the platinum metal with few contributions from the p-orbitals of the ligands, the green color represents the positive charges and the red color represents the negative charges. From our calculations, the E_{gap} is 4.517 eV in which the cis-platin has insulating behavior. The electrostatic potential ESP in fig.4 shows the charges are highly dragged towards the ligands chlorine atoms according to their largely electronegativity in comparison with the other atoms in the compound.

Table.3: The HOMO, LUMO energies and energy gap of the cis-platin.

Method	E_{HOMO} (eV)	E_{LUMO} (eV)	E_{gap} (eV)
Present work	-6.2432	-1.7951	4.4481
Reference [17]	-6.313	-1.796	4.517

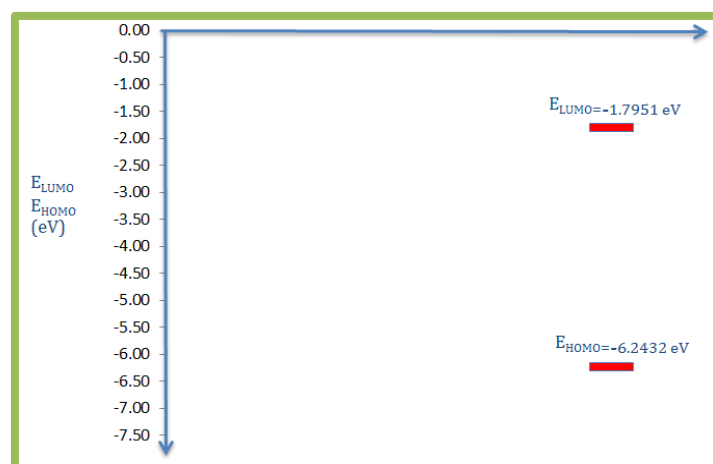


Fig.2: The LUMO-HOMO gap of the cis-platin.

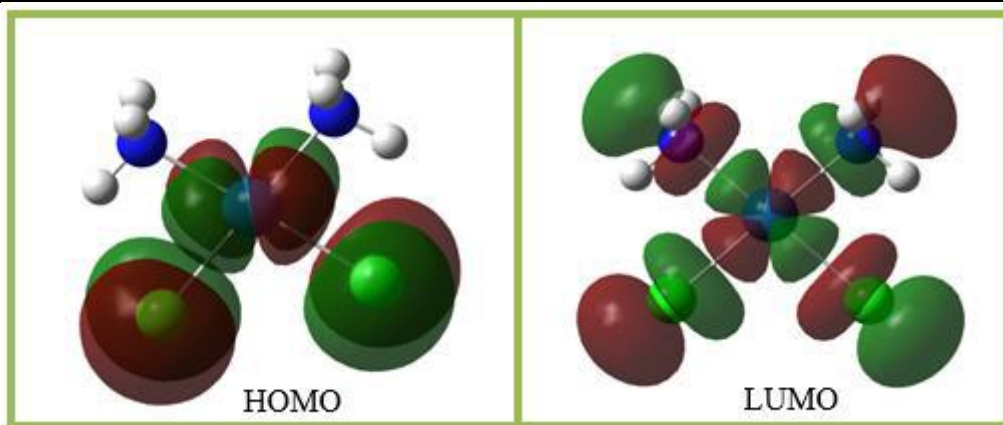


Fig. 3: The 3-D distribution of HOMO and LUMO of the cis-platin.

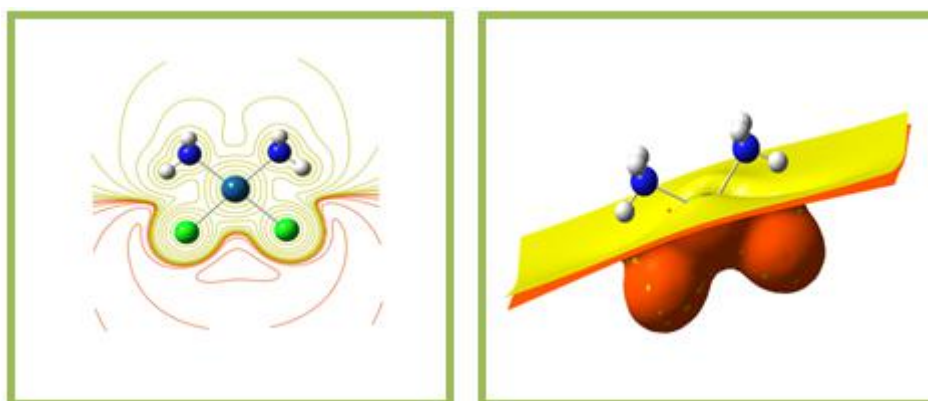


Fig. 4: The ESP distribution of the cis-platin.

Some of electronic properties of cis-platin are listed in Table 4. A good value was obtained for virial ratio ($-V/T = 2.0770$) of the compound without any imaginary frequency in which refers to good relaxation obtained for the studied structure. The calculated values of ionization energy I_E and electron affinity E_A showed the cis-platin has very low ability to donating/ accepting an electron to becomes cation/anion, these results are correspond to the large value of energy gap of the compound and it has

insulating behavior. The results showed the cis-platin has low value of electronic softness S , so, the calculated values of electronegativity X , electrochemical hardness H , chemical potential μ and electrophilic index ω in this work using SDD basis sets are in good agreement with those in ref.[17]. Above results declare the cis-platin needs to high excitation energy to electron transfer or to accepting an electron from the surrounding species.

Table.4: Some electronic variables of the cis-platin.

Property	The present work (DFT-B3LYP/SDD)	Reference [17] (DFT-B3PW91/LANL2DZ)
E_T (a. u)	-1152.9958	----
$\frac{-V}{T}$	2.0770	----
I_E (eV)	6.2432	----
E_A (eV)	1.7951	----
(XeV)	4.0192	4.054
H (eV)	2.2240	2.258
S (eV) ⁻¹	0.2248	----
μ (eV)	-4.0192	-4.054
ω (eV)	3.6315	3.639

IV. CONCLUSION

From the results of the structural and electronic properties of the cis-platin using SDD/DFT, one can conclude the following:

1. the calculated values of bonds and the angles are in good agreement with other studies.
2. A wide gap was obtained between the valence and conduction bands, means, cis-platin has insulating behavior. The great contribution for constructing the molecular orbitals is due to the outer electrons in the platinum metal with few contributions from the p-orbitals of the ligands.
3. The charges are highly dragged towards the ligands chlorine atoms and the ESP was distributed due to the coordination of all atoms in the compound.
4. A good relax was obtained for the studied structure via the calculated value of virial ratio without any imaginary frequency.
5. The cis-platin has very low ability to donating or accepting an electron to becomes cation or anion.
6. The cis-platin has low value of electronic softness and it needs high excitation energy to electron transfer or to accepting an electron from the surrounding species.

V. ACKNOWLEDGEMENTS

We acknowledge the staff of theoretical physics group, physics dep., college of science, university of Babylon for their valued support.

REFERENCES

- [1] C. Zhang, E.BaribefeNaziga, and L.Guidoni,"Asymmetric Environmental Effects on the Structure and Vibrations of cis-[Pt(NH₃)₂Cl₂] in Condensed Phases,"The Journal of Physical ChemistryB,DOI: 10.102,pp.1-130,(2014).
- [2] F. AndreLeRoy,"Interactions of Platinum Metals and Their Complexes in Biological Systems,"Environmental Health Perspectives, 10,pp. 73-83, (1975).
- [3] S. Adnan Abu-Surrah and K. Mika, " Platinum Group Antitumor Chemistry: Design and development of New Anticancer Drugs Complementary to Cisplatin" Current Medicinal Chemistry, Vol. 13, No. 11,(2006).
- [4] A. Imran, A. WaseemWani, K.Saleem and A.IHaque,"Platinum Compounds: A Hope for Future Cancer Chemotherapy"Anti-Cancer Agents in Medicinal Chemistry,13,pp. 296-306,(2013).
- [5] Rosenberg, B., Van Camp, L.,Krigas and T.," Inhibition of cell division in Escherichia coli by electrolysis products from a platinum electrode" Nature, 205, pp.698-699,(1965).
- [6] I. Nicolay Dodoff," A DFT/ECP-Small Basis Set Modelling of Cisplatin: Molecular Structure and Vibrational Spectrum", Computational Molecular Bioscience, 2, pp.35-44, (2012).
- [7] M. Ana Amado,M. SóniaFiuza, P. M. Maria Marques, and A. E. Luis Batista de Carvalho,"Conformational and vibrational study of platinum(II) anticancer drugs: Cisdiamminedichloroplatinum..."The Journal of Chemical Physics, 127, 185104 (2007).
- [8] Z. Hang, A. Matthew Cooperand M. ZytaZiora,"Platinum-based anticancer drugs encapsulated liposome and polymeric micelle formulation in clinical trials,"Biochemical Compounds,4, ISSN 2052-9341, (2016).
- [9] R. Wysokinski, K.Hernik, R.Szostak and D.Michalska,"Electronic structure and vibrational spectra of cis-diammine-(orotato)platinum(II), a potential cisplatin analogue: DFT and experimental study"Chemical Physics, 333,pp. 37-48,(2007).
- [10] M.Sonia Fiuza, M. Ana Amado, P. M. Maria Marques, and A. E. Luis Batista de Carvalho,"Use of Effective Core Potential Calculations for the Conformational and Vibrational Study of Platinum(II) Anticancer Drugs. cis - Diamminedichloroplatinum(II) as a Case Study,"J. Phys. Chem., 112,pp. 3253-3259 (A 2008).
- [11] M. B.Baile, N. S.Kolhe, P. P.Deotarse, A. S.Jain and A. A Kulkarni, "Metal Ion Complex -Potential Anticancer Drug- A Review",International Journal of Pharma Research & Review, August; 4(8):pp.59-66,(2015).
- [12] S.Rafique, M.Idrees, A.Nasim, H. Akbar and A.Athar,"Transition metal complexes as potential therapeutic agents,"Biotechnology and Molecular Biology Reviews, 5(2), pp.38-45, (2010).
- [13] F.Arneseano, A.Boccarelli, D.Cornacchia, F.Nushi, R.Sasanelli, M.Coluccia, and Giovanni Natile,"J. Med. Chem., 52,pp. 7847-7855 7847,(2009).
- [14] C. AthanassiosTsipis,"DFT flavor of coordination chemistry"Coordination Chemistry Reviews,272,pp. 1-29,(2014).
- [15] P. W. Abegg and T. K. Ha, "Ab initio calculation of spin-orbit-coupling constant from Gaussian lobe SCF molecular wavefunctions," Mol. Phys., 27,pp. 763-67,(1974).
- [16] V. P. Ting ,M.Schmidman, C. C. Wilson and M. T. Weller, "Cisplatin: Polymorphism and Structural Insight into an Important Chemotherapeutic Drug," AngewanChemie, International Edit dte ion, 49, 49,pp.9408-9411, (2011).

- [17] Z. BolboliNojini, F. Yavari, S. Bagherifar, "Preference prediction for the stable inclusion complex formation between cucurbit [n=5-7]urils with anticancer drugs based on platinum (II): Computational study," *Journal of Molecular Liquids*, 166, pp. 53-61, (2012).

Energy and Exergy Analysis of a CI engine fuelled with biodiesel fuel from palm kernel oil and its blends with petroleum diesel

Iortyer H. A, Likita Bwonsi

University of Agriculture Makurdi, Faculty of Engineering, Department of Mechanical Engineering, Nigeria

Abstract— Exergy analysis method has been widely used in the design, simulation and performance assessment of various types of engines for identifying losses and efficiencies. In this study, the first and second Laws of thermodynamics are employed to analyze the quantity and quality of energy in a single -cylinder, direct injection diesel engine using petroleum diesel fuel and biodiesel fuel from palm kernel. The experimental data were collected using steady-state tests which enable accurate measurements of air, fuel, and all the relevant temperatures. Balances of energy and exergy rates for the engine were determined and then various performance parameters and energy and exergy efficiencies were calculated for each fuel operation and compared with each other. The results of tested biodiesel from palm kernel showed similar energetic and exergetic efficiencies as petroleum diesel fuel although exergy efficiency of petroleum diesel was higher than that of palm kernel oil biodiesel and its blends. Therefore, as biodiesels derived from Palm Kernel oil (Pkl 100) have comparable performances to diesel fuel, it was concluded that they can be used as substitutes for petroleum diesel without much power loss.

Keywords— Diesel engine, energy analysis, exergy analysis, Palm kernel biodiesel.

I. INTRODUCTION

The basic human needs met through transportation, agriculture and industrial activities hinge on the role played by the petroleum fuels. The increasing energy demand, increasing harmful emissions and depletion of fossil fuel resources inevitably necessitate the optimum utilization of exhaustible fossil fuel and non-renewable energy resources. Hence, researchers are looking for alternative fuels and biodiesel is one of the best available sources to fulfill the energy demand of the world (Mukul *et al.*, 2009). The concept of using vegetable oil as fuel dates back to 1895 to the work of Rudolf Diesel. Although vegetable oils hold promise as alternative fuels (Murungesan *et al.*, 2009),

using raw oils in diesel engines can lead to engine-related problems such as injector coking and piston ring sticking. Biodiesel is a sulfur-free, non-toxic, biodegradable, and oxygenated alternative diesel fuel with a higher cetane number and lubricity (Sekmen *et al.*, 2007). Many researchers (Sahoo *et al.*, 2009 and Zheng *et al.*, 2008) have studied biodiesel fuels and their blends with petroleum diesel fuel as an alternative energy source in the compression ignition engine. The performance, emissions and combustion characteristics of the engine have been analyzed. The results show that for biodiesel fuels, brake specific fuel consumption (Bsfc) increases since these fuels have lower heating values. Based on these studies, biodiesel can be used as a substitute for diesel in diesel engine. Some studies show that almost 1/3 of the energy of a fossil fuel is destroyed during the combustion process in power generation. This has caused a renewed interest in exergy analyses since effective management and optimization of thermal systems is emerging as a major modern technical problem (Graves *et al.*, 2004). An exergy-based performance analysis is the performance analysis of a system based on the second law of thermodynamics that overcomes the limit of an energy-based analysis (Rakopoulos *et al.*, 2006). In this type of analysis of a thermodynamic system, second law equations are presented and discussed thoroughly (Moran *et al.*, 2000) and are used to analyze the operation of power plants (Rosen *et al.*, 2003). Series of papers have been published on second law or exergy analysis applied to internal combustion engines in the last few decades. A review study was published by (Caton 2000) and was extended by Rakopoulos *et al.* (2005). It can be seen from these review papers that numerous studies have been performed on the application of exergy analysis of SI engines (Bourhis *et al.*, 2009) and compression ignition engines using hydrocarbon fuels and/or alternative fuels (Caliskan *et al.*, 2009). Various investigators have conducted some studies on exergy

analysis of ICEs at fixed dead state temperatures (Kanoglu *et al.*, 2005) using same characteristic engines using different fuels. Kanoglu *et al.* (2008) and Caliskan *et al.* (2009) conducted experiment on the effects on exergy efficiencies of different dead state temperatures using alternative fuels in a four stroke, four-cylinder, turbocharged diesel engine. The results obtained showed that exergetic efficiency increased as dead state temperature decreased. The combustion process is the most important stage during IC engine operation and modeling of combustion in a realistic way is very important for exergetic computations. In furtherance of research in this area, this work is geared towards the use of exergy analysis to evaluate the performance of an internal combustion (IC) engine fuelled with biodiesels derived from Nigerian palm kernel oil and its blends with petroleum diesel.

II. THEORETICAL ANALYSIS

Relations presented in equation 1-17 are taken mostly from Caliskan *et al.* (2010). For a thermodynamic system, mass and energy balances for a control volume expressed as follows:

2.1 Energy Analysis:

Energy analyses are conducted by balancing mass and energy flows of the control volume.

The mass and energy balances for a control volume can be expressed by equations (Caliskan *et al.*, 2008)

$$\sum \dot{m}_{in} = \sum \dot{m}_{out} \quad (1)$$

$$\dot{Q} + \dot{W} = \sum \dot{m}_{out} h_{out} - \sum \dot{m}_{in} h_{in} \quad (2)$$

Equation (1) and (2) are mass and energy balance for a control volume of a general thermodynamic open system respectively where the subscripts *in* and *out* represent inlet and exit (output) states respectively while \dot{Q} denotes heat rate, \dot{W} work rate, \dot{m} mass flow rate and h specific enthalpy. These balances describe what is happening in a system an instantaneous time between two instants of time. Energy input rate (\dot{E}_{fuel}) is found using the lower heating values (H_U) and the mass flow rate (\dot{m}_{fuel}) defined in relation as:

$$\dot{E}_{fuel} = \dot{m}_{fuel} H_U \quad (3)$$

Net work (\dot{W}) is calculated with experimental data using the equation

$$\dot{W} = \omega T \quad (4)$$

Where ω is the angular velocity in (rad/s) and T is the torque (NM)

Heat losses (\dot{Q}_{loss}) are evaluated as differences between the energy input rate and net work as follows:

$$\dot{Q}_{loss} = \dot{E}_{fuel} - \dot{W} \quad (5)$$

The thermal efficiency is defined as the ratio of the network to the fuel energy input rate as follows:

$$\eta = \frac{\dot{W}}{\dot{E}_{fuel}} \quad (6)$$

2.2 Exergy Analysis:

Exergy balance of a control volume is written as follows

$$\dot{E}x_{heat} + \dot{E}x_w = \sum \dot{m}_{in} \varepsilon_{in} - \sum \dot{m}_{out} \varepsilon_{out} - \dot{E}x_{dest} \quad (7)$$

(Kanoglu *et al.*, 2009)

Where, $\dot{E}x_{heat}$ is the exergy transfer rate associated with the heat transfer at temperature T , $\dot{E}x_w$ is exergy work rate, \dot{m} is mass flow rate, ε is specific flow exergy and $\dot{E}x_{dest}$ is exergy destruction (irreversibility) rate.

Input exergy rate (fuel exergy rate, $\dot{E}x_{fuel}$) include the chemical exergy rate or specific exergy of the fuel (ε_{fuel}) and the mass flow rate described by the relation

$$\dot{E}x_{in} = \dot{m}_{fuel} \varepsilon_{fuel} \quad (7)$$

$$\text{But, } \varepsilon_{fuel} = H_U \varphi \quad (8)$$

Where, φ is the chemical exergy factor and hence defined as follows:

$$\varphi = 1.0401 + 0.1728 \frac{h}{c} + 0.0432 \frac{o}{c} + 0.2169 \frac{\alpha}{c} \left(1 - 2.0628 \frac{h}{c} \right) \quad (9)$$

Where, $\frac{h}{c}$, $\frac{o}{c}$ and α are hydrogen / carbon, oxygen/ carbon and hydrogen carbon ratio respectively.

Table.1: Some Properties of the fuels used in the test

Property	Diesel 100	PKL100
Typical formula*	$C_{18.27}H_{34.04}$	$C_{18.24}H_{34.01}O_2$
Heating value, (MJ/Kg) ^a	0.07874	0.07874
Sulphur content(wt/wt) ^a	0.1287	0.0307
Cetane number ^b	47.98	52.51
Viscosity@40°C ^b	4.57	7.31
FLASH POINT °C ^b	63	122
ANILINE POINT°F ^b	136.76	101.3

*Source: Centre for Advanced Nanotechnology programme Akure. (NASeni)

^a Source: Lighthouse petroleum engineering co.LTD, warri, Delta State, Nigeria.

^b Source: Warri refinery and petrochemicals company, a subsidiary of Nigerian National Petroleum Corporation, Quality Control Department.

Net Exergy work rate is equal to the Net Energy work rate.

$$\dot{E}x_w = \dot{W} = \omega T \tag{10}$$

Heat transfer Exergy rate ($\dot{E}x_{heat}$) is defined by

$$\dot{E}x_{heat} = \sum \left(1 - \frac{T_o}{T_{cw}} \right) \dot{Q} \tag{11}$$

But the quantity $\frac{T_o}{T_{cw}} = 0$ since the engine is air cooled.

Therefore, the relation becomes

$$\dot{E}x_{heat} = \dot{Q} \tag{12}$$

But,

$$\dot{Q} = \dot{m}_{fuel} H_U - (\dot{E}x_w + m_{out} \Delta h_{out})$$

Where, $\Delta h = h -$

h_o , while h and h_o is enthalpies of exhaust gases at measured exhaust temperature

m_{out} is the total mass of exhaust gas species.

Exhaust exergy (output exergy, $\dot{E}x_{ex}$) contains thermomechanical and chemical exergies

$$\dot{E}x_{ex} = \sum \dot{m}_i (\varepsilon_{tm} + \varepsilon_{chem})_i \tag{13}$$

Where, \dot{m}_i is the mass rate of the combustion products, ε_{tm} and ε_{chem} are specific thermo-mechanical and chemical exergies of the exhaust gases respectively.

While,

$$\varepsilon_{tm} = (h - h_o) - T_o(S - S_o) \tag{14}$$

h and S are specific enthalpy and entropy respectively easily found using the exhaust temperatures of the fuels. and subscript “o” denotes the dead reference state.

The chemical exergy of the exhaust gases was found using relation.

$$\varepsilon_{chem} = \bar{R} T_o \ln \frac{y}{y^e} \tag{15}$$

\bar{R} is the general gas constant, T_o is the environmental temperature, y is the mole fraction of the component given under the definition of the environment as measured y^e is the mole fractions of the exhaust gases and were calculated by balancing real combustion reactions of the fuels by means of emission measurement.

Exergetic efficiency (Ψ) is defined as ratio of net exergy work rate and the Input (fuel) exergy rate.

$$\Psi = \frac{\dot{E}x_w}{\dot{E}x_{in}}$$

III. MATERIALS AND METHODS

The Test-bed Techquipment TD 114 with the engine specification given as shown in Table 1 was used for the engine test experiment. The system has two major units; the engine and instrumentation units.

Table.1: Engine Specification

S/N	Description	Specification
1.	Engine Manufacturer/Model	Techquipment TD 114
2.	Type	Single Cylinder, Air Cooled, Naturally Aspirated 4-Stroke Diesel Engine
3.	Bore/Stroke	70mm/57mm
4.	Compression Ratio	17:1
5.	Maximum Torque	8.2 Nm at 2700 rpm
6.	Maximum Brake Power	2.6 kW at 3600 rpm
7.	Fuel Injection Timing	24 to 33° BTDC
8.	Fuel Injection Pressure	180psi



Plate.1: Engine set-up for the experiments

The engine unit consists of the following parts: Base plate, steering handle, ignition switch, dynamometer, carburetor with speed adjustment screw, magneto ignition system with spark plug, throttle and control lever, exhaust muffler, air inlet, power shaft, torque arm and spring balance.

3.2.1 Description of the engine:

The engine is bolted to base plate. The engine is started by switching on the ignition switch and pulling the handle of the engine. The carburetor of the engine mixes the air and fuel and supplies the combustion chamber where the magneto ignition system with spark plug initiates the combustion processes. The inflow of fuel is controlled by the throttle through the cable and control lever. The power generated from the combustion reaction is transmitted through the power shaft by a means of flexible coupling to the dynamometer. The engine drives the dynamometer paddles inside the dynamometer casing. The casing is partially filled with water. Water enters through the fine control valves and leaves through gate valves (coarse control). There is a vent and outlet to the drain. The paddle has vanes to accelerate the water in the dynamometer which pushes against vanes in the casing. The result is a shearing of the water, causing resistance to the rotation of the engine and a force turning the dynamometer casing on its trunnions (supporting bearings). This force (torque) is measured by the spring balance connected by the torque arm. The load on the engine is dependent on the amount of the water in the

dynamometer casing which is controlled by the two valves. The tachometer is driven by an extension of the dynamometer shaft. The tachometer is a magnetic device for measuring the speed of the engine. The instrumentation units are equipped with the necessary indicators of measurable variables.

3.2.3.1 Precautions:

The following precautions were taken before and during the course of the experiment;

- i. Sufficient diesel samples that will enable the test sequence to be completed were ensured (i.e 2 liters of each of the sample)
- ii. It was ensured that there was a supply of clean water to the Dynamometer
- iii. There were no obstructions for air entering the orifice.
- iv. It was ensured that the dynamometer arm was horizontal.
- v. Initial readings on the instrumentation unit were set and noted.
- vi. After each experiment the engine was flushed with the next sample to be used.
- vii. for statistical reason each experiment was repeated three times.

3.2.3.3 Engine Adjustment for the experiment:

- i. The experiment was conducted by adjusting the engine to the predetermined speed of 3200 rpm. The engine,

at the set speed, was run with four variable loads of 25%, 50%, 75% and 100%. At each loading, the speed was maintained constant by re-adjusting the throttle. After allowing the engine to run smoothly, measurements were taken accordingly.

ii. The experiment was conducted for the two different fuel samples (i.e PKL 100 and Diesel 100). Engine

performance parameters measured were torque, break power(BP), break specific fuel consumption, break thermal efficiency, engine exhaust temperature and exhaust emissions such as carbon monoxide (CO), unburnt hydrocarbon (HC), nitrogen oxides (NO_x) and smoke opacity.

IV. RESULTS AND DISCUSSION

4.1 Fuel Energy rate:

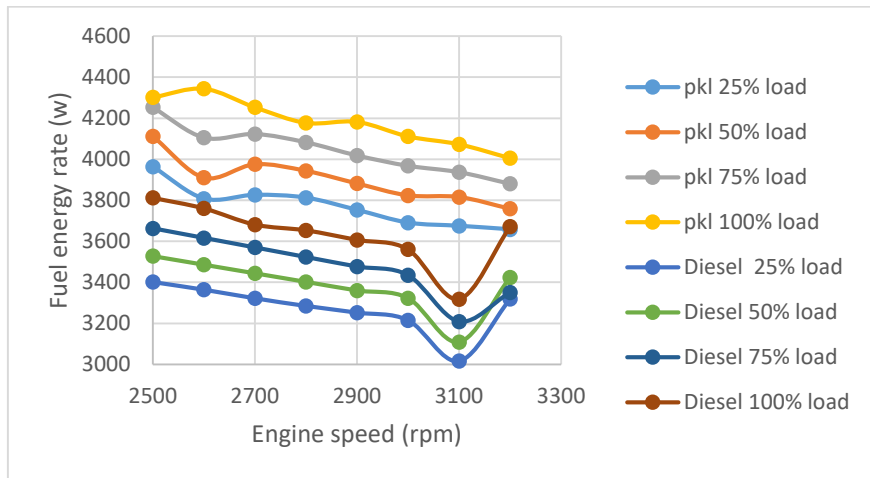


Fig.1: Fuel Energy rate versus engine speed for fuel sample PKL 100 and Diesel 100 .

Fig. 1 shows the effect of speed and load on the fuel energy rate. The graph for both Pkl 100 and Diesel 100 follows the same trend for all the engine loads. The trend shows that, as the engine load increases the fuel energy rate increases. This so because as the load increases, more fuel is combusted to provide the energy required to maintain the desired speed levels (Cem, 2010). Also, with Diesel 100, as the engine speed increases, fuel energy rate reduces to minimum at 3100rpm, and increases at 3200rpm to maximum whereas Pkl100 reduces almost linearly at all the

operational speeds. The maximum values (3812.3 watt) for Diesel 100 was at (2500 rpm, 100% load) and 4344.06 watt for Pkl 100 at (2600rpm, 100% load) .which shows that Pkl100 has the highest fuel energy rate compared to Diesel 100. This is due to the lower heating value of Pkl100 as compared to Diesel 100, more of Pkl 100 is required to compensate it's lower heating value for the same engine operation.

4.2 Heat energy rate:

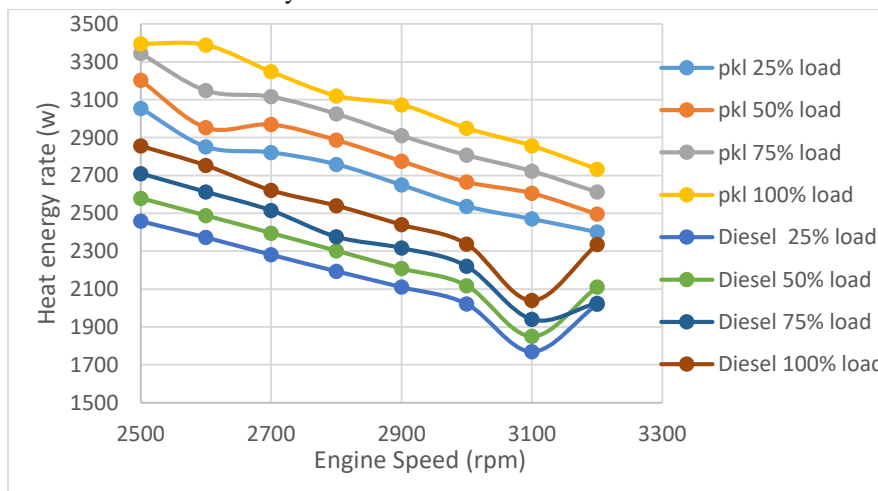


Fig.2: Energy Heat loss rate with Engine speed for fuel sample PKL 100 and Diesel 100.

Fig. 2 shows the effect of engine speed and load on the heat energy loss. The graph follows similar trend with all the load variation. The trend for energy heat loss shows that, as the engine load increases the energy heat loss increases. Also, as the engine speed increases, heat energy loss rate for diesel 100 reduces to minimum at 3100rpm, and increases at 3200rpm to maximum whereas Pkl100 reduces almost linearly at all the operational speeds.

The maximum values (2855.9watt) for Diesel 100 was at (2500 rpm, 100% load) and 3388.42 watt for Pkl 100 was at (2600rpm, 100% load) .which shows that Pkl100 has the

highest heat energy loss rate compared to Diesel 100. Heat transfer is a significant performance loss and affects engine operation loss of available energy, its magnitude is much from the burned gas (Heywood 1988). Heat energy loss is mostly due to friction developed as a result of high viscosity and flash point associated with Pkl 100 (biodiesels); also radiation operation of auxiliary components and heat transfer across the cylinder thermal boundary layer in most cases are causes of heat energy losses (Bilal *et al.*, 2007

4.3 Fuel exergy rate:

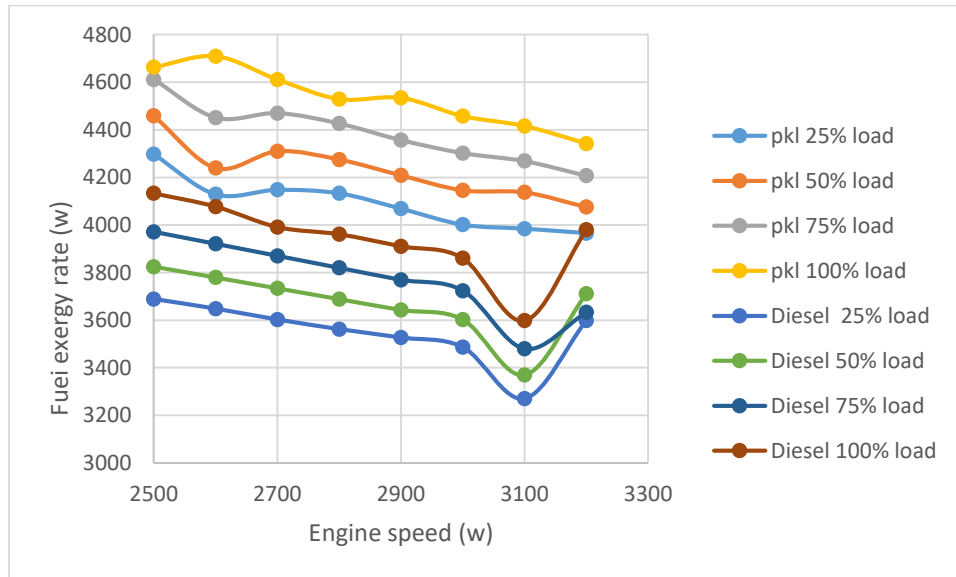


Fig.3: Fuel Exergy rate versus engine speed for fuel sample PKL 100 and Diesel 100.

Figs. 3 shows that as the engine load increases the fuel exergy rate increases. This so because as the load increases, more fuel is combusted to provide the energy required to maintain the desired speed levels (Cem, 2010). Also, with Diesel 100, as the engine speed increases, fuel energy rate reduces to minimum at 3100rpm, and increases at 3200rpm to maximum whereas Pkl100 reduces almost linearly at all the operational speeds.

The maximum values (4133 watt) for Diesel 100 was at (2500 rpm, 100% load) and 4709.52 watt for Pkl 100 was at

(2600rpm, 100% load) .which shows that Pkl100 has the highest fuel exergy rate compared to Diesel 100. This is because Diesel 100 has high value of the lower heating value as compared to Pkl 100. The low calorific value of pkl 100 is always compensated with increase in fuel exergy rates for the same engine operation as compared with diesel (Yilbasi *et al.*, 2007).

4.4 Effective power rate:

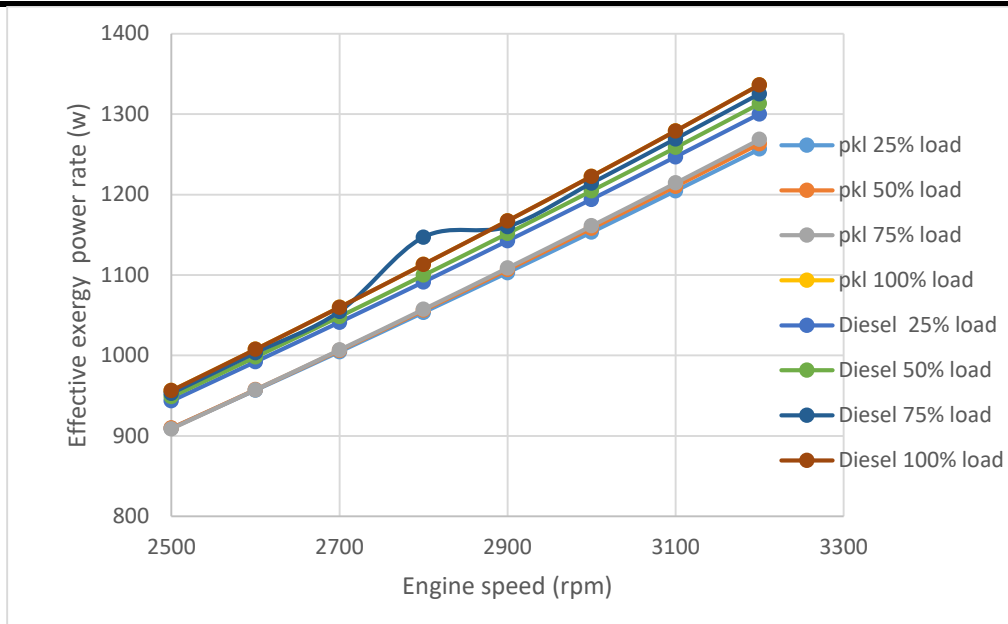


Fig.4: Effective power exergy rate versus engine speed for fuel sample PKL 100 and Diesel 100.

From fig.4 effective exergy power rate is directly proportional to engine speed and inversely proportional to the engine load. This is due to the fact that increasing engine load reduces the developed engine torque but the torque increases with increase in the engine speed (Gumus *et al.*, 2012). It can be observed that the trend of this parameter as a function of speed for pkl 100 is almost found

to be similar to the diesel fuels. Diesel 100 has the highest effective exergy power rate of 1336.4watt, and Pkl 100 has 1268.66watt, this may be due to the fact that diesel fuel has higher heating value than Pkl100.

4.5 Heat exergy rate

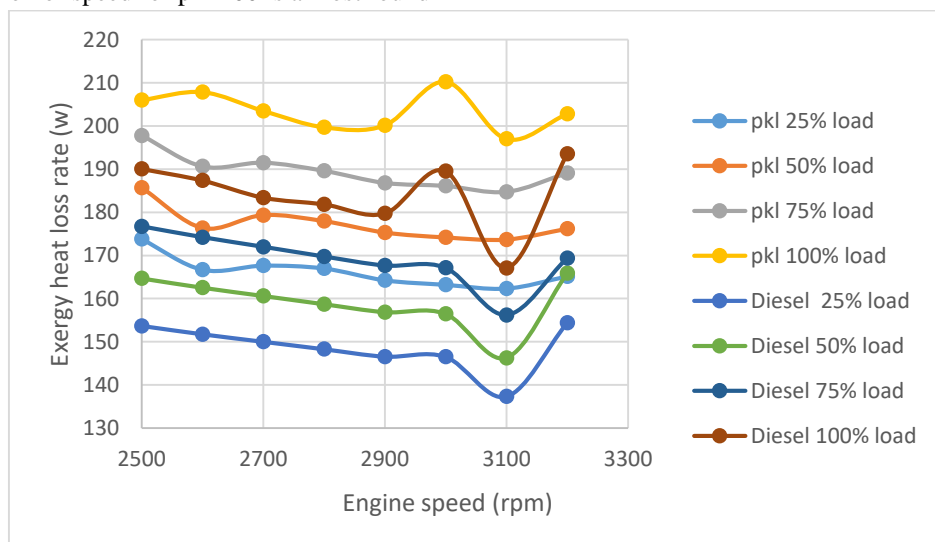


Fig.5: Exergy Heat loss rate versus engine speed for fuel sample PKL 100 and Diesel 100.

Fig.5 shows the trend for exergy heat loss, as the engine load increases the exergy heat loss increases also, and as the engine speed increases the exergy heat loss for Diesel 100 reduces to minimum at 3100rpm, and increases at 3200rpm to maximum. Pkl100 reduces from 2500rpm to 2600rpm and increases almost linearly through 3200rpm. The

maximum exergy heat losses (192.8 watt) for diesel 100 was at 3200 rpm and 100% load and (210.27 watt) for Pkl 100 was at (3000rpm, 100% load). Exergy Heat loss is due to forced convectional heat transfer across the cylinder thermal boundary layer influenced by flame geometry and charge motion/turbulence level (Bilal *et al.*, 2007).

4.6 Exhaust exergy rate:

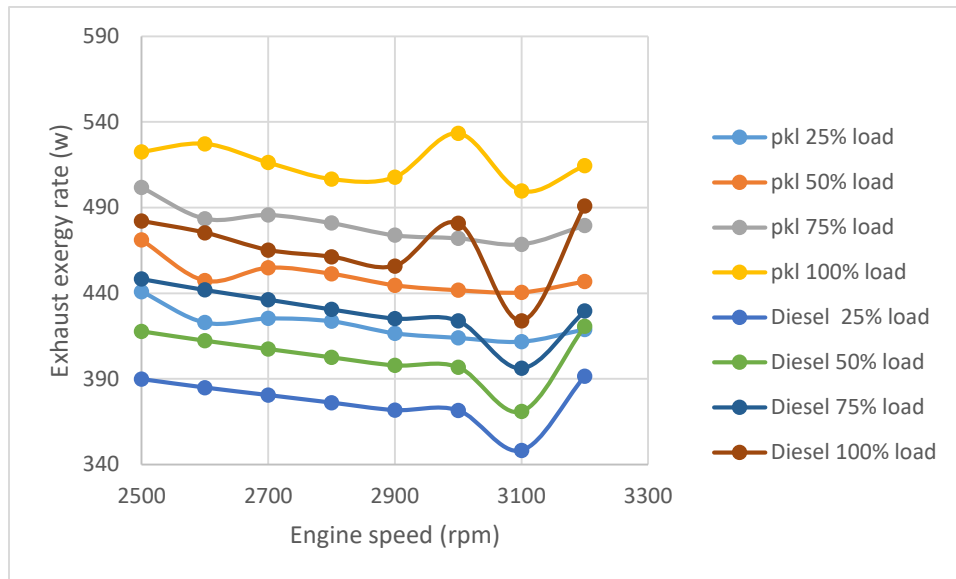


Fig.6: Exhaust Exergy rate with Engine speed for fuel sample PKL 100 and Diesel 100.

The trend for Exhaust exergy (Figs. 6) shows that, as the engine load increases the exhaust exergy increases. Also, as the engine speed increases the exergy heat loss for Diesel 100 reduces to minimum at 3100rpm, and increases at 3200rpm to maximum. Pk1100 reduces from 2500rpm to 2600rpm and increases almost linearly through 3200rpm. The maximum exergy heat losses (490.964 watt) for diesel 100 was at 3200 rpm and 100% load and (533.377 watt) for Pkl 100 was at (3000rpm, 100% load). Because of the higher exhaust temperatures the exergy loss accompanying the exhaust gas is higher in pkl 100 fuel. Consequently, for

the same power output, operation with pkl 100 yields higher rate of heat transfer from the engine. It is also important to note that load has significant bearing on the exhaust gas temperature. As the load increases, exhaust gas temperature for both the Pk1100 and diesel100 fuel increases. But in the case of Pkl 100 fuel, exhaust gas temperature is higher at the lower loads than that of diesel fuel signifying better combustion of diesel fuel at the lower loads then the Pkl100, and hence it causes lower specific fuel consumption for the diesel fuels (Sumitaat *et al.* 2011).

4.7 Exergy Destruction rate:

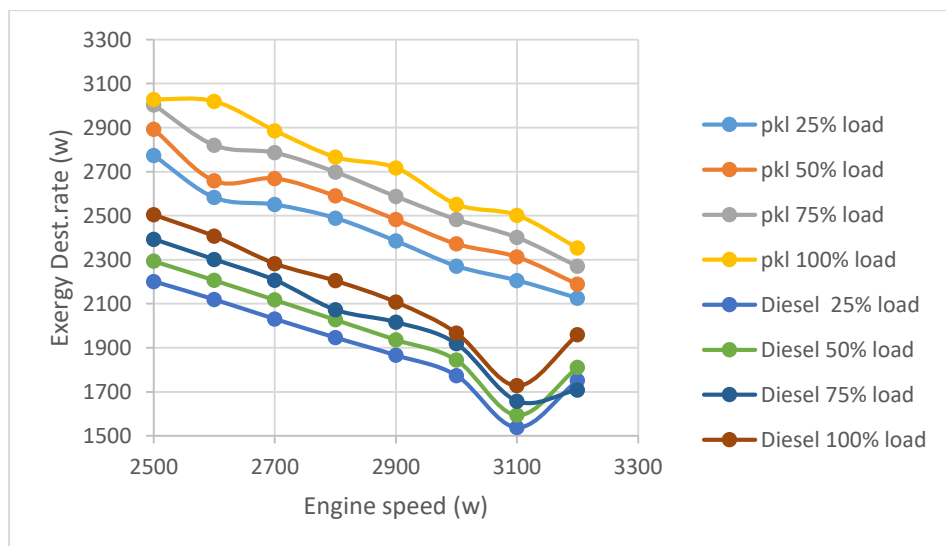


Fig.7: Exergy Destruction rate versus engine speed for fuel sample PKL 100 and Diesel 100.

Fig. 7 shows the effect of engine speed and load on exergy destruction rates. The trend for exergy destruction rates shows that, as the engine load increases the exergy destruction rate increases and as the engine speed increases, the rate of exergy destruction for Pkl 100 reduces to minimum at 2600rpm and increases to 2700rpm and slightly reduces through 3200rpm whereas with diesel 100 as the engine speed increases the exergy destruction rate reduces to minimum at 3100rpm and increases at 3200rpm to maximum. The maximum value was 2504.4w for diesel 100 at (2500 rpm, 100% load) and for Pkl 100 was 3028.52watt at (3200 rpm, 100% load). This means that the destruction

rate is more with fuel sample Pkl 100 and less with Diesel 100. The combustion process in an engine is complex, and is a major source for the destruction of a significant portion of the availability (Kopac *et al.*, 2005). The high viscosity of Pkl 100 as compared to that of Diesel leads to unfavorable pumping, inefficient mixing of fuel with air which contributes to incomplete combustion. Also, the high flash point results in increased carbon deposit formation; these problems lead to increased combustion temperatures, hence the increase in the rate of exergy destroyed in the engine.

4.8 Thermal efficiency:

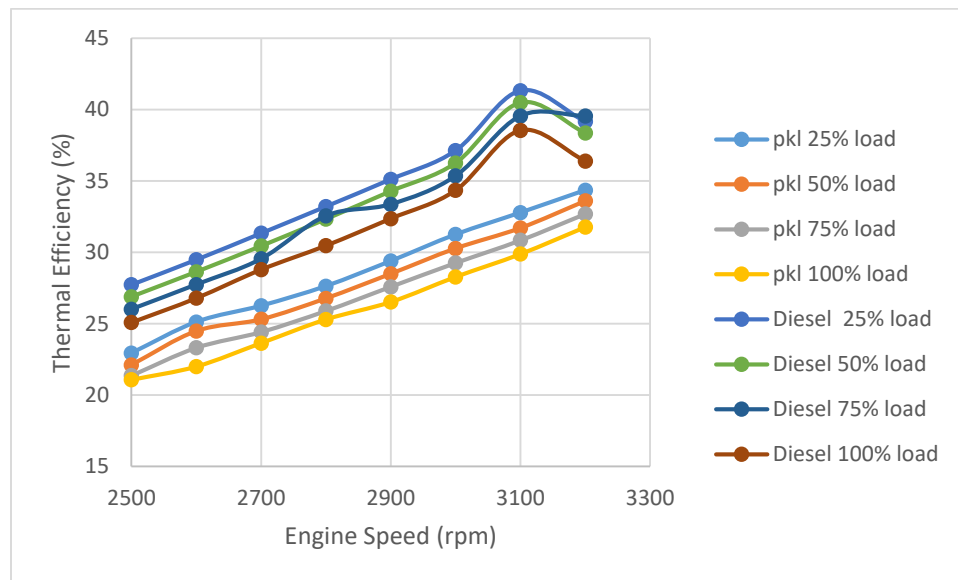


Fig.8: Energy (thermal). Efficiency versus engine speed for fuel sample PKL 100 and Diesel 100.

Fig. 8 shows the effect of engine speed on Energy (thermal) efficiency. The thermal efficiency reduces as the engine load increases while it increases as the engine speed increases. The thermal efficiency for fuel sample Pkl 100 increases almost linearly at all operational speeds. For diesel 100, as the engine speed increases the thermal efficiency increases to maximum at 3100rpm. The maximum thermal efficiency for fuel sample Pkl 100 was 34.35% at (3200rpm, 25% load) and for Diesel 100 was

41.33% at (3100rpm, 25% load). The increase in thermal efficiency means that a larger portion of combustion heat has been converted into work. The low efficiency of Pkl 100 as compared to Diesel 100 may be due its low volatility, slightly higher viscosity and higher density which affects mixture formation of the fuel and thus leads to slow combustion.

4.9 Exergy Efficiency:

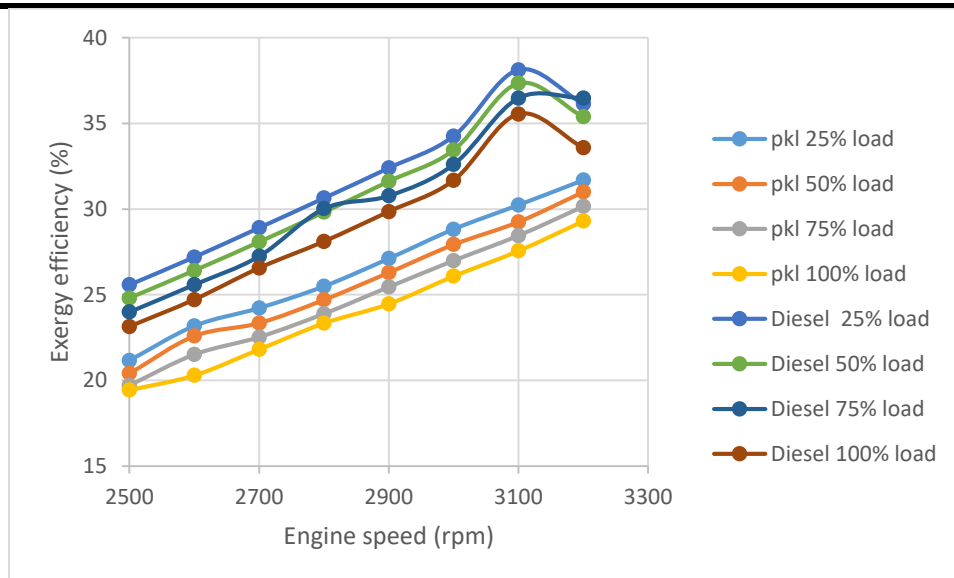


Fig.9: Exergetic Efficiency versus engine speed for fuel sample PKL 100 and Diesel 100.

The effect of engine speed on exergy efficiency is shown in fig. 9. Exergy efficiency relationship with engine load is inverse but direct with engine speed to a maximum value and decreases with further increase in speed. As the engine speed increases the exergy efficiency of fuel sample Pkl 100 increases almost linearly at all operational speeds. But for diesel 100, as the engine speed increases the exergy efficiency increases to maximum at 3100rpm. The trend also revealed that the maximum exergy efficiency for fuel sample Pkl 100 was 31.68% at (3200rpm, 25% load) and for Diesel 100 was 38.12% at (3100rpm, 25% load). The exergy efficiency is to large extent a function of combustion processes. The interaction of the fuels and the engine across the various phases of combustion processes accounts for the overall exergy efficiency (Cem, 2010).

Because biodiesel fuels have different properties than petroleum diesel, such as higher viscosity, higher cetane number, higher specific gravity and lower heating value, when used in unmodified diesel engines, these fuel properties may affect the engine performance and emissions considering that the engines were originally optimized with petroleum diesel (Graboski and McCormick, 1998).

V. CONCLUSIONS

Based on the experiment carried out the following conclusions are reached.

- i. Both thermal and exergy efficiencies reduce with increasing load and increase with increasing speed. Exergy efficiency maximum values range from

28.18% to 38.12%; diesel 100 is the most efficient and fuel sample B60 is the least efficient.

- ii. Comparatively, petroleum diesel (Diesel 100) is more efficient than the biodiesels derived from palm kernel oil (PKL100). However, biodiesels derived from Palm Kernel oil (Pkl 100) have comparable performances to diesel fuel and can be used as substitutes for the petroleum diesel.

REFERENCES

- [1] Bourhis G., and P. Leduc,(2009) Energy and Exergy Balances for Modern Diesel and Gasoline Engines, Oil & Gas Sci. & Tech.–Rev. IFP, DOI: 10.2516/ogst/2009051;
- [2] Caliskan, H., Tat, M.E., Hepbasli, A. and Van Gerpen, J.H. (2010) ‘Exergy analyses of engines fueled with biodiesel from high-oleic soybeans based on experimental values’, International Journal of Exergy, Vol. 7, No. 1, pp.20–36.
- [3] Caliskan N H., M.E. Tat, A. (2009) Hepbasli, Performance Assessment of an Internal Combustion Engine at Varying Dead (Reference) State Temperatures, Applied Thermal Engineering, 29(16), 3431–3436,
- [4] Caton J. N, (2000)On The Destruction of Availability (Exergy) Due to Combustion Processes-with Specific Application to Internal-Combustion Engines, Energy, 25(11), 1097–1117,
- [5] Graves R., S. Daw, J. Conklin, V. K. Chakravarthy, (2004) Stretch Efficiency in Combustion Engines with

- Implications of New Combustion Regimes, FY 2004 Progress Report,.
- [6] Kanoglu, M., Dincer, I. and Rosen, M.A. (2008) 'Exergetic performance investigation of a
- a. turbocharged stationary diesel engine', *International Journal of Exergy*, Vol. 5, No. 2,
 - b. pp.193–203.
- [7] Kanoğlu M., S.K. Işık, and A. Abuşoğlu, (2005) Performance Characteristics of a Diesel Engine Power Plant, *Energy Conversion and Management*, 46(11-12), 1692–1702,
- [8] Moran M.J., and H.N. Shapiro, (2000) *Fundamentals of Engineering Thermodynamics*, 2nd Edition, Wiley New York,
- [9] Mukul S., R. Agarwal (2009), Energy and Exergy Analysis of Brayton-Diesel Cycle, *Proceedings of the World Congress on Engineering Vol II*, July 1-3, 2009, London, U.K, ISBN:978-988-18210-1-0
- [10] Murugesan A., C. Umarani, R. Subramanian, N. Nedunchezian, (2009), Biodiesel as an Alternative Fuel for Diesel Engines-A Review, *Renewable and Sustainable Energy Reviews*, 13(3), 653–662, 2009.
- [11] Rakopoulos C.D, E.G. Giakoumis, (2006) Second-law Analyses Applied to Int. Comb. Engines Operation, *Progress in Energy&Comb. Science*, 32(1), 2–47,
- [12] Rosen M.A., I. Dincer, (2003) Exergy–Cost–Energy–Mass Analysis of Thermal Systems and Processes, *Energy Conv.& Management*, 44(10), 1633–1651,.
- [13] Şahin Z., (2006) The Research for Increasing Exergy Efficiency of Energy Plants with Gas- Solid Fuels, MSc Thesis, ZKU Graduate School of Natural&Applied Sciences Dept of Mech. Eng., Zonguldak,
- [14] Sahoo P.K., L.M. Das, Combustion Analysis of Jatropa, Karanja and Polanga Based Biodiesel As Fuel In a Diesel Engine, *Fuel*, 88(6), 994–999,.
- [15] Sekmen Y., (2007) Use of Watermelon and Flax Seed Oil Methyl Estera as a Fuel in a Diesel Engine, *Technology*, 10(4), 295-302, 2007. Application of Energy and Exergy Analyses to a Ci Engine Using Biodiesel Fuel.
- [16] Sezer I., and A. Bilgin, (2008) Mathematical Analysis of Spark Ignition Engine Operation Via The Combination of The First And Second Laws of Thermodynamics, *Proc. R. Soc. A*, 464, 3107–3128.
- [17] Zheng M., C.M. Mwila, G.T. Reader, M. Wang, D.S.K. Ting, J. Tjong, (2008), Biodiesel Engine Performance and Emissions in Low Temperature Combustion, *Fuel*, 87(6), 714–722.

The Effect of various Sterilization Procedure on Number of Colony-Forming units of isolated endophytic bacteria from *Cosmos caudatus* Kunth. leaf

Fiqih Ramadhan, Fikri Ainur Risma Hardianti Oktavia, Luluk Mukarramah, Ria Yulian, Nurul Hilyatun, Iis Nur Asyiah

Biology Education, Faculty of Teacher Training and Education, University of Jember, Indonesia

Abstract— The purpose of this study was to determine the effect of different concentration and time sterilization on the number of colony-forming units of isolated endophytic bacteria from *Cosmos caudatus* kunth. leaf. The sterilizing agents were used is sodium hypochlorite (NaOCl). The research consisted of four treatments P1 (NaOCl 5.35%; 3 minutes), P2 (NaOCl 5.35%; 1,5 minutes), P3 (NaOCl 3%; 3 minutes), and P4 (NaOCl 3%; 1,5 minutes). Every treatments have one control medium and three repetition. The control medium treated by make streak using *C. caudatus* leaf that had sterilized and the three repetition treated by inoculating 100 µL suspension of *C. caudatus* leaf with 10^{-1} serial dilution. Result on the control medium is sterile and indicated that the bacteria in treatments medium is endophytic bacteria. The CFU in treatments P1 (0×10^2 CFU/ml), P2 ($2,9 \times 10^3$ CFU/ml), P3 ($2,9 \times 10^3$ CFU/ml), and P4 ($2,8 \times 10^3$ CFU/ml). The conclusion from this study is there was no significantly different of different concentration and time sterilization on the number of colony-forming units of isolated endophytic bacteria from *Cosmos caudatus* kunth. Leaf.

Keywords— Sodium hydroxide, endophytic bacteria, leaf *Cosmos caudatus*.

I. INTRODUCTION

Cancer or carcinoma is a group of diseases characterized by the growth and development of uncontrolled and abnormal cells. Nowadays, cancer is one of the main threats and causes of death for human. According to data from the IARC in 2012, cancer has been the cause of death of 8,201,575 people worldwide. While in Indonesia cancer rates by 1.4% (Ministry of Health Republic of Indonesia. 2015). In cancer, the cancer cells can multiply and spread to the far location from the origin place This is what causes the cancer becomes deadly disease. Current cancer treatment was assessed to be less secure. Surgery, chemotherapy, radiation therapy and others still have

severe side effects. Therefore one of alternative cancer treatment is to use natural ingredients that can reduce the side effects of cancer treatment today.

Cosmos caudatus Kunth. is one of the plants that are considered to have anticancer agents and has been widely used in traditional medicine. *C. caudatus* Kunth produce one form of secondary metabolites flavonoids that assessed can be used as an anticancer agent., Existing research results showed *C. caudatus* Kunth leaves contain antioxidant compounds are quite high at 70 mg/L (Lotulung et al., 2001). In another study, methanolic extract of *C. caudatus* Kunth leaves contain flavonoids and quercetin glycosides (Abas et al., 2003). This makes the plant *C. caudatus* Kunth can be used as drugs in the treatment of cancer. Research on the use of *C. caudatus* Kunth as a cancer drug has been widely reported among others as triggers apoptosis (programmed cell death) (Ren et al., 2003); can induce apoptosis of colon cancer cells, and leukemia (Taraphdar, 2001); and also induces apoptosis in breast cancer cells (Pebriana, et al., 2008).

Utilization *C. caudatus* Kunth as an anticancer drug is still in the laboratory scale. For large-scale use (industry), the use of *C. caudatus* Kunth or other plants as anticancer plant drugs still have limitations. This is because if it is produced as an herbal medicine on an industrial scale will cause the limitations of raw materials because most of the raw materials of herbal medicine taken from the mother plant. So it is feared that these biological resources will be destroyed due to the constraint in cultivation. In *C. caudatus* Kunth plant itself has a life cycle that is greatly influenced by the environment, it will affect the growth of plants *C. caudatus* Kunth including the leaves. Besides, *C. caudatus* Kunth are not able to produce a compound which is pretty much in a relatively short time.

Sterilization of plant organs that will be used as materials for endophytic bacteria isolation becomes very important. This is because the sterilization stage determines whether the bacteria isolated are plant endophytic bacteria or are

contaminant bacteria attached to the surface of the plant organ. Sodium hypochlorite (NaOCl) is one of the most commonly used materials in surface sterilization. This material is widely contained in commercial whitening products such as *Fast* and *Clorox* and can be diluted according to the desired concentration (Mahmoud and Al-Ani, 2016). The concentration of NaOCl used for surface sterilization is different for each plant organ and also different for each plant species. In addition to the concentration factor, the duration of sterilization also determines the successful isolation of endophytic bacteria. Sterilization time difference is determined by the morphology of each organ and plant species. For hard plant organs such as a rod needs a longer time than leaves. The improper concentration and duration of sterilization will cause tissue damage to plants that can cause endophytic bacteria that are located on the tissue become die.

The present study aimed to present the effective sterilization procedure in both the NaOCl concentration and the duration of sterilization on the number of colonies resulting from endophytic bacterial isolation from the leaves of the *C. caudatus* Kunth

II. METHODOLOGY

Cosmos caudatus Kunth. plants obtained from Tidar Hill, Jember, East java, Indonesia. The leaf excised from health and maximally growth of 3rd-5th leaf, that growth from the top of shoot.

In this study variation of sterilization method that used are different concentrations and time exposure. The sterilizing agents was use is, sodium hypochloride (NaOCl) which contain (5,25%) NaOCl as active agent with varying concentrations. The variation threatment are consist of four treatments P1 (NaOCl 5.25%; 3 minutes), P2 (NaOCl 5.25%; 1,5 minutes), P3 (NaOCl 3%; 3 minutes), and P4 (NaOCl 3%; 1,5 minutes), which every treatments have one control medium and three repetition. TSA (Tryptic Soy Agar) Merck were applied for growing the isolated endophytic bacteria.

In all treatments, the leaf washed under running tap water to remove microorganisms and dust particles from the surface. 1 gram of *Cosmos caudatus* leaf were used for each treatment, these leafe than exposed to sterilization agent. First immersed in 70% ethanol for one minute, afterward exposed to the NaOCl with different concentrations and time exposure for every treatment, with few drops of Tween 80 were added to the solutions. The use of ethanol and NaOCl is to reduce contamination and by adding the Tween 80 is to enhance the coverage of the solution on the leaf. The sterilized leaf were then rinsed thoroughly with sterile distilled water 3 times each time to remove the disinfectant completely.

Using the stirilized leaf, it streak on the TSA medium as the control. The leaf than crushed and than suspended in 0.8% of physiological salt and it homogenized using vortex. 100 μ L suspension of *C. caudatus* leaf with 10⁻¹ serial dilution, is taken and inoculated on medium using spread methode, than it incubated overnight in temperature 37 °C.

The result of each threatment and control than observed. If the control medium is setrile, means the sterilization process is successful and the growing bacteria on the repetition medium is endopitic bacteria. The number of colonies than determined by counting the number of Colony Forming Units (CFU/mL). Data were subjected to analysis of variance (ANOVA) (degree of true= 95%), signification is 0.067 and means were compared by the Duncan's multiple range test at p<0.05 using the SPSS ver.20 (SPSS Inc., USA).

III. RESULTS AND DISCUSSION

The result (Table 1) showed that number of colony forming unit of endothypic bacteria decrease with an increase in NaOCl concentration and time of exposure. Results also show that at treatment P2 with 5,35% of NaOCl and 1,5 minutes time of exposure and P3 with 3% of NaOCl and 3 minutes time of exposure had best impact on viability of endothypic bacteria. At that treatment, 2,9 X 10³ bacteria colony are formed.

Table.1: Results of various concentrations and time exposure of NaClO on number of colony forming unit

Treatment	NaOCl Consentration	Time Exposure	Number of CFU/ml
P1	5, 35%	3 minute	0 x 10 ²
P2	5, 35 %	1,5 minute	2,9 X 10 ³
P3	3 %	3 minute	2,9 X 10 ³
P4	3 %	1,5 minute	2,8 X 10 ³

Surface sterilization of *Cosmos caudatus* kunth. leaf using method I (P1) showed that with NaOCl 5,35% in 3 minute was effective to eliminate microorganisms on the leaf surface. NaOCl 5,35% in 3 minute possess antimicrobial activity and efficiently in eliminating the

microorganism. At the same time, this treatment method give impact to the number colony forming unit of endophytic bacteria. In this treatment the less number colony forming unit of endophytic bacteria can growth. 0 x 10² colony of endophytic bacteria are formed. It's mean

that at this treatment NaOCl bactericide activity is stronger than the three other treatment.

In method III which has the same result with method (P2), there are no contamination on the control treatment. This treatment also performs good sufficient to eliminate surface microorganisms. Meanwhile the II and III methods show the best impact on colony forming unit of endophytic bacteria. $2,9 \times 10^3$ colony of bacteria can grow at the medium. Sodium hypochlorite in concentration combining with time exposure give the different impact to the colony forming unit of endophytic bacteria. At high concentration with long time of exposure, potentially to eliminate the microorganism in the surface of *Cosmos caudatus* Kunth leaf. But also as the bactericide to the endophytic bacteria.

Sodium hypochlorite NaOCl is a common use for surface sterilization. It is available as commercial bleach product and can be diluted to proper concentrations. Generally it is used by immersing the target organ in this solution for 5-20 minutes. A balance between concentration and time should be verified for each type of plants. Sodium hypochlorite being known as effective disinfectant agent against many bacteria. At the case that some bacteria can survive, it might be due to resistance towards sodium hypochlorite. The bactericidal activity of hypochlorite solution (Bleach) is the NaOCl (OCl⁻) ion with the former being more active so that the disinfecting efficiency of chlorine is best in slightly acid hypochlorite solution (George, 1993 and Russel, 1996).

The results of Mahmoud and Al-Ani (2016), showed that treatment with sodium hypochlorite (NaOCl) had satisfactory results and Singh (2011) also showed that the best concentration of NaOCl is 3%, which can reduce bacterial contaminations up to 95%. Our results are in agreement with earlier studies on attempts using various sterilization methods. The sodium hypochlorite showed a high in reducing the contamination of bacteria because of its is very effective as disinfectant agent against many bacteria. Hypochlorite (OCl⁻) as a strong oxidant can denature by aggregating essential proteins of bacteria as previously described (Winter *et al*, 2008).

In our study the combination between concentration and time exposure of NaOCl proved to be a sterilizing agent that has different impact to the endophytic bacteria colony forming unit. In summary, 5, 35 % of NaOCl with 1,5 minute time exposure and 3 % of NaOCl with 3 minute of time exposure, show as the best sterilization method to be very effective in eliminating surface microorganisms with high viability in endophytic bacteria.

IV. CONCLUSION

From the results obtained, it can be concluded that the effect of various concentrations and time exposure of NaClO on number of colony forming unit of endophytic

bacteria of *Cosmos caudatus* Kunth. Leaf The conclusion from this study is there was no significantly different effect of different concentration and time sterilization on the number of colony-forming units of isolated endophytic bacteria from *Cosmos caudatus* Kunth. leaf.

REFERENCES

- [1] Abas, F., Shaari, K., Lajis, N.H., Israf, D.A., dan Kalsom, Y.U., Antioxidative and Radical Scavenging Properties of the Constituents Isolated from *Cosmos caudatus* Kunth. *Nat. Prod. Sciences* 9 (4): 245-248.
- [2] George EF. (1993). *Plant Propagation By Tissue Culture, Part 1. The Technology (2nd edn)*, exeter, westbury, UK.
- [3] Lotulung, P.D.N., Minarti dan Kardono, L.B.S. 2005. Penapisan Aktivitas Antibakteri, Antioksidan dan Toksisitas Terhadap Larva Udang *Artemia salina* Ekstrak Tumbuhan Asteraceae, Abstrak, Pusat Penelitian Kimia LIPI
- [4] Mahmoud, S. N. and Al-Ani, N. K (2016). Effect of Different Sterilization Methods on Contamination and Viability of Nodal Segments of *Cestrum nocturnum* L. *International Journal of Research Studies in Biosciences (IJRSB)*, 4, p. 4-9.
- [5] Mc.donnell G, Russell AD. (1999). Antiseptics and disinfectants: Activity, action, and resistance. *Clin Microbiol Rev* 12 p.147-179.
- [6] Ministry of Health Republic of Indonesia. 2015. *Situation of Cancer*. Jakarta: Data Center and Information Ministry of Health Republic of Indonesia.
- [7] Pebriana R.B., Wardhani B.W.K., Widayanti E., Wijayanti N.L.S., Wijayanti T.R., Riyanto S., dan Meiyanto E., 2008, Pengaruh Ekstrak Metanolik Daun Kenikir (*Cosmos caudatus* Kunth.) terhadap Pemacuan Apoptosis Sel Kanker Payudara, *Pharmacon*, 9(1), 21-26.
- [8] Ren, W., Qiao, Z., Wang, H., Zhu, L., Zhang, L., 2003, Flavonoids: Promising Anticancer Agents, *Medicinal Research Reviews*, 23 (4), 519-534
- [9] Singh, V., et al., Identification and prevention of bacterial contamination on explant used in plant tissue culture labs. *International Journal of Pharmacy and Pharmaceutical Sciences*, 3. p.160-163.
- [10] Taraphdar, Amit, K., Madhumita, Roy, dan Bhattacharya, R.K., 2001, Natural products as inducers of apoptosis: Implication for cancer therapy and prevention, *Current Science* 80(11): 1391.
- [11] Winter J, Ilbert M, Graf PC, Ozcelik D, Jakob U. (2008). Bleach activates a redox regulated chaperone by oxidative protein unfolding. *Cell* 135: 691-701.

Studies on Preparation of Custard Apple Vinegar

S. J. Raichurkar¹, R. A. Dadagkhair²

¹Department of B. Voc. (Food Processing Technology), Modern College of Arts, Science and Commerce, Ganeshkhind Pune
16, Maharashtra, India

²Scientist, Directorate of Cashew Research, Puttur, Karnataka, India

Abstract— Custard apple (*Annona squamosa*) is highly susceptible to spoilage, softens very rapidly during ripening, and becomes squashy and not easy to consume fresh. The custard apple has nearly 24% sugars; it was hypothesized that this can be further processed by fermentation into a valuable product such as vinegar. The present study was carried out to develop vinegar from custard apple and it was compared with market vinegars sample for sensory evaluation. The physiochemical properties of custard apple vinegar were analysed. The custard apple vinegar production process took 30 days and had physiochemical characteristics of 1.019 gm/ml specific gravity, 1 % alcohol content, 5.39% (v/v) acetic acid, 2.0°Brix, and pH of 2.8 which complied with the standard ranges of brewed vinegar after complete fermentation. The sensory evaluation of vinegar samples was done by ten panel members. The overall acceptability of the market vinegar samples were rated as like extremely on the nine point hedonic scale, while custard apple vinegar was rated as like very much on the nine point hedonic scale.

Keywords— acetic acid fermentation, Custard apple, custard apple vinegar, sensory evaluation.

I. INTRODUCTION

The custard apple (*Annona squamosa*) is one of the important dry land fruit grown in waste land on rain water cultivated throughout the country. A relatively less moist soil and temperate environment will yield the custard apple fruit with good nutritional constituent (Shaha, 1959). Custard apple is popularly known as Sitaphal is grown in 40,000 Ha and the production is 136000 MT in 2012-2013 in India. The fruit is not indigenous to India, but it first originated from Caribbean region but has spread across the central and South America as well as Africa and Asia. It is exported in large quantity from India to UAE, Saudi Arabia, Bangladesh and Kuwait (Chadha, 1995). Fruits have an edible, soft, granular, juicy and sugary pulp with mild flavor and with slight acidity (Butani, 1976). Fruits are considered for their medicinal value besides their general use in juice, milk shakes and

soft drink (Luciana *et al.*, 2010) ice cream, confectionery and certain milk products (Broughton, 1979).

Custard apple is considered as one of the delicious and nutritionally valuable fruit (Mariappan and Saxena, 1983). It contains about 28-55% of edible portion consisting of 73.30% moisture, 1.60% protein, 0.30% fat, 0.70% mineral matter, 23.90% carbohydrates, 0.20% calcium, 0.40% phosphorus, 1.0% iron, 12.4-18.15% sugar, 0.26-0.65% acidity and with caloric value of 105K.Cal/100g (Nissen *et al.*, 1988; Popale *et al.*, 2012 and Sravanthi *et al.*, 2014). Custard apple is highly susceptible to spoilage, softens very rapidly during ripening, and becomes squashy and not easy to consume fresh (Okigbo and Obire, 2009; Pareek, *et al.*, 2011). Hence there is greater need to processing the ripe custard apple fruits in to suitable products to minimize the post-harvest losses. Storage of the fresh fruits of *A. squamosa*, has limitations, since it is perishable, and cold storage is not promising because of the development of an unattractive brown colour on the skin which decreases the market value (Purohit, 1995). Canning of the custard apple pulp is problematic because of the development of bitterness and browning on heating beyond 55°C (Bhatia, Sastry, Krishnamurthy, Nair, and Lal, 1961; Martinez, Medina, Fans, and Gill, 1988; Salunkhe and Desai, 1984). In addition, an unpleasant off-flavour develops in the pulp when heated beyond 65 °C (Nanjunda Swamy & Mahadevaiah, 1993). Vinegar, from the French *vin aigre*, meaning “sour wine,” can be made from almost any fermentable carbohydrate source, including wine, molasses, dates, sorghum, apples, pears, grapes, berries, melons, coconut, honey, beer, maple syrup, potatoes, beets, malt, grains, and whey. Initially, yeasts ferment the natural food sugars to alcohol (Naseem Ullah *et al.*, 2014). This paper reports an attempt to utilize custard apple for the production of vinegar. Vinegar is produced by fermentation of alcohols to acetic acid by bacteria (Anchanarach *et al.*, 2010). The acetic acid bacteria break down the sugars or starch in the substrate converting it to alcohol and then further to acetic acid by different enzymes (Anchanarach *et al.*, 2010). The vinegar can then be used in dressing salads, manufacture of useful

medicines, preservation of food stuffs, provision of antioxidants or as an antibacterial agent (Johnston *et al.*, 2004; Shizuma *et al.*, 2011; Soltan and Shehata, 2012). Vinegar is commonly obtained from good wine, cider, fruits and starchy foods (Silva and Swarnakar, 2007; Krusong and Assanee, 2010). These undergo fermentation by acetic acid bacteria during the process of secondary fermentation.

Since the custard apple has nearly 24% sugars, it was hypothesized that this can be further processed by fermentation into a valuable product such as vinegar. The production of vinegar from the custard apple can be of great value to the country both economically (by increasing the economic value of custard apple, providing locally made vinegar on the market, creating jobs and reducing seasonal losses of the fruits) and will also provide an avenue to utilize the underutilized or culinary fruit.

II. MATERIALS AND METHODS

Custard apples (*Annona squamosa*) fruits were procured in bulk from the local market. Chemicals used in experimentation and analysis were of analytical grade, purchased from standard Indian companies. Media and chemicals used for microbial analysis were also from standard companies.

2.1 Extraction of pulp

Fully ripened fruits were selected and the pulp was extracted manually under hygienic conditions. The seeds and pulp were separated from each other by rubbing the mixture on a 30 mesh sieve leaving the seeds and the covering sheath of the capillary pulp (Seema *et. al.*, 2008 and Mysore *et. al.*, 2008).

2.2 Preparation of custard apple must

The physicochemical properties of the extract were measured and recorded in Table 1. The brix of the extract was adjusted to 22°Brix and ammonium sulphate (111ppm) added to stabilize the must and to provide a nitrogen source for yeast. The pH of the must was adjusted to 4 by adding 120 ml of vinegar. The treated must was pasteurized at 63°C for 30 minutes and then allowed to cool to room temperature of 25°C.

2.3 Preparation of the yeast starter culture

A small amount of must (20 ml) was inoculated with viable wine yeast (*Saccharomyces cerevisiae*) at a rate of 0.3g/L and left to incubate in a water bath for approximately 20 minutes.

2.4 Must inoculation for alcoholic fermentation

Approximately 3.8 liters of standardized must was poured into a 10 liter sterile plastic jerry-can and inoculated with 20 ml of the yeast starter culture. The jerry-can was tight fitted with an air lock filled with distilled water. The inoculated must was subjected to primary fermentation at ambient temperature for 7 days to produce custard apple

wine, which was then filtered using a sterile folded muslin-cheese cloth after complete primary fermentation. After alcoholic fermentation alcohol content must checked only 0 – 1 % TSS must remain. Fermentation was started for sedimentation and strained through cloth and clarified supernatant is taken in bottle up to ¾ capacities.

2.5 Must preparation and Acetic acid fermentation

The wine obtained after the alcoholic fermentation contained 11.50% (v/v) alcohol. It was filtered and alcohol wort added for vinegar production. The addition of alcohol wort for vinegar production was conducted by taking out 4 L of unpasteurized vinegar with about 6% (w/v) acidity and adding 2.8 L of alcohol wort with 11.50% (v/v) alcohol content. For vinegar fermentation the alcohol content of the fermented liquor was adjusted to 7 – 8 % by diluting with water. (Byarugaba-Bazirake *et al.*, 2014)

2.6 Acetic acid fermentation

The acetic fermentation was conducted by seeding the wine obtained at alcoholic fermentation with acetic acid bacteria @ 10 % v/v stirred and the bottle mouth was closed by cork with the two holes in it for proper aeration as *Acetobacter aceti* is aerobic and their activity is greatly reduced by light so kept in dark.

2.7 Aging

As the vinegar prepared was turbid and does not possess a good taste. It was stored in container during which the vinegar develops a good aroma and flavour and becomes mellows.

2.8 Pasteurization

It was poured in previously sterilized bottles, corked air tight and the bottles were heated in hot water at 71 to 77°C for 15 – 20 min so that growth of vinegar bacteria was stopped and the strength of vinegar was maintained during storage.

2.9 Routine analyses

A sample of vinegar was analysed every two days for the ethanol content, pH, and total acidity. Monitoring of the per cent alcohol production (%v/v) was done by gravimetric Analysis, Percent acetic acid production (w/w) was done by neutralizing samples at pH 7.2 with 0.1N NaOH; it was assumed that all medium acidities were due to acetic acid, pH was estimated using pH meter; (Hanna) and total soluble solids as degrees Brix using RHB-32 (ATC) refractometer; ATAGO) (Ranganna, 1986)acquired over a period of 30 days at room temperature.

2.10 Sensory evaluation of vinegar

The quality attributes like taste, flavour, color and overall acceptability were judged by panel members on the basis of nine point's hedonic scale. A single portion of vinegar preparation was served in a glass bowl. The judges were

instructed to fill the nine point hedonic score card for each vinegar.

III. RESULTS AND DISCUSSION

Table 1 depicted the physiochemical properties of the custard apple extract, and was found that the total sugars

were quite high as 22.5 %, TSS 28 °Bx and acidity 0.45%. The results were compared to those obtained by Sravanthi *et. al.*, (2014), i.e. 28 °Bx and 21.42% TSS, total sugars, respectively and similar results were also reported by Kolekar and Tagad, 2012.

Table.1: Physiochemical Properties of Custard Apple Extract

Sr. No	Parameters	Content
1.	Edible portion(g)	45
2.	Moisture (%)	70
3.	Total sugars (%)	22.5
4.	Protein (%)	1.5
5.	Fat (%)	0.3
6.	Minerals (%)	0.9
7.	Acidity (%)	0.45
8.	TSS(°Bx)	28
9.	Vitamins(mg)	37
10.	Ascorbic acid (mg/ 100g)	9.20

Primary fermentation was carried out at room temperature (25°C). The process undergoes to form various intermediate products through glycolysis in anaerobic condition. This resulted in a light brown colored custard apple wine with an alcohol content of 11.50% (v/v).The custard apple wine obtained (Table 2) was then subjected

to a two-step fermentation system using a batch process. This involved enzymatic oxidation where the ethanol substrate was first oxidized to acetaldehyde and subsequently oxidized to the final product, acetic acid. This process was carried out over a period of 30 days.

Table.2: Physiochemical properties of wine and vinegar*

Sr. No	Parameters	Content	
		Wine	Vinegar
1.	TSS (°Bx)	6±1.00	2±0.00
2.	Alcohol content (%)	11.50	1.0
3.	Specific gravity (gm/ml)	0.984±0.00	1.019±0.001
4.	pH	3.5±0.00	2.8±0.01
5.	Total acidity (%)	0.16±0.001	5.39±0.00

* Values are means ±SD of triplicate determinations.

Before the initial mixing of the inoculum and fresh wine a very short lag phase with no significant acid production was observed. This may be due to the sudden change in the medium conditions at the initial mixing that affected fermentative microorganisms. According to Brock and Madigan (1991), the observed microorganisms response can be explained as an adaptation phase in which the required enzymes for substrate degradation are synthesized. During the lag phase, acetic acid bacteria use the main proportion of their energy resources in this synthesis. It is therefore not surprising that no net production of acetic acid was produced.

The decrease in alcohol concentration was corresponded to the gradual rise in acetic acid concentration (T.T.A)

which accumulated from 11.50 to 1.0% (v/v) over a fermentation progress period of 30 days. The ethanol content in garlic vinegar was nil and onion vinegar have 2g/l (Horiuchi *et al.*, 1999). Alcohol induces stress in yeast cells causing their death and flocculation, but the stress of yeast is more related to acetaldehyde which is the first intermediate product of ethanol biological oxidation by *Acetobacter aceti*. This acetaldehyde disrupts the enzymatic activity of yeast. The beginning of acetic acid formation is related to maximum cellular growth and sufficient biomass density to start the acetification process (Seyram *et al.*, 2009).

The pH of the vinegar during the secondary fermentation was recorded to decrease slightly from pH 3.5 to pH 2.8.

The result obtained was similar to recommendations of Sassou *et al.*, 2009 who recommended that pineapple vinegar has a pH 2.8. This slight initial increase in acidity provided optimal growth conditions to initiate acetification. This fall in pH can be accredited to accumulation of acetic acid and other volatile short chain organic acids such as propionic, tartaric and butyric acids, which are important in development of the flavor and aroma of vinegar (Seyram *et al.*, 2009).

The alcohol content continued to decrease with time from 11.50% to about 1% by the 30th day. This deduces that the alcohol conversion to acetic acid reaches one when acetic acid reaches to the maximum in the medium. The vinegar produced from the custard apple extract contained 5.39% (v/v) acetic acid and was comparable with 6.33% (v/v) and 6.11% (v/v) vinegar obtained by Torija *et al.*, (2010) in their study of two vinegar plants; Laguinnelle (B,Banyuls,France) and Viticultors Masd'en gil(P,bellmunt del priorat, Tarragona,Spain).

There was also a significant amount of sugar recorded (2.0 °Brix) in the custard apple wine vinegar by the end of the fermentation. This denotes that there is better utilization of sugar in the production of custard apple wine vinegar than custard apple wine (see Table 2). Therefore, the presence of fermentable sugars in custard apple can make them ideal substrates for alcoholic fermentation of fruit juice and subsequent secondary fermentation into vinegar.

Table 3 describes the sensory evaluation of custard apple vinegar. The sensory evaluation plays an important role in the quality of food. The overall acceptability of custard apple vinegar was 8.5 score, which were comparable to other market vinegar samples. The data obtained statistically depicts that the quality of the custard apple vinegar is very well comparable with market vinegars in terms of colour, flavour, taste and overall acceptability. It shows the market viability of the product to make it commercial.

Table.3: Sensory Evaluation of Custard Apple Vinegar*

Name of vinegar	Colour	Flavour	Taste	Overall acceptability
Custard apple vinegar	8.2±0.13	8.4±0.33	8.2±0.29	8.5±0.22
Market vinegar 1	8.1±0.11	7.8±0.22	8.8±0.29	8.8±0.21
Market vinegar 2	8.3±0.20	8.5±0.24	8.4±0.30	8.9±0.24
Market vinegar 3	8.4±0.25	8.8±0.26	8.5±0.24	8.7±0.23

* Values are means of ±SD of ten panel members

The overall acceptability of the market vinegar samples were rated as like extremely on the nine point hedonic scale, while custard apple vinegar was rated as like very much on the nine point hedonic scale. Though market vinegar 2 scored higher score (8.9±0.24) in overall acceptability on a total score of 9 than custard apple vinegar (8.5±0.22). The brownish colour of the custard apple vinegar is due to the enzymatic browning during pulping.

IV. CONCLUSION

The custard apple wine vinegar production process took 30 days and had physiochemical characteristics of 5.39% (v/v) acetic acid, 2.0°Brix, and pH of 2.8 which conformed with the standard ranges of brewed vinegar after complete fermentation. The aroma of the vinegar produced was appreciated by the consumers who were acquainted with vinegar. This study therefore, showed that custard apple can be used as an ideal substrate for production good quality vinegar. This not only increases the economical and food value of custard apple but also provides a way of utilizing custard apple in India.

REFERENCES

- [1] W.K. Anchanarach, G.T. Heeragool, T.I. Noue, T.Y. Akushi, O.A. Dachi, and K.M. Atsushita, "Acetic acid fermentation of *acetobacter pasteurianus*: relationship between acetic acid resistance and pellicle polysaccharide formation," Biosci Biotechnol Biochem., vol. 74, pp.1591–1597, 2010.
- [2] B. S. Bhatia, L. V. Sastry, G. V. Krishnamurthy, K.G. Nair and G. Lal. "Preservation of custard apple (*Annona squamosa* L.)," J. of Science of Food and Agriculture, vol.12, pp.529–532, 1961.
- [3] T.D. Brock and M.T. Madigan Biology of microorganisms. Englewood Cliffs, NJ: Prentice-Hall. 6th Ed. 1991. pp. 874.
- [4] W. J. Broughton and T. Guat, "Storage conditions and ripening of the custard apple *Annona squamosa* L.," Scientia Horticulturae, vol.10, Issue 1, pp. 73–82, 1979.
- [5] D. K. Butani, "Insect pests of fruit crops and their control - custard apple," Pesticides, vol.10, Issue 5, pp. 27-28. 1978.

- [6] G. W. Byarugaba-Bazirake, W. Byarugaba, M. Tumusiime and D. A. Kimono, "The technology of producing banana wine vinegar from starch of banana peels," African J. of Food Science and Technology, vol.5. Issue.1, pp.1-5. 2014.
- [7] K. L. Chadha, "Export of fresh fruits and nuts from India," J. of Appl. Hort, vol. 1. Issue.2, pp.1-18. 1995.
- [8] J. I. Horiuchi, T. Kamo and M. Kobayachi, "New vinegar production from onions," J. of Bioscience and Bioengineering, vol.88. Issue.1, pp.107-109, 1999.
- [9] C. Johnston, C. Kim and A. Buller, "Vinegar improves insulin sensitivity to A high-carbohydrate meal IN subjects with insulin resistance OR type 2 diabetes," Diabetes care. vol, 27, pp. 272–290. 2004.
- [10] T. N. Kolekar and V. B. Tagad, "Studies on Physico-chemical properties Of Custard Apple Fruit," Indian Streams Research J, vol. 2. Issue. 8, pp. 1-4, 2012.\
- [11] W. Krusong and V. Assanee, "An investigation of simultaneous pineapple vinegar fermentation interaction between acetic acid bacteria and yeast," Asian J. of Food and Agro-Industry, vol. 3, pp. 192–203. 2010.
- [12] A.R Luciana, L. Santos, P.S.P Lucia and D. Maria, Amelia, "Boaventura acetogenins from *Annona cornifolia* and their antioxidant capacity," Food Chem., vol. 122, pp.1129–1138. 2010.
- [13] V. Mariappan and R. C. Saxena, "Effect of custard-apple oil and neem oil on survival of nephotettix virescens (homoptera: cicadellidae) and on rice tungro virus transmission," J. of Economic Entomology, vol.76, Issue.3, pp.573-576. 1983.
- [14] C. M. Martinez, L.S. Medina, M.J. Fans and S. Gill, "Cherimoya.(*Annona cherimola* Mill), polyphenol oxidase, monophenolase and dihydroxyphenolase activities," J. of Food Science., vol. 53, pp.1191–1194, 1988.
- [15] N. S. Mysore, R. Baskaran., J.R. Lingamall, Munusamy. and R.V. Somasundaram and R. Rajarathnam, "Influence of processing conditions on flavour compounds of custard apple (*Annona squamosa* L)," LWT - Food Science and Technology., vol.41, Issue.2 pp. 236-243.2008.
- [16] A. M. Nanjunda Swamy and M. Mahadevaiah, Fruit processing. In: K. L. Chadha, and O. P. Pareek (Eds.), Advances in horticulture, Vol. 4, New Delhi: Malhotra Publishing House, 1993, pp. 1835.
- [17] Naseem Ullah, Javed Ali, Shahzeb Khan, Farhat Ali Khan, Zia-ur-Rehman and Arshad Hussain, "Production and quality evaluation of garlic (*Allium sativum*) vinegar using *acetobacter aceti*," Life Science Journal, vol.11, pp.158-160.2014.
- [18] R. J. Nissen, B.I. Brown, A.P. George and L. S. Wong, "Comparative studies on the postharvest physiology of fruit from different species of *Annona* (custard apple)," J of Horti. science, vol. 63 Issue. 3, pp.521—528. 1988.
- [19] R.N. Okigbo and O. Obire, "Mycoflora and production of wine from fruits of soursop (*Annona muricata* L.)," International J. of Wine Research, vol. 1, pp. 1–9 2009.
- [20] S. Pareek, E.M. Yahia, O. P. Pareek and R.A. Kaushik, "Post-harvest physiology and technology of *Annona* fruits," Food Research International, vol. 44, pp.1741–1751.2011.
- [21] S. R. Popale, S. B. Gaikwad and R. A. Dagadkhair, "Studies on preparation of custard apple wine by using *Sacchromyces cerevisiae var. Ellipsoide*," Beverage and Food World, vol. 12, pp. 38-39. 2012.
- [22] A.G. Purohit, "Annonaceous fruits. In D. K. Salunkhe, & S. S. Kadam (Eds.), Hand book of fruit science and technology," New York: Marcel Dekker Press. 1994. pp. 377–385.
- [23] S. Ranganna, "Hand Book of analysis and quality control for fruits & vegetables products," 2nd edition Tata Mc Graw Hill Publishing Co. Ltd. New Delhi. 1986.
- [24] D.K. Salunkhe and B.B. Desai, "Custard apple. In Post-harvest biotechnology of fruits," Boca Raton, FL: CRC Press. 1984, pp. 133.
- [25] S.K. Sassou, Y. Ameyapoh, S.D. Karou and C. Sauzade, "Study of pineapple peelings processing into vinegar by biotechnology," Pakistan J. of Biological Sciences, vol.12, Issue. 11, pp. 859- 865. 2009.
- [26] M. K. Seema, G. K. Jayaprakasha, and R.P. Singh, "Antioxidant activity of custard apple (*Annona squamosa*) peel and seed extracts," J. of Food Science and Technology, vol. 45, Issue. 4, pp. 349-352. 2008.
- [27] K. Seyram, Sossou, Yaovi Ameyapoh Simplicie, D. Karou. and Comlan De Souza," Study Of pineapple peelings processing into vinegar by biotechnology," Pakistan J. of Biological Sciences, vol.12, Issue.11, pp.859- 865. 2009.
- [28] T. Shizuma, K. Ishiwata, M. Nagano, H. Mori and N. Fukuyama, "Protective effects of fermented rice vinegar sediment (*Kurozu moromimatsu*) in a diethylnitrosamine induced hepatocellular carcinoma animal model," J. of Clinical Biochemical Nutrition, vol. 49, pp. 31–35.2011.
- [29] F. L. H. Silva and R. Swarnakar, "Cashew wine vinegar production: alcoholic and acetic

- fermentation,” *Brazilian J. of Chemical Engineering.*, vol. 24, pp.163–169. 2007.
- [30] S. Soltan Sahar and M. M. E. M Shehata, “Antidiabetic and hypocholesterolemic effect of different types of vinegar in rats,” *Life Science J*, vol. 9, pp. 2141–2151.2012.
- [31] T. Sravanthi, K. Waghrey and Jayasimha Rayalu Daddam, “Studies on preservation and processing of custard apple (*annona squamosa*) pulp,” *International J. Of Plant, Animal And Environmental Sciences*, vol. 4, Issue. 3, pp. 676-682. 2014.
- [32] M. J. Torija, A. Mas, C. Vegas, M. Estibaliz, A. Gonzalez, M.C. Guillamon, and M. Poblet, “Population dynamics of acetic acid bacteria during traditional wine vinegar production,” *Food Microbiology*, vol. 27, pp. 257–265.2010.

Health benefits of Green and Black Tea: A Review

K.H.G.K. Kodagoda, I. Wickramasinghe

Department of Food Science and Technology, Faculty of Applied Sciences, University of Sri Jayewardenepura, Gangodawila, Nugegoda, Sri Lanka

Abstract— *Tea, (Camellia sinensis) is grown in about thirty countries and next to water, is the most widely consumed beverage in the world. Based on the type of the processing, three tea types can be identified as Green, Black and Oolong tea. Drinking tea has been considered a health-promoting habit since ancient times. The modern medicinal research is providing a scientific basis for this belief. Various studies have suggested the health promoting effects of green and black tea is due to its polyphenolic compounds mainly catechins. Unlike green tea, health benefits of consuming black tea are not extensively discussed. This review is mainly focused on the health benefits of consuming green and black tea.*

Keywords— *Black tea, Green tea, health benefits, polyphenols.*

I. INTRODUCTION

Tea is the most consumed beverage in the world after water. Legends of China and India have indicated that the tea consumption is one of the very ancient habits. Traditionally, tea was drunk to improve blood flow, eliminate toxins, and to improve resistance to diseases [1]. The spread of tea cultivation to India between 1818 and 1834 can be considered as the origin of the modern tea industry. Through cultivation, tea has become an important agricultural product throughout the world, particularly in regions lying close to the equator [2]. Tea, from the plant *Camellia sinensis*, is consumed in different parts of the world as green, black or oolong tea [3].

Green tea is prepared by dehydration of tea leaves which does not lead to the oxidation of constituent polyphenols, therefore green tea, contains high concentrations of monomeric polyphenols from the catechins group [4]. Black tea, obtained by tea leaves with fermentation, is oxidized and contains mainly multimeric polyphenols, whose biological activity is not well documented [5]. And Oolong tea is a partially oxidized product [6]. Green tea is best studied for decades for its health benefits, including cancer chemo preventive and chemotherapeutic effects [7], [8] but in recent years, black tea is also extensively investigated mainly regarding its influence on human health [9].

II. PROCESSING OF GREEN AND BLACK TEA

Green and black tea is mainly produced from *Camellia sinensis* var. *sinensis*. The primary goal in the manufacture of green tea is the preservation of the leaf catechins. The steps of processing include plucking, rapid enzyme inactivation by steaming or pan firing, rolling, and high temperature air drying. Glycosides of aromatic and terpene alcohols found in the growing leaf are rapidly hydrolyzed after plucking to form the free volatile alcohols. The rolling process imparts a twist which improves appearance. During the final drying step many new aromatic compounds are formed which impart important characteristics of green tea flavour. Green tea composition is similar to that of the fresh leaf with regard to the major components [6].

The black tea production begins with plucking, withering, maceration (rolling) and finally drying. During withering, the leaves take on a form facilitating the rolling process. This process results in disrupting the cell structure of the leaves and the fermentation process then begins [10]. In the black tea production process, about 75% of catechins contained in the tea leaves undergo enzymatic transformation consisting in oxidation and partial polymerization [11], [12]. Because the main enzyme taking part in these processes is tea leaf polyphenol oxidase, it is essential to assure its direct contact with polyphenols and atmospheric oxygen. The resulting black tea composition depends on the technological process of its production [10].

III. COMPOSITION OF GREEN AND BLACK TEA

Normally the composition of tea leaf varies with climate, season, horticultural practices, variety of the plant, and age of the leaf, i.e. the position of the leaf on the harvested shoot [6]. With regard to the major components, green tea composition is similar to that of the fresh leaf. Green tea contains polyphenolic compounds, which include flavanols, flavandiols, flavonoids, and phenolic acids. These compounds account for up to 30% of the dry weight of green tea leaves. Most of the polyphenols present in green tea are flavanols, commonly known as catechins. Some major catechins present in green tea are (-)-epicatechin

(EC²), (-)-epicatechin-3-gallate (ECG), (-)-epigallocatechin (EGC), and (-)-epigallocatechin-3-gallate (EGCG). In addition, caffeine, theobromine, theophylline, and phenolic acids such as gallic acids are also present in green tea [11].

It is difficult to state a definitive composition for black tea beverage, as it varies with different preparations [6]. In the process of manufacturing of black tea catechins are mostly oxidized to theaflavins or thearubigins. For tropical black tea they occur as 15-20% thearubigins, 1-2% theaflavins and 5-10% catechins on a dry-weight basis [13]. In addition, methylxanthines are present with 2 to 4% as caffeine and as a small amount of theophylline and of theobromine [14].

Table.1: Green and Black Tea composition [2]

Compound	Green Tea (% wt/wt solids)	Black tea (% wt/wt solids)
Catechin	30	9
Theaflavins	-	4
Simple polyphenols	2	3
Flavonols	2	1
Other polyphenols	6	23
Theanine	3	3
Amino acids	3	3
Peptides/Proteins	6	6
Organic acids	2	2
Sugars	7	7
Other Carbohydrates	4	4
Lipids	3	3
Caffeine	3	3
Other methylxanthines	<1	<1
Potassium	5	5
Other minerals/ash	5	5
Aroma	Trace	Trace

IV. HEALTH BENEFITS OF GREEN AND BLACK TEA

4.1 Cancer prevention

Accumulation of reactive oxygen species in cells and resulting modifications in DNA structure, enzymatic activity, and defense mechanisms all influence the development of the cancer pathogenesis [15]. Tea consumption has been reported to have beneficial effects against different types of cancers due to its antioxidants which have the ability to prevent and control cancer development. Many *in vivo* studies conducted with rodents have shown that tea protects against many types of cancer and at most stages of carcinogenesis [16]. Green tea and green tea polyphenols have been shown to have anti-cancer activity in a number of laboratory studies, which could be mediated through antioxidant or pro-oxidant mechanisms

[17]. Green tea polyphenols such as EGCG inhibit cell viability and induce apoptosis in a number of cancer cell lines such as osteogenic sarcoma [18], lymphoblastoid cells [19], leukemia cells [20], melanoma cells [21], T lymphocytes [22] and larynx carcinoma [23]. EGC can inhibit breast cancer cell viability through induction of apoptosis, yet not in normal breast cells [24]. Green tea can induce apoptotic cell death in cancer better than other teas as it has the highest concentration of polyphenols [25]. The activity of the tea and its polyphenols on the inhibition of the skin tumorigenesis has been well studied [4]. Early studies have demonstrated that topical application or ingestion of green tea polyphenols or EGCG inhibit tumor initiation and promotion by chemical carcinogens and UV light in mice [26]-[29]. Black tea has similar effects [29]-[32]. Topical application of a green tea polyphenolic fraction on mice skin papillomas can decrease significantly the conversion of benign tumors to malignant tumors [33]. Reduction in lung tumor number is observed when mice are treated with green or black tea, EGCG, or decaffeinated teas prior to chemical induction of lung tumorigenesis [25], [34].

Tea polyphenols; theaflavine gallate of black tea and epigallocatechin gallate of green tea can inhibit the formation of heterocyclic amines from cooked fish and meat which are genotoxic carcinogens associated with cancer of the breast, colon and pancreas [11].

Tea drinking was associated with reduced risk of lung cancer in male cigarette smokers in a case control study in Uruguay [35]. In a population-based case-control study in Shanghai, China, consumption of green tea was associated with a reduced risk of lung cancer among non-smoking women and the risk decreased with increasing consumption [36]. In a case control study, a protective effect of frequent, daily or several times/week black tea drinking appeared among non-smoking women [37].

4.2 Cardiovascular disease (CVD) prevention

Consumption of tea is increasingly being shown to be associated with enhanced cardiovascular and metabolic health [25]. In coronary heart diseases, atherosclerotic plaque formation is caused by the deposition and the oxidation of low-density lipoprotein (LDL) at the lesion sites of artery walls when the tocopherol levels are depleted. Studies testing the antioxidant effect of tea polyphenols on LDL and VLDL (very low-density lipoproteins) oxidation indicate that EGCG is very effective and has a lipoprotein bound antioxidant activity greater than tocopherol [38]. Black tea extract also increases the resistance of LDL to oxidation in a concentration dependent manner [39], but at low concentrations, tocopherol is more effective [40]. Green tea catechins affect lipid metabolism by different pathways and prevent the appearance of atherosclerotic plaque [25].

4.3 Diabetes

Various studies have shown that tea may affect glucose metabolism and insulin signaling, causing interest in the health effects of tea consumption on diabetes [25]. Green tea can reduce blood glucose levels in aged rats, an indicator of diabetes frequently observed in the aging population [41]. Tea suppresses the activity of glucosetransporters in the intestinal epithelium and is believed to reduce dietary glucose intake [42]. In another study conducted in Iran with forty-six patients with type II diabetes mellitus, it was found that regular intake of black tea extracts had anti-oxidative and anti-inflammatory effects in the patients [43].

4.4 Anti-bacterial effect

Tea polyphenols are also known for their antibacterial activity. In general, antibacterial activity decreases when the extent of tea fermentation is increased, implying stronger activity in green tea than black tea [44],[45]. Green tea catechins, particularly EGCG and ECG, have antibacterial activity against both Gram-positive and Gram-negative bacteria [46]-[48]. Broadly, Gram-positive bacteria are more sensitive to tea extracts than Gram-negative bacteria [47]. The antibacterial activity of black tea has also been reported [44]-[46]. Tea extracts exhibits inhibitory effects against several food pathogens, including *Staphylococcus aureus*, *Shigelladisenteriae*, *Vibrio cholerae*, *Campylobacter jejuni*, *Listeria monocytogenes*, etc. [49],[50]. Drinking tea also leads to a reduction of enterobacteria which produce ammonia, skatole and other harmful amines and a beneficial increase in the level of *lactobacilli* and *bifidobacteria* which produce organic acids and lower the intestinal pH [51],[52].

4.5 Oral health

Linke and LeGeros[53] indicated that frequent intake of green tea can significantly decrease caries formation, even in the presence of sugars in the diet. In vivo animal studies have shown that specific pathogen-free rats infected with *Streptococcus mutans* and then fed with a cariogenic diet containing green tea polyphenols have significantly lower caries scores [54]. Several studies have indicated that polyphenols from green tea inhibit growth, acid production, metabolism, and glucosyltransferase enzyme activity of *S. mutans* and dental plaque bacteria [55].

Adults rinsing with black tea 10 times a day for 7 days had a significantly less pronounced pH fall, lower plaque index ($P < 0.05$), and numerically fewer *S. mutans* and total oral *Streptococci* in plaque but not in saliva. Fluoride concentrations in plaque and saliva increased, reaching a maximum at day 7 [56]. It is evident that black tea and its polyphenols also benefit human oral health by inhibition of dental plaque, its acidity, and its cariogenic microflora [55].

4.6 Bone mineral density

Bone Mineral Density also is positively associated with tea consumption, which may optimize bone health [57]. Specifically, green tea appeared to benefit bone health more than other kinds of tea (e.g., black, oolong), which may be due to decreased oxidative stress [58], [59], increased activity of antioxidant enzymes [58], and decreased expression of pro-inflammatory mediators [58],[59]. Tea-derived flavonoids and lignans may also improve bone mineral density [60]-[62], particularly in older women with low concentrations of endogenous oestrogen.

4.7 Obesity

Obesity and the comorbidities associated with obesity remain a global health problem [63]. Epidemiological evidence and several randomized controlled intervention trials have shown an inverse relationship between habitual tea consumption (predominately green tea) and levels of body fat and waist circumference [64],[65]. While green tea contains an array of compounds, the putative antiobesity effects have been most commonly attributed to the polyphenolic fraction of green tea, specifically the catechins [66]. Green tea catechins induces antiobesity effects by thermogenesis and substrate oxidation which are mediated by sympathetic nervous system activity, modifications in appetite control, down-regulation of enzymes involved in hepatic lipid metabolism, and decreased nutrient absorption [63]. But according to Pan et al.,[67]black tea polyphenols are more effective than green tea polyphenols in body weight reduction. Black tea polyphenols inhibit lipid and saccharide digestion, absorption and intake, promote lipid metabolism and block pathological processes of obesity and the comorbidities of obesity by reducing oxidative stress [67].

V. CONCLUSION

Green and black tea can be considered as a healthy drink rather than a traditional beverage due to its pharmacologically active molecules. It is increasingly recognized that tea contains polyphenols and other components that may reduce the risk of developing chronic diseases such as cancer, cardiovascular diseases, diabetes, promote weight loss and oral health and increase bone mineral density. As the human clinical evidence is still limited, future research needs to define the actual magnitude of health benefits, establishes the safe range of tea consumption associated with these benefits, and elucidates the mechanisms of action. The development of biomarkers for green and black tea consumption, as well as molecular markers for their biological effects, will facilitate future research in this area.

REFERENCES

- [1] Balentine D.A., Wiseman, S. A. and Bouwens, L. C. (1997). The chemistry of tea flavonoids, *Crit. Rev. Food Sci. Nutr.* 37,pp.693–704.
- [2] Harbowy, M., Balentine, D., Davies, A. and Cai, Y. (1997). Tea Chemistry. *Critical Reviews in Plant Sciences*, 16(5), pp.415-480.
- [3] Chacko, S., Thambi, P., Kuttan, R. and Nishigaki, I. (2010). Beneficial effects of green tea: A literature review. *Chinese Medicine*, 5(1), p-13.
- [4] Dufresne C. J. and Farnworth, E. R. 2001). A review of latest research findings on the health promotion properties of tea. *J NutrBiochem*, 12,pp.404– 412.
- [5] Haslam, E. (2003).Thoughts on thearubigins. *Phytochemistry*,64,pp.61 – 73.
- [6] Graham, H. N. (1992). Green tea composition, consumption, and polyphenol chemistry. *Preventive Medicine*, 21(3), pp.334-350.
- [7] Khan, N., Afaq, F. and Mukhtar, H. (2008). Cancer chemoprevention through dietary antioxidants: progress and promise. *Antioxid Redox Signal*,10,pp. 475–510.
- [8] Khan, N. and Mukhtar, H. (2008).Multitargeted therapy of cancer by green tea polyphenols. *Cancer Lett.*,269, pp.269–680.
- [9] Retveld, A. and Wiseman, S. (2003). Antioxidant effects of tea: evidence from human clinical trials. *J Nutr.*,133, pp.3285– 3292.
- [10] Luczaj, W. and Skrzydlewska, E. (2005). Anti-oxidative properties of black tea. *Preventive Medicine*, 40(6),pp. 910-918.
- [11] Katiyar, S. and Mukhtar, H. (1996). Tea in chemoprevention of cancer. *International Journal of Oncology*.8,pp.221-238
- [12] Mikhail A. Bokuchava , Nina I. Skobeleva and Gary W. Sanderson (1980). The biochemistry and technology of tea manufacture, *C R C Critical Reviews in Food Science and Nutrition*, 12:4, 303-370, DOI: 10.1080/10408398009527280
- [13] Hara, Y. (2001). *Green tea:health benefits and applications*. New York: Marcel Dekker,pp.22-25
- [14] Hara, Y., Luo, S. J., Wickremashinghe, R. L. and Yamanishi, T. (1995a). Botany (of tea). *Food Rev. Int.*, 11, pp.371-374.
- [15] Mate´s, J. M. and Sa´nchez-Jime´nez, F. M. (2000). Role of reactive oxygen species in apoptosis: implications for cancer therapy, *Int. J. Biochem. Cell Biol.*, 32,pp.157–170.
- [16] Dreosti, I. E., Wargovich, M.J. and Yang, C. S. (1997). Inhibition of carcinogenesis by tea: the evidence from experimental studies, *Crit. Rev. Food Sci. Nutr.* 37, pp.761–770.
- [17]Forester, S. and Lambert, J. (2011). The role of antioxidant versus pro-oxidant effects of green tea polyphenols in cancer prevention. *Molecular Nutrition & Food Research*, 55(6), pp.844-854
- [18] Ji, S. J., Han, D. H. and Kim, J. H. (2006). Inhibition of proliferation and induction of apoptosis by EGCG in human osteogenic sarcoma (HOS) cells. *Arch Pharm Res.*29, pp.363–368.
- [19] Noda, C., He, J., Takano, T., Tanaka, C., Kondo, T., Tohyama, K., Yamamura, H. and Tohyama, Y. (2007). Induction of apoptosis by epigallocatechin-3-gallate in human lymphoblastoid B cells. *BiochemBiophys Res Commun.*362, pp.951– 957
- [20] Nakazato, T., Ito, K., Miyakawa, Y., Kinjo, K., Hozumi, N., Ikeda, Y. and Kizaki, M. (2005). Catechin, a green tea component, rapidly induces apoptosis of myeloid leukemic cells via modulation of reactive oxygen species production in vitro and inhibits tumor growth in vivo. *Haematologica*. 90, pp.317–325.
- [21] Nihal, M., Ahmad, N., Mukhtar, H. and Wood, G. S. (2005). Anti-proliferative and proapoptotic effects of (–)-epigallocatechin-3-gallate on human melanoma: Possible implications for the chemoprevention of melanoma. *Int. J Cancer*. 114, pp.513–521.
- [22] Li, H. C., Yashiki, S, Sonoda J, Lou H, Ghosh SK, Byrnes JJ, Lema C, Fujiyoshi T, Karasuyama M, Sonoda S. (2002). Green tea polyphenols induce apoptosis in vitro in peripheral blood T lymphocytes of adult T-cell leukemia patients. *Jpn J Cancer Res.*, 91, pp. 34–40.
- [23] Lee JH, Jeong YJ, Lee SW, Kim D, Oh SJ, Lim HS, Oh HK, Kim SH, Kim WJ, Jung JY. EGCG induces apoptosis in human laryngeal epidermoid carcinoma Hep2 cells via mitochondria with the release of apoptosis-inducing factor and endonuclease G. *Cancer Lett.* 2010;290:68–75.
- [24] Vergote D, Cren-Olive C, Chopin V, Toillon RA, Rolando C, Hondermarck H, Le Bourhis, X. F. (2002). (–)-epigallocatechin (EGC) of green tea induces apoptosis of human breast cancer cells but not of their normal counterparts. *Breast Cancer Res Treat.*, 76, pp. 195–201.
- [25] Khan, N. and Mukhtar, H. (2013). Tea and Health: Studies in Humans. *Current Pharmaceutical Design*, 19(34), pp.6141-6147.
- [26] Yang, C. S. and Wang, Z. Y. (1993). Tea and cancer: review, *J. Natl. Cancer Inst.* 85, pp. 1038–1049.
- [27] Wang, Z. Y., Huang, M.T., Chang, R., Ma, W., Ferraro, T., Reulh, K. R., Yang, C. S. and Conney, A. H. (1992). Inhibitory effect of green tea on the growth of established skin papillomas in mice, *Cancer Res.* 52, pp. 6657–6665.

- [28] Wang, Z. Y., Huang, M. T., Ferraro, T., Wong, C. Q., Lou, Y. R., Reulh, K., Latropoulos M., Yang, C. S. and Conney, A. H. (1992). Inhibitory effect of green tea in the drinking water on tumorigenesis by ultraviolet light and 12-O-tetradecanoylphorbol-13-acetate in the skin of SKH-1 mice, *Cancer Res.* 52, pp.1162–1170.
- [29] Conney, A. H., Lu, W. -P., Lou, Y. -R., Xie, J. -G. and Huang, M. -T. (1999). Inhibitory effect of green and black tea on tumor growth, *Proc. Soc. Exper. Biol. Med.* 220, pp.229–233.
- [30] Katiyar, S. K. and Mukhtar, H. (1997). Inhibition of phorbol ester tumor promoter 12-O-tetradecanoylphorbol-13-acetate-caused inflammatory responses in SENCAR mouse skin by black tea polyphenols, *Carcinogenesis* 18, pp. 1991–2006.
- [31] Wang, Z. Y., Huang, M. T., Lou, Y. R., Xie, G. J., Reulh, K. R., Newmark, H. L., Yang, C. S. and Conney, A. H. (1994). Inhibitory effects of black tea, green tea, decaffeinated black tea, and decaffeinated green tea on ultraviolet B light-induced skin carcinogenesis in 7,12-dimethylbenz[a]anthracene-initiated SKH-1 mice, *Cancer Res.* 54, pp. 3428 – 3435.
- [32] Lu, Y.-P., Lou, Y.-R., Xie, J.-G. , Yen, P., Huang, M.-T. and Conney, A. H. (1997). Inhibitory effect of black tea on the growth of established skin tumors in mice: effects on tumor size, apoptosis, mitosis and bromodeoxyuridine incorporation into DNA, *Carcinogenesis* 18, pp.2163–2169.
- [33] Katiyar, S. K., Agarwal, R. and Mukhtar, H. (1993). Protection against malignant conversion of chemically induced benign skin papillomas to squamous cell carcinomas in SENCAR mice by a polyphenolic fraction isolated from green tea, *Cancer Res.*, 53, pp. 5409–5412.
- [34] Cao, J., Xu, Y., Chen, J. and Klaunig, J. E. (1998). Chemopreventive effects of green and black tea on pulmonary and hepatic carcinogenesis, *Fund. Appl. Toxicol.*, 29, pp. 244–250.
- [35] Mendilaharsu M, De Stefani E, Deneo-Pellegrini H, Carzoglio JC, Ronco A. (1998). Consumption of tea and coffee and the risk of lung cancer in cigarette-smoking men: a case-control study in Uruguay. *Lung Cancer*, 19, pp.101–107.
- [36] Zhong, L., Goldberg, M. S., Gao, Y. T., Hanley, J. A., Parent, M .E. and Jin, F. A.(2001).population-based case-control study of lung cancer and green tea consumption among women living in Shanghai, China. *Epidemiology*,12, pp.695–700.
- [37]Kubik, A. K., Zatloukal, P., Tomasek, L. et al. (2004). Dietary habits and lung cancer risk among non-smoking women. *Eur J Cancer Prev.*, 13, pp.471–480.
- [38] Vinson, J.A., Jang, J., Dabbagh, Y. A., Serry, M. and Cai, S. (1995). Plant polyphenols exhibit lipoprotein-bound antioxidant activity using an *in vitro* oxidation model for heart disease, *J. Agric. Food Chem.*, 43, pp.2798–2809.
- [39] McAngelis, G. T., McEneny, J., Pearce, J. and Young I. S. (1998). Black tea consumption does not protect low density lipoprotein from oxidative modification, *Eur. J. Clin. Nutr.*, 52, pp.202–206.
- [40] Nicolisi, R. J., Lawton, C. W. and Wilson, T. A. (1999). Vitamin E reduces plasma low density lipoprotein cholesterol, LDL oxidation, and early aortic atherosclerosis compared with black tea in hypercholesterolemic hamsters, *Nutr. Res.* 19, pp.1201–1214.
- [41] Zeyuan, D.,Bingying, T. X. L., Jinming, H. and Yifeng, C. (1998). Effect of green tea and black tea on the blood glucose, the blood triglycerides, and antioxidation in aged rats, *J. Agric. Food Chem.* 46, pp.875–878.
- [42] Shimizu M. (1999). Modulation of the intestinal function by food substances, *Nahrung* 43, pp.154–158.
- [43] Neyestani TR, Shariatzade N., Kalayi, A. et al. (2010). Regular daily intake of black tea improves oxidative stress biomarkers and decreases serum C-reactive protein levels in type 2 diabetic patients. *Annals of Nutrition and Metabolism*, 57, pp.40–49.
- [44] Tiwari R. P., Bharti, S. K., Kaur, H. D., Dikshit, R. P. and Hoondal, G. S. (2005). Synergistic antimicrobial activity of tea and antibiotics. *Indian J Med Res.*, 122(1), pp.80–94
- [45] Almajano, M. P., Carbó, R., Jiménez J. A. and Gordon, M. H. (2008). Antioxidant and antimicrobial activities of tea infusions. *Food Chem.*, 108(1), pp.55–63.
- [46] Bancirova, M. (2010). Comparison of the antioxidant capacity and the anti-microbial activity of black and green tea. *Food Research International*, 43(5), pp, 1379–1382.
- [47] Toda, M., Okubo, S., Hiyoshi, R. and Shimamura, T. (1989). The bactericidal activity of tea and coffee. *LettApplMicrobiol.* 8(4), pp.123–125.
- [48] Hamilton-Miller, J. M. T. (1995). Antimicrobial properties of tea (*Camellia sinensis* L.) *Antimicrob Agents Chemother.*, 39(1), pp.2375–2377.
- [49] Negi, P. S., Jayaprakasha, G. K. and Jena, B. S. (2003). Antioxidant and antimutagenic activities of pomegranate peel extracts. *Food Chemistry*, 80(3), pp.393–397
- [50] Taguri, T., Tanaka, T. and Kouno, I. (2004). Antimicrobial activity of 10 different plant polyphenols against bacteria causing food-borne

- disease. *Biological and Pharmaceutical Bulletin*, 27(12), pp.1965–1969.
- [51] Yamamoto T., Juneja, L. R., Chu, D. C. and Kim, M. (1997). *Chemistry and Applications of Green Tea*. CRC Press LLC: Boca Raton, USA
- [52] Ernst, P. (1991). Review article: the role of inflammation in the pathogenesis of gastric cancer, *Aliment. Pharmacol. Therapeutics* 13 (Suppl. 1), pp. 13–18.
- [53] Linke, H. A. B. and LeGeros, R. Z. (2003). Black tea extract and dental caries formation in hamsters. *Int J Food Sci Nutr.*, 54:89–95
- [54] Otake, S., Makimura, M. and Kuroki, T. (1991). Anticaries effects of polyphenolic compounds from Japanese green tea. *Caries Res.*, 25, pp.438–442
- [55] Wu, C. D. and Wei, G. X. (2002). Tea as a functional food for oral health. *Nutrition* 18, pp.443–444
- [56] Wu, C. D., Wefel, J. S. and Lingstrom, P. (2001). Anticariogenic potential of black tea. *Proceedings of the American Society for Microbiology Annual Meeting*, 327
- [57] Shen, C., Yeh, J., Cao, J. and Wang, J. (2009). Green tea and bone metabolism. *Nutrition Research*, 29(7), pp.437–456
- [58] Shen C. L., Wang, P., Guerrieri, J., Yeh, J. and Wang, J. S. (2008). Protective effect of green tea polyphenols on bone loss in middle-aged female rats. *Osteoporosis Int.*, 19(7), pp.979–990.
- [59] Shen, C. L., Yeh, JK, Liu X-Q, Dunn DM, Stoecker BJ, Wang P, et al. (2008). Effect of green tea polyphenols on chronic inflammation-induced bone loss in female rats. *FASEB J*.22, pp.314.3.
- [60] Delaissé JM, Eeckhout Y, Vaes G. (1986). Inhibition of bone resorption in culture by (+)-catechin. *Biochem Pharmacol.*, 35(18), pp. 3091–3104
- [61] de Aloysio, D., Gambacciani, M., Altieri, P., Ciaponi, M., Ventura, V. and Mura, M., et al. (1997). Bone density changes in postmenopausal women with the administration of ipriflavone alone or in association with low-dose ERT. *Gynecol Endocrinol.*, 11(4), pp.289–293.
- [62] Whelan, A. M., Jurgens, T. M. and Bowles, S. K. (2006). Natural health products in the prevention and treatment of osteoporosis: systematic review of randomized controlled trials. *Ann Pharmacother*, 40(5), pp.836–849.
- [63] Rains, T. M., Agarwal, S. and Maki, K. C. (2011). Antiobesity effects of green tea catechins: a mechanistic review. *Journal of Nutritional Biochemistry*. 22(1), pp.1–7.
- [64] Wu, C. H., Lu, F. H., Chang, C. S., Chang, T. C., Wang, R. H. and Chang, C. J. (2003). Relationship among habitual tea consumption, percent body fat, and body fat distribution. *Obes.*, 11, pp.1088–95.
- [65] Phung O. J., Baker, W. L., Matthews, L. J., Lanosa, M., Thorne, A. and Coleman, C. I. (2010). Effect of green tea catechins with or without caffeine on anthropometric measures: a systematic review and meta-analysis. *Am J Clin Nutr.*, 91, pp.73–81.
- [66] Nagle, D.G., Ferreira, D. and Zhou, Y. D. (2006). Epigallocatechin-3-gallate (EGCG): chemical and biomedical perspective. *Phytochemistry*, 67, pp.849–855.
- [67] Pan, H., Gao, Y. and Tu, Y. (2016). Mechanisms of Body Weight Reduction by Black Tea Polyphenols. *Molecules*, 21(12), p.1659.

Removal of Zinc Metal Ions from Electroplating Industrial Waste Water by Using Bio-Sorbent

Mr. Vivek S. Damal, Mrs. V. U. Khanapure

Department of Civil Engineering, SCOE, Savitribai Phule Pune University, India

Abstract— The adsorption of Zinc from electroplating industrial effluent by banana peel powder was investigated. The influence of pH of sample, adsorbent dosage, temperature and contact time were evaluated on the bio-sorption studies. The present study aims to investigate efficiency of banana peel as an adsorbent for removal of zinc from effluent by batch experiments. In order to investigate the bio-sorption isotherms, two equilibrium models, Langmuir and Freundlich isotherms were analyzed. This study focuses on optimization of contact time, pH, temperature and adsorbent dosage of banana peel for removal of heavy metals from effluent of electroplating industry.

Keywords— Adsorption, Zinc, Banana Peel, Electroplating industry.

I. INTRODUCTION

Electroplating industrial waste water is one of the major contributors to heavy metal pollution in surface water. Removal of heavy metals from industrial waste water is important because they are not only contaminating water bodies but also toxic to human being and animals. For the removal of heavy metals from industrial waste water streams the bio-sorption process is used with use of natural, alternative and cheaper adsorbents. The purpose of this study is to check feasibility of bio-sorbent for removal of zinc ion from electroplating industrial waste water.

Problem Statement:

At present scenario industries directly discharge their effluent into municipal waste water because there is lack of regulations regarding disposal of such effluent and also due to costlier treatment techniques available. Objective of the study is to suggest economical and environment friendly technique by use of banana peels which is easily available as bio-sorbent for removal of zinc from electroplating industrial effluent.

II. EXPERIMENTAL ANALYSIS

Preparation of Adsorbent from Banana Peel:

The banana peels used to prepare adsorbent in form of powder. This adsorbent used for removal of zinc from the electroplating effluent. These are collected from various

fruit juice centers. Firstly Banana peels washed with distilled water 3-4 times to remove other soluble substances. Then banana peels dried in sun light for 5 days. Then this banana peels dried in an oven at 90°C for 10 hrs. Afterward's this product again dried in an oven at 100°C for 5 hrs. This banana peel product cooled at room temperature and grinded to powder.

Sampling:

The effluent samples were collected from the Electroplating industry, Super Auto Plating Pvt. Ltd, Bhosari Pune, Maharashtra, India.

Batch Adsorption:

All experiments are carried out at room temperature (25-30°C) in batch method. Batch method was selected because of its simplicity and reliability. The experiments were carried out by taking 100ml effluent sample in a flask and after pH adjustment a 1gm of dried adsorbent was added. The flask was agitated at near about 60 to 70 rpm for 60 minutes using a mechanical stirrer. After shaking, the suspension was allowed to settle. The residual biomass adsorbed with metal ion was filtered using whatman-1 filter paper. Metal ion estimation using Atomic adsorption spectrophotometer. The percent removal of metals from the solution was calculated by the following equation. Percent removal of metals from the solution was calculated by the following equation.

$$\% \text{removal} = \frac{(C_o - C_e)}{C_o} \times 100$$

Where,

C_o = is the metal ion concentration (mg/l)

C_e = is the final ion concentration (mg/l)

$$\text{amount adsorbed, } q_e = \frac{(C_o - C_e)}{m} \times V$$

Where,

M = mass of adsorbent

C_o = initial concentration of metal ion in the solution

C_e = Final concentration of metal ion in the solution (mg/lit)

V = volume of solution (lit),

q_e = amount of metal ion adsorbed per gram

Characteristics of Adsorbent (Banana Peel):

1. Energy-dispersive X-ray spectroscopy - Scanning Electron Microscopy (EDX-SEM)

Element	Weight%	Atomic%
C K	51.04	59.70
O K	43.40	38.11
Mg K	0.18	0.10
Si K	0.68	0.34
P K	0.21	0.09
Cl K	1.00	0.40
K K	3.04	1.09
Ca K	0.46	0.16
Totals	100.00	

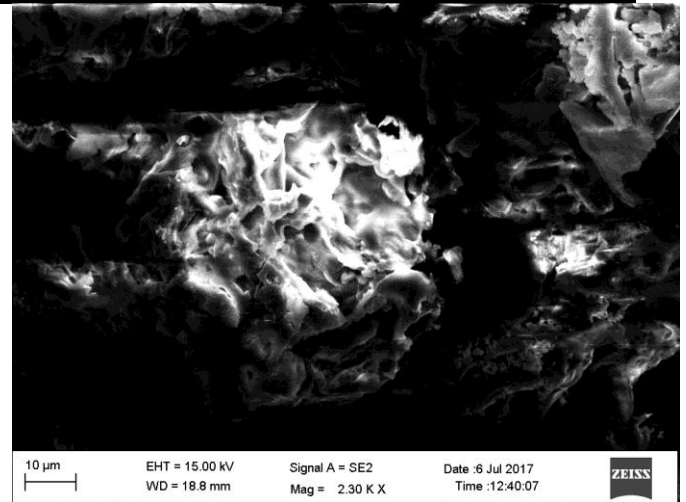


Fig.3: After Adsorption

Parameters affecting Adsorption Process:

1. Effect of pH

The effect of pH on percentage removal of zinc banana peel from effluent sample is shown in following figure. It is observed that the percentage removal of zinc increases slowly with increasing pH from 2 to 4 and thereafter drops slowly. The maximum percentage removal of zinc by banana peel was 97.15%. The optimum pH at which maximum removal of zinc is observed is to 4.0

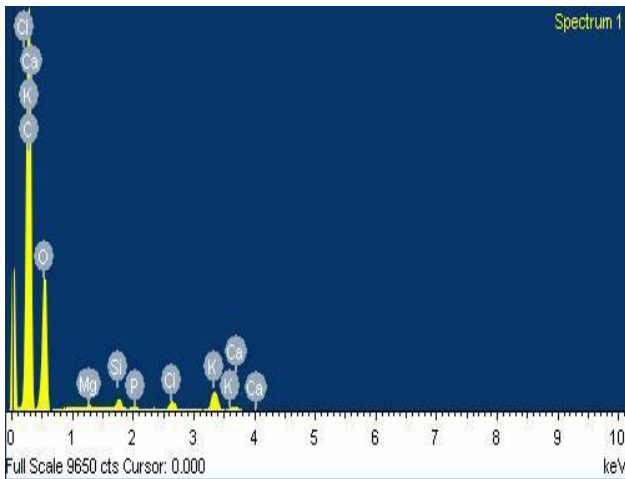


Fig.1: EDX-SEM analysis

1. Scanning Electron Spectroscopy (SEM)

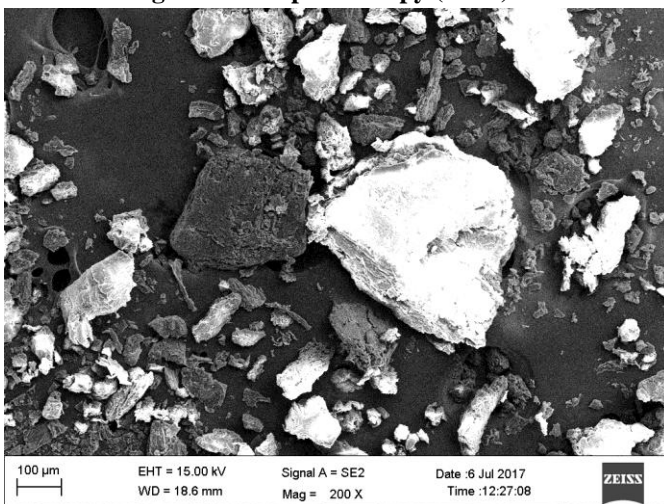


Fig.2: Before Adsorption

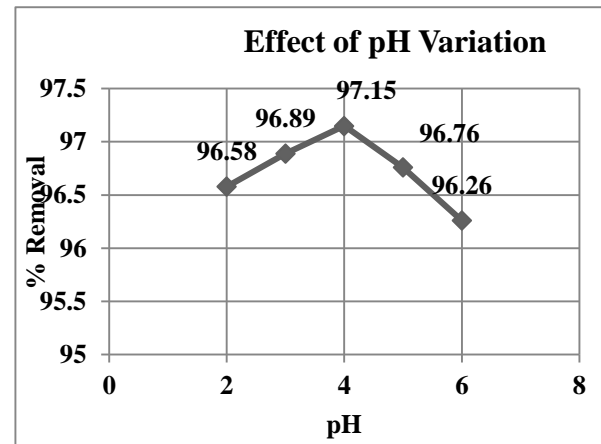


Fig.4: Relation between pH and percentage removal of zinc.

2. Effect of Adsorbent Dose

The effect of adsorbent dosage on percentage removal of zinc from effluent sample is shown in following figure no.2. It is observed that initially the percentage removal of zinc increased rapidly with an increase in adsorbent dosage, but after certain adsorbent dosage the removal efficiency did not increase.

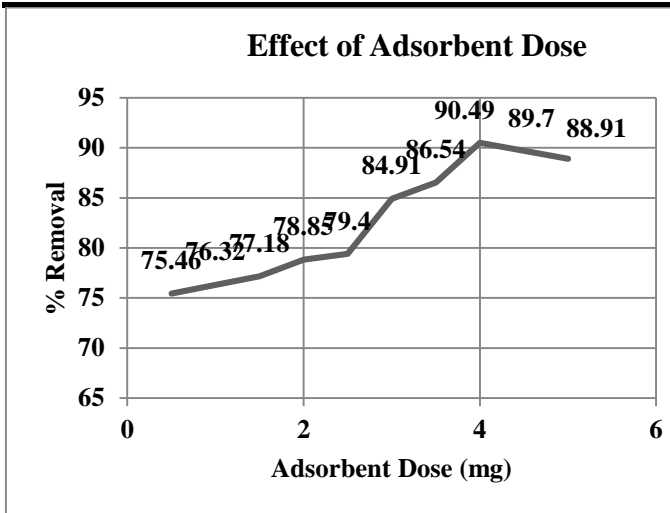


Fig.5: Relation between adsorbent dose and percentage removal of zinc.

3. Effect of Temperature

The effect of temperature on percentage removal of zinc from effluent sample is shown in following figure no.3. With the increase in temperature percentage removal of zinc decreased. For banana peel, zinc removal decreases from 85.05 % to 79.35 % due to the increase in temperature from 30° to 50°C.

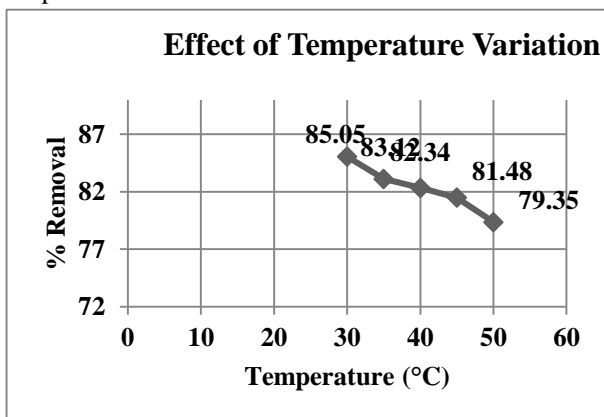


Fig.6: Relation between adsorbent dose and percentage removal of zinc.

The percentage removal is decreased with increase of temperature, so it was concluded that the adsorption reactions are exothermic. Bio sorption capacity also increased with decrease in temperature. The decrease of bio-sorption capacity at higher temperature may be due to the damage of active binding sites in the biomass. The maximum zinc removal is observed at 30°C.

4. Effect of Contact Time

The effect of contact time on batch adsorption of zinc at 30°C and at pH 4.0 by banana peel is shown in following figure. During the experiment contact time was varied from 0 to 270 min. The results showed that the percentage

removal of metal ion by adsorbent increased by increasing contact time. The maximum removal of zinc is observed at 270 min.

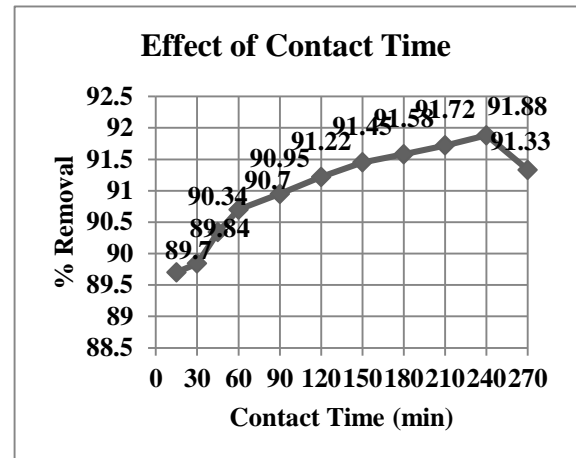


Fig.7: Relation between Contact Time and percentage removal of zinc.

III. ADSORPTION ISOTHERMS

Adsorption isotherms i.e. Langmuir and Freundlich isotherms are used to characterize the bio sorption.

Langmuir Isotherm:

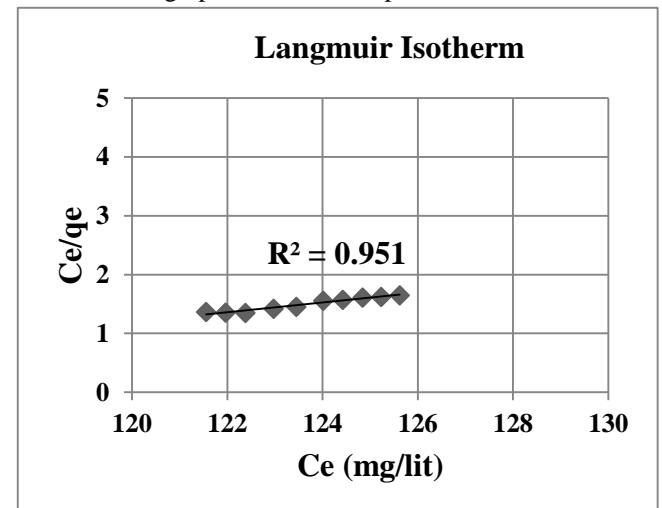
The Langmuir model makes assumptions such as monolayer adsorption and constant adsorption energy. Langmuir equation of adsorption isotherm is:

$$1/q = 1/q_{max} + 1/(b \cdot q_{max}) (C_f)$$

Where,

q_{max} and b are the Langmuir constants.

The graph of isotherm is plotted below:



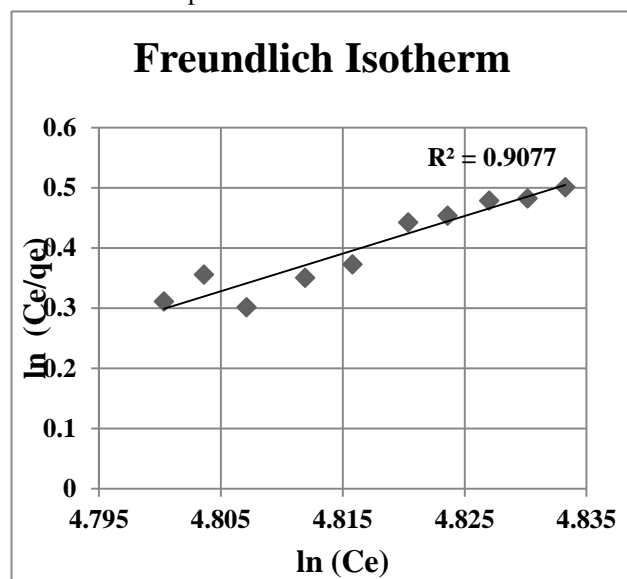
Graph.1: Langmuir Isotherm plots for removal of zinc for banana peel.

Freundlich Isotherm

Freundlich model deals with heterogeneous adsorption. The Freundlich equation of adsorption isotherm is:

$$\log q = \log K + (1/n) \log C_f$$

Where q is the amount adsorbed per unit mass of adsorbent and C_f is equilibrium concentration. The graphs of isotherms are plotted below:



Graph.2: Freundlich Isotherm plots for removal of zinc

IV. CONCLUSION

The experimental data on batch study showed the maximum removal of 90% was obtained at 4gm of adsorbent and 100ml of zinc sample. The removal of zinc from sample strongly depends on pH of the solution, adsorbent dosage, temperature and contact time. The maximum adsorption of zinc was obtained at pH 4.0, adsorbent dosage of 4 gm, contact time 240 min and temperature at 30°C. The best fitting of experimental results to the proposed isotherms was observed in isotherm models that assume that ionic species bind first at energetically most favorable sites with multi layer adsorption taking place simultaneously. Values of correlation coefficient for Langmuir isotherm is 0.951 whereas for Freundlich isotherm is 0.907. It indicates that Langmuir isotherm's correlation coefficient value is near to 1 and hence Langmuir isotherm fit well for adsorption equilibrium. Decrease in percentage of adsorption with increase in temperature indicates that the process is exothermic in nature and increase in adsorbent dose gave increased adsorption for zinc. These findings will be used in further works for the optimization of the sorption experimental conditions using banana peel powder in continuous processes since this adsorbent may be an alternative to more costly materials as activated carbon for the treatment of liquid wastes containing metals.

ACKNOWLEDGEMENTS

I would like to express the deepest gratitude to my project advisor and mentor **Mrs. V. U. Khanapure** for her supervision, advice and guidance.

REFERENCES

- [1] Madhukar J. Phadtare, S.T. Patil, "The Removal heavy metals from industrial waste water", International Journal Advanced Engineering and Research Studies, April-June 2015.
- [2] Ali S.M., Khalid A.R., Majid R.M., "The Removal of Zinc, Chromium and Nickel from industrial waste water using Corn cobs", Iraqi Journal of Science, 2014, Vol 55, No.1, pp:123-131.
- [3] Achanai Buasri, Sutteera Panphrom, "Bio-sorption of Heavy Metals from Aqueous Solutions Using Water Hyacinth as a Low Cost Biosorbent", Civil and Environmental Research ISSN 2222-1719 (Paper) ISSN 2222-2863 (Online) Vol 2, No.2, 2012.
- [4] Muhammad Aqeel Ashraf, Karamat Mahmood, Abdul Wajid, "Study of low cost bio-sorbent for biosorption of heavy metals", International Conference on Food Engineering and Biotechnology IPCBEE vol.9 (2011) IACSIT Press, Singapore.
- [5] M.A. Ashraf, M.J. Maah, I. Yusof, "Study of mango biomass (*Mangifera indica* L) as a cationic biosorbent", International Journal of Environment and Science Technology, 581-590, summer 2010 ISSN: 1735-1472 IRSEN, CEERS, IAU.
- [6] Wanna Saikaew, Pairat Kaewsarn, "Cadmium ion removal using biosorbents derived from fruit peel wastes", Songklanakari Journal Science and Technology 31 (5), 547-554, Sep.-Oct. 2009.
- [7] G.O. El Sayad, H.A. Dessouki, S.S. Ibrahim, "Removal of Zn(II), Cd(II) AND Mn(II) from Aqueous Solutions by Advanced Maize Stalks", The Malaysian Journal of Analytical Sciences Vol.15 No 1 (2011): 8-21.
- [8] Amuda, O. S., & Ibrahim, A. O. (2006). Industrial waste water treatment using natural material as adsorbent. African Journal of Biotechnology. 5, 16, pp 1483-1487.
- [9] Dikshit, V., Agarwal, I. C., Shukla, P. N., & Gupta, V. K. (2006). Application of low-cost adsorbent for dye removal. Journal of Environmental Management, 90, 8, pp 2313-42.
- [10] Dermentzis, K., & Christoforidis, A. (2011). Removal of Nickel, Copper, Zinc and Chromium from synthetic and industrial waste water by electrocoagulation. International Journal of Environmental Science. 1, 5, 697-710.
- [11] Muhammed Ersoy Ensar Oguz, "Removal of Cu²⁺ from aqueous solution by adsorption in a fixed bed column and Neural Network Modelling," Chemical Engineering Journal, vol. 164, pp. 56-62, 2010.
- [12] Gupta, V.K., Arshi, R., Saini, V.K., and Neeraj, J.. Biosorption of copper (II) from aqueous solutions

- by Spirogyra species. 2006, *J Colloid Interf Sci.* 296, 59-63.
- [13] Hossain, S. M., and Anantharaman, N. Studies on Copper (II) Biosorption using *Thiobacillus ferrooxidans*, *J Univ Chem Technol and Metall*, 2005, 40, 227-234.
- [14] B. Benguela and H. Benaissa, "Cadmium removal from aqueous solutions by chitin: kinetic and equilibrium studies," *Wat. Res.* Vol. 36, pp. 2463-2474, 2002.M.
- [15] A. Hanif, R. Nadeem, H. N. Bhatti, N. R. Ahmad and T. M. Ansari, "Ni (II) biosorption by *Cassia fistula* (Golden Shower) biomass," *J. Hazard. Mater.* Vol. 139, pp. 345-355, 2007.
- [16] Kurniawan, T. A., Chana, G.Y.S., Lo, W.H., & Babel, S., Physico-chemical treatment techniques for wastewater laden with heavy metals, *Chem. Eng. J.* 118, (2006) 83-98.
- [17] Sunil Rajoriya, Balpreetkaur, "Absorptive Removal of Zinc from Waste Water by Natural Bio-sorbents", *International Journal of Engineering Science Invention*, Volume 3 Issue 6, June 2014, PP.60-80
- [18] Maryam Sahranavard, Ali Ahmadpour, Mohammad Reza Doosti. Biosorption of Hexavalent Chromium Ions from Aqueous Solutions using Almond Green Hull as a Low-Cost Biosorbent: *European Journal of Scientific Research* ISSN 1450-216X Vol.58 No.3 (2011), pp.392-400.
- [19] Matis, K. A., Zouboulis, A. I., Gallios, G.P., Erwe, T., Blocher, C., Application of flotation for the separation of metal-loaded zeolite, *Chemosphere.* 55, (2004) 65-72.
- [20] Mavrov, V., Erwe, T., Blocher, C., Chmiel, H., Study of new integrated processes combining adsorption, membrane separation and flotation for heavy metal removal from wastewater, *Desalination.* 157, (2003) 97-104.
- [21] Kalavathy, M. H., Miranda, L. R., *Moringa oleifera*—a solid phase extractant for the removal of copper, nickel and zinc from aqueous solutions. *Chem. Eng. J.* 158, (2010) 188-199.

Antioxidants and antioxidant activity common eight banana varieties in Kerala

Siji .S*, Nandini. P.V

Abstract— The objective of this research were to study antioxidants and antioxidant compounds from selected eight varieties of banana and the antioxidant activity were analysed using two methods such as total antioxidant activity and DPPH (2,2-diphenyl-1-picrylhydrazyl) radical scavenging activity using different solvents such as petroleum ether, methanol and water. In the present study revealed that variety Red banana showed highest β carotene and (8.53 $\mu\text{g}/100\text{g}$). Ascorbic acid content of banana varieties ranged between 1.52 - 5.35 mg/100g. Highest ascorbic acid content was noticed in Red banana (5.35 mg). Highest dopamine content was exhibited in variety Robusta (13.3 mg/100g) and lowest was found in variety Rasakadali (3.2mg/100g). The total antioxidant activity revealed that variety Robusta had the highest DPPH activity with an IC_{50} value of 43.6 $\mu\text{g}/\text{ml}$ in petroleum ether solvent. With regard to total antioxidant activity, variety Padatti exhibited highest activity with an IC_{50} value of 41.2 $\mu\text{g}/\text{ml}$ in petroleum ether while variety Rasakadali (48.4) and Poovan (48.4) showed maximum activity in methanol followed by variety Red banana with an IC_{50} value of 44.4 $\mu\text{g}/\text{ml}$ in methanol.

Keywords— Antioxidants, Antioxidant activity, β carotene, Ascorbic acid, Dopamine, Total Antioxidant Activity, DPPH Radical Scavenging Activity.

I. INTRODUCTION

Kaur and Kapoor (2002) are of the opinion that diets rich in fruits and vegetables are associated with lower incidence of disease risks, including cardiovascular and cancer. They also argue that processing or cooking can enhance the health promoting effects of fruits and vegetables.

Now a day's consumption of fruits has been increased due to its nutritional and therapeutic effects on the human health due to the presence of phytochemicals and antioxidants. Studies evidence revealed that a healthy eating habit with increased consumption of fruits plays an important role in the prevention of chronic diseases, such as heart diseases, cancer, stroke, diabetes, Alzheimer's diseases and cataract (Willett, 2002; Wright *et al.*, 2008).

Free radicals are involved in both the process of aging and the development of cancer. To deal with the free radicals,

the body equipped with an effective defense system which includes various enzymes and high and low molecular weight antioxidants. The best sources of antioxidants are fruits and vegetables. The consumption of fruits and vegetables has been inversely associated with morbidity and mortality from degenerative diseases (Terry *et al.*, 2001).

Aurore *et al.* (2009) reported that banana, an herbaceous climacteric fruit, represents one of the most significant fruit crop in world export trade after coffee, cereals, sugar and cocoa and is one of the most important fruit crops grown throughout Kerala (Shanmughavelu *et al.*, 1992).

Bananas are one of the most popular food in the world contain various antioxidant compounds such as gallic catechin and dopamine which protects the body against the ill effects of free radicals. Since banana fruits are widely available, they have been used as food without apparent toxic effect. Hence, the present study is an evaluation of antioxidants and antioxidant activity present in eight selected banana varieties available in Kerala.

II. MATERIALS AND METHODS

Eight ripe banana varieties used for table purpose were selected for the study. The varieties selected were Palayankodan (AAB), Rasakadali (AB), Robusta (AAA), Poovan (AAB), Nendran (AAB), Kadali (AA), Red banana (AAA), Padatti (AAB). The banana varieties were procured at the time when the characteristic fruit colour developed for each type. They were collected from Instructional Farm, Vellayani and local markets of Trivandrum. To assess the antioxidants and antioxidant activity of banana varieties such as β carotene, ascorbic acid, dopamine, total antioxidant activity, DPPH radical scavenging activity were analysed.

β carotene

Method suggested by Sadasivam and Manickam (2008) was used for the estimation of β carotene.

Ascorbic acid

Ascorbic acid was estimated titrimetrically using 2, 6 dichloro indophenol dye (Ranganna, 2001).

Dopamine

Dopamine was estimated spectrophotometrically using the method suggested by (Li *et al.*, 2009) using dopamine hydrochloride as standard.

Total Antioxidant Activity

The total antioxidant activity was determined through phosphomolybdate method (Buratti *et al.*, 2001). The banana extract was dissolved in phosphomolybdate reagent and incubated in water bath for 90 min. It was allowed to cool and absorbance was measured at 765 nm against the blank.

DPPH Radical Scavenging Activity

Determination of 1,1-diphenyl-2-picrylhydrazyl was carried out using the method described by Ribeiro *et al.* (2008).

The percentage inhibition of DPPH radical was calculated by comparing the result of the test with control (methanol and 1ml DPPH) using the formula (Schlesier *et al.*, 2002).

Percentage inhibition

$$= \frac{(\text{Absorbance of control} - \text{Absorbance of test})}{\text{Absorbance of control}} + 100$$

In the present study, antioxidant activity of banana varieties was studied by the total antioxidant activity and DPPH assay in different solvents such as petroleum ether, methanol and water.

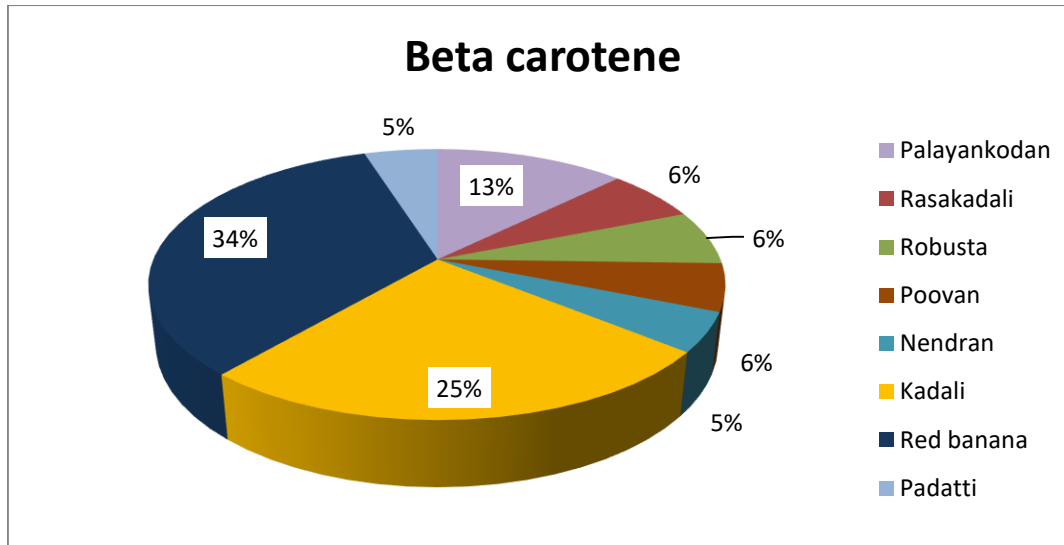
STATISTICAL ANALYSIS

All the analyses were done in triplicates. In order to obtain suitable interpretation the generated data was subjected to statistical analysis like One-way Analysis of Variance (ANOVA) at 0.05% significant level and graphical interpretation of analyzed data was also adopted.

III. RESULTS AND DISCUSSION

Beta carotene, a strong antioxidant can neutralize free radicals and reactive oxygen molecules which may lead to the development of cardiovascular disease and cancer. The data on beta carotene is presented in the Fig 1.

Significant differences ($p < 0.05$) were seen among the banana varieties in terms of the β carotene content. Beta carotene is an important antioxidant present in fruits in different concentration. In the present study, highest beta carotene was found in variety Red banana (21.19 $\mu\text{g}/100\text{g}$) and was significantly different from other varieties. The lowest beta carotene content was noticed in variety Nendran (2.19 $\mu\text{g}/100\text{g}$). The results of the present study showed a wide variation in β carotene levels among the bananas studied. The findings are in close agreement with other studies (Arora *et al.*, 2008; Amorim *et al.*, 2009) who had reported wide variability in β carotene content in bananas.



Ascorbic acid, a water soluble vitamin protects the body from ill effects of free radicals (Elekofehinti and Kade, 2012). Fresh fruits, vegetables and synthetic tablets supplement the ascorbic acid requirement of the body (Frei and Traber, 2004). However, stress, smoking, infections and burns deplete the ascorbic acid reserves in the body.

The ascorbic acid content of the banana varieties was observed to range between 1.52 - 5.35 mg/100g. The highest ascorbic acid was observed in variety Red banana (5.35 mg) and the lowest for variety Robusta (1.52 mg) (Table 1).

A study conducted by Poongodi (2012) on locally available banana in Tamil Nadu revealed that vitamin C

content varied from 0.71-4.69 mg g⁻¹ fresh tissues. The highest vitamin C content was present in Poovan and on the other hand, least content was found in Robusta. Sreedevi (2013) conducted a study on organically cultivated banana varieties like Nendran, Palayankodan and Rasakadali and found that vitamin C level was high in Rasakadali (6.46mg) followed by Nendran (6.4mg) and Palayankodan (3.33 mg).

Dopamine, 4-(2-aminoethyl) - benzene-1, 2-diol control movement, emotional response, and ability to experience pleasure and pain (Liu *et al.*, 2004) and also important for cardiovascular, hormonal, renal and central nervous

system functions in the body (Hussain and Lokhandwala, 2003; Zare *et al.*, 2006).

Variations in the yield of extracts, extracting compounds, type of soil and agro- climatic condition also affect dopamine content of banana (Hsu *et al.*, 2006).

The dopamine content of the different banana varieties was observed to range between 3.2- 13.3 mg/100g. The highest dopamine content was observed in variety Robusta (13.3 mg) and the lowest for variety the Rasakadali (3.2g) (Table 1).

According to Pereira and Marcelo (2014), the dopamine content in the banana pulp at 4-6 stages is 9.1±3.1 mg/100g.

Table.1: Ascorbic acid and dopamine content of banana varieties

Treatments	Name	Ascorbic acid (mg/100g)	Dopamine (mg/100g)
T ₁	Palayankodan (AAB)	2.19	8.4
T ₂	Rasakadali (AB)	2.18	3.2
T ₃	Robusta (AAA)	1.52	13.3
T ₄	Poovan (AAB)	4.26	5.3
T ₅	Nendran (AAB)	3.36	6.1
T ₆	Kadali (AA)	3.50	7.2
T ₇	Red banana (AAA)	5.35	11.0
T ₈	Padatti (AAB)	1.73	7.2
	CD(0.05)	0.382	0.051

The banana varieties analyzed for antioxidant capacity are presented in Table 2. It was revealed that antioxidant activity was higher for petroleum ether extract followed by methanol extracts when compared to aqueous extract. The antioxidant activity of the banana varieties ranged between 41.2-49.2 µg/ml, 44.4-51.6 µg/ml and 46.4-54.8 µg/ml in petroleum ether, methanol and aqueous medium

respectively. Highest antioxidant activity was reported in variety Padatti with an IC₅₀ value of 41.2 µg/ml and 46.4 µg/ml in petroleum ether and aqueous medium respectively. Where as in methanol solvent, highest activity was exhibited by variety Red banana with an IC₅₀ value of 44.4 µg/ml.

Table.2: Total antioxidant activity of banana varieties

Treatments	Name	IC ₅₀ values (µg/ml)		
		Petroleum ether	Methanol	Water
T ₁	Palayankodan (AAB)	48.0	49.2	53.6
T ₂	Rasakadali (AB)	43.6	51.6	54.0
T ₃	Robusta (AAA)	49.2	50.0	52.2
T ₄	Poovan (AAB)	44.0	49.2	49.2
T ₅	Nendran (AAB)	44.0	46.0	48.4
T ₆	Kadali (AA)	44.6	46.4	54.8
T ₇	Red banana(AAA)	43.6	44.4	51.2
T ₈	Padatti (AAB)	41.2	46.0	46.4

The concentration of sample that could scavenge 50% free radical (IC_{50}) was used to determine antioxidant capacity of sample compared to standard. The varieties having lowest IC_{50} had the highest antioxidant capacity. According to Blois (1992), "sample that had $IC_{50} < 50$ ppm, was considered as very strong antioxidant, 50-100 ppm strong antioxidant, 101-150 ppm medium antioxidant, while weak antioxidant with $IC_{50} > 150$ ppm".

Poongodi *et al.* (2012) conducted a study on the antioxidant activity of the pulp extracts of nine varieties of banana, via Kadali, Karpooravalli, Monthan, Pachainadan, Poovan, Rasthali, Robusta and Sevvazhai. The total antioxidant capacity of banana pulp extracts was expressed as number of equivalents of ascorbic acid. According to the results, different pulp extracts exhibited various degrees of antioxidant capacity. The ethanol extracts of variety Rasathali banana showed highest $\mu\text{mol g}^{-1}$ antioxidant

activity in the range of $6.60 \mu\text{mol g}^{-1}$ compared to other varieties of banana pulp, whereas ethanolic extract of poovan banana showed least activity in the range of $3.80 \mu\text{mol g}^{-1}$.

The variations in the antioxidant potential reported by various authors can be attributed to differences in cultivars, extraction procedures, geographical location and prevailing conditions such as soil, temperature, sunlight, horticulture practices and so on (Kim *et al.*, 2001).

In the present study, free radical scavenging capacity of banana varieties were studied by the DPPH assay in different solvents such as petroleum ether, methanol and water. Table 3 illustrates the results of DPPH activity of the banana varieties. The IC_{50} value was calculated from the graph (it was noted as the concentration of sample needed to scavenge the free radicals at 50 per cent inhibition).

Table .3: DPPH radical scavenging activity of banana varieties

Treatments	Name	IC_{50} values ($\mu\text{g/ml}$)		
		Petroleum ether	Methanol	Water
T ₁	Palayankodan (AAB)	50.8	52.4	54.4
T ₂	Rasakadali (AB)	45.6	48.4	53.8
T ₃	Robusta (AAA)	43.6	50.4	50.8
T ₄	Poovan (AAB)	50.0	48.4	52.0
T ₅	Nendran (AAB)	51.2	55.2	55.6
T ₆	Kadali (AA)	46.8	53.6	58.0
T ₇	Red banana (AAA)	48.0	56.8	57.6
T ₈	Padatti (AAB)	46.0	51.3	58.8

The results of present study revealed that antioxidant activity ranged from IC_{50} values of $41.2 \mu\text{g/ml}$ to $54.8 \mu\text{g/ml}$ in the banana varieties studied. Maximum antioxidant capacity was observed in variety Padatti ($41.2 \mu\text{g/ml}$) and minimum antioxidant capacity observed in variety Kadali ($54.8 \mu\text{g/ml}$).

A study conducted by Pongoodi *et al.* (2012) reported that Karpooravalli banana showed least DPPH radical scavenging activity. Similar findings were also reported by Rungnapa *et al.* (2007) on Thai bananas.

Qusti *et al.* (2010) and Miller *et al.* (2000) conducted a study on antioxidant activity of fresh fruits using DPPH assay and found that plant variety, growing condition, maturity, season, geographic location, fertilizer application, soil type, storage conditions and amount of sunlight

received are some of the factors which affect the DPPH assay.

IV. CONCLUSION

The present study highlighted that selected banana varieties serve as a natural store of various health beneficial antioxidant compounds. Antioxidant activity and antioxidant capacity of different selected banana varieties determined by different methods indicated that banana is rich in various health beneficial various bioactive compounds such as ascorbic acid, beta carotene, dopamine, having potent antioxidant activities and free radical scavenging activity. Banana is cheaper in price and easily available so that everyone can include their daily diet. This antioxidant compounds and antioxidant activity synergistically act to reduce the risk of degenerative

diseases like cardiovascular diseases, cancer etc. We can say confidently banana is a “poor man’s apple”.

REFERENCES

- [1] Amorim, E. P., Vilarinhos, A. D., Cohen, K. O. and Amorim, V. B. O. 2009. Genetic diversity of carotenoid- rich bananas evaluated by Diversity Arrays Technology (DarT). *Genet. Mol. Biol.* 32 (1): 96-103.
- [2] Arora, A., Choudary, D., Agarwal, G. and Singh, V. P. 2008. Compositional variation in beta carotene content, carbohydrate and antioxidant enzymes in selected banana cultivars. *Int. J. Food Sci. Tech.* 43 (11): 1913-1921.
- [3] Aurore, G., Parfait, B. and Fahrasmane, L. 2009. Bananas, raw materials for making processed food products. *Trends Food Sci Technol.* 20: 78-91.
- [4] Blois, M. S. 1992. Antioxidant determination by the use of stable free radicals. *J. Nature.* 181(4): 1199-2000.
- [5] Buratti, S., Nicoletta, P., Francesco, V. and Furio, B. 2001. Direct analysis of total antioxidant activity of olive oil and studies on the influence of heating. *J. Agric. Food Chem.* 49(5): 2532-2538.
- [6] Elekofehinti, O.O and Kade, I. J. 2012. “Aqueous extract of Solanumanguivi Lam. Fruits (African egg plant) inhibit Fe²⁺ and SNP induced lipid peroxidation in rat’s brain – in vitro,” *Der Pharmacia Lettre.* 4(5):.1352-1359.
- [7] Frei, E. C. and Traber, A. R. 2004. Effect of drying method and length of storage on tannin and total phenol concentrations in Pigeon pea seeds, *Food Chem.* 86 (1): 17-23.
- [8] Hussain, T. and Lokhandwala. M. F. 2003. Renal dopamine receptors and hypertension. *Exp. Biol. Med.* 228 (2): 134-142.
- [9] Hsu, B. Coupar, I. M. and Ng, K. 2006. Antioxidant activity of hot water extract from the Doum palm, *hyphaenethebaica.* *Food Chem.* 98 (2): 317-328.
- [10] Kaur, C. and Kapoor, H.C. 2002. Processed fruits and vegetables are healthier. *J. Indian Hort.* 47 (6) : 35-37.
- [11] Kim, Y.C., Koh, K. S. and Koh, J. S. 2001. Changes of flavonoids in the peel of jeju native fruits during maturation. *Food Sci. Tech.* 10: 483-487.
- [12] Li, G., Yan Z. and Quanmin, L. 2009. Spectrophotometric determination of dopamine hydrochloride in pharmaceutical, banana, urine and serum samples by potassium ferricyanide-(Fe-III). *Analytical Sciences.* 25 (4):1451-1455.
- [13] Liu, R.H. 2004. Potential synergy of phytochemicals in cancer prevention: mechanism of action. *J. Nutr.* 134: 3479S-3485S.
- [14] Miller, H. E., Rigelhof, F., Marquart, L., Prakash, A. and Kanter, M. 2000. Antioxidant content of whole grain breakfast cereals, fruits and vegetables. *J. Am Coll Nutr.* 19(3): 312-319.
- [15] Pereira, A. and Marcelo, M. 2014. Banana (*Musaspp*) from peel to pulp: Ethnopharmacology, source of bioactive compounds and its relevance for human health. *J. Ethnopharmacol* 160 (4):149-163.
- [16] Poongodi. 2012. Determination and comparison of non enzymatic antioxidants from different local varieties of banana (*Musasp*). *Int. J. Pharm. Bio. Sci.* 3(4): 17-24.
- [17] Qusti, S. Y., Ahamed, N., Abo-khatwa. and Mona, A. B. 2010. Screening of antioxidant activity and phenolic content of selected food items cited in the Holly Quran. *EJBS.* 2(1): 40-51.
- [18] Ranganna, S. 2001. Hand book of analysis and quality of fruit and vegetable products. Second edition. Tata McGraw Hill Publishing Compony Ltd, India, p. 112.
- [19] Ribeiro, S. M. R., Barbosa, L. C., Queiroz, J. H., Knodler, M. and Schieber, A. (2008). Phenolic compounds and antioxidant capacity of Brazilian mango (*Mangifera indica L.*) varieties. *Food Chemistry.* 110 (3) : 620-626.
- [20] Rungnapa, M., Waya, S., Jirawan, B., Rungthip, K. and Weerachai, P. 2007. Fatty acid content and antioxidant activity of Thai bananas. *Mj. Int. J. Sci. Tech.* 1(2): 222-228.
- [21] Sadasivam, S. and Manickam, A. 2008. Biochemical Methods. 3rdedn. New Age International Publications, New Delhi, India. pp.19-22.
- [22] Schlesier, K. M., Harwat, V. B. and Bitsch, R. 2002. Assessment of antioxidant activity by using different in vitro methods. *Free Radical Res.* 36 (2): 177-187.
- [23] Shanmugavelu, K. G., Aravindakshan, K. and Sathiamoorthy, S. 1992. Banana, Taxonomy, breeding and production Technology; Metropolitan Book Co. Pvt. Ltd. New Delhi. India, p.459.
- [24] Sreedevi, L. 2013. Quality evaluation of organic ripe banana. M.Sc (HSc) thesis, Kerala Agricultural University, Thrissur. pp. 41-46.
- [25] Terry, P., Terry, J.B., and Wolk, A. 2001. Fruits and vegetable consumption in the prevention of cancer: an update. *J. Intrn. Med.* 250:280-290.

- [26] Willett, W.C. 2002. Balancing lifes-style and genomics reaserch for disease prevention.*Science*. 296: 695-698.
- [27] Wright, M.E., Park, Y., Subar, A.F., Freedaman, N.D., Albanes, D., Hollenbeck, A., Leitzmann, M.F., and Schatzkin, A. 2008. Intake of fruit, vegetables and specific botanical groups in relation to lung cancer risk in nih-aarp diet and health study.*Am J. Epidermology*. 168:1024-1034.
- [28] Zare, H. R., Rajabzadeh, N., Nasirizadesh, N. and Ardakani, M. M. 2006. *J. Electroanal. Chem.* 589-560.

Theoretical Study of Electronic and Electrical Properties of Pure and Doped Graphene Sheets

Hamid I. Abbood, Hakiema S. Jabour

Babylon University, College of Science, Physics Department, Iraq

Abstract—The studied graphene sheets were design at Gaussian View 5.0.8 program and initially relaxed at Gaussian 09 program. The last relaxation of these structures was done using the SIESTA-trunk-462 program. All calculations are carried out using GOLLUM program. The results showed the presence of fluorine atoms in the sheet has not an effect on the geometrical parameters of carbon-carbon bonds. Pure graphene sheet has zero band gap and large electronic softness with higher electrical and thermal conductivities due to the multi channels of electron transport it has in comparison with the two doped graphene sheets, the presence of fluorine atoms in the rings leads to rise the energy gap and decrease the open channels of electron transfer, the electrical conductivity is linearly proportionality decreasing with the number of added fluorine atoms. The I-V characteristics of the studied graphene sheets was analyzed and observed resistance behavior for pure graphene sheet.

Keywords—Graphene, Electrical Conductivity, Electronic Softness, I-V Curve.

I. INTRODUCTION

Graphene is a two-dimensional atomic layer of carbon atoms, the building block of the 3-D structure graphite. While graphite has been a well-known and utilized material since antiquity, a single graphene layer was not isolated and studied until relatively recently [1-3]. Graphene was generated by several different chemical techniques in the 1960s and 1970s, but it was not until 2004 when K. S. Novoselov, A. K. Geim, and coworkers at the University of Manchester introduced a simple technique involving the mechanical exfoliation of graphite to isolate single graphene layers [1,4,5]. The availability of graphene flakes made the study of its properties possible and led to the enormous interest and intense activity in graphene research currently ongoing [5-8].

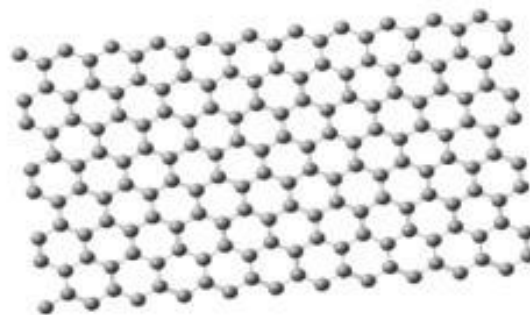
Graphene is a material with unique electronic transport properties such as a high Fermi level, outstanding carrier mobility, and a high carrier saturation velocity. These properties are complemented by excellent thermal conductivity, high mechanical strength, thinness, and flexibility. These characteristics make graphene an

excellent candidate for advanced applications in future electronics [7-9]. In particular, the potential of graphene in high-speed analog electronics is currently being extensively explored [3,6,8]. In current paper, we discuss briefly the basic electronic structure and transport properties, I-V characteristic of pure GR1 and doped graphene sheets with different number of fluorine atoms GR2 and GR3.

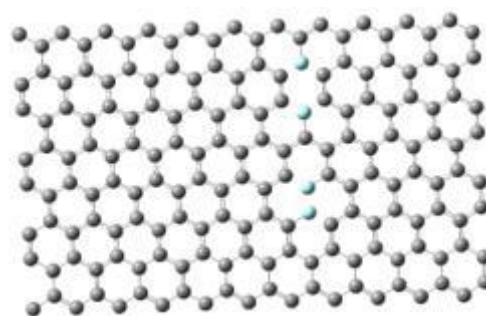
II. COMPUTATIONAL DETAILS

The calculated properties of graphene sheets in figure 1 are carried out using density functional theory LDA/SZ basis sets method. The structures of the studied sheets are designed at Gaussian View 5.0.8 program [10], the relaxation of the studied structures was initially done using Gaussian 09 package of programs and then using the SIESTA-trunk-462 program [11], all the calculations are carried out using GOLLUM program " version 1.0 " [12].

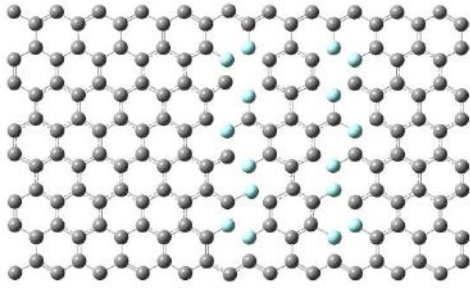
III. RESULTS AND DISCUSSION RESULTS



GR1



GR2



GR3

Fig.1: The relax structure(Carbon (C)≡ gray: Fluorine (F) ≡ green).

The three suggested relax structures in Fig. 1 are the pure graphene sheet GR1, the doped graphene with four fluorine F atoms GR2 and the doped graphene with sixteen fluorine F atoms GR3. We showed the addition of fluorine atoms in the pure graphene sheet to construct the doped graphene sheets has not an effect on the bonds C-C, C=C and C-C=C in the structure, these bonds are remain in the same ranges of carbon rings structures[13,14].

Fig. 2 shows the calculated values of total energy E_T obtained from the relaxation of the studied structures. E_T was decreased with adding the fluorine atoms in place of carbon atoms, it depends on the number of electrons in each structure, E_T was decreased with increasing fluorine atoms in the sheet.

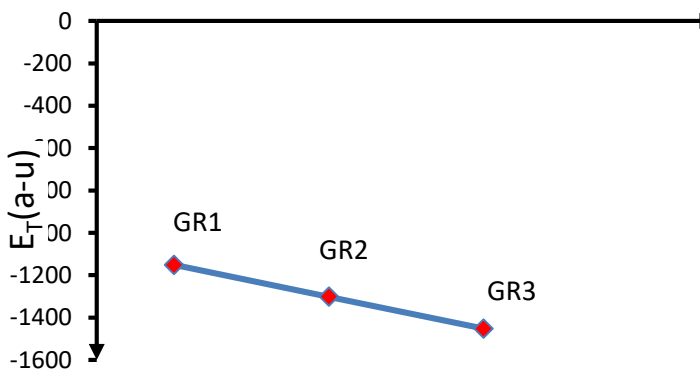


Fig.2: The total energy of the relax structures

Fig. 3 showed the calculated value of the energy gap E_g of the pure graphene sheet GR1 is the lowest ($E_g = 0.0168$ eV), this value was raised to (0.1109 and 0.0553) eV for GR2 and GR3, respectively. E_g is independent of the increasing of the number of fluorine atoms in the sheet, GR2 and GR3 are new molecular electronics have new electronic applications. Fig. 4 observed the electronegativity X of the studied sheets, it is in the order of $GR1 > GR2 > GR3$, this corresponds to the results of ionization energy IE and electron affinity EA, where IE and EA are in the order of $GR1 > GR2 > GR3$. Fig.5

illustrates the electronic softness S of the studied sheets, we showed the pure GR1 has the higher S , the increasing of electronic softness is the main future as a sign for that band gap goes to be rather soft and lowering the resistance of the structure to lose an electron.

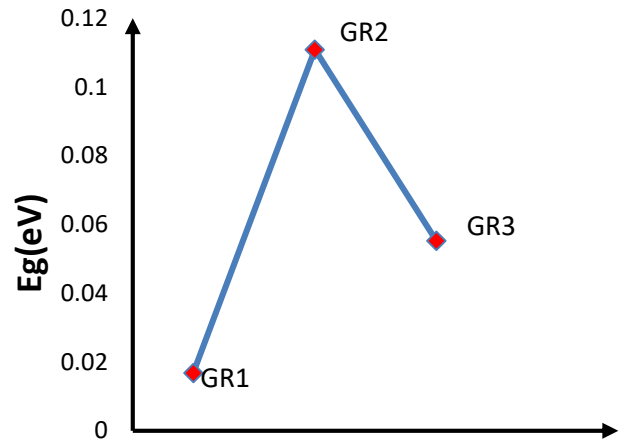


Fig. 3: The energy gap of the relax structures

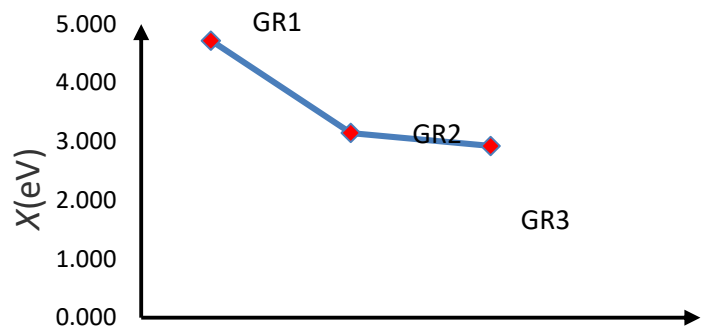


Fig. 4: The electronegativity of the relax structures

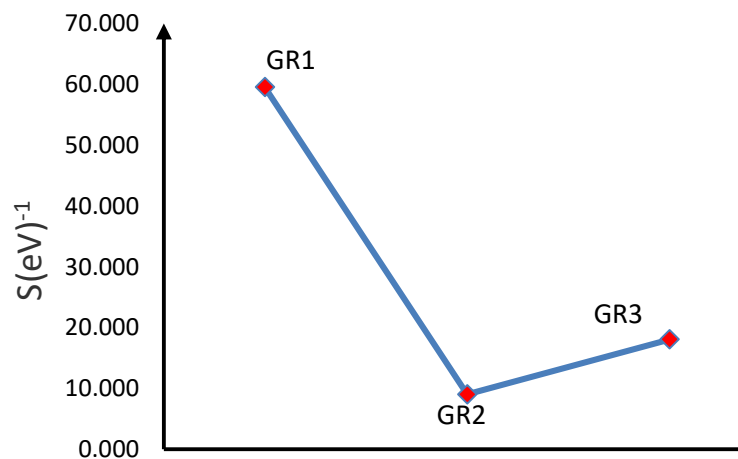


Fig. 5: The electronic softness of the relax structures

Fig.6 showed the electrical conductivity of all graphene sheets holds the stationary state approximately after (50) K in the range of temperature to (400) K. Generally, the pure GR1 has the higher electrical conductivity (2) μS due to that the pure sheet has multi channels of electron

transport in comparison with the two others. The electrical conductivity of GR2 is (0.897) μ S and GR3 is (0.0519) μ S, the presence of fluorine atoms in the rings decreased the open channels of electron transfer and therefore reduces the electrical conductivity of the sheet. The decreasing of the electrical conductivity is linearly proportionality with the increasing the number of added fluorine atoms.

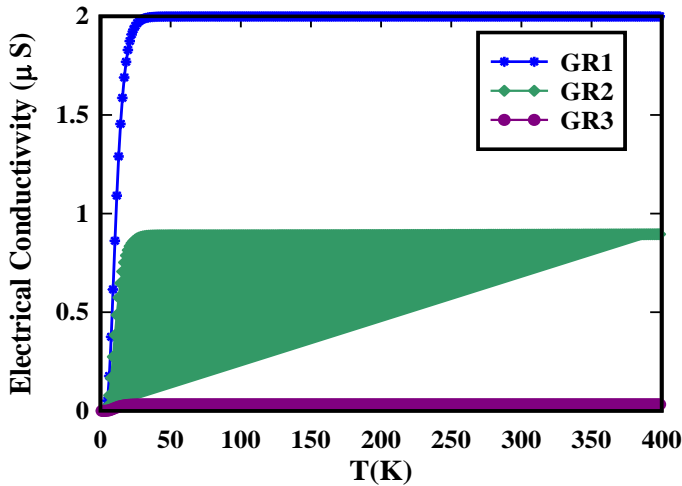


Fig.6: Electric conductivity in (μ S) of the pure and doped graphene sheets.

Figure 7 declare the thermal conductivity of the studied graphene sheets has the same behavior of the electrical conductivity, it is increasing with increase of the temperature. At (300)K, GR1 has the higher thermal conductivity (1.141×10^{-9})W/m. K, GR2 has (5.153×10^{-10})W/m. K and GR3 has thermal conductivity of (3.710×10^{-11})W / m. K. Means, the increasing the number of fluorine atoms in the sheet decreases the number of open channels that the electrons can passthrough and therefore, gave the sheet low electrical and thermal conductivities[15-17].

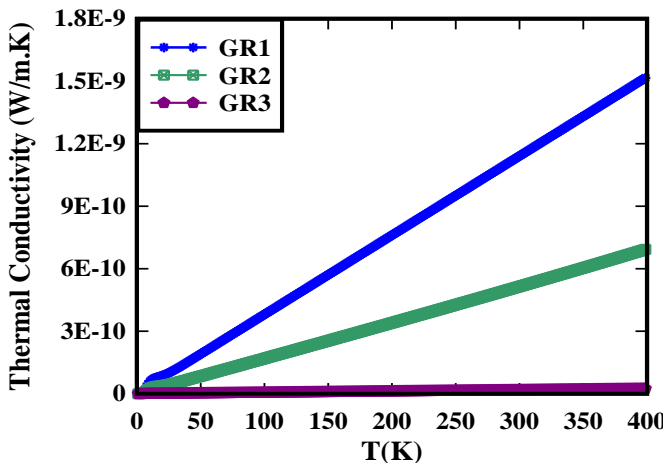


Fig.7: Thermal conductivity of the pure and doped graphene sheets.

Fig. 8 shows the I-V curve of the pure GR1 and doped GR2 and GR3 sheets. After each sheet inserted in between two gold contacts electrodes with a suitable anchor atom between the electrode and the sheet, a bias voltage of (2 V) was applied in the direction of the axis connecting both the anchor atoms. The Fermi level of the electrode was fixed and was considered lying in the middle of LUMO-HOMO gap. From I-V curve, for GR1 we observed a linear relationship between the current and the voltage reaches to (1.6 V), means GR1 has resistance behavior, after this value, we observed sensing behavior at (1.6 V) bias voltage and (-1.6V) reverse voltage. The response of the I-V curve was reduced with adding the fluorine atoms in the sheet. This responsively was lowered with increasing the number of fluorine atoms, as seen for GR2 and GR3. A very valuable result obtained from above behavior, since this behavior reduces completely the high temperature effects that appear in the old macro devices. The I-V curve indicates to that the appropriate contact with the electrodes have rather limited effect on the sensing performance of the doped graphene sheets.

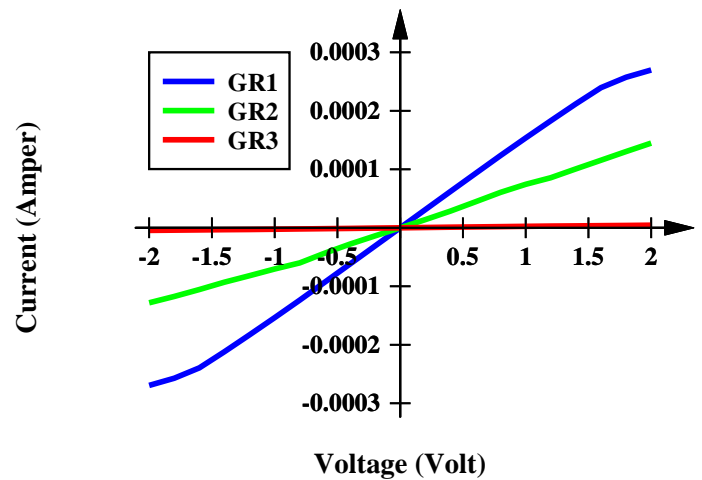


Fig.8: The I-V curve of the pure and doped graphene sheets.

IV. CONCLUSION

From the above results in present study, one can conclude the following:

1. The number of the fluorine atoms added in the sheet has a significant role in the electrical conductivity values.
2. Pure graphene sheet has zero band gap with high electrical conductivity in comparison with the other doped sheets, the pure graphene has the largest electrical conductivity multi channels of electron transport it has, the presence of more and more of fluorine atoms in the sheet decreases the

number of channels that the electrons can pass through.

3. Thermal conductivity was decreased with increasing the number of fluorine atoms. Thermal conductivity has the same behavior of electrical conductivity.
4. Pure graphene sheet has the largest value of electronic softness in comparison with the doped sheets.
5. Pure graphene sheets show I-V curve very much similar to resistance type. This behavior reduces completely the high temperature effects that appear in the old macro devices.

V. ACKNOWLEDGEMENTS

We acknowledge the staff of theoretical physics group, physics dep., college of science, university of Babylon for their valued support.

REFERENCES

- [1] K. S. Novoselov, A. K. Geim, S. V. Morozov, D. Jiang, Y. Zhang, S. V. Dubonos, I. V. Grigorieva, and A. A. Firsov, *Journal of Science*, Vol. 306, PP. 666–669, 2004.
- [2] K. S. Novoselov, A. K. Geim, S. V. Morozov, D. Jiang, M. I. Katsnelson, I. V. Grigorieva, S. V. Dubonos, and A. A. Firsov, *Journal of Nature*, Vol. 438, PP. 197–200, 2005.
- [3] Y. Zhang, Y. Tan, H. L. Stormer, and P. Kim, *Journal of Nature*, Vol. 438, PP. 201–204, 2005.
- [4] A. K. Geim and K. S. Novoselov, *Journal of Nature Mater*, Vol. 6, PP. 183–191, 2007.
- [5] Ph. Avouris, *Journal of Nano Lett.*, Vol. 10, PP. 4285–4294, 2010.
- [6] P. R. Wallace, *Journal of Physics Rev.*, Vol. 71, PP. 622–634, 1947.
- [7] J. S. Moon, D. Curtis, M. Hu, D. Wong, C. McGuire, P. M. Campbell, G. Jernigan, J. L. Tedesco, B. VanMil, R. Myers-Ward, C. Eddy, Jr., and D. K. Gaskill, *Journal of IEEE Electron Device Lett.*, Vol. 30, PP. 650–652, 2008.
- [8] Y.-M. Lin, K. A. Jenkins, A. Valdes-Garcia, J. P. Small, D. B. Farmer, and P. Avouris, *Journal of Nano Lett.*, Vol. 9, PP. 422–426, 2009.
- [9] Y.-M. Lin, C. Dimitrakopoulos, K. A. Jenkins, D. B. Farmer, H.-Y. Chiu, A. Grill, and P. Avouris, *Journal of Science*, Vol. 327, PP. 662, 2010.
- [10] R. Dennington, T. Keith and J. Millam, "Gauss View 5.0.8", SemichemInc, 2008.
- [11] E. Artacho, J. Gale, A. Garc, J. Junquera, P. Ordej, D. Sanchez-Portal and J. Soler, "SIESTA-trunk-462", Fundaci on General Universidad Autonoma de Madrid, 2013.
- [12] J. Ferrer, C. Lambert, V. García-Suarez, S. Bailey, S. Hatf, D. Manrique, "GOLLUM version 1.0", Lancaster University, 2014.
- [13] L. Pauling, "The Nature of the Chemical Bond", Cornell University Press, United States, 1960.
- [14] F. Allen, D. Watson, L. Brammer, A. Orpen and R. Taylor, *Journal of International Tables for Crystallography*, Vol.C, PP.790-811, 2006.
- [15] J. Soren and R. Morten, "Electronic and optical properties of graphene and grapheneantidot structures", Master Thesis , University of Aalborg , 2013.
- [16] F. Molitor, "Electronic properties of graphene Nanostructures", Ph.D. Thesis, ETH, 2010
- [17] B. Ghavami, A. Ebrahimzadeh, *Journal of Mesoscale and Nanoscale Physics*, Vol.1, PP. 1-6, 2015.
- [18] Sabah N. Mazhir, Hamid I. Abbood and Hawraa A. Abdulridha, *Electron Transport in Graphene-B/P compound Hetero-junction Using LDA/SZ*, *International Journal of Advanced Engineering Research and Science (IJAERS)*, Vol.3, 2016.
- [19] Hawraa A. Abdulridha, Sabah N. Mazhir and Hamid I. Abbood, *Room Temperature Conductance of Graphene Sheet as a Function of Some Variables Using LAD/SZ Method*, *Advances in Physics Theories and Applications*, Vol.52, 2016.

Nutritional Evaluation of Different Mango Varieties available in Sri Lanka

Kothalawala S.G., Jayasinghe J.M.J.K.

University of Sri Jayewardenepura, Gangodawila, Nugegoda, Sri Lanka.

Abstract— The study was carried out to evaluate the nutritional properties of five varieties (Willard, Karthakolomban, Malwana, Bettiamba and Gira Amba) of mango. Nutritional properties were significantly ($p < 0.05$) varied among the different mango varieties. The highest edible portion (79.49%), total soluble solids (0.75%), ash, total carbohydrate, sugar (30.56 mg/100 gm) and crude fiber were found in Karthakolomban. The highest amount of fat and moisture content were found in Malwana. The maximum amount of caloric value was found in Bettiamba. Gira Amba variety indicated the highest amount of protein content among the other mango varieties. Gira Amba has the highest titratable acidity meanwhile Karthakolomban has the lowest value considerably. Mango varieties in this study possess pH values without any significant deviations and Bettiamba was recorded as the variety with highest pH value meanwhile Malwana claimed to be the lowest. Therefore, this study contributed to the identification of the characteristic biochemical properties of several prominent Sri Lankan mango varieties.

Keywords— Sri Lankan mango, Nutrient analysis, Chemical property analysis.

I. INTRODUCTION

Mango is a tropical and subtropical fruit scientifically known as *Mangifera indica* L. India, Pakistan, Mexico, Brazil, Haiti, Philippines and Bangladesh are known to be the leading cultivators of mango. The genus of *Mangifera* consists of 69 species and mostly restricted to tropical Asia [1]. As a South Asian country, A narrow range of mango cultivars presently grows widely throughout Sri Lanka in dry, intermediate and wet zones. Best and adaptable varieties are only chosen for the cultivation to get a higher yield from a mango tree. Fruits are provided annually from most of the Sri Lankan mango cultivations. Sri Lanka produces several superior varieties of mango namely Karthakolomban, Willard Vellaicolomban, Ambalavi, Chembatan, Malwana, Betti Amba, These mango varieties have their own demand and have commercial importance in food industries. Mango is not only delicious but also rich in prebiotic dietary fiber, vitamins, minerals and polyphenolic flavonoid antioxidant compounds. It also contains sugar, small amount of protein, fats and other

nutrients. Mango is frequently eaten fresh. It's also been partaken as desserts such as juices, jellies, jams, nectars as well as crisp mango chips [2]. Mangoes are consumed in both raw and cooked form in South Asian countries and also, they are consumed at all stages of fruit development from the tiny fruit stage, that shed abundantly on to develop beyond the initial stage to the fully mature ones. Nutritional properties of mango fruit vary from variety to variety and developmental stages [3]. Many scientific research approaches on analyzing the physicochemical characteristics of different mango varieties were recorded in past few decades [4], [5], [6], [7]. Physicochemical and nutritional characteristics of most of the varieties of mango grown in Sri Lanka were not properly analyzed. Considering the above fact, the present study was designed to evaluate the nutritional status of five different mango varieties (Willard, Karthakolomban, Malwana, Bettiamba and Gira Amba) grown in Sri Lanka to recommend their use in daily life and commercial purposes.

II. MATERIALS AND METHODS

Sample collection

The experiment was conducted inside a food processing and analyzing laboratory in the Department of Food Science and Technology, University of Sri Jayewardenepura, Sri Lanka. Five popular varieties of mangoes were analyzed in this study. These include Willard, Karthakolomban, Malwana, Bettiamba and Gira Amba. Selected mangoes were collected from five local markets in Colombo city.

Sample preparation

Fresh mango samples free from insect's bites were collected and washed with deionized water in order to eliminate visible dirt. Excessive dripping water on the surface was removed quickly with a blotting paper. Those were then cut into small pieces, homogenized. Accurate quantity was weighed as required for different analysis. Every experiment was replicated nine times to have a result for each parameter.

Determination of nutritional properties

The edible portion of the fruit was calculated by subtracting the weight of indigestible parts of fruits from

the weight of whole fruits. The pH of fruit extract was determined with the use of a digital pH meter (HQ11d). Moisture content was determined by digital moisture analyzer (A&D MX-50). Titratable acidity was estimated with the visual acid base by digital method [8]. The total soluble solid (TSS) was determined with a hand refractometer (Ade Advanced Optics, Model-REF234). Reducing sugar and total sugar contents were determined by Lane and Eynon method [9]. The estimation of total protein was made by Kjeldahl method [10]. Determination of the crude fibre and fat were carried out according to AOAC procedure [11]. Ash content of the mango was determined by incinerating and heating sample in a muffle furnace at 600°C for six hours until a constant weight was reached [12]. The total carbohydrate amount was determined by the following equation [13]

$$\text{Total Carbohydrate (\%)} = 100 - \{\text{Moisture (\%)} + \text{Protein (\%)} + \text{Fat (\%)} + \text{Ash (\%)}\}$$

The gross food energy was estimated by using a bomb calorimeter [14]

Table.1: Maturity stage, organoleptic properties, edible portion, and moisture content of mango varieties

Mango Variety	Maturity stage	Taste	Colour	Edible portion	Moisture content
Willard	Ripen	Sweet	Red and yellow	75.34 ± 2.58	75.34 ± 3.34
Karthakolomban	Over Ripen	Very sweet	Green and Yellow	78.28 ± 2.35	71.63 ± 4.46
Malwana	Ripen	Sweet	Green and yellow	65.49 ± 2.54	84.28 ± 2.39
Bettiamba	Ripen	Sweet	Green and yellow	74.88 ± 4.28	72.56 ± 2.12
Gira Amba	Ripen	Very sweet	Green and Yellow	69.67 ± 3.43	77.23 ± 3.89

Nutritional properties

Maturity stage, taste and colour of different mango varieties were depicted in table 1. Willard, Malwana, Bettiamba and Gira Amba were found in ripe stage but Karthakolomban was found in over ripe stage. The tastes of mango varieties varied sweet to very sweet. While Karthakolomban and were identified as very sweet while Willard, Malawana, Bettiamba and Gira Amba were found as sweet. Colour of different mango varieties was visually observed and most of the mangoes were bicolour almost all the varieties consisted with red, yellow and green colours at the stage of observation.

Edible portion and moisture content of different mango varieties were differed significantly ($p < 0.05$) as shown in Table 1. The highest amount of edible portion was found in Karthakolomban (78.28%) and the lowest amount of edible portion was found in Malwana (65.49%). Karthakolomban, Bettiamba and Gira Amba resulted in higher (above 70%) edible portion. Previously conducted similar study indicates that the Karthakolomban possess 78% edible portion and Willard contains 76% edible portion which are comparatively accurate with the current study. Moisture content was observed more than 70% in all varieties. The highest and lowest moisture content was found in Malwana (84.28 %) and Karthakolomban (71.63 %), respectively. It was reported that most fruits are

Statistical analysis

The data were statistically analyzed using SPSS (Statistical Package for Social Sciences version 22.00) to assess and compare of physico-chemical, nutritional properties of the mango varieties.

III. RESULTS AND DISCUSSION

The outcome of nutritional properties including their physical characters of five different mango varieties were analyzed and compared. Each value represents the average from nine replications and the results expressed as mean values ± standard deviations (SD). After performing ANOVA (Analysis of variance) test it is evident that two physical characteristics (edible portion and moisture content) are significantly different ($p < 0.05$). It is also found that chemical properties such as pH, Titratable acidity, TSS and the macro nutrients such as Total Sugar, Reducing Sugar, Total protein, Total fat, Crude fiber, Ash, Total carbohydrate, Total energy of different varieties of mango had a significant variation. ($p < 0.05$).

composed of 70% to 90% of water [15] [16]. Therefore, the observations obtained clarify the previously reported results.

Significant chemical properties such as pH, total soluble solids, titratable acidity, total sugars and reducing sugars of different varieties of mangoes are included in the Table 2. All values were found to be varied significantly ($p < 0.05$) among all the mango varieties. It is observed that pH value of mango varieties ranged from 4.31 to 4.67. Bettiamba was found with highest pH (4.67) and Malwana with the lowest pH (4.31) value. The pH values for Willard (4.34) and Karthakolomban (4.41) are bit contradictory to another previously mentioned study. However, this study contains lower values comparatively to the previous study due to variables such as ripening stage. Titratable acidity was found to be maximum in Gira Amba (0.68%) followed by Willard (0.67%) and Bettiamba (0.54%). A previous study reported, higher pH (4.2 to 5.7) and lower acidity (0.05 to 0.22%) in mango grown in Mediterranean subtropical climate [17]. According to another study titratable acidity of mango varies from 0.25 to 0.60% [18]. Because of the maturity stage of mango, the acidity in varieties we observed, ranges from 0.26% to 0.75%. The variations in pH value and titratable acidity of mangoes cause due to ripening and their storage period [19].

Total soluble solids content was also differed significantly ($p < 0.05$) and found maximum in Karthakolomban (21.96 %) followed by Bettiamba (18.43 %) and it was minimum in Gira Amba (16.56 %). Total soluble solids (TSS) are directly correlated with the acidity of fruit. Generally, acidity of fruit decreases and total soluble solids increases during maturity and ripening stage of fruit [20] [21]. It was also reported Total soluble solids in Willard is 23.5% even though the current study indicates it as 20.17%. But the

TSS value for the Karthakolomban was not quite deviated from the previous study.

The amount of total sugar and reducing sugar of different mango varieties varied significantly ($p < 0.05$). Total sugar ranged from 4.27% to 5.48% and reducing sugar ranged from 4.61% to 3.04%. The maximum amount of both the total sugar and reducing sugar were found in Karthakolomban, 5.96% and 5.14%, respectively and minimum amount of total sugar and reducing sugar was found in Malwana (4.32 % and 4.13 %), respectively.

Table 2. pH, Titratable acidity, total soluble solid, total sugar, reducing sugar of mango varieties

Mango Variety	pH	Titratable acidity	Total soluble solids	Total sugar	Reducing sugar
Willard	4.34 ± 0.14	0.67 ± 0.04	20.17 ± 0.32	5.14 ± 0.24	4.32 ± 0.16
Karthakolomban	4.41 ± 0.23	0.35 ± 0.04	23.96 ± 1.24	5.96 ± 0.83	5.14 ± 0.24
Malwana	4.31 ± 0.15	0.43 ± 0.02	17.46 ± 0.54	4.32 ± 0.54	4.13 ± 0.18
Bettiamba	4.67 ± 0.16	0.54 ± 0.08	18.43 ± 0.67	4.58 ± 0.28	4.28 ± 0.34
Gira Amba	4.34 ± 0.32	0.68 ± 0.06	16.56 ± 0.48	4.43 ± 0.43	4.17 ± 0.12

Significant variation ($p < 0.05$) of total protein, total fat, crude fiber, ash, total carbohydrate and total energy content was observed among the different varieties of mango (Table 3). It is seen that the total protein content ranged between 0.17 gm/100 gm and 0.28 gm/100 gm. The highest amount of total protein was found in Gira Amba

(1.18 gm/100 gm) and lowest amount of total protein (0.07 gm/100 gm) was found in both the Karthakolomban. According to previous studies conducted, maximum protein content in all the fruits varies from 1.57 to 5.42% and maximum protein content in the different varieties of tropical fruits vary from 0.4 to 0.8% [22].

Table 3: Total protein, total fat, crude fiber, ash, total carbohydrate and total energy of mango varieties

Mango Variety	Total protein	Total fat	Crude fiber	Ash	Total carbohydrate	Total energy
Willard	0.21 ± 0.03	0.67 ± 0.03	1.17 ± 0.05	0.39 ± 0.04	23.39 ± 0.04	95.75 ± 2.56
Karthakolomban	0.17 ± 0.02	0.41 ± 0.02	3.16 ± 0.06	0.58 ± 0.03	27.21 ± 0.02	100.57 ± 1.89
Malwana	0.18 ± 0.01	0.86 ± 0.02	1.46 ± 0.03	0.32 ± 0.04	14.36 ± 0.03	60.06 ± 2.04
Bettiamba	0.24 ± 0.02	0.59 ± 0.02	1.98 ± 0.04	0.22 ± 0.02	26.39 ± 0.04	103.91 ± 1.56
Gira Amba	0.28 ± 0.02	0.72 ± 0.04	2.06 ± 0.04	0.24 ± 0.03	21.53 ± 0.03	85.48 ± 2.76

The total fat ranged from 0.41 gm/100 gm to 0.86 gm/100 gm. Malwana variety was found rich in total fat content (1.20 gm/100 gm) and Karthakolomban (0.41 gm/100 gm) was found with the lowest amount of fat content. It was reported that usually fat content of different fruits is not greater than 1% [23].

Both crude fiber and ash contents possess a significant variation ($p < 0.05$) in different mango varieties. The maximum amount of crude fiber was found in Karthakolomban (3.16 gm/100 gm) followed by Gira Amba (2.06 gm/100 gm) and Bettiamba (1.98 gm/100 gm). The lowest amount of crude fiber was found in Willard (1.17 gm/100 gm). The highest amount of ash was found in Karthakolomban (0.58 gm/100 gm) and lowest in Bettiamba (0.22 gm/100 gm). Regarding ash content, [24] reported that the total content of mineral salt as ash in fruits varied from 0.2% to 1.5%, which range is almost similar to our observed findings.

Total carbohydrate and total energy of different mango varieties were also significantly ($p < 0.05$) varied (Table 3). Generally, carbohydrate of fruit is less concentrated than cereals because of their high-water content. Fruits

rich in carbohydrate provides a high amount of energy. In this study, Bettiamba indicated the highest amount of energy (103.91 Kcal/100 gm) due to its high carbohydrate content (26.39 gm/100 gm) followed by Karthakolomban (100.57 Kcal/100 gm) and the lowest amount of energy showed in Malwana (46.05 Kcal/100 gm) due to its low carbohydrate content (14.36 gm/100 gm).

IV. CONCLUSION

The study has indicated that the mango is an adequate source of energy and macronutrients such as carbohydrate and crude fibre. Bettiamba and Karthakolomban have high amount of carbohydrate and both are rich sources of contains high carbohydrate hence provides more energy. Malwana contains highest moisture content and Karthakolomban possesses the highest edible portion when compared. It also consists with the highest total soluble solids, total sugar and reducing sugar. Considering the nutritional facts, Karthakolomban is highly nutritive and fibrous. Gira Amba contains higher percentage of protein, and a higher fat content with respect to the other varieties compared. Malwana contains low reducing sugar, low total

sugar and low total soluble solids. Therefore, such varieties and their processed products may be suitable for diabetic patients. As for the conclusion, nutritional properties of these main mango varieties of Sri Lanka were systematically addressed under their nutritional parameters. This may assist the consumers, dietitian and food processors. Further analysis like vitamin and mineral profile will be required for complete nutritional information of these mango varieties.

REFERENCES

- [1] Gulcin, I., Uguz, M., Oktay, M., Beydemir, S. and Kufrevioglu, O. (2004). Evaluation of the antioxidant and antimicrobial activities of Clary Sage (*Slaviasclarea L.*). *Turkey Journal of Agricultural Forestry*, 28, pp.25-33.
- [2] Hamdard, M., Rafique, M. and Farroq, U. (2004). Physico – chemical characteristics of various mangos, *Mangifera indica L.* varieties. *Journal of Agricultural Research*, 42(2), pp.191-199.
- [3] Leghari, M., Sheikh, S., Memon, N., Soomro, A. and Khooharo, A. (2013). Quality attributes of immature fruit of different mango varieties. *Journal of Basic and Applied Sciences*, 9, pp.52-56.
- [4] Bhuyan, M. and Islam, M. (1990). Physico morphological characters of some popular mango cultivars. *Bangladesh Journal of Agriculture*, 14, pp.181-187.
- [5] Rajput, S. and Pandey, S. (1997). Physico-chemical characteristics of some mango cultivars under Chhattisgarh region of Madhya Pradesh. *Horticulture Journal*, 10(1), pp.9-14.
- [6] Hamdard, M., Rafique, M. and Farroq, U. (2004). Physico – chemical characteristics of various mangos, *Mangifera indica L.* varieties. *Journal of Agricultural Research*, 42(2), pp.191-199.
- [7] Akhter, S., Naz, S., Sultan, T., Mahmood, S., Nasir, M. and Ahmad, A. (2010). Physicochemical attributes and heavy metal content of mangoes (*Mangifera indica L.*) cultivated in different regions of Pakistan. *Pakistan Journal of Botany*, 42(4), pp.2691-2702.
- [8] Nielsen, S. (2010). *Food analysis*. 4th ed. New York [etc.]: Springer, pp.227-232.
- [9] Ranganna, S. (1986). *Handbook of analysis and quality control for fruit and vegetable products*. New Delhi: Tata McGraw-Hill, pp.12-123.
- [10] Nielsen, S. (2010). *Food analysis*. 4th ed. New York [etc.]: Springer, pp.136-138.
- [11] Official methods of analysis of AOAC International. (2005). 18th ed. Gaithersburg, Md.: AOAC International, pp.8-21.
- [12] Nielsen, S. (2010). *Food analysis*. 4th ed. New York [etc.]: Springer, pp.108-110.
- [13] Pearson, D. (1976). *The Dictionary of Nutrition and Food Technology*. 15th ed. London: Butter Worth Publisher.
- [14] Official methods of analysis of AOAC International. (1995). 16th ed. Arlington, VA: AOAC International.
- [15] Ueda, M., Sasaki, K., Utsunomiya, N., Inaba, K. and Shimabayashi, Y. (2000). Changes in Physical and Chemical Properties during Maturation of Mango Fruit (*Mangifera indica L.* 'Irwin') Cultured in a Plastic Greenhouse. *Food Science and Technology Research*, 6(4), pp.299-305.
- [16] Haque, M., Saha, B., Karim, M. and Bhuiyan, M. (2010). Evaluation of Nutritional and Physico-Chemical Properties of Several Selected Fruits in Bangladesh. *Bangladesh Journal of Scientific and Industrial Research*, 44(3).
- [17] Pleguezuelo, C., Zuazo, V., Fernandez, J. and Tarifa,, D. (2012). Physico-chemical quality parameters of mango (*Mangifera indica L.*) fruits grown in a Mediterranean subtropical climate (SE Spain). *Journal of Agricultural Science and Technology*, 14, pp.365-374.
- [18] Hamdard, M., Rafique, M. and Farroq, U. (2004). Physico – chemical characteristics of various mangos, *Mangifera indica L.* varieties. *Journal of Agricultural Research*, 42(2), pp.191-199.
- [19] Prusky, D., Kobilier, I., Zauberman, G. and Fuchs, Y. (1993). PREHARVEST CONDITIONS AND POSTHARVEST TREATMENTS AFFECTING THE INCIDENCE OF DECAY IN MANGO FRUITS DURING STORAGE. *Acta Horticulturae*, (341), pp.307-320.
- [20] Padda, M., do Amarante, C., Garcia, R., Slaughter, D. and Mitcham, E. (2011). Methods to analyze physico-chemical changes during mango ripening: A multivariate approach. *Postharvest Biology and Technology*, 62(3), pp.267-274.
- [21] Sajib, M., Jahan, S., Islam, M., Khan, T. and Saha, B. (2014). Nutritional evaluation and heavy metals content of selected tropical fruits in Bangladesh. *International Food Research Journal*, 21(2), pp.609-615.
- [22] Gopalan, C., Rama, S. and Balasubra, S. (1993). *Nutritive Value of Indian Foods*. 2nd ed. Hyderabad: Indian Council of Medical Research.
- [23] Norman, N. (1976). *Food Science*. 2nd ed. INC-Westport, Connecticut: The Avi publishing company.
- [24] Gardner, V., Bradford, F. and Hooker, H. (1952). *The Fundamentals of Fruit Production*. 3rd ed. New York: McGraw-Hill Book Co.

Five New Ways to Prove a Pythagorean Theorem

Nurul Laily, Hobri, Dafik

Department of Mathematics Education, University of Jember, Indonesia

Abstract— Pythagoras is one of the mathematicians who developed the basic theories of mathematics. One of his taunts that are well-known even by primary school students is a Pythagorean Theorem. This theorem states that in a right-angled triangle, the square of the hypotenuse is equal to the sum of each other sides square. There are many proofs which have been developed by a scientist, we have estimated up to 370 proofs of the Pythagorean Theorem. In this paper, we are trying to develop five new proofs of Pythagorean Theorem by using algebraic-geometric proof. The first proof is proven by the trapezoidal shape constructed by five right triangles. The second and third Proofs are proven by using the constructed parallelograms consisting four right triangles and two isosceles trapezoids. The fourth proof is proven by trapezoidal shape constructed of three pieces of a congruent trapezoid, and the fifth proof is proven by using a rectangle constructed by congruent square. Thus, we conclude that the proof of the Pythagorean Theorem can be proven by using the construction of flat trapezoid, parallelogram, square, and rectangular by means of a right-angle triangle.

Keywords— Pythagoras theorem, right-angle triangle, Trapezoid, Square, Rectangle..

I. INTRODUCTION

Pythagorean Theorem becomes an important base in the calculation of the length side of the flat straight sides with the help of right-angled triangles, because the Pythagorean Theorem is a fundamental theorem in mathematics. The Pythagorean Theorem has been introduced to students from elementary school until secondary school. Pythagoras discovery in the field of music and mathematics remains alive today. Pythagorean Theorem is taught in schools and used to calculate the distance a side of a right triangle. Before Pythagoras, there were no proofs or assumptions underlying on right triangle systematic. Pythagoras was the first person who coined that axioms, postulates outlined in advance in developing geometry.

The famous Pythagorean Theorem states that the square of the hypotenuse of a right triangle is equal to the sum of each other sides square. Although the development of the various version of other proofs has been widely known

before Pythagoras, all proof related to the right triangle is still addressed to the Pythagorean Theorem, because he was the first to prove the observation mathematically in a right triangle.

One of the benefits of this theorem is as a tool in the calculation of the natural phenomena. The Pythagorean Theorem was a base of proving Fermat's theorem in 1620: $x^n + y^n = z^n$, which was firstly proven by Sir Andrew Wiles in 1994. After that, some math calculations in a quite complicated technique were resolved.

The book: *The Pythagorean Proposition* written by ES Loomis, second edition published since 1940 is a major collection of proofs of Pythagoras theorem. This book has been collected as many as 370 different proofs of Pythagorean Theorem. A proof given by Euclid, as well as a modern mathematician like Legendre, Leibniz and Huygens, also ex-president of the United States (James Garfield) have enriched the collection of that book.

In that book, Loomis classify all evidence into four categories. Most evidence are categorized in algebraic or geometric proof. In algebra, the proof of this theorem is shown by the number of squares of the two legs lengths which are equal to the length of the hypotenuse. While the geometrical proof is indicated by the box area developed from two foot square areas that are equal, to that, produced on the hypotenuse. That book consists of 109 algebraic proof and 255 geometric proof geometric. (There are also 4 "quaternionic" evidences and two "dynamic" evidences). Furthermore, the total calculation of all category, the proof is reaching 370. In addition there are five journaled latest evidences, such as the evidence in the category of geometry-trigonometry. Therefore, the total is 375 evidentiary proof.

The spread of Pythagoras Theorem is very fast. So many books and internet portals review this theorem and its proof. Since the days of Pythagoras, many different proofs of the Pythagorean Theorem are published. In the second printed book: *"The Pythagorean Proportion"* Lomis ES 370 has collected and classified the evidence of this famous theorem.

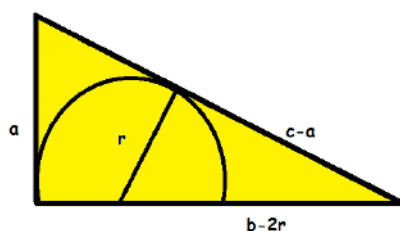
Proofs of Pythagoras that have been found by researchers are a five-proof algebraic - geometric proof. The first proof is given in a trapezoidal ABGD constructed of five pieces of a right triangle, there are two pairs of right-

angled triangles congruent with the side of the base a and (ba) to the height of each b and $(a + b)$. Then, the triangle elbow with a base and height c , is a way to apply $a^2 + b^2 = c^2$. The second Proof is known in parallelogram ABCD. It is constructed of four right-angled triangle, two of which are congruent triangle with each pedestal is $a, c, (ba)$ and the height $b, c, \text{ and } (b + a)$. This is a way to apply $a^2 + b^2 = c^2$. The third Proof is in parallelogram AELH which is constructed of two pieces of congruent isosceles trapezoid, each trapezoid constructed by six right-angled triangle, two pairs of which are congruent right-angled triangles with base a and height b , the two others are a right triangle with the base length and height is c . It is a way to apply $a^2 + b^2 = c^2$. The fourth proof is given in trapezoidal of ABIH square which is constructed from ABCD trapezoid and DCIH square. ABCD is made of EHGFSquare with sides c and four congruent right-angled triangles with the pedestal a and high b . Trapezoid DCIH is formed from three pieces of right-angled triangles, two of which is a right triangle with base a and height b , and a right triangle with base and height c . In proving the fifth, rectangle ABDE is constructed of two congruent square, each square constructed of square PQRS with sides (ba) and four right-angled triangle with the base a and b . It applies that $a^2 + b^2 = c^2$. The next Pythagorean Theorem comes from the 20th president of US, J.A Garfield in 1876. The area of the trapezoid below can be calculated in two ways, so that the Pythagorean theorem can be proven by trapezoid coincides extension with the three right-angled triangle, then $a^2 + b^2 = c^2$.

On the Square ABCD, in which it creates four right-angled triangle with sides a, b , and c as the hypotenuse and unknown a, b , as the triangular straightener.

Is it proven that square ABCD equals the number of extensive third-angled triangle and square PQRS, then apply $a^2 + b^2 = c^2$.

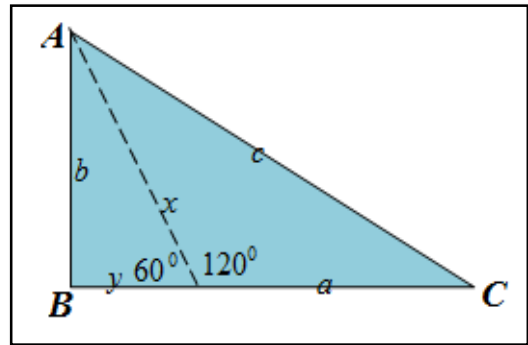
The next theorem was proven by *J. Molokach*, on May 19, 2015 by writing a half-circle to the right-angled triangle. r is the radius of the semicircle. This is determined by the proportion of (the equality of two triangles).



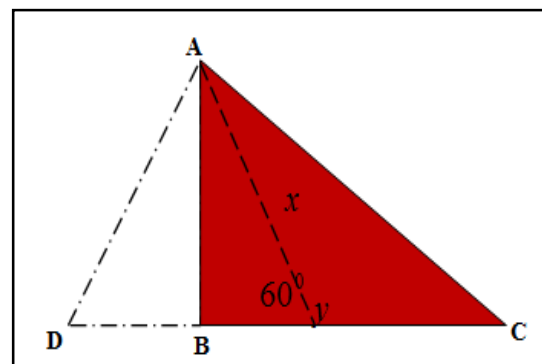
Proof of J. Molokach

To prove the Pythagorean Theorem, it is applied to the intersection of two chords in a circle equation, then apply $a^2 + b^2 = c^2$.

The Evidence of Pythagoras made by Burkard Polster and Marty Ross published in Mathematics Magazine (VOL. 89, No.1, February 2016 pages:47-54). The Pythagoras proof discovery is an evidence of the cosines law with angles of 60° and 120° . The evidence depends on the Pythagorean Theorem and the general law of cosines.



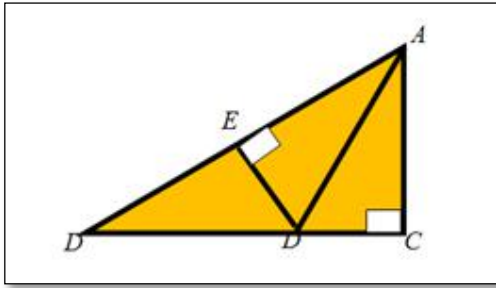
Pythagoras Burkard Polster- Marty Ross



Pythagoras Burkard Polster- Marty Ross

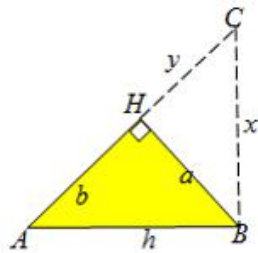
In this case, the evidence refers to the van floor Lamoen discovery derived from the general statement of the Pythagorean Theorem of right isosceles triangle case. Pythagorean Theorem through an angle of 60° and 120° , any right-angled triangle can be divided into one angle of 60° and the other 120° angle. Using the notation in the diagram refers to the results of the Polster and Ross. Pythagorean Theorem through 60° and 120° obtained: $b^2 + a^2 = c^2$.

Proofs of Pythagoras have been published in *the American Mathematical Monthly Magazine*, with an editor record (vol.116 2009, October 2009, p 687) Although this evidence does not appear and known, it is the rediscovery of the evidence, which first appeared printed, and the evidence has been presented by Sang Woo Ryoo, a student of Carlisle High School, Carlisle, PA. Loomis took credit for evidence. Figure AD, angle bisector of the angle A, and DE is perpendicular to AB.



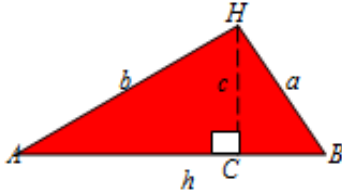
Evidence by Ryoo Sang Woo

the proof leads to $(cb)(c + b) = A^2$ and to the Pythagoras identity. Thus it obtains the equation: $b^2 + c^2 = A^2$.



Loomis evidence to 16

Given HB is perpendicular to the air conditioner to form three right-angled triangles namely: $\triangle ABC$, $\triangle AHB$, and $\triangle BCH$. So it uses: $b^2 + a^2 = h^2$.



HC is perpendicular to AB. So, to form three right-angled triangle need: $\triangle ACH$, $\triangle BCH$, $\triangle AHB$, using the ratio of $AC:AH = AH:AB$. then it uses; $h^2 = a^2 + b^2$.

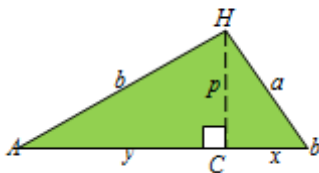
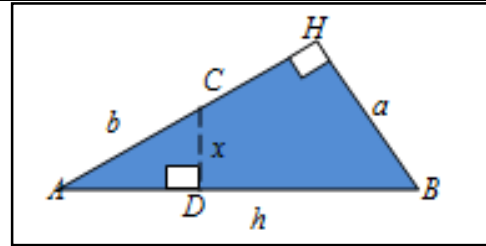


Fig.1: Trapezoid ABDG

By using the ratio:

$$x^2 + p^2 = x^2 + xy = x(x + y) = a^2,$$

it applies, $h^2 = a^2 + b^2$



An ABC triangle with the elbows in H uses the comparison:

$$\frac{a}{x} = \frac{b}{h-a}; \frac{b}{h-a} = \frac{h}{b-x};$$

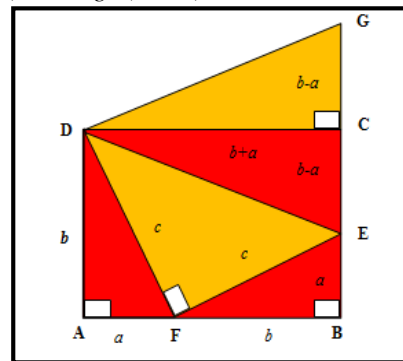
then is obtained: $a^2 + b^2 = h^2$.

There are still many ways that can be served to motivate new verification techniques to prove this Pythagorean Theorem.

II. RESULTS AND DISCUSSION

The following will be presented new evidence in the Pythagoras theorem. Proof of the Pythagorean Theorem developed in this article is categorized in the form of evidence algebraic geometry, wherein each is accompanied by a proof of the theorem, evidence and geometry images to get easier in its presentation. There are four new theorems that found new evidences related to the Pythagoras theorem.

Theorem 1: an ABCD trapezoid with a ABDG rectangular and DCG triangle, the ABCD square constructed by $\triangle DAF$ with right-angled at A with a pedestal, height b, and hypotenuse c. Pulled straight line segment from point F to point B with side lengths b, draw a line segment perpendicular to AB, from point B to point E with a side length. Connect the dots from point E to F with side length c, and from point D to point E, so $\triangle DFE$ is a right triangle. Pull straight line segment from point E to point C with a long ba. Connect the line segment from point D to point C, draw a line segment from point C to point G with the long side (ba), draw a line segment from point D to point G, so that ABGC is a trapezoid with a base $(3b-a)$ and high $(b + a)$, then shows $a^2 + b^2 = c^2$.



Proof:

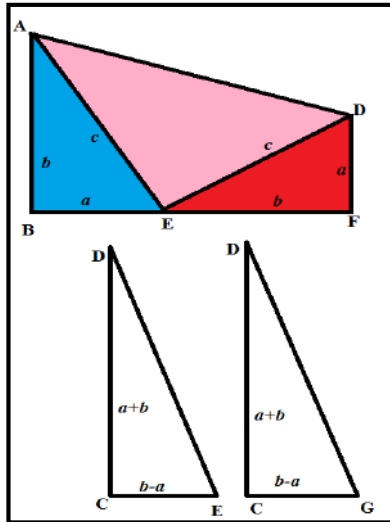


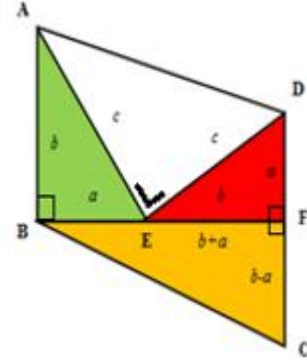
Fig.2: Parallelogram ABCD

The rectangle ABCD is composed of four right-angled triangle that is $\triangle DAF$, $\triangle FBE$, $\triangle DFE$, $\triangle DCE$. On board a $\triangle DAF \cong \triangle FBE$ length and height b , $\triangle DCE$ have a high pedestal and c , and $\triangle AFD \cong \triangle FBE$ have a side length and height b . Line segment drawn from point C to point to point G sided $(b a)$ and a line segment drawn from point G to point D. As such DCG triangle is a right triangle in C with the length of the base (ba) and high $(b + a)$, then apply $a^2 + b^2 = c^2$.

Trapezoid broad ABGD are:

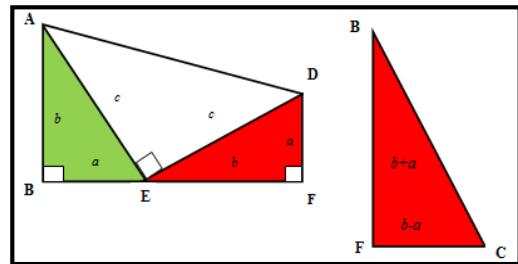
$$\begin{aligned}
 &= \text{Area } \Delta_1 + \text{Area } \Delta_2 + \text{Area } \Delta_3 + \text{Area } \Delta_4 + \text{Area } \Delta_5 \\
 &\frac{1}{2} \cdot (3b - a) \cdot (b + a) = \frac{ab}{2} + \frac{ab}{2} + \frac{c^2}{2} + \frac{b^2 - a^2}{2} + \frac{b^2 - a^2}{2} \\
 &\frac{3b^2 - ab + 3ab - a^2}{2} = \frac{ab}{2} + \frac{ab}{2} + \frac{c^2}{2} + \frac{b^2 - a^2}{2} + \frac{b^2 - a^2}{2} \\
 &3b^2 + 2ab - a^2 = 2ab + c^2 + 2b^2 - 2a^2 \\
 &b^2 + a^2 = c^2
 \end{aligned}$$

Theorem 2: a triangle ABE is a right triangle in B, drawn segment of the straight line from point E to point F with the long side b , drawn the line segment perpendicular to BF, from point F to point D with length a , connect line segment from point A to point D and from point D to point E with a length c , draw a line segment perpendicular to BF with point F to point C of length (ba) , connect the line segment from point B to point C, such that ABCD is a parallelogram with base $(b + a)$ and b high, then apply $a^2 + b^2 = c^2$.



Proof:

a parallelogram ABCD consists of trapezoidal ABFD and right-angled triangle BFC. The length of the side $AB = b$, the $DF = a$, and high $BF = (a + b)$. Trapezoid ABFD has two pairs of right-angled triangles with the $\triangle ABE$ and $\triangle ADF$ high pedestal a and b , and a right triangle with sides of length $\triangle AED$ high pedestal and is c . Two line segments drawn from point F to point C with side lengths $(b a)$ and from point B to point C on the side BF. $\triangle CFB$ is such that the right-angled triangle in F with the high pedestal of a and b , then apply $a^2 + b^2 = c^2$.



The vast of parallelogram ABCD =

$$\begin{aligned}
 &\text{Area } \Delta_1 + \text{Area } \Delta_2 + \text{Area } \Delta_3 + \text{Area } \Delta_4 \\
 &\frac{1}{2} (a+b)(a+b) + \frac{1}{2} (a+b)(b-a) = \frac{1}{2} ab + \frac{1}{2} c^2 + \frac{1}{2} ab + \frac{1}{2} (b+a)(b-a) \\
 &\frac{a^2 + 2ab + b^2 + b^2 - a^2}{2} = \frac{ab}{2} + \frac{c^2}{2} + \frac{ab}{2} + \frac{b^2 - a^2}{2} \\
 &\frac{a^2 + 2ab + 2b^2 - a^2}{2} = \frac{c^2 + 2ab + b^2 - a^2}{2} \\
 &a^2 + 2ab + 2b^2 - a^2 = c^2 + 2ab + b^2 - a^2 \\
 &a^2 + b^2 = c^2
 \end{aligned}$$

Theorem 3: right triangles ABF and FBC with the base a , height b and hypotenuse c , drawn straight line segments from the point F to the point I with a side length b , drawn the line segment perpendicular to AB, from the point F to point I to the length of the side b . Pull the line segment perpendicular to the IF, from the first point to duck H and from point I to point J with a side length. Line segment drawn from point A to point H and F sides with side length c . Line segment drawn from point H to point A and from point A to point. Connect both isosceles trapezoid ACJH and CELJ to trapezoidal AELH, such

that trapezoidal $ACJH \cong CELJ$, then come into force $a^2 +$

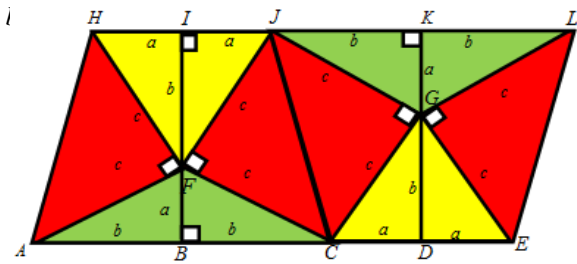


Fig.3: Parallelogram AEHL

Proof:

In a parallelogram AELH constructed from two congruent trapezoids ACJH and CELJ. In trapezoid ACJH consists of three pairs of right-angled triangles are congruent ie $\Delta ABF \cong \Delta CBF$ and $\Delta HIF \cong \Delta JIF$ which has a high pedestal of a and b, and $\Delta AFH \cong \Delta CFJ$ which has a high pedestal and c, such a parallelogram AELH has eight right-angled triangles are congruent with the high pedestal of a and b, and four congruent right-angled triangle with the base and the height is c, then come into force $a^2 + b^2 = c^2$.

Area AELH = $4 \times$ Area FHI + $4 \times$ Area AFH + $4 \times$ Area ABF

$$2\left(\frac{1}{2}(2a+2b)(a+b)\right) = 4\left(\frac{1}{2}ab\right) + 4\left(\frac{1}{2}c^2\right) + 4\left(\frac{1}{2}ab\right)$$

$$2a^2 + 2ab + 2ab + 2b^2 = 2ab + 2c^2 + 2ab$$

$$2a^2 + 4ab - 4ab + 2b^2 = 2c^2$$

$$2a^2 + 2b^2 = 2c^2$$

$$a^2 + b^2 = c^2$$

Theorem 4: a trapezoid ABIH constructed of ABCD square and DCIH trapezoid. On the square ABCD constructed from EBJ right triangle with the base a, height b and hypotenuse c, drawn straight line segment from point J to point C to length b and from point E to point A with a side length. Pull the line segment perpendicular to AB from point A to point F with the length b, connect the line segment from point E to point F. Pull the line segment perpendicular to BC from point C to point G with length a and from the point G to point D with a length b. Pull the line segment with a length c from point J to point G and point F to point G, draw a line segment perpendicular to BC, from point D to point H and from point C to point I. Connect the line segment from point H and I to point G, and, I point to point H, such that $ABHF \cong HCDE$ DCIH then come to form $a^2 + b^2 = c^2$.

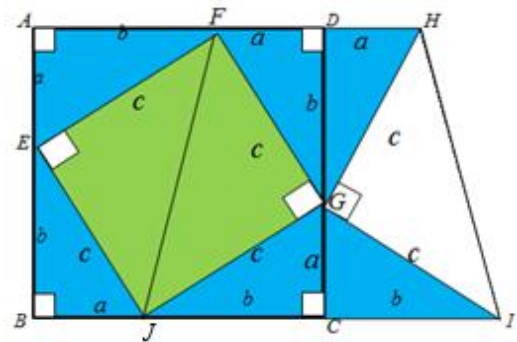


Fig.4: Trapezoid ABIH

Proof:

A square ABCD constructed of four right-angled triangles with a pedestal length and height b, and two right-angled triangles with a base and height c. In the wake square ABCD, drawn a line segment from point D to point H to the base a, and drawn a line segment from point C to point I with a side length b and retractable segment line from point G cut CD at point H and I each had side length c. Line segment drawn from point H to the point I with the length $\sqrt{2}c$, so that $\Delta EBJ \cong \Delta EAF \cong \Delta EDG \cong \Delta JCG \cong \Delta HDG \cong \Delta ICG$ and $\Delta FEH \cong \Delta FGH \cong \Delta HGI$, then apply $a^2 + b^2 = c^2$.

Area of rectangle ABCD + Area of rectangle CDHI = 6. area triangle Area AEF + 3 Area of triangle EFH

$$(a+b)(a+b) + \frac{1}{2}(a+b)(a+b) = 6\left(\frac{1}{2}ab\right) + 3\left(\frac{1}{2}c^2\right)$$

$$\frac{2a^2 + 4ab + 2b^2 + a^2 + 2ab + b^2}{2} = \frac{6ab + 3c^2}{2}$$

$$3a^2 + 6ab + 3b^2 = 6ab + 3c^2$$

$$3a^2 + 3b^2 = 3c^2$$

$$a^2 + b^2 = c^2$$

Or,

Area ABIH = 6. Area AEF + 3. Area EFH

$$\frac{1}{2}(a+2b)(2a+b)(a+b) = 6\left(\frac{1}{2}ab\right) + 3\left(\frac{1}{2}c^2\right)$$

$$\frac{3a}{2} = \frac{6ab + 3c^2}{2}$$

$$3a^2 + 6ab + 3b^2 = 6ab + 3c^2$$

$$3a^2 + 3b^2 = 3c^2$$

$$a^2 + b^2 = c^2$$

Theorem 5: an ABDE rectangle is constructed from two square pieces ABCF and CDEF. Each square constructed of four right-angled triangles are congruent with the base a and height b, and a square PQRS with

sides $(b-a)$, drawn line segment from point F and point C , such that $ABDE$ form a rectangle with a length $2c$ and width c , then apply $a^2 + b^2 = c^2$.

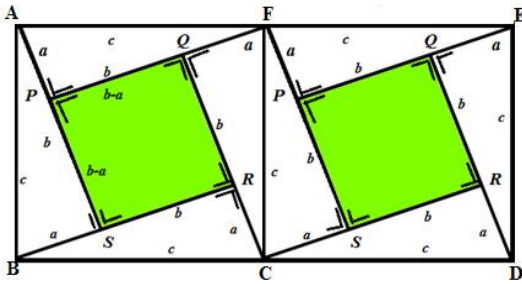


Fig.5 : Rectangle ABDE

Proof:

A rectangle $a b d e$ of two square pieces is congruent. $ABDC$ square with sides c . $ABDC$ square have the four right-angled triangles are congruent with the high pedestal of a and b , and square $PQRS$ with sides $(b-a)$. Such that $AP = BS = RC = FQ = a$, and $AS = CQ = FP = BR = b$, then apply $a^2 + b^2 = c^2$.

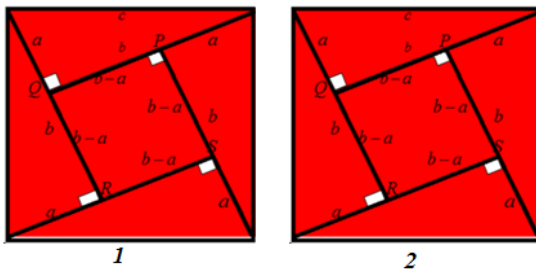


Fig.6 : Rectangular ABCD

To prove the Pythagorean theorem above note the following:

Area Rectangle = 2.(4. Area of triangle ARB + Area of rectangle PQRS)

$$p.l = 2 \cdot \left(4 \cdot \frac{1}{2} ab + (b-a)^2 \right)$$

$$2c \cdot 2c = 2 \cdot (2ab + b^2 - 2ab + a^2)$$

$$2c^2 = 2 \cdot (b^2 + a^2)$$

$$2c^2 = 2a^2 + 2b^2$$

$$c^2 = a^2 + b^2$$

III. CONCLUSION

The above discussion has discovered the five new ways of proving Pythagoras Theorem. The fifth way is quite effective in a very famous proving and rewarding theorem. However, the five new evidences above are pretty easy to be understood by teachers and students in the school.

ACKNOWLEDGEMENTS

We gratefully acknowledge the support from FKIP-University of Jember

REFERENCES

- [1] G Leonardo da Vinci (April 15, 1452 - May 2, 1519)
- [2] Loomis, E., S. *The Pythagorean Proportion of 1927.*
- [3] Maor, E., *The Pythagorean Theorem, A 4,000-Year History*, Princeton University Press, Princeton, N.J., 2007, p. xii..
- [4] Maor, E., *The Pythagorean Theorem, A 4,000-Year History*, Princeton University Press, Princeton, N.J., 2007, p. 5.
- [5] Maor, E., *The Pythagorean Theorem, A 4,000-Year History*, Princeton University Press, Princeton, NJ, 2007, p. 17.
- [6] Paulus Gerdes, *Zum erwachenden geometrischen Denken*, Dresden, Maputo, 1985.
- [7] Wagner, Donald B, 2004. *A proof of the Pythagorean Theorem by LiuHui.* [Online]. <http://donwagner.dk/Pythagoras/Pythagoras.html>

Survival Analysis in Patients with Dengue Hemorrhagic Fever (DHF) Using Cox Proportional Hazard Regression

Luluk Handayani, Mohamat Fatekurohman, Dian Anggraeni

Mathematics Depart. University of Jember, Indonesia

Abstract—Indonesia is a tropical country that has two seasons: the rainy season and dry season. In the rainy season frequent flooding or puddles of water that could become mosquito breeding and the spread of various diseases, one of which is the dengue fever. Dengue Hemorrhagic Fever (DHF) is the cause of public health problems with a very rapid deployment and can lead to death within a short time. This causes dengue become one of the attractions to be investigated further. This study discusses the survival analysis and the factors that affect the healing rate of dengue patients using Cox proportional hazard regression based on data from the medical records of hospitalized dengue patients at the Jember Klinik Hospital. The results showed that the factors of age, gender, hemoglobin, trombonist, and hematocrit affect the healing rate of DHF patients.

Keywords—survival analysis; DHF; cox proportional hazard.

I. INTRODUCTION

Indonesia is a tropical country that has two seasons, namely the rainy season and the dry season. In the rainy season, for various reasons, there are floods or puddles that can become a mosquito breeding and spread various diseases, one of which is dengue fever disease. Dengue Haemorrhagic Fever (DHF) is an acute febrile illness caused by dengue virus that enters the bloodstream through the bite of *Aedes Aegypti* mosquito (Wikipedia, 2012), which spreads very quickly and can result in death in a short time. Dengue Hemorrhagic Fever (DHF) is one of the diseases that almost always cause public health problems and the number is always there, even tended to increase. It is known that since the first DBD appeared in Indonesia, precisely in Surabaya in 1968, it quickly spread to other areas so that in 1980 all provinces in Indonesia have been infected with DHF (Darmowandowo, 2006). Indonesia is the country with the highest incidence of DHF in Southeast Asia since 1968-2009 (WHO, 2009). This causes DBD to be one of the interesting objects to be studied and studied further, for example, to know the length of time to survive the

DHF patients to recover. The application of statistical methods that can be used to analyze the case is survival analysis.

Survival analysis is a statistical analysis that is specifically used to analyze data or cases related to the time or length of time until a particular event occurs. This survival analysis is usually used in the health field (Kleinbaum and Klein, 2012). Observational data for survival analysis are survival data, ie observation data about the time period from the beginning of observation until the occurrence of an event, the event could be death, healing or other symptoms (Lee, 1992). According to Collett (1994), survival data do not meet the statistical standard procedure requirements used in data analysis, since survival data is usually not symmetrically distributed. The histogram model of survival time in a group of individuals will tend to be skewed to the right, so it is possible that survival data is not only normally distributed. There are several other distributions that are commonly used in survival analysis, ie, exponential distributions, Weibull distributions and lognormal distributions. The distribution used in a survival analysis can be determined from the estimation of the survival data distribution with some statistical test methods, such as Anderson Darling test and Chi-Squared test. While some of the models known in this analysis include binary logistic regression, Bayesian Mixture Survival model, Random Survival Forests (RSF), Multivariate Adaptive Regression Splines and Cox Proportional Hazard regression.

Several previous studies have been conducted on DHF cases using survival analysis, such as Nisa '(2012) about survival analysis with Multivariate Adaptive Regression Splines approach in DHF case in the district.

II. LITERATURE REVIEW

A. Survival Analysis

The survival analysis or survival analysis is a time-related data analysis, from the beginning to the occurrence of a specific event (Collett, 2003). Duration

from the beginning of the observation (time origin) until the occurrence of a special event (end point or failure event) is called the time of survival. The particular event (failure event) may be a failure, death, relapse or recovery from an illness, a response from an experiment, or another event chosen according to the researcher's interest. The survival analysis has a special characteristic, namely the distribution of data in the form of long life time (skewed) right because the value will always be positive and the data is censored (Lee, 1992).

1. SurvivalTime

Survival time can be defined as the time from the beginning of observation to the occurrence of events, can be in days, months, and years. Such events may be the development of a disease, the response to treatment, the recurrence of an illness, death or other event chosen in accordance with the interests of the researcher. Therefore, the time of survival can be the time of recovery from the disease, the time from start of treatment to the occurrence of response and time to death (Lee and Wang, 2003). In determining survival time, there are three factors that are needed (Le, 1997):

- a. Time of origin (time origin or startingpoint)
- b. End events / end time (ending event of interest)
- c. Time scale as the measurement scale for the passage of time.

2. CensoredData

The difference between survival analysis and other statistical analysis is the presence of censored data. Censored data is recorded data when there is information about individual survival times, but does not know the exact time of survival (Kleinbaum & Klein, 2012). Censorship is one of the steps that must be taken to overcome the incompleteness of an observation data. The data is said to be censored if the data can not be observed completely because the research subject is lost or resigned or until the end of the research the subject has not experienced a certain incident, while the data can be observed completely until the end of research called uncensored data (Lee & Wang, 2003). The causes of censored data are:

- a. Loss to follow up, occurs when objects move, dies or
- b. refuses to participate. Drop out, occurs when the treatment is stopped
- c. for some reason. Termination of study, occurs when the study period ends intermediate object observed has not reached the failure event.

The 3 (three) types of sensors used in survival analysis (Collet, 1994) are as follows:

- a. RightSensorSensors that occur when a failure event has not occurred until the end of the study.
- b. LeftSensorSensors that occur when a failure event

occurs before the research begins.

c. IntervalSensorSensors that if termination in data collection and event failure occur between these time intervals.

3. SurvivalFunction and HazardFunction

The function of survival and hazard function is a fundamental function in survival analysis. In theory, the survival function can be described with a smooth curve and has the following characteristics (Kleinbaum & Klein, 2012):

- 1. Not increase, curve tends to decrease when t increases
- 2. For $t = 0$, $S(t) = S(0) = 1$ is the beginning of the study, since no object has an event, the probability of survival time 0 is 1
- 3. For $t = \infty$, $S(t) = S(\infty) = 0$ theoretically, if the period of study increases without limit then none survives so that the survival curve approaches

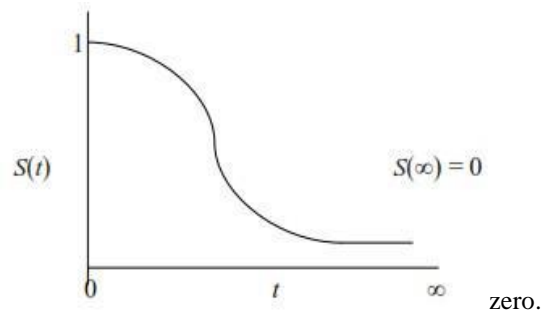


Fig.2.2: Survival Function Curve (Kleinbaum & Klein, 2005)

The survival function is essential in survival analysis, since there is a survival probability for various t values that is important information from survival data. The survival function is used to represent the individual probability of surviving from the initial time to some time. The survival function, $S(t)$, is defined as the probability that an individual survives greater than t time (Le, 1997), thus:

$$S(t) = P(T > t) = 1 - P(T \leq t) = 1 - F(t) \quad (2.1)$$

with $F(t)$ is the Cumulative Distribution Function (CDF) of the data distribution.

In contrast to survival functions that focus on non-occurrence of events, hazard functions focus on the occurrence of events. Therefore, hazard function can be viewed as the information giver that is opposite to the survival function. Similar to the survival survival curve, the hazard function curve also has characteristics, namely (Kleinbaum and Klein, 2012):

- 1. Always nonnegative, ie equal to or greater than zero
- 2. Has no upper limit
- 3. In addition the hazard function is also used for reasons:
- 4. Giving an overview of the failure rate
- 5. Identify the specific model shape

6. Creating a mathematical model for survival analysis is usually written in the form of a hazard function. The hazard function $h(t)$ is the probability of a person failing after a given time unit, which is the opposite of the survival function $S(t)$. The hazard formula can be interpreted as the probability of occurrence at a time interval between t and $t + \Delta t$ where the survival time T is greater than or equal to t .

$$h(t) = \lim_{\Delta t \rightarrow 0} \frac{P(t \leq T \leq t + \Delta t | T \geq t)}{\Delta t} \quad (2.2)$$

$$h(t) = \lim_{\Delta t \rightarrow 0} \frac{P(\text{an individual } t \text{ age dies at an interval up } t + \Delta t)}{\Delta t} \quad (2.3)$$

$$h(t) = dt = P(t \leq T \leq t + \Delta t | T \geq t) \quad (2.4)$$

In other words, the hazard function $h(t)$ estimates the proportion of deaths of individuals or individuals experiencing an event in time t (Kleinbaum and Klein, 2012). When the hazard function is always constant, it will get a constant-risk model (exponential). The following is the functional relationship between cumulative hazard function, $H(t)$, and survival function, $S(t)$ (Le, 1997) are:

$$H(t) = -\ln S(t) \quad (2.5)$$

B. Kaplan Meier

The purpose of survival analysis is to estimate and interpret survival function. In this research, the method used is Kaplan-Meier method. Kaplan-Meier method is a technical type of survival analysis that is often used. This product is often referred to as product limit method, the method is not made a certain interval and the effect is calculated exactly when it happens. The length of each subject's observations is composed of the shortest to the longest, with the censored records included or calculated, this is considered to be proportional to numerical measurements. This research is nonparametric statistical research with censored data, so use Kaplan-Meier's method is the best.

Actually, a life-table method is the same as Kaplan-Meier, but in the life-table object is classified based on certain characteristics which each character is arranged with interval by considering the chance of effect during the interval period is constant so that the data obtained will be more general. While the Kaplan-Meier method is analyzed according to their original time. This results in a definite proportion of survival because it uses precise time survival in order to obtain more accurate data. In addition, Kaplan-Meier is a method used when no model is feasible for survival data (Sari, 2011).

Log Rank Test

The log rank test is a significance test for comparing survival functions between the two groups. This test is a nonparametric statistic test and is suitable to be used when data is not symmetrical ie data tilted to the right. In addition, the Log Rank test is widely used in clinical

trials to look at the efficiency of a new treatment compared to the old treatment when measured is the time until an event occurs. To calculate the log rank there are several stages, namely:

- Count the number of risky subjects in each group at the time of failure (n_{ij}).
- Calculates the number of subjects who experienced events in each group at the time of failure (m_{ij}).
- Calculates the number of subjects who experienced the expected event for each group at the time of failure (e_{ij}).

$$e_{ij} = \frac{n_{ij}}{n_{1j} + n_{2j}} \times (m_{1j} + m_{2j}) \quad (2.6)$$

- Calculates The Log Rank

$$x^2 = \frac{(O_i - E_j)^2}{\text{var}(O_i - E_j)} \quad (2.7)$$

With :

$$(O_i - E_j) = \Sigma(m_{ij} - e_{ij}), i = 1, 2, \dots \quad (2.8)$$

- Cox Regression (Cox Proportional Hazard Regression)

The function of survival and hazard function is an analysis used to see the difference of 2 or more groups. However, if there are covariate variables that want to be controlled or if using some explanatory variables in explaining the relationship between survival time then cox regression is used. Thus cox regression can be used to create a model that describes the relationship between time of survival as a dependent variable with a set of independent variables. This independent variable can be either continuous or categorical.

Cox proportional hazard is the model used in survival analysis which is a semiparametric model. Cox proportional hazard regression is used when the observed outcome is the length of time of an event. Initially this modeling was used in the branch of statistics, especially biostatistika, which is used to analyze the death or life expectancy of a person. But over the development of the modeling era is widely used in various fields, including academic, medical, social, science, engineering, agriculture and so on (Sari, 2011).

When investigating a case in medicine for example the case of a patient with a particular disease, a relationship between the patient's survival time and the clinical characteristics of the patient's medical data is required. By denoting the average hazard function $h_0(t)$ can be determined hazard $h(t)$ of a given patient, by:

$$h(t) = (t)h_0(t) \quad (2.9)$$

The cox model formula is the multiplication of two magnitudes, the baseline hazard function and the exponential form for the linear summation of $\beta_i X_i$, ie the sum of the independent variables X (Kleinbaum and Klein, 2012). The Bazine hazard function is the hazard rate when it is an unknown function because the distribution of survival time (T) is unknown. This function is time-dependent only and does not contain X . This exponential quantity depends only on X called time independent covariate. This is because X does not depend on time, so X is called an independent time covariate. However, when X is time dependent, a different method is needed to model the hazard.

In the general regression model hazard function h depends on t and dependent covariates $X_1, X_2, \dots, X_m(t)$. And on a simple proportional hazard cox model, with the covariates X_1, X_2, \dots, X_m is independent of t the hazard function is as follows:

$$h(t, v_1, \dots, x_m, \beta_1, \beta_2, \dots, \beta_m) = h_0(t) \exp\{\beta_1 x_1 + \beta_2 x_2 + \dots + \beta_m x_m\} \quad (2.10)$$

$$h(t) = h_0(t) \exp\{\beta_1 x_1 + \beta_2 x_2 + \dots + \beta_m x_m\} = h_0(t) \exp\{\beta' x\} \quad (2.11)$$

The most specific of these formulas is the proportional hazard assumption of baseline hazard is a function of t but does not involve the variable X . Unlike the exponential form involving variable X but does not involve t . X is said to be time independent (independent of time). The assumption on the proportional hazard cox model is the hazard ratio that compares the two categories of independent variables is constant at all times or is independent of time. If this assumption is not met or time dependent (X depends on time) then the model used is extended cox model. Another important characteristic of the cox model is that the baseline hazard, $h_0(t)$, is an unspecified function. This is what makes cox proportional hazard a parametric model.

The cox proportional hazard model is a well-known model for survival analysis. According to Kleinbaum and Klein (2012) the causes of this model are well known and widely used include:

1. The cox model is a non-parametric model.
2. Can estimate hazard ratio without the need to know $h_0(t)$ or baseline hazard function.
3. Can estimate $h_0(t)$, $h(t, X)$ and survival function. Although, $h_0(t)$ is not specific.
4. Is a robust model so that the results of the model cox almost the same with the parametric model results.
5. The safe model is chosen when in doubt to determine its parametric model, so there is no fear about the choice of the wrong parametric model.
6. Better than the logistics model when it

comes to timing survival and censorship. The purpose of cox regression:

1. Estimate the hazard ratio
2. Testing the hypothesis
3. Looking at the confidence interval of the hazard ratio

The assumption in the Cox Proportional Hazard model is that the hazard ratio comparing the two categories of predictors is constant at all times or is independent of time. In general, there are three approaches to assessing proportional hazard assumptions, namely:

1. With the graph approach

You do this by plotting the Log Minus Log (LML) plot of the survival function. In this plot for each strata must be parallel / parallel. This method can only be used for categorical variables. For continuous variables should be converted into categorical (2 or 3 groups). If each strata of the tested variable is parallel, then the assumption is satisfied. If it is not parallel then the proportional assumption is not met.

2. Using time dependent variable in extended cox model

The trick is to make the interaction between independent variables with survival time then see the significance value. The proportional assumption is met when the value

3. Using goodness of fit test.

The trick is to look at the value of p (Chi-square). If the value then the proportional assumption is met.

These three ways have advantages and disadvantages, for that a researcher should use at least two ways to test the proportional assumptions.

Candidate variable included in the interaction test is the independent variable that influences the survival time ($p < 0,25$). Next test the interaction between independent variables by using likelihood ratio test. If the value included in the model. Cox (Cox Proportional Hazard) regression model is:

$$h(t) = h_0(t) \exp\{\beta_1 x_1 + \beta_2 x_2 + \beta_i x_i\} \quad (2.12)$$

If the assumption is not met then the model used cox regression is recommended with time dependent covariate or extended cox model and can also use cox stratification model.

D. Dengue Hemorrhagic Fever (DHF)

Dengue Hemorrhagic Fever (DHF), a medical language called Dengue Hemorrhagic Fever (DHF), is a disease caused by dengue virus that is transmitted through the bite of *Aedes Aegypti* and *Aedes Albopictus* mosquitoes, which causes disruption of the capillary blood vessels and the blood clotting system, resulting in bleeding. The disease is found in many tropical regions

such as Southeast Asia, India, Brazil, America, including all over Indonesia, except in places more than 1.000 meters above sea level.

Incubation period for 3 - 15 days since someone attacked by dengue virus, furthermore patient will show various signs and symptoms of dengue as follows:

1. High fever suddenly 2-7 days (38 - 40 degrees Celcius).
2. On examination tourniquet test, it appears there larva (puspura)bleeding.
3. The presence of bleeding in the inner eye (conjunctiva), nosebleeds (epitaxis), defecation with the feces (mucous) mucus mixed with blood (melena), and others.
4. Enlarged liver (hepatomegaly).
5. Blood pressure decreases causing shock.
6. On the laboratory examination (blood) day 3 - 7 there was a decrease in platelet count below $150.000/\text{mm}^3$ (thrombocytopenia), an increase in hematocrit value above 20% of the normal value (hemoconcentration).
7. Occurrence of some accompanying clinical symptoms such as nausea, vomiting, decreased appetite (anorexia), abdominal pain, diarrhea, chills, seizures and headaches.
8. Experiencing bleeding on the nose (nosebleeds) and gums.
9. Fever felt by the sufferer causing complaints of sore / pain in the joints.
10. The appearance of red spots on the skin due to rupture of blood vessels.

III. METHODOLOGY

A. Research Data

Data used in this research is secondary data in the form of patient data of Dengue Hemorrhagic Fever (DHF) at Jember Clinic Hospital in September until December 2016 obtained from medical record of Jember Clinic Hospital as many as 100 patients

B. Research Variabel

In this study the variables used are response variables and predictor variables, with the description as follows:

1. Variable Response

Response variable in this research is survival time, that is time needed by patient to survive from time of early patient of DHF patient in hospital (start point) until patient stated recover (failure/end point). The response variable in this study is denoted by the letter T with time units in days.

2. Predictor Variables

Predictive variables in this study are data predicted to affect the survival time of DHF patients

obtained from medical record data at Jember Clinic Hospital, namely:

a. Age (X_1)

The age variable is the age of DHF patients at the beginning of admission to hospitalization at Jember Clinic Hospital.

b. Gender (X_2)

The gender variable is the sex of DHF patients who are hospitalized in Jember Clinic Hospital, which is classified into two categories:

1 = Male

2 = Female

c. Hemoglobin (X_3)

Hemoglobin variable that is hemoglobin level of DHF patients during undergoing hospitalization at Jember Clinic Hospital.

d. Trombosit/Platelets (X_4)

Platelet variable is the number of thrombocyte of DHF patients during undergoing inpatient at Jember Clinic Hospital, which is divided into two categories, namely:

1 = below normal ($<150.000 / \text{mm}^3$)

2 = normal ($150,000 - 400,000 / \text{mm}^3$)

(Gandasoebrata, 2009)

e. Hematocrit (X_5)

Hematocrit variable that is the percentage of hematocrit of DHF patients during undergoing inpatient at Jember Clinic Hospital.

C. Research Steps

The steps taken in this research are as follows:

1. Conducting a descriptive statistical analysis to determine the characteristics of DHF patients.
2. Make a Kaplan Meier Curve and perform a Log-Rank test on a categorical independent variable (predictor).
3. Conduct analysis of factors that affect the healing rate of DHF patients.

IV. RESULTS AND DISCUSSION

Descriptive Statistics Analysis

The following is the result of descriptive statistical analysis on the characteristics of DHF patients during undergoing inpatient at Jember Clinic Hospital as many as 100 patients.

a. Survival Time, Age, Hemoglobin, Platelets and Hematocrit

Descriptive statistical analysis of DHF patients in RSP Jember Clinic for survival time, age, hemoglobin, platelets and hematocrit are presented in Table 4.1. Especially for hemoglobin, thrombocyte and hematocrit are divided into two, namely at the time of admission and during the last medical record of each DHF patient.

Table 4.1 Descriptive Statistics Analysis Time Survival, Age, Hemoglobin, Platelets and Hematocrit

Variabel	Min	Max	Mean	Normal			
Survival Time	1	9	3,093				
Age	1	59	19,13				
	Saat Awal Masuk Rawat Inap			Saat Rekam Medis Terakhir			
	Min	Max	Mean	Min	Max	Mean	
Hemoglobin	10,40	18,10	13,55	9,80	17,30	12,94	Male (14 – 18 gr/dL) Female (12 – 16 gr/dL) Children (10 – 16 gr/dL)
Trombosit	8.000	363.000	103.750	19.000	325.000	131.520	150.000 – 400.000 sel/mm ³
Hematokrit	31,00	53,30	41,02	31,00	52,40	39,28	3 times Hemoglobin

Table 4.1 provides information that the average length of hospital stay (survival time) is 3 days with the shortest hospitalization is 1 day and the longest is 9 days. While the patient age is 19 years on average, the youngest patient is one year old and the oldest is 59 years (patients aged 0 - 12 months are assumed to be 1 year old). DHF patients declared cured is indicated by the results of a medical examination under normal circumstances. Medical examination in question includes the examination of hemoglobin levels, platelets and hematocrit.

At baseline admission to hospitalization, the average hemoglobin of patients tended to be normal at 13.55 g/dL. But not all patients have normal hemoglobin levels. The lowest hemoglobin level was 10.40 g/dL and the highest hemoglobin level was 18.10 g/dL. While for platelets, the average platelet count of patients below normal is 103.750/mm³ (normal platelets 150,000 - 400,000/mm³). At baseline admission the lowest platelet count is 8,000 / mm³ and the highest platelet level is 363.000/mm³. As for hematocrit, hematocrit level is said to be normal if the percentage is 3 times the hemoglobin level or according to Kusriastuti (2011), the normal percentage of hematocrit for children 33-38%, adult male 40-48% and adult female 37-43%. From Table

4.1 the mean percentage of hematocrit level of DHF patients is 41.02%, it shows that the mean hematocrit level of DHF patients is normal, although not all patients have normal hematocrit level. At the beginning of admission hospitalization hematocrit lowest level 31.00% and highest 53.30%.

Table 4.1 also provides information on hemoglobin levels, platelets and hematocrit of DHF patients when the last medical record. At the time of the last medical record, the average patient's hemoglobin was lower when compared to the initial admission to hospitalization, which was 12.94 gr/dL, but still relatively normal. As for platelets, the average patient had elevated platelet levels when compared to early entry. According to Kusriastuti (2011), new patients can be discharged one of the conditions is if the platelet count is greater than 50.000/mm³. From Table 4.1, the average platelet

count of DHF patients was 131.520/mm³, so the average patient's platelet level was normal. As for hematocrit, the average hematocrit level of patients is normal that is 39.28%. Thus, from Table 4.1 it can be seen that during the last medical record, hemoglobin, tomocyte and hematocrit levels of DHF patients were normal.

Gender

b. Data of in-patient DHF in Jember Clinic Hospital from September to December of 2016 were 100 patients, obtained from medical record of Jember Clinic Hospital, consist of 58 male patients and 42 female patients.

Kaplan Meier Analysis and Log-Rank Test

The characteristics of survival time of DHF patients at Jember Clinic Hospital during inpatient care can be shown with Kaplan Meier's survival curve. Kaplan Meier's survival curve is a curve describing the probability of surviving DHF patients. In this study, the event studied was the recovery of dengue patients (patients had clinical improvement). Thus the Kaplan Meier curve explains the probability of the patient not recovering (not undergoing clinical improvement). Based on the duration of hospitalization of DHF patients obtained from medical record data of Jember Clinic Hospital, Kaplan Meier survival curve was obtained as in Figure 4.1.

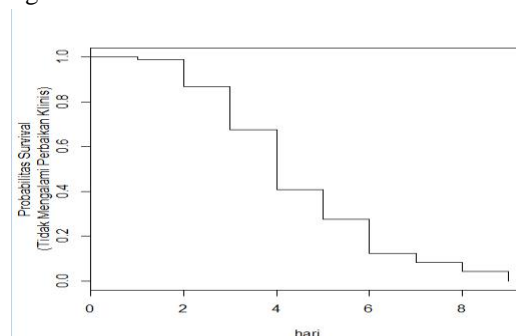


Fig.4.1: Kaplan Meier Survival Curve Based Survival Time

Figure 4.1 informs visually that the longer DHF patients undergo inpatient (t), the probability of a DHF patient not recovering (not undergoing clinical improvement) until the time t is less close to zero, meaning the longer the patient is hospitalized (the longer Get medical treatment) then the greater the probability of patients to recover (clinical improvement). Description of probability of healing DHF patients can be see in Table 4.2.

Table.4.2: Probability of DHF Patients

time	n.risk	n.even	survival	std.err	lower	upper
t						
1	100	1	0,9900	0,00995	0,9707	1,0000
2	98	12	0,8688	0,03392	0,8048	0,938
3	85	19	0,6746	0,04728	0,5880	0,774

4	66	26	0,4088	0,04967	0,3222	0,519
5	40	13	0,2760	0,04517	0,2002	0,380
6	27	15	0,1227	0,03316	0,0722	0,208
7	12	4	0,0818	0,02770	0,0421	0,159
8	8	4	0,0409	0,02002	0,0157	0,107
9	4	4	0,0000	NaN	NA	NA

trombosit	0,0000	3,524	0,0004
hematokrit	0,0444	0,935	0,3496

Table 4.4 The value of Akaike's Information Criterion (AIC)

Variabel	AI
All Independent Variable	882,1166
Age, Gender and Hematokrit	891,0849
Gender, Trombosit and Hematokrit	888,4697
Age, Hemoglobin and Trombosit	878,9539
Age and Trombosit	877,0109

In Table 4.2, time indicates days, n.risk indicates the number of patients diagnosed with DHF, n.event shows the number of dengue fever patients and survival indicates the probability of patients not recovering. Further explained about the characteristics of DHF patients in Jember Klinik Hospital based on sex which is suspected to affect Kaplan Meier survival curve, as in Figure 4.2.

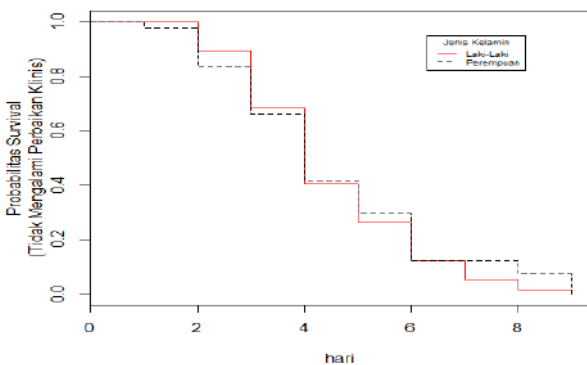


Fig.4.2: Kaplan Meier Survival Curve By Gender

Figure 4.2 shows a dotted line (black) more dominating above a straight line (red) indicating that the probability of not recovering female patients is greater than that of male patients, meaning that the survival time of the male gender is better than patients with female gender.

The next step is to do a log-rank test to find out the differences between the survival probability curves in Figure 4.2. From the log-rank test results obtained p-value value of 0,604. When compared with chi-square of 0.3 with degrees of freedom 1, it shows that the probability of survival of DBD patients of either male or female sex does not differ significant.

Factors Affecting the Healing Rate of DHF Patients

To know what factors influence the rate of healing of DHF patients, then modeling between response variables (survival time) and predictor variables used. Modeling with all predictor variables is shown in Table 4.3.

Table.4.3: Parameter Significance Test

Variabel	Parameter Estimates	z	P-value
age	0,0256	3,088	0,0020
gender	0,0548	0,232	0,8164
hemoglobin	0,1328	0,874	0,3819

Table 4.4 shows that the smallest AIC value is 877,0109 when doing cox proportional hazard regression without gender, hemoglobin and hematocrit variables. So the best model is obtained by doing regression cox proportional hazard using age and trombosit variables. Estimation of the parameters for each variable based on the best model can be seen in Table 4.5.

Table 4.5 Estimation of Cox Regression Parameters in the Best Model

Variabel	Parameter Estimates	z	P-value
age	0,025650	3,546000	0,00039
trombos	0,0000054	3,648000	0,00026
it			40

So, the best model can be written as follows:

$$\begin{aligned} \hat{h}(t) &= \exp(\beta'x) \\ &= \exp(-0,02565 \text{ age} \\ &\quad + 0,0000054 \text{ trombosit}) \\ &= \exp(-0,02565X_1 + 0,0000054 X_4) \end{aligned}$$

V. CONCLUSION

Descriptive statistical analysis showed that from 100 DHF patients admitted to RSP Jember Klinik, the average clinical condition improved within 3 days, with 53 patients belonging to productive age group (15- 59 years) and 58 male sexually transmitted Men. At the time of admission was 83 patients whose platelet count was below normal (less than 150,000 / mm3). While during the last medical record there was a decrease in the number of patients with under-normal platelets to 64 patients. The mean hemoglobin and thrombocyte levels of DHF patients at baseline were 13.55 g / dL and 41.02% respectively, while during the last medical record the mean hemoglobin and platelet counts were 12.94 grams / DL and 39.28%. While the factors that significantly influence the rate of improvement of clinical condition of DHF patients are age and platelets.

Suggestions that can be given from the results of this study, for the medical team is expected to control the factors that affect the rate of improvement of the clinical condition of DHF patients. While for further research, it is suggested to add factors that theoretically can influence the rate of improvement of clinical condition of DHF patients and can develop survival analysis in other fields, such as in industry or education.

REFERENCES

- [1] Collett, D. (2003). *Modelling Survival Data in Medical Research*. 2nd edision . Chapman and Hall/CRC, London.
- [2] Darmowandowo, W. (2006). *Continuing Education*. Divisi Tropik & Infeksi Bagian Ilmu Kesehatan Anak FK Unair RSUD Dr. Soetomo, Surabaya.
- [3] Gandasoebrata, R. (2009). *Penuntun Laboratorium Klinik*. Dian Rakyat, Jakarta.
- [4] Kleinbaum, D.G. & Klein, M. (2012). *Survival Analysis: A Self-Learning Text*. Springer, London.
- [5] Kusriastuti, R. (2011). *Modul Pengendalian Demam Berdarah Dengue*. Kementerian Kesehatan RI, Jakarta.
- [6] Le, C.T. (1997). *Applied Survival Analysis*. John Wiley and Sons Inc, New York.
- [7] Lee, E.T. & Wang, J.W. (2003). *Statistical Methods for Survival Data Analysis*. 3rd edision. John Wiley and Sons Inc, Canada.
- [8] Mufidah, A.S. (2016). Analisis Survival Pada Pasien Demam Berdarah *Dengue* (DBD) di RSUD Haji Surabaya Menggunakan Model Regresi Weibull. *Jurnal Sains dan Seni ITS*, 5(2), p. 2337-3520.
- [9] Nisa', S.F. (2012). Analisis Survival Dengan Pendekatan Multivariate Adaptive Regression Splines Pada Kasus Demam Berdarah *Dengue* (DBD). *Jurnal Sains dan Seni ITS*, 1(1), p.318-323.
- [10] Sari, N. (2011). Aplikasi Regresi Cox Propotional Hazard Pada Analisis Kesintasan Dan Identifikasi Faktor Resiko. *Skripsi*. Departemen Matematika Fakultas Matematika dan Ilmu Pengetahuan Alam Universitas Sumatra Utara, Medan.
- [11] Omurlu, I.K., Ture, M. & Tokatli, F. (2009). The Comparisons of Random Survival Forest and Cox Regression analysis with Simulation and an Application Related to Breast Cancer. *Journal International of Expert Systems with Applications*, 36, p. 8582-8588.
- [12] WHO. (2009). *Dengue, Guidelines For Diagnosis, Treatment, Prevention, and Control*. Special Programme for Research and Training in Tropical Disease (TDR), France.

An Efficient Energy Savings Schemes using Adjacent Lossless Entropy Compression for WSN

Cisil Baby¹, Dr .H. N. Suresh³

¹ Research scholar, Dept. of ECE, Jain University, Bangalore, Karnataka, India.

² Professor & Research coordinator, Bangalore Institute of Technology, Dept. of IT, VV puram, Bangalore, India

Abstract—The proposed work aims at designing routing method and data compression algorithm for WSN's. An ad-hoc network (WANET) is considered and based on certain criteria the data is forwarded dynamically. Various parameters such as Compression Ratio, Packet Delivery Rate, Energy consumption are considered to determine the efficiency of the network. One of the primary parameters to be considered in the configuration of Wireless Sensor Networks (WSN) is the energy consumption of the nodes and the data throughput. Since the nodes are controlled by batteries with lower energy limit, it is required to minimize the energy utilization. Henceforth a proficient routing technique in light of LEACH protocol is proposed alongside the utilization of A-LEC data compression strategy. The simulations are carried out through Network Simulator 2 (NS2). The compression code is written in GNU-C

Keywords— Multi-hop routing, LEACH, LEC compression, Energy consumption., network lifetime,

I. INTRODUCTION

Due to the inception of nano technology and MEMS [1] (Micro electro Mechanical systems), WSN's have been realized to create network with actuators and sensors. Similarly, technological emergence in communication hardware, low power VLSI design and embedded computing are combinely helpful towards making the innovation show up as a reality, the combination of computing and communications has the capability to create revolution everywhere. It incorporates financial aspects, ecological checking, mining, meteorology seismic observing, acoustic discovery, medicinal services applications, process observing, foundation assurance, setting mindful figuring, undersea route, brilliant spaces, stock following and strategic military reconnaissance.

The adequacy of the WSNs lie in their detecting quality, adaptability, vitality utilization, versatility, system lifetime, versatility, scope, and so on they can offer. WSNs normally turn into the principal decision with

regards to organization in remote and dangerous environment.

A definitive objective of such WSNs sent in the above scenarios is to send the detected information from sensors to sink followed by further examination at the sink. The performance of such WSN's depends on the way data is collected, the sensor topology, amount of data travelling in the network and so on. To achieve good performance, many network topologies and their routing protocols have been proposed for information gathering. Administration of topology plays an important role in diminishing various limitations like failure of node and communication, crisis of computational resource, less energy, traffic, delay and so on.

The type of routing path – unicast or broadcast, the size of data packets, overhead are determined by the topology. The performance, lifetime, network coverage and the Quality of Service of the network depend directly on the topology. Hence it is important to choose the right topology to enhance the network parameters. Energy consumption is one of the significant parameters which has a significant role in performance of WSN. The energy consumption depends upon the distance between the sensor nodes. The power consumption is proportional to the distance to be transmitted between the nodes

II. LITERATURE SURVEY

Few of the existing methodologies are overviewed in this section. The focus is more on lossless data compression algorithms: C M Salder and M. Martonosi [1] have proposed a low complex data compression algorithm for WSN's that lack resources. It is a modified form of the Lempel-Ziv-Welch algorithm. In this paper, the Sensor LZW is modified and the better energy saving is obtained by using different amounts of compression. The data sets from several real world data are used and Oreduction in energy consumption upto 4.5 x is obtained.

F. Marcelonni and M. Vechio [2] have proposed a lossless compression algorithm comprising of predictive coding in which encoder and predictor are used. The aim

is to reduce the computational and storage resources. Huffman coding is used to code the residues obtained from the predictor. The compression algorithm is implemented and simulated on Avrora and environmental dataset is used as input. A compression ratio of 27.25% is obtained for Temperature data and a ratio of 42.57% is obtained for relative humidity. Though compression is performed here the energy consumption is not analyzed. The comparison of compression ratio is performed w.r.t gzip and bzip2 and is found to outperform both the methods. It is also noted that the algorithm is not effective when the correlation of data changes since it does not adapt to changing data.

J Tehola [3] developed an algorithm for lossless compression based on Golomb Coding. The basic form of Golomb Code consists of prefix code and rail code separated by a separator bit which is usually a zero bit. This is applicable for coding run-length sequences which mainly consists of clusters of either 0's or 1's. For example if the original binary code consists of clusters of zero's, the prefix code is the group of 1's representing the clusters in k th powers of 2 of zeros (Sub-Clusters). The construction of Golomb Code is modified by representing the sub clusters of zero's by grouping them in exponentially increasing order of k th powers of 2. By doing so the size of prefix code decreases. Large compression ratios of upto 64.99% were obtained by choosing an optimal k .

H. Nakayama and N. Ansari [4] proposed a movable sensor node around the area of sensing which essentially collects data from the nodes, and the energy is balanced effectively. Due to the advancement in MEMS, complicated sensors are available and as a result mobile nodes and sinks are conceivable. The proposed method here uses several mobile sinks to gather data. The data gathering method is faster and hence the data would be collected in a real time manner. By using mobile nodes along with hierarchical routing the paper demonstrates conserving energy as efficiently as possible. The disadvantage is the non-possibility of deploying mobile nodes and sinks in various areas.

J Al-Karaki and Ahmed E. Kamal [5] have made a survey on routing techniques in WSN. The routing methods surveyed are categorized into flat, hierarchical and location-based based on the structure. The protocols are classified as: multipath based, query-based, negotiation-based and QoS based. All the above structures have the same purpose of increasing the network lifetime without affecting the delivery of data.

C K Toh [6,7] wrote a paper on Maximum Battery life routing for Wireless Ad hoc networks. During simulation here, five different routes selection methods are analyzed

: Minimum transmission power, Minimum battery cost, Min-Max battery cost, Conditional Max-Min battery cost and Stability of Association. Among these, the Conditional Max-Min Battery Cost was found to be most effective assuming the transmission power of each node is equal in all the cases. The proposed algorithm here is conditional max-min battery capacity routing which selects a shorter path if the nodes in all routes possess enough battery capacity. A threshold γ is set. If the node energy falls below it, every route going through the node is avoided.

W. Heinzelman and A. Chandrakasan [8,9] have analyzed Low energy adaptive clustering hierarchy, a protocol for Wireless Micro Sensor Networks. Here, a protocol architecture consisting of efficient energy cluster method routing along with data aggregation is used. The results of using LEACH shows that the network lifespan can be increased by an order of magnitude in comparison with general multi-hop techniques. In addition the method here shows a reduction in energy dissipation and latency [10,11,12].

III. PROPOSED PROTOCOL METHODOLOGY

We proposed a method to minimize the energy utilization of the nodes including effective routing with data compression. Filter calculation is utilized to course the data and A-LEC technique is utilized to pack the data got by the nodes.

Lossless Entropy compression encodes the residue/difference sequence using modified Golomb code. The residues $r_i = (i = 1, 2, 3, \dots, N)$, where N is the size of data block) of LEC are assumed to be uncorrelated to each other. Therefore they are coded independently. LEC performs well if the differential predictor captures the temporal correlation roughly, based on residue independence. Otherwise it would perform badly in cases where the residue sequence is dependent and correlated. By considering that the residue sequence is correlated, it is possible to devise a modified form of LEC known as A-LEC (Adjacent LEC) which can exploit the correlation better and yield a higher compression ratio.

3.1 LEC Overview:

The residue sequence of integers produced by the differential predictor is packed into groups which increase exponentially in size. Codeword of LEC mainly consists of two parts:

- 1) Entropy Code indicating the group
- 2) Index in the group indicating the position of the residue in the group

Subsequent groups in the table differ by 1 bit in the entropy code. The size of each group increases

exponentially with n. Hence the group size is equal to 2n. Therefore by having a common code entropy code for a large number of group entries, the code word reduces substantially, since it is seen that that the residues normally won't exceed the 8th group.

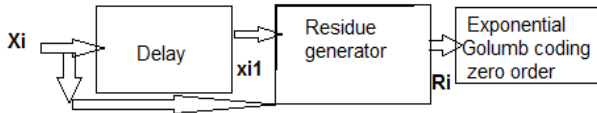


Fig.1: Block diagram for LEC Compression:

Above Figure explains the working principle of LEC Compression. Based on the modified method of exponential Golomb Coding, the integer residues xi's obtained from the residue generator is divided into two groups whose size increase exponentially. Referring to table 1, for residue Ri not equal to zero, Ri coded as hi|ai, where hi represents the code for the group to which the residue belongs to and ai represents the index or the position of the residue in the group to which it belongs to. The table consists of sixteen groups. For if the obtained residue is say +9, the group it belongs to is (+8, ... ± 15) where hi = 101 and its position in the group (+8,-8,+9,-9 · · · ± 15) is 3 whose binary representation is 011. Therefore ai = 011. The representation of +9 would be a concatenation of hi and ai which is 011101. Similarly other residues are coded. If residue is 0, ai is omitted.

Table.1: LEC Coding

n	h(n)	g(n)
0	00	0
1	010	-1,+1
2	011	-2,+2,-3,+3
3	100	-4,+4,-5,+5
4	101	-6,+6,-7,+7
5	110	-8,+8,-9,+9
6	1110	-10,+10,-11,+11
7	11110	-12,+12,-13,+13
8	111110	-14,+14,-15,+15
9	1111110	-16,+16,-17,+17
10	11111110	-18,+18,-19,+19
11	111111110	-20,+20,-21,+21
12	1111111110	-22,+22,-23,+23
13	11111111110	-24,+24,-25,+25
14	111111111110	-26,+26,-27,+27
15	1111111111110	-28,+28,-29,+29

3.2 A-LEC Method :

Adjacent LEC is a modified form of LEC devised for robustness. The context information among the residues is exploited by the algorithm. A-LEC uses an extra codeword si into the main codeword. Si acts as a set of status bits which specify one among the four conditions as shown in table 2. The concept here is that while coding the present residue the contextual information of the previous residue is considered.

Table.2: A LEC coding table

Si	Context Data	Codeword for h(n _i)	Group
00	n _i = n _{i-1}	No codeword for h	Same
01	n _i = (n _{i-1}) - 1	No codeword for h	Neighbor above
10	n _i = (n _{i-1}) + 1	No codeword for h	Neighbor Below
11	Otherwise	h(n _i)	Otherwise

- For Si = 00, the present residue is same as the previous residue and the code word for h in the present residue is omitted.
- For Si = 01, the present residue belongs to the group just above the group of previous residue. Here again, the code word for hi is omitted.
- For Si = 10, the present residue belongs to the group just below the group of previous residue .Again, the code word for hi is omitted.
- For Si = 11, the present residue belongs to a non-neighbor different group. Here the code word for hi should exist in the main code word.

The number of nodes in the area comprising the hotspots is less when compared to other area in the network. Therefore the volume of data generated by the hotspot area is small in comparison with the amount of data flowing into the hotspot area. This suggests that majority of the power consumption in the hotpot area is by forwarding the data coming from outside the hotspot. To decrease the energy consumed in the hotspot, the volume of data sent to the hotspot must be decreased. The energy required to transmit the data is proportional to the amount of data to be transferred. Data compression can reduce the amount of data. Since in general the environmental data collected by the sensors (temperature, humidity, and atmospheric pressure) is correlated, it can be compressed. The extent of compression or the compression ratio depends on the amount of correlation in the data. The proposed scheme here utilizes hierarchical routing outside the hotspot and flat multi-hop routing inside the hotspot area. Hierarchical routing makes sure data is The performance of the network is studied under 4 scenarios and comparisons are made.

- 1) CC-BTS transmission without compression
- 2) CC-BTS transmission with compression
- 3) CC-CC transmission without compression
- 4) CC-CC transmission with compression

The simulations are conducted in NS2 and the following graphs for the residual energy was obtained. Compressed before sending it to the hotspot and flat multi-hop routing optimizes the distance metric in the hotspot area.

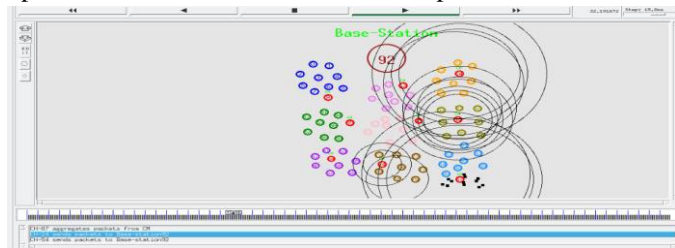


Fig.2: CC 24 and CC 54 sends data packets to the sink

As shown in fig 2. above, CC 24 and CC 54 send data packets to the sink. The data is compressed using A-LEC method (Adjacent Lossless Energy Compression). In LEC, the data collected by the nodes is given to a difference computation block whose output is a sequence of residues r_i ($i=1,2, \dots, M$). The residue sequence is encoded by the entropy encoder and are considered to have no correlation amongst each other and hence are coded independently. The central idea here is to formulate a coding method that would exploit the temporal correlation in the residue sequence and thereby resulting in higher compression ratio.

IV. RESULTS AND PERFORMANCE EVALUATION

The environmental monitoring real world data sets from Sensor-Scope [7] are used. The comparison of LEC and S-LZW is made for temperature and relative humidity measurements. Le-Genepi and stbernanrd from Sensor Scope deployments are tested. The size of the data sets range from 31253 to 71536 samples. The temperature and humidity readings are connected to an ADC. The outputs of ADC for the raw relative humidity and raw temperature are represented with resolutions of 14 and 12 bits. These raw outputs are then converted [8] to physical measures expressed as t and h as shown by the code below. The t and h values are then used as inputs for A-LEC Compression.



Fig.3: Throughput of CC-BTS Topology without compression

Fig 3 is a plot of data throughput versus the round number..

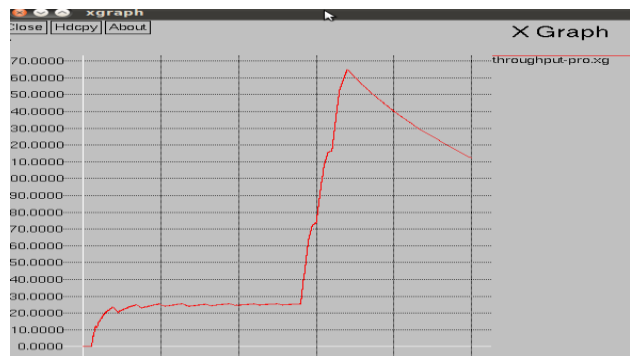


Fig.4: Throughput of CC-BTS with Compression

The data throughput as shown in Fig 4, has increased since throughput depends on the packet loss and the packet loss substantially reduces when lossless compression is used.



Fig.5: Throughput of CC-CC without compression

Fig 5 is a plot of node number against the residual energy in the respective node at the end of 100 rounds. The data packets move from the cluster head of one to another and finally to the sink in a multi-hop fashion. Since the transmission distance of each cluster head is less, the energy consumed for transmission is also less, thereby the residual energy is more as seen from the graph and the network lifespan is also more. The throughput is seen to be higher in this case.

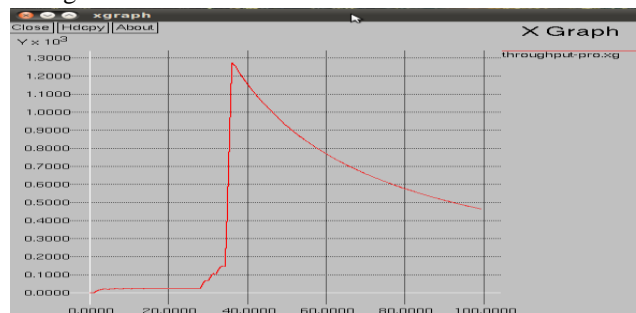


Fig.6: Throughput for CC-CC with Compression

Fig 6 is plot of node number versus the residual energy the corresponding node the end of 100 rounds. Initially

the energy of the nodes was 100 Joules. After several rounds of operation the final energy possessed was found to be more in CC-CC transmission with the use of A-LEC data compression. The number of negative peaks is lesser, indicating that the energy is distributed equally among the nodes. The compression performance was evaluated by compression ratio as follows: $R = 1 - (z/z')$ where z and z' denote the original raw data size and compressed data size in bits respectively. The throughput obtained is also seen to be the maximum.

V. CONCLUSION

The routing of data in the networks is performed using hierarchical multi-hop method. Simulations are conducted in NS2 in different scenarios and the one with Hierarchical Multi-hop routing is found to be most efficient. A-LEC compression method is adopted and is compared with S-LZW and LEC compression methods. The A-LEC shows a higher degree of ruggedness and hence it is adaptive to changes in the data pattern. Four Scenarios related to routing are compared and the energy utilization is also compared. It shows that CC-CC with data compression is most effective since it consumes least amount of energy. The data sets are collected from sensor scope and compression ratio is computed for the prescribed algorithm for different types of data. Since different types of data have different temporal correlations, the prescribed algorithm effectively utilizes the temporal correlations and adapts better to different kinds of data

REFERENCES

- [1] M. Sadler and M. Martonosi, "Data compression algorithms for energy-constrained devices in delay tolerant networks," in *Proc. 2006 International Conference on Embedded Networked Sensor Systems*, pp. 265–278.
- [2] F. Marcelloni and M. Vecchio, "A simple algorithm for data compression in wireless sensor networks," *IEEE Commun. Lett.*, vol. 12, no. 6, pp. 411–413, 2008.
- [3] J. Teuhola, "A compression method for clustered bit-vectors," *Inf. Process. Lett.*, vol. 7, no. 6, pp. 308–311, 1978.
- [4] H. Nakayama, N. Ansari, A. Jamalipour, Y. Nemoto, N. Kato, On data gathering and security in wireless sensor networks, in: Sarnoff Symposium, IEEE, 2007, pp. 1–7 (30 2007-May 2).
- [5] J. Al-Karaki, A. Kamal, Routing techniques in wireless sensor networks: a survey, *IEEE Wireless Communications* 11 (6) (2004) 6–28.
- [6] C.-K. Toh, Maximum battery life routing to support ubiquitous mobile computing in wireless ad hoc networks, *IEEE Communications Magazine* 39
- [7] W. Heinzelman, A. Chandrakasan, H. Balakrishnan, An application-specific protocol architecture for wireless microsensor networks, *IEEE Transactions on Wireless Communications* 1 (4) (2002) 660–670.
- [8] T A Welsch "High Performance Data compression", *computer* Vol 17
- [9] P Elias "Predictive coding" *IRE Transf. Information Theory* Vol 7 [10] Shivashankar and Varaprasad. G, Implementing a New Power Aware Routing Algorithm Based on Existing DSR Protocol for MANETs, *International Journal of Communication Networks and Distributed Systems*, Vol. 10, Issue 2, 2012,
- [10] Karthikeyan. N, Palanisamy V, Duraiswamy. K, A Performance Evaluation Of Proactive And Reactive Protocols Using ns-2 Simulation, *International Journal of Engineering Research & Industrial Applications*, Vol.2, No.11, pp 309-326, 2009.
- [11] Mohd Izuan Mohd Saad Performance Analysis of Random-Based Mobility Models in MANET Routing Protocol, *European Journal of Scientific Research*, Vol.32, No.4, pp.444-454, 2009.

Reactive Power Control in Power System using Modified UPFC

Engr. M. Bilal¹, Engr. Dr. Ejaz Hassan², Engr. Hamza Zafar³

^{1,2}Department of Electrical Engineering, University of Engineering and Technology Taxila,(APCOMS Campus), Pakistan

³ Department of Electrical Engineering, University of Engineering and Technology Taxila, Pakistan

Abstract—The power system is an exceptionally nonlinear system that works in an always showing signs of change condition, loads, generator yields, topology and key working parameters changes consistently. The stability of the system depends on the nature of the disturbance as well as the initial operating condition. The power congestion known as the limitations to how much power can be transferred across a transmission interfaces and further that there is an incentive to actually desire to transfer more power. The old approach was to correct congestion lies in reinforcing the system with additional transmission capacity. Although easy to perform, this approach is complex, time consuming and costly. It is ending up noticeably progressively hard to get the licenses to building new transmission passages, or even grow existing ones. This issue can be solved by introducing Facts devices in the transmission system. Facts Devices play an imperative part in controlling the reactive and active power flow to the power network and thus both the system voltage variances and transient stability. Among Facts device Unified Power Flow Controller (UPFC) is the most versatile and complex power electronic equipment which can increase reliability and can serve as an alternative to new investments in overhead lines, which are difficult due to a lack of public support. The proposed work is based on control of reactive power in power system utilizing modified Unified Power Flow Controller (UPFC). The impact of customary UPFC and modified UPFC on the power flow of transmission lines were analyzed.

Keywords— Flexible AC Transmission System (FACTS), Modified DC Link Capacitor, Matlab Simulink. Power System, Reactive Power, Unified Power Flow Controller (UPFC).

I. INTRODUCTION

In this world of ever expanding consumers the design of a particular device is to be done with utmost care. It is well known that with the help of present overhead (OH) transmission line it will become impossible to laying a new transmission line for increase in consumers to supply them their electric needs. So to supply the electric need of every consumer after 10-20 years we have done to lay a

new transmission line as these so called FACTS devices are available in the market.

Unified power flow Controller (UPFC) is the most versatile converters among the Flexible AC Transmission System (FACTS) devices [1-5]. It comprises of two voltage source converters (VSC), one is connected with parallel with transmission line to insert a reactive power in the transmission line and other is connected with series with the transmission line to insert active power in the transmission line, by this way this converter will compensate the reactive power and active power all together or independently [6]. The UPFC is a combination of static synchronous compensator and static synchronous series compensator which are connected via a common DC link, as shown in fig.1 to allow bi-directional flow of real power between series output terminals of SSSC and the shunt terminals of the STATCOM, and is allowed to provide concurrent real and reactive power compensation. These two devices are two voltage source inverters (VSI), operated from a common DC link provided by a DC storage capacitor.

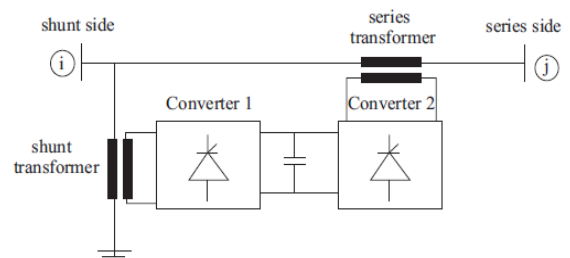


Fig. 1: Schematic Diagram of Conventional UPFC

Ratings of this DC link capacitor bank may have a significant impact on the cost and physical size of the UPFC. The capacitor is sized for a specified ripple voltage, typically 10% of the nominal voltage. The main drawback with this DC link capacitor is its design for maintaining the desired ripple [7]. Also this capacitor has shorter life when compared to AC capacitor of same rating. This limits the life and reliability of the voltage source inverter [8].

II. THE PROPOSED SCHEME OF UPFC

An effort has been taken to remove the DC link capacitor in the UPFC without affecting its performances. The DC link of conventional UPFC has been modified with lengthened the DC link as in field and one extra transmission line need to be lay. Finally the combined responses are compared for simplicity. Various observations are made only on a single phase Unified Power Flow Controller (UPFC). As the exchange of active and reactive power is taking place in between the shunt and series part, the location of series and shunt part is of most important. The power system stability, efficiency and disturbance problems in power system are undefined in the grid. To enhance the power system strength efficiency, the shunt portion of Unified Power Flow Controller UPFC ought to be situated in the place from where it can diminish the impact of voltage changes and the series part ought to be situated in where its parameter changes impact the variation of active and reactive power the most [9,10,11]. Ignoring the cost involved in laying one extra line, this approach can be used to improve the system stability condition using UPFC with lengthening DC link, and where we can install the UPFC in our required location as shown in fig.2 and fig.3.

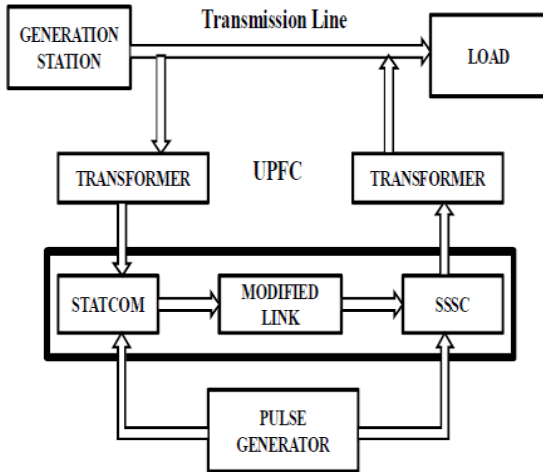


Fig. 2: Block Diagram of Modified UPFC

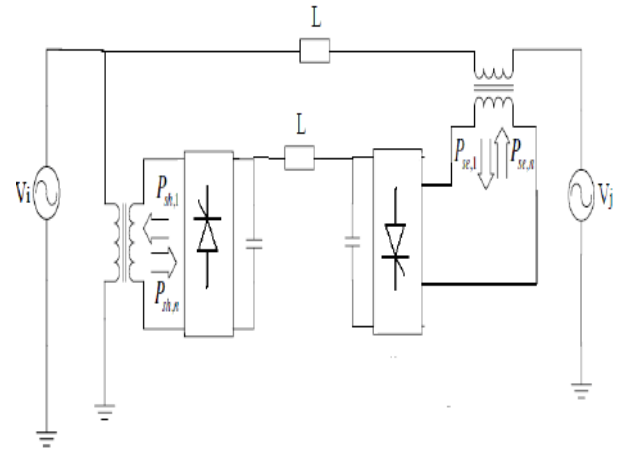


Fig. 3: Schematic Diagram of proposed UPFC

III. SIMULINK MODEL OF 22KV TRANSMISSION LINE

Experiments carried out for 22kv transmission line system for three different cases.

- a. Without UPFC
- b. Conventional UPFC
- c. Modified UPFC.

3.1 Without UPFC

In this model of transmission line, there is a 22 kV voltage source is feeding to an RL load. For measurement of current a current measurement block named CT is connected in the circuit, whose output can be taken from the scope 'current' connected to this block. A block for voltage measurement named V is connected across the load. The output of this voltage measurement block is fed to the scope named voltage for voltage waveform. Further a block for power measurement is connected the circuit to calculate the power consumed by the load. This power measurement block is further connected to the demux, for obtaining the power in terms of real and reactive power. The power outputs of this demux can be obtained from the two scopes connected to it. All the blocks used in this transmission line model are taken from the SimPower System toolbox of Matlab Simulink.

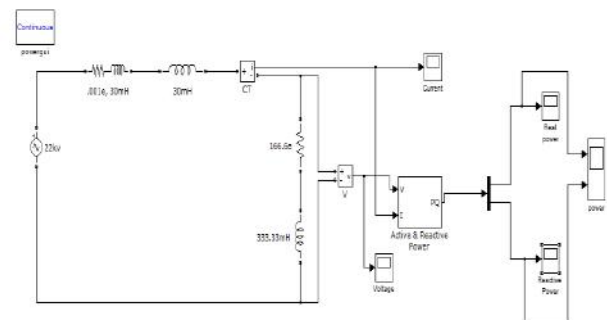


Fig. 4: Simulink Model of 22 k V Transmission Line without UPFC

3.2 With Conventional UPFC

The following model in fig 5 shows the Simulink model of 22kv transmission line when conventional UPFC is incorporated in system. The conventional UPFC consists of two voltage source inverter with common DC link capacitor.

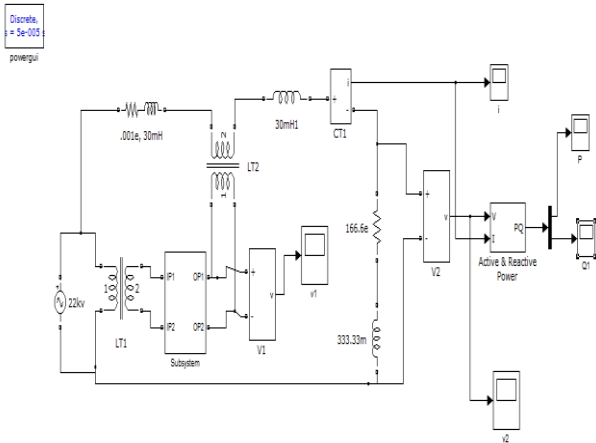


Fig. 5: Simulink Model of 22 k V Transmission Line with conventional UPFC

3.3 With Modified UPFC

The following model in fig 6 shows the Simulink model of 22kv transmission line when modified UPFC is incorporated in system.

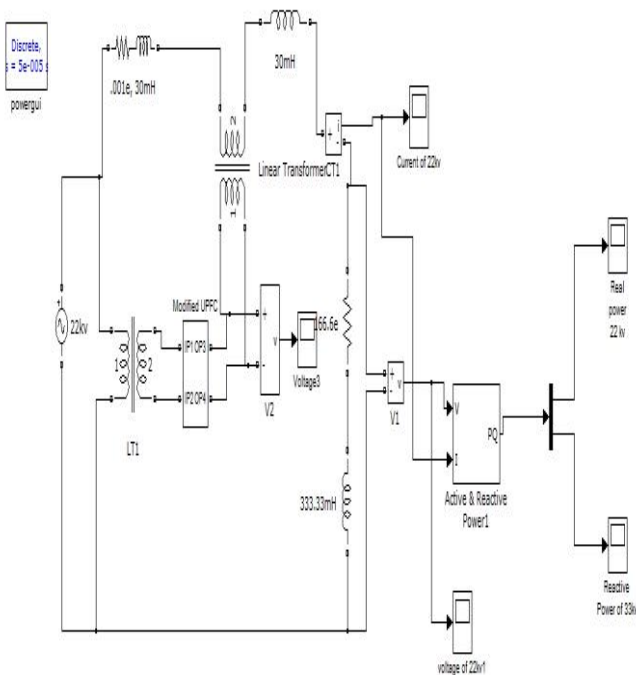


Fig. 6: Simulink Model of 22 k V Transmission Line with modified UPFC

IV. SIMULATION RESULT

4.1 Without UPFC

The following fig. shows the reactive power waveform of 22kV transmission line without UPFC (Simulink model of 22kV transmission line is developed in fig.4). At the steady state time $t=0.02$ sec the Reactive Power is 0.62 MVar.

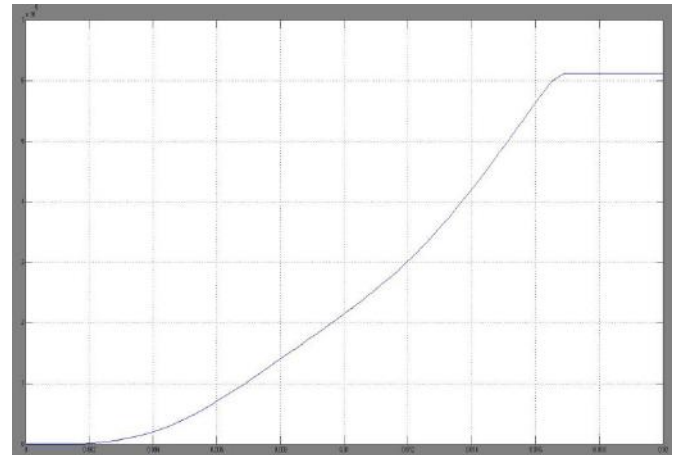


Fig. 7: Reactive Power waveform of 22kV line without UPFC

4.2 With Conventional UPFC

The following fig. shows the reactive power waveform of 22kV transmission line with conventional UPFC (Simulink model of 22kV transmission line is developed in fig. 5). At the steady state time $t=0.02$ sec the Reactive Power is 0.70 MVar.

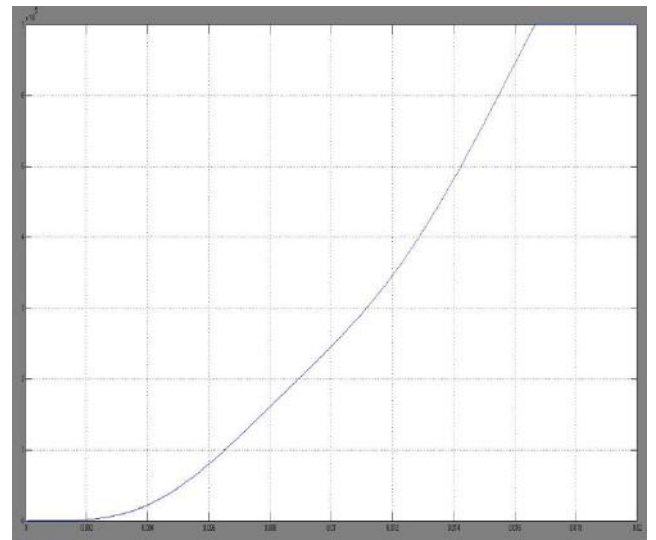


Fig. 8: Reactive Power waveform of 22kV line with conventional UPFC

4.3 With Modified UPFC

The following fig. shows the reactive power waveform of 22kV transmission line with modified UPFC (Simulink model of 22kV transmission line is developed in fig.6).

At the steady state time $t=0.02$ sec the Reactive Power is 0.69 MVar.

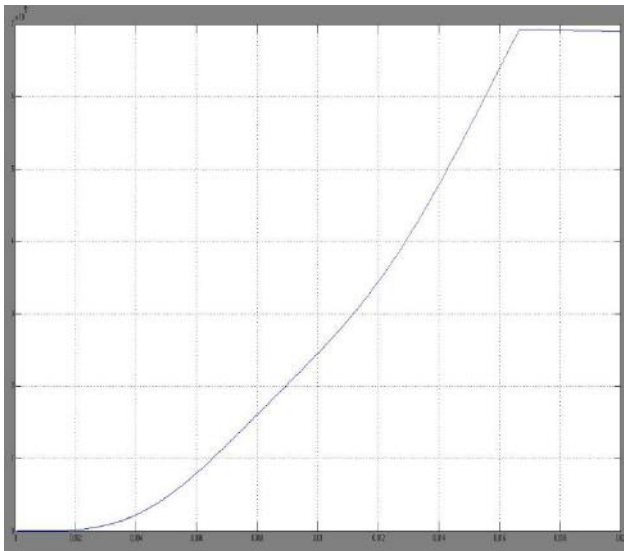


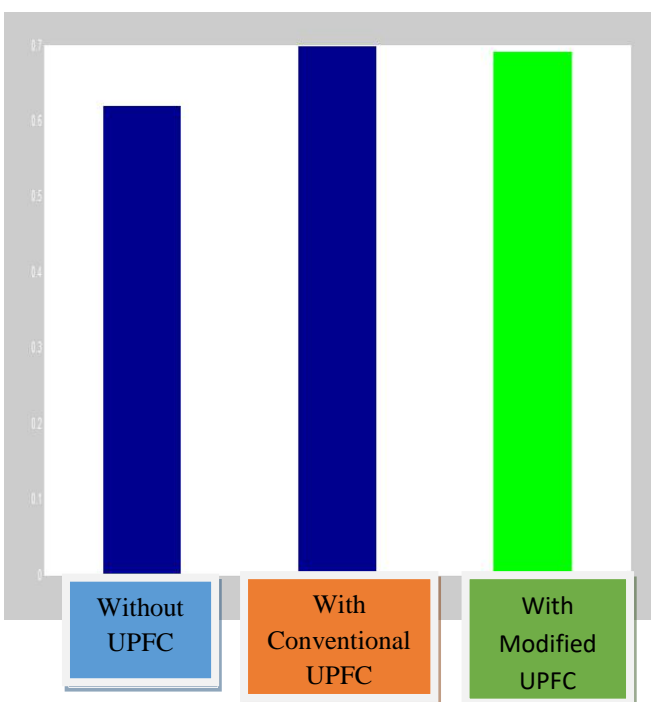
Fig. 9: Reactive Power waveform of 22kV line with modified UPFC

4.4 Comparison of Result

The summary of above results for 22KV line is given below in table.

Parameters	Without UPFC	With Conventional UPFC	With Modified UPFC
Reactive Power	0.62 MW	0.70 MW	0.69 MW

The summary of above results for 22KV line is given below using bar chart.



V. CONCLUSION

This work presents a single phase new UPFC concept of transmitting power with modified DC link between series and shunt part of UPFC, which gives more flexibility of UPFC installation. The active power exchange between shunt and series is transmitted through a single DC transmission line. The UPFC can be install at different location with extended DC link which will reduces the effect of harmonics problems encounter in UPFC with eliminated DC link. However it reduces the power transmission capability slightly as shown in result and additional lossless in the transmission line and transformers. But both the modified UPFC have the full function as conventional UPFC. The separated series part of this UPFC will reduce the cost significantly and have a lot of extra benefits, such as higher reliability, convenient for installation and maintenance.

The performance of the proposed schemes has been analyzed with MATLAB/Simulink assuming that the UPFC is connected with the 22 kV transmission line of sample power system. The proposed schemes of UPFC interfaced in the power system accomplish a similar performance as that of a traditional scheme.

REFERENCES

- [1] L. Gyugyi, "Unified Power Flow Control Concept for Flexible AC Transmission Systems," in Proc. 5th International Conference on AC and DC Power Transmission Conf., IEE, Issue 345, pp 19-26, London, UK, 1991.
- [2] I. Papic, P. Zunko, D. Povh, M. Weinhold, "Basic Control of Unified Power Flow Controller," IEEE Transactions on Power Systems, v. 12, n.4, p.1734-39, Nov. 1997.
- [3] Z. Huang, et al., "Application of Unified Power Flow Controller in Interconnected Power Systems – Modeling, Interface, Control Strategy and Study Case," IEEE Transactions on Power Systems, v.15, n.2, p.817-24, May, 2000.
- [4] E. Uzunovic, C. Cañizares, J. Reeve, "Fundamental Frequency Model of Unified Power Flow Controller," in Proc. North American Power Symposium NAPS, Cleveland, Ohio, Oct.1998, pp. 294-99.
- [5] K. K. Sen, E. J. Stacey, "UPFC-Unified Power Flow Controller: Theory, Modeling and Applications," IEEE Transactions on Power Delivery, Vol. 13, No. 4, Oct. 1998. pp.1953-60.
- [6] A. Karami-Mollae and M. R. Karami-Mollae, "A new approach for instantaneous pole placement with recurrent neural networks and its application in control of nonlinear time-varying systems," *Systems & Control Letters*, vol. 55, pp. 385-395, 2006.

- [7] D.Soto, T.C. Green. A comparison of high power converter topologies for the implementation of Facts controllers, IEEE Trans, Ind. Electron.49 (October, 5 2002).
- [8] Y. Minari, K. Shinohara, R. Veda PWM rectifier/voltage source inverter without DC link capacitor for induction motor drive, IEE, Proc. – B140 (November, 6 1993.)
- [9] I. Pabic, P. Zunko, D. Povh, M. Weinhold, “Basic Control of Unified Power Flow Controller,” IEEE Transactions on Power Systems, v. 12, n.4, p.1734-39, Nov. 1997.
- [10] Z. Huang, et al., “Application of Unified Power Flow Controller in Interconnected Power Systems – Modeling, Interface, Control Strategy and Study Case,” IEEE Transactions on Power Systems, v.15, n.2, p.817-24, May, 2000.
- [11] Vasquez Arnez, R. L; Zanetta, L.C.; Effective Limitation of Line Fault Currents by Means of Series-Connected VSI-Based FACTS Devices. In: X Symposium of Specialists in Electric Operational and Expansion Planning, Florianópolis, Brasil, X SEPOPE, 2006.

Revolutionary Automatic Traffic Controller

Satyendra Pratap Singh, Rajan Tiwari

Mechanical Engineering Department, Rajarshi Rananjay Sinh Institute of Management and Technology, Amethi – 227405, Uttar Pradesh, India

Abstract— Here, the focus is to control the traffic on bridge as well as on road by using the traffic control optimizer, this setup is provided for the foot path and also the divider of the road which is used to control the traffic by providing extra space on the road during over crowd conditions.

Traffic is a major problem in modern era. Morning to evening, till late night, each one is facing a problem every day. According to the survey, According to “TRAFFIC CORPORATION OF INDIA and IIM KOLKATA” in the year 2012 there is loss of 60,000 crore rupees of India per year due to traffic jam. The study revealed that on 17 big routes of country there is a national fuel mileage of 3.96 kilometres per litre. According to the survey of “Centre for Transforming India” in 2010, there is loss of 2.5 litre of fuel per day in car and 0.7 litre of fuel per day in bike. Due to traffic jam, there is a loss of 90 minutes per day of an average person, if we would calculate it in years, about 23 days an average person wastes in traffic. According to study of IBM the 40% of productivity of the country decreases due to wasted time in traffic jams. Thus the main purpose of making this optimizer is to control the jam by shift down of the footpath (using IR sensor), if there is no crowd on other side of lane then it shifts the divider towards the other side of road at some definite length. In this whole phenomena, IR sensor which sends signal to the microcontroller and operates motorised scissor jack which provides path on the road.

Keywords— IR sensor, Arduino Programmed Microcontroller, Motorised Scissor Jack, Linear Actuator, Fibre Divider Railing, Modified Traffic Light.

I. INTRODUCTION

As we know that traffic is a major problem of the modern age. Population of country is increasing day by day, but our resources are fixed due to which many problems are in existence such as pollution, less space, disease traffic etc. Traffic causes more problems such as wastage of time, consumption of fuel, noise pollution etc. The main factor to which the overcrowded traffic affects is the precious time of man. In today's era, no one wants to waste his time on traffic. Adjusted for the large population, India has less than 3.8km of road per 1000 people including its paved and unpaved & also bridge on the river. The size(width) of the road is fixed according to the free

space. Due to limited space on road and more population, the traffic problems are very common in today's scenario. For this we have tried to introduce a system which can be operated in this limited space for control of the traffic in efficient manner, this set up is designed for the national highways, bridges. This operates when the over traffic is on the road. It distributes the traffic and maintains the stabilisation on the road. By using this, we can save time, heavy consumption of fuel, accidents and jams also. This system helps to circulate the traffic in an efficient way.



Fig1: River Bridge



Fig 2: Road Traffic

II. BASIC DESCRIPTION OF IDEA

Today's heavy traffic on roads is a severe headache for municipal authorities. Due to over traffic, we waste our time as well as some times money also. Today we see that the size of the roads are fixed and also its various components such as divider, footpath are static due to which during jam conditions, the space of footpath are free after some duration when the pedestrian are passed out. Basically jam occurs in two conditions, first, sometime jam is seen on the half of road (i.e. one side) and other half is free (i.e. second side) as compared to the first half and vice versa, and sometimes both sides are completely jam. To overcome this problem, we are going to discuss a solution to control this problem. Our idea is that if the jam exists at half of road and other half is free, then sensor (IR) senses the free & occupied space after which linear actuator shifts the divider towards the other side to a appropriate distance and provides more space. Eventually sensor senses again and footpath track goes

downward side which provides space on road, on doing so we can distribute the jam and can control the disturbed traffic easily. As soon as the traffic is optimised, therefore the traffic light signals to move on from the foot path & also from the divider and comes under the safe line and it toward its original position. This process would occur again if this condition is vice versa.

On the other hand if there is a traffic jam on both sides of road, in that condition sensor senses and then only footpath track moves downward side and divider is kept static in this whole phenomena. This all phenomena is controlled by the arduino programmed microcontroller.

III. DESCRIPTION OF THE ELEMENT

- a) Movable fibre divider
- b) Modified traffic light with two signals
- c) IR sensor
- d) Arduino programmed microcontroller
- e) Linear actuator
- f) Scissor jack

As we know that the road is designed with several component such as divider, footpath railing, traffic light etc. In this approach the old phenomena of the road such as fixed footpath and fixed divider is replaced by the innovative movable divider and movable footpath railing. The working phenomena is given below –

a) Movable Fibre divider - The old concrete divider is replaced by the fibre made divider. The basic work of divider is to divide the road in two parts for up and down motion. The divider is connected with linear actuator, which provides sliding motion to the divider during shifting condition, due to which we can acquire the required space on the road.



Fig.3: Linear Movable Divider

b) Footpath – In the old phenomena of the road the foot path is made of the concrete and at some height, its width is near about 2.5 feet to 3 feet and modified footpath is in the level of road, also it is only separated by the railing, which is made up of cast iron pipe or fibre pipe. This is lifted by the motor operated scissor jack.

c) IR sensor- An infrared sensor is an electronic instrument which is used to sense the certain

characteristics of its surrounding by either emitting or by detecting radiation. Infrared sensor is also capable of measuring the heat being emitted by an object and detecting motion.



Fig.4: IR Sensor

d) Arduino Programmed Control Board – Arduino is used to provide proper interface between the sensors and other electronic and electrical equipment.

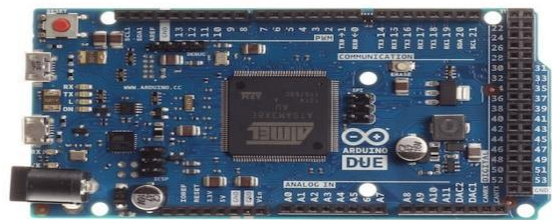


Fig.5: Ardiuno Programmed Control Board

e) Scissor Jack –The scissor jack is mechanical equipment which is used to lift the load. A scissor jack is operated simply by turning the crank which is inserted into one end of scissor jack. This crank is usually of “Z” shape when this crank is turned by the electric motor, the screw turns and this raises the jack. The screw acts like a gear mechanism. It has teeth, which turn and move the two arms, producing work. By only turning the screw thread, scissor can lift load of thousand pounds.



Fig.6: Scissor Jack

f) Electro-Mechanical Linear Actuator- A linear actuator is an actuator that creates motion in a straight line, in contrast to the circular motion of convectional electric motor. Mechanical linear actuator typically is operated by conversion of rotary motion into the linear motion. For accurate and repeatable positioning, index mark may be used on the electric motor. This actuator includes an encoder and digital poisoning readout. These are similar to knob used in the CNC machine and the micrometre, except their purpose is to adjust position rather than position measurement.



Fig.7: Linear Actuator

g)Linear Encoder- Basically encoder is a device, circuit transducer, software program, that converts the information from one format or code to another, for the purpose of standardization, speed or compression.

Linear encoder is a sensor which is read a head paired with scale that encodes position. The sensor reads the scale in order to convert the encoded position into an analogy or digital position by digital read out or motion control. It control in positioning of the object which is attached to the actuator.

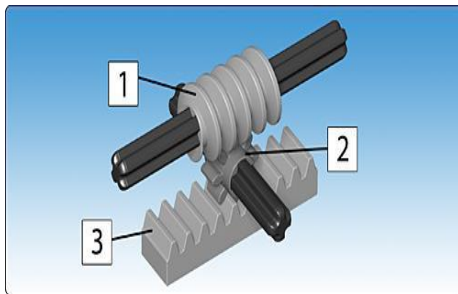


Fig.8: Mechanism of linear actuator

IV. ACTUAL SET UP AND IT'S WORKING

Now in this, we are going to explain the actual set up of the different component of the system. That is given below -

- 4.1. Divider with its additional component
- 4.2. Modified traffic signal
- 4.3. Foot path railing with its additional component
- 4.4. Programmable Arduino micro control board

4.1. Divider with its additional component

Here the divider is made of the fibre with the moving wheel in its base. In the divider, we had provided IR sensor to its both side of the face for detecting the crowd and signalling to the microcontroller to blink the light. And the electromechanical linear actuator is also provided in this set up. The one end of the linear actuator is fixed with the movable divider and other end is fixed with other side of the road at last end of the footpath and further it is attached to the programmable microcontroller.

4.2. Modified Traffic signal

This traffic signal is used for showing the motion of the divider as well as the motion of the footpath railing. This signal is operated by the microcontroller. This shows the motion of different object with different light which

always pays attention from the motion of the object to the traveller. Here, we had given different colour indication which shows the different motion.

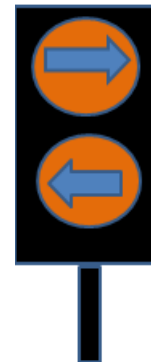


Fig.9: Signal indicating the movement of Divider



Fig.10: Signal indicating the motion of the footpath

4.3. Footpath with Additional Component

Here the footpath railing is made of cast iron or fibre. This foot path railing is laced with the IR sensor, the motorised scissor jack and the traffic signal light. This motion occur when there is bumper to bumper jam on the road, at that time the IR sensor senses and signals to the microcontroller which send signal to the traffic light for showing the indication of motion of footpath in downward direction to the traveller, and same at that time the microcontroller sends signal to the electric motor to start and rotates screw jack. For the lifting condition, it rotates motor in clockwise direction and for downward motion it rotates motor in anticlockwise direction.

4.4. Programmable Arduino Micro Controlled Board

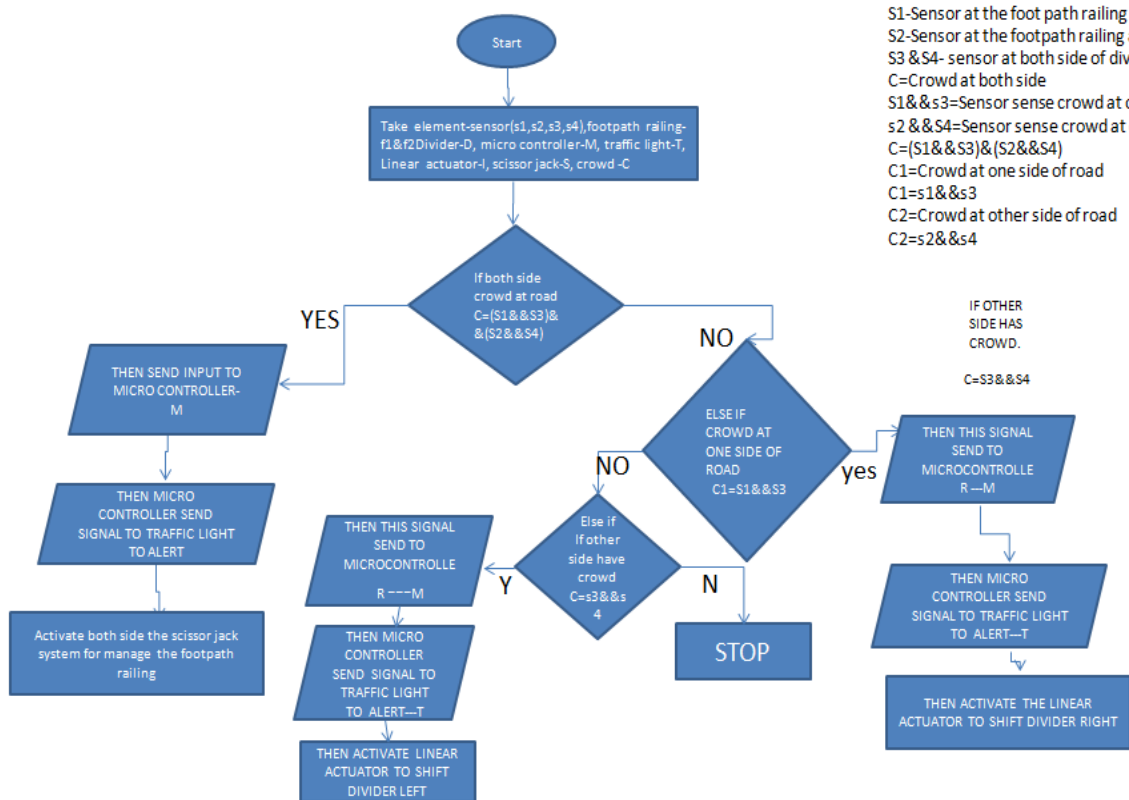
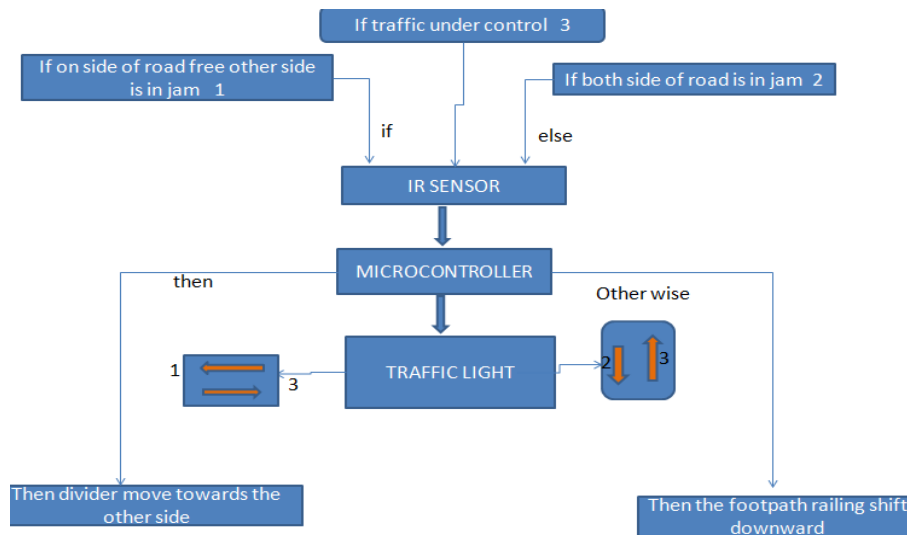
This is the brain of whole system. This whole system is provided to the traffic signal stand. From where it receives the signal of the sensor element and gives the signal to the traffic light & the linear actuator & the electric scissor motor to operate their operations. At the entrance of the bridge as well as road, at both the sides

from up and down side, there is a traffic light which shows the signal of up and down motion of foot path railing. If foot path railing is coming upward side then it gives signal to travellers to not to come in the same direction of the footpath railing. This whole phenomenon is controlled by our programming on the microcontroller. A special instruction is also given at the entrance of the bridge and road, is that, move towards the left side of the road if there is no traffic on the road and to make a proper distance from divider. If at other side of road is

approximately free space then sensor senses the traffic and linear actuator shifts the divider to other side as it feed during programming duration of microcontroller.

Model is working on the following condition-

- When one side of road is free and other is in jam condition or vice versa.
- When the both side of road is filled with traffic.



S1-Sensor at the foot path railing at going side f1
 S2-Sensor at the footpath railing at coming side f2
 S3 & S4- sensor at both side of divider D
 C=Crowd at both side
 S1&s3=Sensor sense crowd at one side of road
 S2 & S4=Sensor sense crowd at other side of road
 C=(S1&S3)&(S2&S4)
 C1=Crowd at one side of road
 C1=s1&s3
 C2=Crowd at other side of road
 C2=s2&s4

When one side of road is free and other is in jam and vice versa-

In this condition the sensor, senses the position of the vehicles on the free road and send signals to the microcontroller which in turn gives the signal to traffic light to show the motion of divider in pictorial form, and when the vehicles are away from divider at that duration the microcontroller send signals to the linear actuator to provide the linear motion in the divider. Due to this we have some space on the other side of road, but for further increasing the space on the road the footpath sensor senses and give signals to microcontroller, which in turn gives signals to traffic light to show the pictorial motion

of divider in led and then after that the microcontroller send signals to the electronic scissor jack to come downward side and hence footpath comes in the level of road and the vehicles can easily pass over them due to which, we can distribute the traffic easily. After some time when the traffic is optimised, the sensor senses and send signals to microcontroller and again it sends signals on the entrance traffic signal, which shows the upward motion of footpath railing. Due to which vehicles are not allowed to come over the footpath. And it gives the signal of motion of the divider on its original position which is shown by the line of blue paint.



Fig.11: Shows basic motion of vehicle on the road



Fig.12: Shows the moment of divider towards the rightward

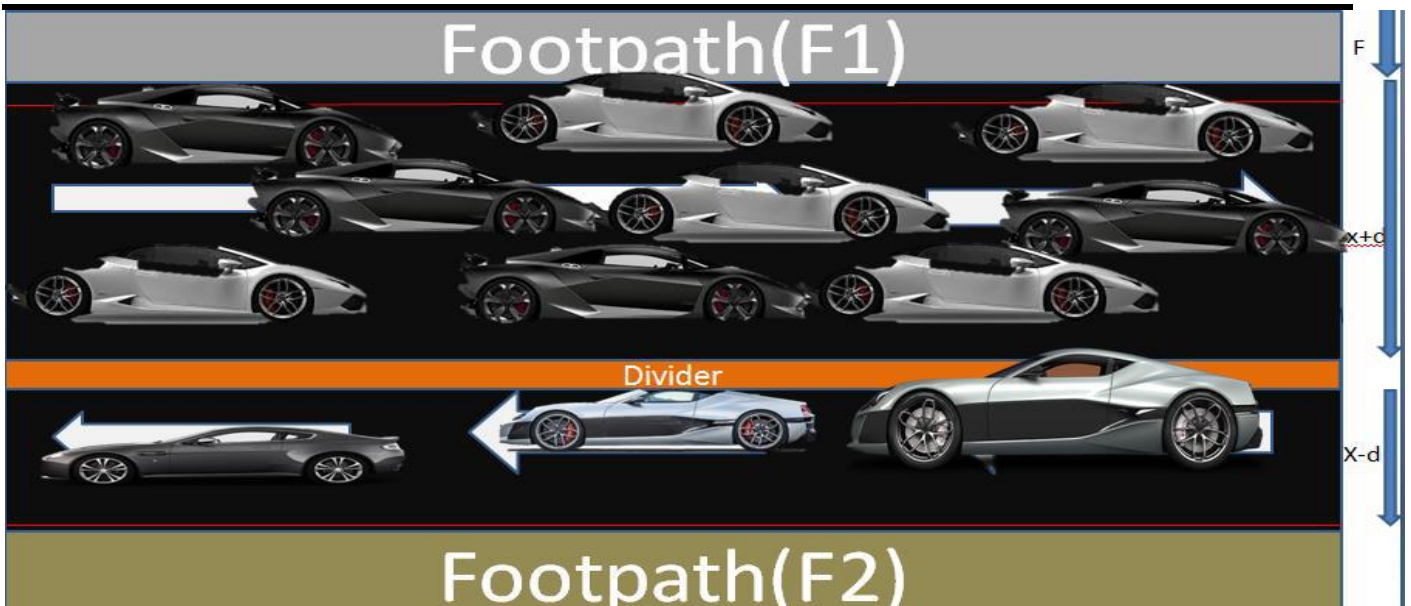


Fig.13: Shows the moment of divider towards the left side

For producing more efficiency, we can also put down the footpath railing and get extra space on the road. As shown in the fig.

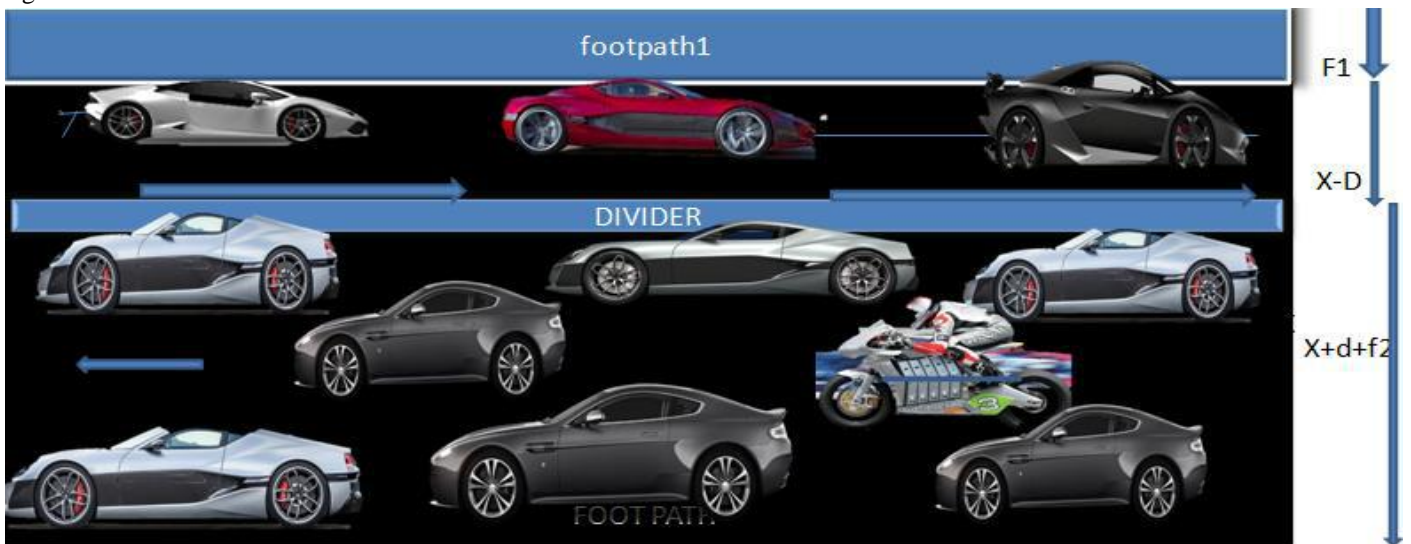


Fig.14: Shows the moment of divider towards right side and motion of foot path downward

When both the side of the road is filled with crowd

In this condition, the sensor of divider as well as the sensor of the footpath sense traffic on the road. In the condition when the both side of the divider is completely filled with jam then in that condition microcontroller does not allow to start the linear actuator. It is totally based on the programming of the microcontroller. But the sensor of the footpath sends signals to the microcontroller which allows the traffic light to show the sign of downward motion of footpath, with orange light starts blinking and the microcontroller is allowed to start the electric motor

of scissor jack which moves downward the footpath railing, due to this we can get extra space at both side of road for coming and going both side. For getting extra space vehicle shift towards the free space. By doing so vehicle can easily pass. After controlling of jam the microcontroller send signals to the both sides of the traffic control light which is present at the entrance of the road to show the sign of coming up the footpath which indicates to be away from the foot path. After that microcontroller send signals to the electric scissor motor to operate for lifting the footpath.

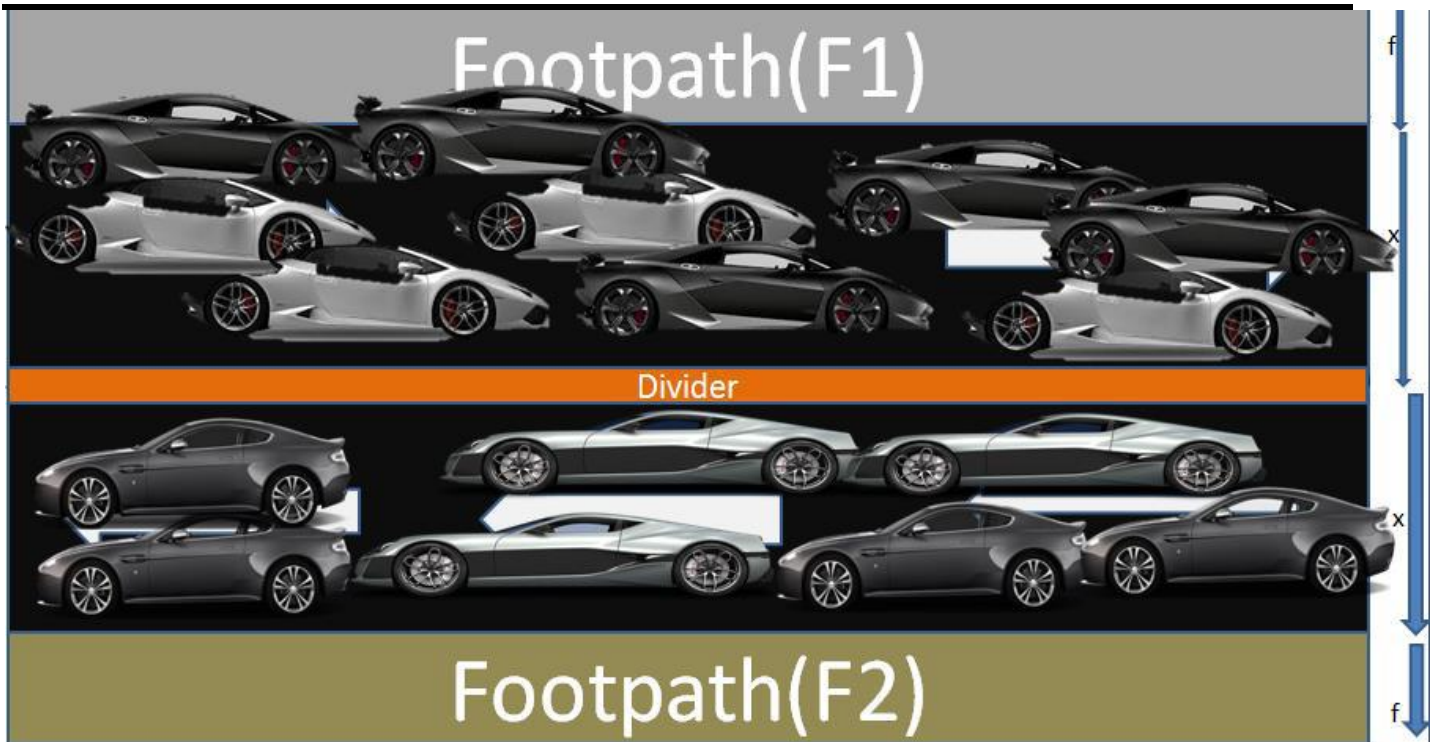


Fig.15: Shows traffic on both side and all components on its basic position



Fig.16: Shows the motion of foot path on both side of road

V. CONCLUSION & RESULTS

- We can shift our upward footpath in downward motion so that the extra space is provided by the

road. Around 3 feet will be helpful for the control of the traffic.

- If the condition is still not in control or over loading on the road then we can use the extra space provided

by the divider and approximately 4 feet extra space could be provided. Around 27 feet of the road will be helpful to control the traffic.

- The same procedure will be done for the morning shift when no. of vehicles coming decreases, the road will increase, we will follow the same procedure or vice versa for above mentioned point.
- The controlling of traffic should be totally depended upon the signal light. We have to provide the different types of relevant signal light for the movement of movable divider or foot path.
- As we already use three lights for the different purpose for the traffic control, so we have to apply different coloured lights, say orange with up and down motion.
(Specially, for particular inspection done on HAZRATGANJ SQUARE, Lucknow)
- Timing: 5:00 pm to 7:00 pm the no. of vehicle from one lane is approximately 80,000.
- If we consider the parts of the road is on its relevant position then the time lag is 2 min, but if we use the extra space then the time lag may be decrease up to 1min.
- Time lag is depended upon the no. of vehicles passing on the same road, if the no. of the vehicle increases so that it will be helpful for decrement of traffic and finally we can have a power full traffic control system.
- The main question arises in our mind that 'what will happen when footpath is converted into the road then where the pedestrian would walk then we can shift both side pedestrian into one side with the help of zebra crossing at the equal distance before or after of roundabout.
- When one side footpath is converted then with the help of zebra crossing, then the second side is converted or shifted to another side.
- The same will be repeated for morning downwards motion.

By the use of traffic optimizer, we can control the traffic as well as provide suitable and comfortable environment to the huge crowded cities. By this system we provided the extra space on the road for the suitability of vehicles with zero disturbance, we can reduce the time lag which can impact on the saving of precious time, money, wastage of fuel and as well as to provide protective environment. This complete system undergoes a pre-deformed scenario of the project describe on this for the human suitability and comfort ability. This idea will drastically change the problems of present era to overcome all the grievances and will provide a fruitful environment among us.

VI. ACKNOWLEDGEMENT

We take this opportunity to express our deep sense of gratitude & whole hearted thanks to our Institution Rajarshi Rananjay Sinh Institute of Management & Technology, Amethi for inspiring and encouraging us to explore ourselves. The Incubation Centre of the Institute, Is a beehive of intellectual and innovative activities. Under the effective guidance of our teachers & seniors, we have completed the final draft on Revolutionary Automatic Traffic Controller. Our Institute has always focused on providing us a framework for better future for mankind. Also in shaping us to become effective, skilled professionals in coming future. We are very thankful to the Institute's Management & our Director Sir for his kindness, constant encouragement, and influential leadership & for the valuable time which he devoted to us. Also, thanks to our family & friends who directly & indirectly helped, supported & motivated us along the due course of completion of this research paper.

REFERENCES

- [1] Natasha Jones (February 17, 2011). "Police question traffic control costs". Aldergrove Star. Retrieved June 3, 2013.
- [2] "Safety at Street Works and Road Works - A Code of Practice". www.gov.uk. Department for Transport. Retrieved 15 December 2014.
- [3] Kator, Zabi. "traffic control". website. Guard NOW. Retrieved 19 May 2013.
- [4] Xiao-Feng Xie, et al. Real-time traffic control for sustainable urban living. IEEE International Conference on Intelligent Transportation Systems (ITSC), Qingdao, China, 2014: 1863-1868.
- [5] "Dowel Bars for New and Existing Concrete Pavements" (PDF). Washington State Department of Transportation. February 2013. Retrieved 24 March 2014.
- [6] "Traffic-related Air Pollution near Busy Roads". American Journal of Respiratory and Critical Care Medicine Vol 170. pp. 520-526. 2004
- [7] "Road Transport (Europe)". Overview. European Communities, Transportation. 2007-02-15. Retrieved 2007-03-24
- [8] https://www.google.co.in/search?q=sensors+microcontrollers&rlz=1C1CHBD_enIN743IN743&oq=SENSORS+%26+MICROCO&aqs=chrome.1.69i57j0l5.13898j0j7&sourceid=chrome&ie=UTF-8#

Short-term rhGH increases PIIINP, a biomarker of endothelial dysfunction

Graham M. R.*^{1,2}, Gu Y.¹, Evans P. J.³, Cooper S. M.⁴, Davies B.², Baker J. S.⁵

¹Michael. R. Graham*, Research Academy of Grand Health, Ningbo University, China;

²University of South Wales, CF37 1DL, UK.

¹Yaodong Gu, Research Academy of Grand Health, Ningbo University, China.

³P. J. Evans, Royal Gwent Hospital, Newport, South Wales, NP20 2UB, UK.

⁴S. M. Cooper, Cardiff Metropolitan University, Cardiff, CF24 6XD, UK.

²B. Davies, University of South Wales, CF37 1DL, UK

⁵J. S. Baker University of the West of Scotland, Hamilton, Scotland, ML3 OJB, UK.

Abstract— Objectives: In arterial hypertension, amino-terminal propeptide of type III procollagen (PIIINP) is elevated in arterial aneurysm tissue and associated with a poor prognosis following acute myocardial infarction (MI). Recombinant human growth hormone (rhGH) administration attenuates endothelial dysfunction but increases PIIINP. This study was conducted to establish if short-term rhGH administration affects PIIINP, endothelial function and selected cardiovascular disease (CVD) risk factors, in healthy males.

Design: Method: Male subjects (n=48) were randomly assigned into two groups:

(1): control group (C) n=24, mean \pm SD, age 32 ± 11 years; height 1.8 ± 0.06 metres;

(2): rhGH administration group (rhGH) n=24, mean \pm SD, age 32 ± 9 years; height 1.8 ± 0.07 metres.

Blood pressure (BP), heart rate (HR), arterial pulse wave velocity (APWV), and biochemical indices were investigated.

Results: PIIINP (0.28 ± 0.1 vs. 0.42 ± 0.2 , U/ml); Insulin like growth factor-I (159 ± 54 vs. 323 ± 93 , ng.mL⁻¹); resting HR (72 ± 14 vs. 78 ± 11 , b.p.m.) and rate pressure product (RPP) (90 ± 18 vs. 97 ± 14 , bpm x mm.Hg x 10⁻²) all significantly increased ($P < 0.05$). Total cholesterol (4.7 ± 0.9 vs. 4.4 ± 0.7 , mmol.L⁻¹); high sensitivity C-reactive protein (1.77 ± 2.1 vs. 1.29 ± 1.6 , mg.L⁻¹); serum homocysteine (13.2 ± 4.0 vs. 11.7 ± 3.1 , μ mol.L⁻¹) and APWV (9.97 ± 1.38 vs. 9.18 ± 1.6 , m.s⁻¹) all significantly decreased ($P < 0.05$).

Conclusion: Paradoxically, there was an improvement in CVD inflammatory markers and APWV; but PIIINP and resting RPP increased.

Elevated PIIINP may have a confounding adverse effect on the endothelium, but may also provide clinical prognostic information in monitoring arterial hypertension, left ventricular function in the sub-acute phase following MI and endothelial function in aortic aneurysms.

Keywords— APWV; BP; hsCRP; Homocysteine; PIIINP; RPP.

I. INTRODUCTION

Serum amino-terminal propeptide of type III procollagen (PIIINP) is an extension peptide of procollagen type III and reflect its synthesis. It is cleaved off procollagen type III during the biosynthesis of type III collagen, and is a circulating biochemical marker of collagen metabolism which characterizes the early stages of repair and inflammation [1]. PIIINP is associated with the repair process involving collagen deposition which influences endothelial remodeling after myocardial infarction (MI) and increasing levels from ~ 3 to ≥ 5 μ g/L are believed to reflect enhanced collagen turnover, including synthesis and deposition as well as alteration in degradation and elimination [1]. Elevated levels appear to be associated with a poor prognosis of patients following acute non-thrombolysed MI [2]. An elevation of PIIINP greater than 5.0 μ g/L has been identified as an independent predictor of cardiac death or complicating left ventricular heart failure by vascular remodeling [3]. In dilated cardiomyopathy, with restrictive mitral filling pattern and diastolic dysfunction patients with an elevated PIIINP had a worse prognosis [4]. Elevated circulating levels of PIIINP were also associated with a decreased six minute walk distance and an increased resting heart rate (HR) in pulmonary arterial hypertension (PAH) [5].

PIIINP appears to be an important biomarker which may evaluate left ventricular end-diastolic pressure (LVEDP) and may predict cardiac mortality in acute coronary syndrome (ACS) [6].

Collagen is an important protein of the extracellular matrix (ECM) that determines the physiological properties of arteries, especially the aortic wall and the development of abdominal aortic aneurysms (AAA) [7]. PIIINP is increased in AAA tissue compared with normal aortic walls affected by occlusive atherosclerotic disease [7]. A significant difference between plasma PIIINP levels exists in patients with AAAs compared with controls and the turnover of type III collagen increases with the

enlargement of the aneurysm diameter [8]. Degradation of type III collagen in the aneurysmal wall may have an important impact on AAA rupture and the increased levels of PIIINP may also be able to predict AAA prognosis [9]. Collagen production has been identified as being increased in excess growth hormone (GH) production (acromegaly) [10]. Serum PIIINP which is increased in this condition may be used as a marker for monitoring the extent of the disease process [10]. Untreated long standing acromegaly is characterised by a high HR and arterial hypertension (the hyperkinetic syndrome) and concentric biventricular hypertrophy, diastolic dysfunction, rhythm disturbances and valve dysfunction which can all exacerbate acromegalic cardiomyopathy [11].

Systolic function and cardiac performance is markedly decreased in growth hormone deficiency (GHD) but is improved following recombinant human growth hormone (rhGH) replacement [12]. Endothelial dysfunction (ED) determined by flow-mediated endothelium-dependent dilation (EDD) of the brachial artery and measured by B mode ultrasound is prevalent in GH-deficient adults, which is reversed by rhGH replacement for the period of treatment of 18 months [13]. RhGH decreases aortic systolic and diastolic pressure which may reduce cardiovascular disease (CVD) in GHD [14]. RhGH improves vascular ED in patients with chronic heart failure who are not deficient in endogenous growth hormone [15]. Short-term rhGH, four weeks (0.1 and 0.2 IU.kg⁻¹.day⁻¹) and two weeks (0.1 IU.kg⁻¹.day⁻¹) respectively, has been shown to significantly elevate PIIINP in healthy individuals by almost three times baseline levels [16, 17]. The purpose of this original study was to examine the effects of one week's supraphysiological rhGH administration on PIIINP and specific CVD parameters in an apparently healthy group of strength training males. The research team hypothesised that PIIINP would increase and that CVD parameters would decrease, following rhGH administration.

II. METHODS

Subjects. Approval for the study was obtained from the University of South Wales ethics committee, in accordance with the declaration of Helsinki. Ethical registration committee number: HRE916. Prior to data collection, subjects were informed of experimental protocol, signed informed consent, and were instructed that they could withdraw from the study at any time. In addition, a drug screen was performed on each subject to exclude the use of xenobiotic substances. Urinalysis was performed at a world anti-doping agency (WADA) accredited laboratory. All subjects were recreational strength trainers and recreationally active. Subjects in both groups were former testosterone users and followed synchronised training

times and intensity, which did not differ. This was verified by detailed training diaries. In order to avoid confounding effects on biochemical indices, subjects abstained from physical activity for 24 hours before each testing day.

Study design. Male subjects ($n=48$) were randomly assigned, using a single blind procedure, into two groups: (1): control group (C) $n=24$, mean \pm SD, age 32 ± 11 years; height 1.8 ± 0.06 metres; 2): rhGH administration group (*rhGH*) $n=24$, mean \pm SD, age 32 ± 9 years; height 1.8 ± 0.07 metres.

Physiological tests were performed in the same order for both the experimental group and the control group. Subjects were familiarised with testing procedures. Subjects were examined daily over a period of six weeks between the hours of 09:00 and 11:00, to avoid confounding diurnal effects and were anonymous to each other. A dosage of 0.019 mg.kg⁻¹.day⁻¹ rhGH was used and was considered an acceptable dosage that would provide a physiological effect, with minimal side effects, in apparently healthy subjects. An administration diary was recorded. Subjects were examined prior to the commencement of rhGH administration, day 1, day 7, and after cessation, day 14. Dietary intake was strictly monitored, using a fourteen day dietary recall (Nutri-check, Heath Options Ltd, Eastbourne, UK).

Blood sampling. Phlebotomy was conducted in the fasted state, following 30 minutes rest in the supine position [18] using the standard venepuncture method (Becton Dickinson, Rutherford, NJ, USA between the hours of 09:00 and 09:30 accounting for diurnal biological variation of male sex hormones [19].

Serum analytes were measured using standard methods and analysed in duplicate. Serum total cholesterol (TC) and triglycerides (TG) were measured by dry-slide technology on an Ortho Vitros 950 analyzer (Ortho Clinical Diagnostics, High Wycombe, Bucks UK). The inter-assay CVs were: Total cholesterol: 1.95%; Triglycerides: 3.6%. The intra-assay CVs were: Total cholesterol: 3.8%; Triglycerides: 0.9%.

Serum high density lipoprotein cholesterol (HDL-C) was analysed on an ILab 600 using a homogeneous direct method in which reaction with non-HDL cholesterol is prevented by addition of anti-human lipoprotein antibody (Instrumentation Laboratory, Warrington, UK). The inter-assay CV was: 2.8%. The intra-assay CV was: 1.2%. Serum low density lipoprotein cholesterol (LDL-C) was derived from the Friedewald equation.

High sensitivity C-reactive protein (hsCRP) was analysed using a latex-enhanced immunoturbidimetric assay (Randox Laboratories, Crumlin, Northern Ireland). The inter-assay was: 4.95%. The intra-assay CV was: 8%.

HCY was measured from plasma blood by fluorescence polarization immunoassay (FPIA) using the IMX[®] system

analyser IMX[®] reagents (ABBOTT Laboratories, UK). The inter-assay was: 6.1%. The intra-assay CV was: 4.4%.

Testosterone (T, nmol.L⁻¹) was analysed with the chemiluminescent immunoassay on an Advia Centaur analyser (Bayer Diagnostics, Newbury, UK). The inter-assay CV was: 12.0%. The intra-assay CV was: 7%.

IGF-I was analysed using the standard Nichols Institute Diagnostics IGF-I immunoradiometric Assay (IRMA), which employs two region-restricted affinity purified polyclonal antibodies (Nichols Institute Diagnostics, San Clemente, CA 92673 U.S.A.) calibrated against the world health authority 1st IRP IGF-I 87/518.

The inter-assay CV was: 4.5%. The intra-assay CV was: 10.0%, 6.3% and 5.7% at serum concentrations of 61.5, 340.8 and 776.9 ng.ml⁻¹ respectively.

Recombinant and pituitary GH were analysed using two immunofluorometric assays, one measuring 22 kiloDalton hGH and the other total hGH (22 and 20 kiloDalton) [20]. The inter-assay CVs were: 10.0, 4.0, and 5.4% at 1.7, 12.1 and 22.2 ng.ml⁻¹, respectively. The intra-assay CV was 5%.

Serum amino-terminal propeptide of type III procollagen (PIIINP) was measured by a two-stage sandwich RIA (CIS Biointernational; Oris Industries, Gif-Sur-Yvette Cedex, France). The reported intra-assay variability at 0.8, 1.5 and 4.0 U/ml is 2.9, 2.9 and 4.0% respectively. The inter-assay variability at 0.25, 1.5 and 5.6 U/ml is 11.3, 7.8 and 9.3% respectively.

Body composition assessment. Body mass (BM, kg) was measured using a calibrated balanced weighing scales (Seca, Cranlea Ltd, UK) and stature was measured using a stadiometer (Seca, Cranlea Ltd, UK). All measurements were taken barefoot in briefs. Body Mass Index (BMI, kg.m⁻²) was calculated by dividing the subject's weight in kilograms (kg) by the square of the subject's stature in meters. Body density was determined using hydrostatic weighing procedures previously described by [21]. Following a familiarisation trial, underwater weight was determined five times. The mean of five trials was used as the criterion value. Gastrointestinal volume was assumed to be 0.1 litres (L) and residual lung volume (RLV) was estimated to be 24% of forced vital capacity and ranged from 0.9 L-1.4 L, which was within normal limits [22]. Body fat was estimated from body density, using the equation of Siri [23].

Arterial Pulse Wave Velocity (APWV): was measured simultaneously and non-invasively in the supine subject's arm and leg by oscillometry (time resolution \pm 2 ms; QVL SciMed (Bristol, UK). The right arm and right leg were used for all the studies. PWV was derived as the distance between the proximal edges of each pair of cuffs divided by the transit time in m.s⁻¹. Each recording of PWV took 30 seconds. Throughout each study PWV was measured for

the first 12 minutes (12 instructions). Each instruction consists of the artery being in a state of vascular occlusion, at a pressure of 65-70 mmHg, for 30 seconds. PWV was measured for the following 30 seconds, in a state of non-occlusion. After 12 instructions, there was distal vascular occlusion for 5 minutes at a pressure of 65-70 mmHg (instruction 13). Following the five minute occlusion, PWV was repeatedly measured for a further 12 instructions. Reproducibility of supine PWV was assessed by within-subject coefficients of variation over 30 min of consecutive measurements and of measurements repeated one month apart. All subjects attended in the fasted state and at the same time on the morning of each study, having avoided caffeine-containing beverages for 12 h. All interventions and measurements were preceded by a preliminary period of >20 minutes supine rest in a quiet, temperature-controlled room at 22°C [24].

Electrocardiography: A resting 12 lead electrocardiogram (ECG) was performed on all subjects in accordance with the position statement outlined by the American Heart Association [25].

Blood Pressure (BP) Measurement: Blood pressure (BP) was measured in accordance with the American Heart Association Council on High Blood Pressure Research (2005) [26]. BP measurements were obtained by a single physician at the beginning of the physical examination, using a calibrated mercury column sphygmomanometer (Yamasu, Kenzmedico Co., Ltd., Japan). BP was measured from the bared arm, with the subject seated on a chair, with a back support, for five minutes with both feet on the floor and legs uncrossed. The arm was supported at heart level and the appropriate sized cuff was used, ensuring 80% of the circumference of the subject's arm was encircled. The Korotkoff sounds were measured from the brachial artery in the antecubital fossa, using the diaphragm of the stethoscope (Littmann, 3M, Loughborough, England, UK). BP was ascertained from both arms and if the difference was less than 10 mmHg the reading was taken from the right arm. All readings that were finally used were measured from the right arm, since there were no differences between the right and left arm. Two auscultatory measurements in each position were made at an interval of one minute and an average of those readings was used to represent the patient's BP. If these readings did not agree to within 5 mm.Hg for SBP and DBP a further two readings were made and the average of those multiple readings was used.

Calculations and Statistical analyses.

From published research, the sample size of $n=24$, was estimated using the nomogram method described by Altman (1982) [27]. The proposed main variable for the effect of rhGH was considered to be IGF-I and the lowest dose of rhGH required to significantly increase IGF-I, in

healthy young men and women, has been estimated to be $0.0025 \text{ mg.kg}^{-1}.\text{day}^{-1}$ [28]. From the critical difference equation, described by Fraser and Fogarty, (1989) [29], Healy *et al.*, (2003) [30] estimated an increase in IGF-I of 24% was required to demonstrate a physiological effect of IGF-I on metabolism, from rhGH administration. Velloso *et al.*, (2013) [17] monitored a dosage of $0.033 \text{ mg.kg}^{-1}.\text{day}^{-1}/0.1 \text{ IU.kg}^{-1}.\text{day}^{-1}$, which significantly increased PIIINP ($P<0.05$). A dosage of $0.019 \text{ mg.kg}^{-1}.\text{day}^{-1}/0.058 \text{ IU.kg}^{-1}.\text{day}^{-1}$ was assumed to be an acceptable dosage that would provide a physiological effect, with minimal side effects, in a cohort of apparently healthy subjects.

Data were analysed using a computerised statistical package (PASW 22.0 for Windows, Surrey, England) using parametric statistics. Significance was set at the $P<0.05$ level. Data are presented as means \pm standard deviation (SD). The power of the test was calculated at 95%. Confirmation that all dependent variables were normally distributed was assessed via repeated Kolmogorov-Smirnov tests. Changes in selected dependent variables as a function of time and condition were assessed using a two way repeated measures analysis of variance (ANOVA). Following simple main and interaction effects, Bonferroni-corrected paired samples *t*-tests were applied to make *posteriori* comparisons of the effect of time at each level of the condition factor. The rate pressure product (RPP) was calculated as heart rate multiplied by systolic SBP.

III. RESULTS

The urinary concentrations of testosterone were normal and the serum gonadotrophins and testosterone were within the reference range for eugonadal men (male serum testosterone: 10-35 nmol/L, table 4). Electrocardiography was unremarkable in all subjects, demonstrating no adverse effect of rhGH on cardiac electrical or rhythmical activity.

There were no changes within the control group. Demographic characteristics of the subjects are presented in table 1. Body mass index (BMI, kg.m^{-2}) significantly increased within the rhGH administration group ($P<0.017$). Body fat significantly decreased within the rhGH administration group ($P<0.017$).

Values for APWV (m.s^{-1}) are presented in table 2. The lower limb pre-occlusion velocity was significantly decreased within the rhGH administration group ($P<0.017$).

Results of the effects of rhGH on the cardiovascular responses: heart rate (HR), systolic blood pressure (SBP), and rate pressure product (RPP) responses are shown in table 2. HR and RPP significantly increased on rhGH administration compared with the control group ($P<0.05$).

Results of the effects of the drug on the serum analytes are shown in table 3. Serum Sodium, IGF-I and PIIINP significantly increased within the rhGH administration group ($P<0.017$) and IGF-I and PIIINP also significantly increased compared with controls ($P<0.05$). Serum hsCRP, HCY, and TC, all significantly decreased within the rhGH administration group ($P<0.017$).

IV. DISCUSSION

In this study the administration of rhGH at a dose of $0.019 \text{ mg.kg}^{-1}.\text{day}^{-1}$ for six days, in apparently healthy individuals equated to a mean value of 1.6 mg per day, which was considered a supraphysiological dose. In healthy males and females, the GH level is normally undetectable ($<0.2 \mu\text{g.L}^{-1}$) throughout most of the day. There are approximately 10 intermittent pulses of growth hormone per 24 hours, most often at night, when the level can be as high as $30 \mu\text{g.L}^{-1}$. This equates to an average GH secretion of circa 0.67 mg and 0.83 mg in males and females respectively, per 24 hours [31].

The effect of rhGH in elevating PIIINP and IGF-I, corroborated similar research of short-term (four and two weeks) rhGH administration [16, 17]. PIIINP concentration is currently considered an independent predictor of left ventricular end-diastolic pressure (LVEDP) and correlates with cardiac mortality and revascularization, providing an additional means of evaluating and managing patients with acute coronary syndrome [6]. Arterial PWV is a valid and non-invasive measure of arterial stiffness that may be more directly related to damage of the target organs relative to brachial blood pressure as it is less altered by heart rate, wave reflection, and antihypertensive or lipid-lowering drugs [24]. It has only been suggested as a CVD correlational independent risk marker with PIIINP in recent years [5].

The mechanism by which rhGH exerts these effects is by the stimulation of collagen metabolism which is an important protein of the extracellular matrix (ECM) which determines the physiological properties and remodeling of the arterial endothelium in aortic aneurysms [7]. PIIINP also has an effect on myocardial fibroproliferation following myocardial infarction [3]. It is suggested that this increases arterial and myocardial stiffness, thereby causing systolic and diastolic blood pressure dysfunction resulting in BP elevation [4]. Cardiac echo-reflectivity, which is a reflection of heart collagen content, is increased in patients with active acromegaly and correlates with elevated PIIINP concentrations. After treatment of acromegaly, and reduction in GH production, both parameters revert to normal [32].

Aortic APWV is also considered an important independent risk factor of CVD and an elevation can predict the

occurrence of cardiovascular events independently of classic risk factors, other than age and blood pressure [33]. The elasticity of the proximal large arteries is the result of the high elastin to collagen ratio in their walls, which progressively declines toward the periphery. Endothelium-derived nitric oxide (NO) diffuses toward the underlying vascular smooth muscle, producing relaxation, modulating arterial smooth muscle tone and distensibility [34]. By improving arterial elasticity, endothelium-derived NO reduces the arterial wave reflection and reduces left ventricular work and the pulse pressure within the aorta [34].

However, in acromegaly where GH and IGF-I levels are excessively elevated for prolonged periods of time there is increased oxidative stress coupled with diminished antioxidant capacity and the endothelial dysfunction occurs as a consequence of NO levels [35]. Both hydrogen sulfide (H₂S) and nitric oxide (NO) are gaseous transmitters, which play a critical role in regulating vascular tone. An H₂S and NO conjugated donor can time-dependently and dose-dependently relax sustained contractions induced by phenylephrine in rat aortic rings, suggesting a possible interactive role between H₂S and NO, in vasorelaxation, produced by fluctuating GH and IGF-I levels [36]. Also H₂S induces relaxation of isolated rings of human mesenteric arteries, independently of NO. Endothelium-dependent related mechanisms with the stimulation of ATP-sensitive potassium channels represents important cellular mechanisms for H₂S effect on human mesenteric arteries [37].

In this study, subjects were exposed to the shortest duration supraphysiological dosage of rhGH possible, which was considered to significantly increase PIIINP. This also caused a reduction in the lower limb pre-occlusion APWV. It is unknown whether the increase in PIIINP caused an increased turnover of the ECM in the arterial wall. The reasons for the decrease in APWV might be as a result of the increased IGF-I to a serum concentration where it increased NO [35]. IGF-I is believed to have a vascular protective role because it stimulates NO production from endothelial and vascular smooth muscle cells. The time frame and concentration levels of serum GH and IGF-I, from commencement of excess production, in acromegaly, to pathological symptomatology is still unknown. The research conducted by the GH-2000 and GH-2004 teams did not identify any serious adverse physiological effects despite the administration of double and quadruple the dose (0.033 and 0.067 mg.kg⁻¹.day⁻¹ [38, 16]) for four times longer (one month) than dosages used in the present study (0.019 mg.kg⁻¹.day⁻¹). However, the researchers were attempting to identify a test for doping rather than assess CVD risk factors. The significantly decreased lower limb pre-occlusion APW velocity in the rhGH group is

comparable with the effects of rhGH on endothelial dysfunction (ED) in growth hormone deficiency (GHD) [14] and in heart failure [15].

The most common short term effects following rhGH administration are from sodium and water retention and weight gain, from dependent oedema, which can frequently occur within days [39]. It does this in GHD [39] and in healthy subjects by activation of the renin-angiotensin system, increasing aldosterone secretion, by inhibiting atrial natriuretic peptide secretion and by a direct action on renal tubules [40]. In the present study, the sodium level was significantly increased, but remained within the normal reference range, but this may have accounted for the elevation in resting HR and RPP, which occurs in acromegaly.

Sustained increased plasma levels of IGF-I may predispose an individual to long term ED and may be accounted for by an inverse correlation of NO levels with GH and IGF-I excess [41]. In the present study the effect on HR and RPP which occurred, could be explained by the effects of IGF-I on NO production, impairing baroreceptor function, via activation of the NO-system, elevating HR without affecting BP [42], corroborating similar short-term rhGH administration [39].

The research group had previously identified a significant reduction of independent cardiovascular risk factors, following rhGH administration, without an identification of changes in PIIINP [43]. In coronary artery disease, hsCRP has an important function in initiation of inflammation. It is also a better predictor of mortality than fibrinogen and offers prognostic information beyond that provided by the conventional cardiovascular risk factors [44]. Also acute inflammation, determined by elevated hsCRP, significantly increases arterial stiffness (AS) in older adults [45]. These increases can be reduced in a high cardiorespiratory fitness group, compared with a low cardiorespiratory fitness group [45].

Raised levels of HCY and CRP, which are independent risk factors for atherosclerosis, are thought to elevate blood pressure and cause vascular endothelial dysfunction by reducing NO production in endothelial cells, potentiating oxidative stress, which may result in vasoconstriction and endothelin 1 increase [46].

This significant lowering of both HCY and hsCRP is a unique finding in an unusual cohort of former testosterone using individuals. It is believed that the use of supraphysiological dosages of testosterone sensitises these individuals to microvascular insult, which predisposes them to impaired vascular reactivity [47]. An elevation of HCY had previously been established by the authors' research group in users of testosterone, which might account for the enhancement of oxidative stress and represent a mechanism leading to the destruction of

vascular cells [48]. In this study, the former users of testosterone had an elevation of homocysteine, which may have sensitised the arterial endothelium, initiated atherogenesis and increased AS by modification of DNA methylation [49]. The underlying epigenetic mechanism, which is an alteration of the phenotype without a change of DNA sequence, may have contributed to altered gene expression causing vascular damage [50]. However, following a twelve week washout the baseline values of HCY were within normal limits and the same as controls. By significantly lowering HCY, the administration of short-term rhGH would appear to have exerted a beneficial effect on any adverse effect that sustained elevated HCY might cause.

The vascular protective role of IGF-I has been suggested because of its ability to stimulate NO production from endothelial and vascular smooth muscle cells [51]. IGF-I may also play a role in aging, atherosclerosis and cerebrovascular disease. Just as an excess of GH and IGF-I can cause unfavourable cardiovascular effects [11, 32] so too in cross sectional studies, low GH and IGF-I levels have been associated with unfavourable CVD risk factors, such as abnormal lipoprotein levels and hypertension [51]. In prospective studies, lower IGF-I levels predict future development of ischaemic heart disease [51].

Conclusion. The aim of the present study was to evaluate measurements of PIIINP, following short-term rhGH administration, as a diagnostic tool in relation to endothelial function. Despite the increase in PIIINP there was an improvement in APWV and CVD risk factors consistent with recent research [52]. We postulate that, over a longer period of time, an elevated PIIINP may ultimately have an adverse effect on endothelial structure and function and predict a future breakdown of the endothelium. We believe that such findings preclude the use of rhGH as either an adjunctive therapy in gender hormone replacement therapy (andropause and menopause) or as a solitary treatment of the somatopause.

ACKNOWLEDGEMENTS

The design, execution, data handling, interpretation, and manuscript preparation were entirely the responsibility of the authors. We would like to acknowledge the contribution of Professors Andrew Kicman and David Cowan from the Drug Control Centre, King's College London, in the analysis of IGF-I, PIIINP and urine steroid screen and the contribution of Professor Martin Bidlingmaier for the two immunofluorometric assays for analysis of the GH isoforms.

REFERENCES

- [1] Jensen LT, Hørslev-Petersen K, Toft P et al. Serum aminoterminal type III procollagen peptide reflects repair after acute myocardial infarction. *Circulation* 1990; 81:52–57.
- [2] Høst NB, Jensen LT, Bendixen PM et al. The aminoterminal propeptide of type III procollagen provides new information on prognosis after acute myocardial infarction. *Am J Cardiol* 1995; 76: 869–873.
- [3] Poulsen SH, Høst NB, Jensen SE et al. Relationship between serum amino-terminal propeptide of type III procollagen and changes of left ventricular function after acute myocardial infarction. *Circulation* 2000; 101: 1527–1532.
- [4] Rossi A, Ciccoira M, Golia G et al. Amino-terminal propeptide of type III procollagen is associated with restrictive mitral filling pattern in patients with dilated cardiomyopathy: a possible link between diastolic dysfunction and prognosis. *Heart* 2004; 90: 650–654.
- [5] Safdar Z, Tamez E, Chan W et al. Circulating collagen biomarkers as indicators of disease severity in pulmonary arterial hypertension. *JACC Heart Fail* 2014; 2: 412-421.
- [6] Lee CH, Lee WC, Chang SH et al. The N-Terminal Propeptide of Type III Procollagen in Patients with Acute Coronary Syndrome: A Link between Left Ventricular End-Diastolic Pressure and Cardiovascular Events. *PLoS One* 2015; 10(1): e114097, doi:10.1371/journal.pone.0114097.
- [7] Ghorpade A, Baxter BT. Biochemistry and molecular regulation of matrix macromolecules in abdominal aortic aneurysms. *Ann N Y Acad Sci* 1996; 18: 138-150.
- [8] Treska V, Topolcan O. “Plasma and tissue levels of collagen types I and III markers in patients with abdominal aortic aneurysms”. *Int Angiol* 2000; 19: 64-68.
- [9] Ihara A, Kawamoto T, Matsumoto K et al. Relationship between hemostatic markers and circulating biochemical markers of collagen metabolism in patients with aortic aneurysm. *Pathophysiol Haemost Thromb* 2003; 33: 221-224.
- [10] Verde GG, Santi I, Chiodini P et al. Serum type III procollagen propeptide levels in acromegalic patients. *J Clin Endocrinol Metab* 1986; 63: 1406-1410.
- [11] Lombardi G, Galdiero M, Auriemma RS et al. Acromegaly and the cardiovascular system. *Neuroendocrinology* 2006; 83: 211-2177.
- [12] Cittadini A, Cuocolo A, Merola B et al. Impaired cardiac performance in GH-deficient adults and its improvement after GH replacement. *Am J Physiol* 1994; 267: E219- E225.

- [13] Pfeifer M, Verhovec R, Zizek B et al. Growth hormone (GH) treatment reverses early atherosclerotic changes in GH-deficient adults, *J Clin Endocrinol Metab* 1999; 84: 453-457.
- [14] Smith JC, Evans LM, Wilkinson I et al. Effects of GH replacement on endothelial function and large-artery stiffness in GH-deficient adults: a randomized, double-blind, placebo-controlled study, *Clin Endocrinol* 2002; 56: 493-501.
- [15] Napoli R, Guardasole V, Matarazzo M et al. Growth hormone corrects vascular dysfunction in patients with chronic heart failure. *J Am Coll Cardiol* 2002; 39: 90-95.
- [16] Holt RI, Erotokritou-Mulligan I, McHugh C et al. The GH-2004 project: the response of IGF1 and type III pro-collagen to the administration of exogenous GH in non-Caucasian amateur athletes, *Eur J Endocrinol* 2010; 163: 45-54.
- [17] Velloso CP, Aperghis M, Godfrey R et al. The effects of two weeks of recombinant growth hormone administration on the response of IGF-I and N-terminal pro-peptide of collagen type III (P-III-NP) during a single bout of high resistance exercise in resistance trained young men. *Growth Horm IGF Res* 2013; 23: 76-80.
- [18] Pronk NP. Short term effects of exercise on plasma lipids and lipoproteins in humans. *Sports Med* 1993; 16: 431-448.
- [19] Ahokoski O, Virtanen A, Huupponen R et al. Biological day- to-day variation and daytime changes of testosterone, follitropin, lutropin and oestradiol-17b in healthy men. *Clin Chem Lab Med* 1998; 36: 485-491.
- [20] Wu Z, Bidlingmaier M, Dall R et al. Detection of doping with human growth hormone. *Lancet* 1999; 13: 895.
- [21] Goldman F, Buskirk ER. Body volume measurement by underwater weighing: description of a technique. in: Brozek, Henschel (eds.) 1961; 78-89.
- [22] Wilmore JH. The use of actual, predicted and constant residual volumes in the assessment of body composition by underwater weighing". *Med Sci Sports Exerc* 1969; 1: 87.
- [23] Siri WE. Body composition from fluid spaces and density: analysis of methods, in: J. Brozek, A. Henschel (Eds.), *Techniques for Measuring Body Composition. National Academy of Sciences/National Research Council, Washington, DC* 1961; 223-224.
- [24] Mattace-Raso F, Hofman A, Verwoert GC et al. Determinants of pulse wave velocity in healthy people and in the presence of cardiovascular risk factors: 'establishing normal and reference values'. *Eur Heart J* 2010; 31: 2338-2350.
- [25] Fletcher GF, Blair SN, Blumenthal J et al. Statement on exercise. Benefits and recommendations for physical activity programs for all Americans, a statement for health professionals by the committee on exercise and cardiac rehabilitation of the council on clinical cardiology, American heart association. *Circulation* 1992; 86: 340-344.
- [26] Pickering TG, Hall JE, Appel LJ et al. Council on High Blood Pressure Research Professional and Public Education Subcommittee, American Heart Association. Recommendations for blood pressure measurement in humans: an AHA scientific statement from the Council on High Blood Pressure Research Professional and Public Education Subcommittee. *J Clin Hypertens (Greenwich)* 2005; 7: 102-109.
- [27] Altman DG. How large a sample? In *Statistics in Practice* (eds. SM Gore and DG Altman), London, British Medical Association 1982; 6-8.
- [28] Ghigo E, Aimaretti G, Maccario M et al. Dose-response study of GH effects on circulating IGF-I and IGFBP-3 levels in healthy young men and women. *Am J Physiol Endocrinol Metab* 1999; 276: 69-13.
- [29] Fraser CG, Fogarty Y. Interpreting laboratory results. *Br Med J* 1989; 298: 1659-1660.
- [30] Healy ML, Gibney J, Russell-Jones DL et al. High Dose Growth Hormone Exerts an Anabolic Effect at Rest and during Exercise in Endurance-Trained Athletes. *J Clin Endocrinol Metab* 2003; 11: 5221-5226.
- [31] Melmed S. Medical progress: Acromegaly. *N Engl J Med* 2006; 14: 2558-2573.
- [32] Ciulla MM, Epaminonda P, Paliotti R et al. Evaluation of cardiac structure by echoreflectivity analysis in acromegaly: effects of treatment. *Eur J Endocrinol* 2004; 151: 179-186.
- [33] Cecelja M, Chowienczyk P. Dissociation of aortic pulse wave velocity with risk factors for cardiovascular disease other than hypertension: a systematic review. *Hypertension* 2009; 54: 1328-1336.
- [34] Ramsey MW, Goodfellow J, Jones CJ et al. Endothelial control of arterial distensibility is impaired in chronic heart failure. *Circulation* 1995; 92: 3212-3219.
- [35] Anagnostis P, Efstathiadou ZA, Gougoura S et al. Oxidative stress and reduced antioxidative status, along with endothelial dysfunction in acromegaly. *Horm Metab Res* 2013; 45: 314-318.
- [36] Wu D, Hu Q, Ma F et al. Vasorelaxant Effect of a New Hydrogen Sulfide-Nitric Oxide Conjugated Donor in Isolated Rat Aortic Rings through cGMP

- Pathway. *Oxid Med Cell Longev* 2016; 7075682. doi: 10.1155/2016/7075682.
- [37] Materazzi S, Zagli G, Nassini R et al. Vasodilator activity of hydrogen sulfide (H₂S) in human mesenteric arteries. *Microvasc Res* 2017; 109:38-44.
- [38] Powrie JK, Bassett EE, Rosen T et al. GH-2000 Project Study Group. Detection of growth hormone abuse in sport. *Growth Horm IGF Res* 2007; 17: 220-226.
- [39] Hoffman DM, Crampton L, Sernia C et al. Short term growth hormone (GH) treatment of GH deficient adults increases body sodium and extracellular water, but not blood pressure. *J Clin Endocrinol Metab* 1996; 81: 1123-1128.
- [40] Møller J, Jørgensen JO, Møller N et al. Expansion of extracellular volume and suppression of atrial natriuretic peptide after growth hormone administration in normal man. *Metabolic Effects of Growth Hormone in Humans. J Clin Endocrinol Metab* 1991; 72: 768-772.
- [41] Ronconi V, Giacchetti G, Mariniello B et al. Reduced nitric oxide levels in acromegaly: cardiovascular implications. *Blood Pressure* 2005; 14: 227-232.
- [42] Nyström HC, Klintland N, Caidahl K et al. Short-term administration of growth hormone (GH) lowers blood pressure by activating eNOS/nitric oxide (NO)-pathway in male hypophysectomized (Hx) rats. *BMC Physiol* 2005; 5: 17.
- [43] Graham MR, Baker JS, Evans P et al. Evidence for a decrease in cardiovascular risk factors following recombinant growth hormone administration in abstinent anabolic-androgenic steroid users. *Growth Horm IGF Res* 2007; 17: 201-209.
- [44] Ndrepepa G, Braun S, Tada T et al. Comparative prognostic value of C-reactive protein & fibrinogen in patients with coronary artery disease. *Indian J Med Res* 2014; 140: 392-400.
- [45] Jae SY, Yoon ES, Jung SJ et al. Effect of cardiorespiratory fitness on acute inflammation induced increases in arterial stiffness in older adults. *Eur J Appl Physiol* 2013; 113: 2159-2166.
- [46] Talikoti P, Bobby Z, Hamide A. Hyperhomocysteinemia, Insulin Resistance and High HS-CRP Levels in Prehypertension. *J Clin Diagn Res* 2014; 8: CC07- CC09.
- [47] Lane HA, Grace F, Smith JC et al. Impaired vasoreactivity in bodybuilders using androgenic anabolic steroids. *Eur J Clin Invest* 2006; 36: 483-488.
- [48] Graham MR, Grace FM, Boobier W et al. Homocysteine induced cardiovascular events: a consequence of long term anabolic-androgenic steroid (AAS) abuse. *Br J Sports Med* 2006; 40: 644-648.
- [49] Graham MR, Baker JS, Davies B. Causes and Consequences of Obesity: Epigenetics and Hypokinesia? *Diabetes, Metabolic Syndrome and Obesity: Targets and Therapy* 2015; 8: 455-460.
- [50] Zhou S, Zhang Z, Xu G. Notable epigenetic role of hyperhomocysteinemia in atherogenesis. *Lipids Health Dis* 2014; 13:134.
- [51] Jin C, Guo J, Qiu X, Ma K et al. IGF-1 induces iNOS expression via the p38 MAPK signal pathway in the anti-apoptotic process in pulmonary artery smooth muscle cells during PAH. *J Recept Signal Transduct Res* 2014; 34: 325-31.
- [52] Manhenke C, Ueland T, Jugdutt BI et al. The relationship between markers of extracellular cardiac matrix turnover: infarct healing and left ventricular remodelling following primary PCI in patients with first-time STEMI. *Eur Heart* 2014; 35: 395-402.

Demographic characteristics of the subjects are presented in table 1.

Table.1: Subject demographics.

Variables	Control Group (C)			Administration Group			
	Day	1	7	14	(PRE-rhGH)	(on-rhGH)	(POST-rhGH)
BM (kg)		89.8 ± 12.7	89.6 ± 12.6	89.5 ± 12.7	86.1 ± 12	86.7 ± 12.1	85.5 ± 11.8**
BMI (kg.m ⁻²)		28 ± 3.1	27.9 ± 3.1	27.9 ± 3.1	27.5 ± 3.0	27.7 ± 3.1	27.3 ± 3.0**
Body Fat %		21.9 ± 3.8	21.7 ± 3.8	21.6 ± 4.0	20.0 ± 6.0	19.0 ± 6.0*	19.1 ± 5.8*
RT (years.)		12.2 ± 3.6	12.2 ± 3.6	12.2 ± 3.6	12.2 ± 3.6	12.2 ± 3.6	12.2 ± 3.6
WT (no.week)		4.4 ± 1.1	4.4 ± 1.1	4.4 ± 1.1	4.4 ± 1.1	4.4 ± 1.1	4.4 ± 1.1
TT (mins.)		47 ± 15	47 ± 15	47 ± 15	47 ± 15	47 ± 15	47 ± 15
Energy Intake (KJ.day ⁻¹)		18050 ± 4100	18100 ± 2020	18175 ± 3100	17900 ± 3020	18450 ± 3900	18100 ± 2020
Protein Intake (g.day ⁻¹)		205 ± 60	195 ± 55	213 ± 45	207 ± 35	217 ± 65	210 ± 50

Training history for control (C) group v growth hormone (rhGH) group.

Results are presented as means \pm Standard Deviations (SD)

BM = Body mass; **BMI** = Body mass index; **FFMI** = Fat free mass index; **RT** = Resistance training; **WT** = Weight training; **TT** = Training time.

* = $P < 0.017$ = significantly different to **PRE-rhGH**; ** = $P < 0.017$ = significantly different to **on-rhGH**

Values for Cardiovascular responses are presented in table 2.

Table.2: Arterial Pulse Wave Velocity & Heart Rate and Blood Pressure Responses.

Variables	Control Group (C)			Administration Group			
	Day	1	7	14	(PRE-rhGH)	(on-rhGH)	(POST-rhGH)
UL-PRE-OCC-V (m.s ⁻¹)		8.76 \pm 1.80	8.88 \pm 1.69	8.91 \pm 1.90	9.21 \pm 1.93	8.69 \pm 1.17	8.49 \pm 1.08
UL-POST-OC-V (m.s ⁻¹)		8.31 \pm 1.76	8.67 \pm 1.54	8.63 \pm 1.69	8.96 \pm 1.80	8.65 \pm 1.41	8.27 \pm 0.94
LL-PRE-OCC-V (m.s ⁻¹)		9.64 \pm 1.62	9.79 \pm 1.50	9.75 \pm 1.54	9.97 \pm 1.38	9.18 \pm 1.60*	9.26 \pm 1.52*
LL-POST-OC-V (m.s ⁻¹)		9.28 \pm 1.45	9.48 \pm 1.26	9.37 \pm 1.26	9.84 \pm 1.84	9.27 \pm 1.33	9.35 \pm 1.49
HR-rest (bpm)		66 \pm 16	67 \pm 16	67 \pm 14	72 \pm 14	78 \pm 11†	75 \pm 18
SBP-rest (mm.Hg)		125 \pm 12	124 \pm 12	125 \pm 11	126 \pm 10	125 \pm 12	122 \pm 9

APWV (m.s⁻¹) responses for control (C) group v growth hormone (rhGH) group.

Figures are presented as means \pm Standard Deviations (SD).

UL-PRE-OCC-V = Upper Limb Pre-occlusion Velocity;

UL-POST-OC-V = Upper Limb Post-occlusion Velocity;

LL-PRE-OCC-V = Lower Limb Pre-occlusion Velocity;

LL-POST-OC-V = Lower Limb Post-occlusion Velocity.

Heart rate (**HR**, bpm), Systolic Blood Pressure (**SBP**, mm.Hg),

Rate Pressure Product (**RPP**, bpm. x mm.Hg x 10⁻²) responses, for control (C) group v growth hormone (rhGH) group.

Figures are presented as means \pm Standard Deviations (SD).

-rest = Resting.

† = $P < 0.05$ = significantly different to C

* = $P < 0.017$ = significantly different to **PRE-rhGH**

Serum analytes associated with cardiovascular disease (CVD) are presented in table 3.

Table.3: Serum analytes associated with cardiovascular disease.

Variables	Control Group (C)			Administration Group			
	Day	1	7	14	(PRE-rhGH)	(on-rhGH)	(POST-rhGH)
T (nmol.L ⁻¹)		17.5 \pm 5.2	17.5 \pm 5.6	17.4 \pm 5.4	16.2 \pm 6.0	15.3 \pm 5.7	14.5 \pm 5.0
Na ⁺ (mmol.L ⁻¹)		139.6 \pm 8.4	141.5 \pm 3.1	140.5 \pm 5.8	140.6 \pm 2.7	142 \pm 2.4*	142 \pm 2.4*
hsCRP(mg.L ⁻¹)		1.35 \pm 1.9	1.38 \pm 2.1	1.44 \pm 2.1	1.77 \pm 2.1	1.29 \pm 1.6*	1.7 \pm 2.8
HCY (μ mol.L ⁻¹)		12.5 \pm 4.2	13.3 \pm 4.7	13.1 \pm 4.1	13.2 \pm 4.0	11.7 \pm 3.1*	13.1 \pm 4.3
TG (mmol.L ⁻¹)		1.0 \pm 0.4	1.1 \pm 0.5	1.1 \pm 0.4	1.2 \pm 0.5	1.1 \pm 0.6	1.4 \pm 0.9

HDL (mmol.L ⁻¹)	1.2 ± 0.4	1.3 ± 0.3	1.2 ± 0.3	1.2 ± 0.3	1.2 ± 0.2	1.2 ± 0.3
LDL (mmol.L ⁻¹)	2.7 ± 0.8	2.8 ± 0.8	2.8 ± 1.0	2.9 ± 0.9	2.7 ± 0.7	2.9 ± 0.9
TC (mmol.L ⁻¹)	4.4 ± 1.0	4.6 ± 0.9	4.5±1.1	4.7±0.9	4.4 ± 0.7*	4.7 ± 1.0
IGF-I (ng.mL ⁻¹)	179 ± 47	169 ± 50	175 ± 53	159 ± 54	323±93*†‡	175 ± 61
PIIINP (U/ml)	0.32 ± 0.1	0.30 ± 0.1	0.32 ± 0.1	0.28 ± 0.1	0.42 ± 0.2*†‡	0.35 ± 0.1*

Serum analytes responses for control (C) group v growth hormone (GH) group.

Figures are presented as means ± Standard Deviations (SD)

T = Testosterone; **hsCRP** = high sensitivity C-reactive Protein; **HCY** = Homocysteine; **TG** = Triglycerides;

HDL = High Density Lipoprotein; **LDL** = Low Density Lipoprotein; **TC** = Total Cholesterol;

IGF-I = Insulin-like growth factor-I; **PIIINP** = Amino-terminal propeptide of type III procollagen.

* = $P < 0.017$ = significantly different to **PRE-rhGH**;

† = $P < 0.017$ = significantly different to **POST-rhGH**;

‡ = $P < 0.05$ = significantly different to **C**.

Data modeling diagnostics for share price performance of Islamic Bank in Malaysia using Computational Islamic Finance approach

Nashirah Abu Bakar¹, Sofian Rosbi²

¹Islamic Business School, College of Business, Universiti Utara Malaysia, 06010 Sintok, Kedah, Malaysia

²School of Mechatronik Engineering, Universiti Malaysia Perlis, 02600 Arau, Perlis, Malaysia

Abstract— *Bank Islam Malaysia Berhad is an institution that offers financing activity that complies with shariah (Islamic law) and its practical application through the development of Islamic economics. The objective of this study is to forecast the performance of share price for Islamic Bank in Malaysia. The method implemented in this study is autoregressive integrated moving average (ARIMA). From the analysis, there are two model of ARIMA that developed which are ARIMA (3,1,3) and ARIMA(3,1,4). The model of ARIMA (3,1,4) show larger value of R-squared and lower absolute value of Akaike info criterion (AIC). In addition, the mean absolute percentage error (MAPE) is 0.85% in ex-post data range. This results indicates ARIMA (3,1,4) is a reliable forecasting model. The findings from this study will help investors to select a better portfolio for their investment decision in order to gain better profits. In addition, the findings of this study also will help economists to understand the future condition of economic scenario in Malaysia.*

Keywords— *Islamic banking, Islamic finance, ARIMA model, Share price, Malaysia*

I. INTRODUCTION

The main objective of establish Islamic banking system is to provide a products and services according to *shariah* law. *Shariah* is referring to activities that follow Islamic law. All the transaction must be free from the prohibited element such as *riba*, *gharar* and *maisir*. The main source in Islamic law is Al-Quran and As-Sunnah.

The history of development Islamic banking in Malaysia was started with the establishment of Pilgrim Hajj (Tabung Haji) in 1969. Then, Bank Islam Malaysia Berhad (BIMB) was established in 1983. Since Malaysia was established Islamic banking system, the development of Islamic finance and banking was growth rapidly. According to the Asian Banker Research Group, the World's 100 largest Islamic banks have set an annual asset growth rate of 26.7% and the global Islamic Finance industry is experiencing average growth of 15-20%

annually. Thus, it is important to Muslim peoples to support Islamic banking products and services.

Many researches study the outstanding performance of Islamic bank in Malaysia such as Ab Rahim et al. (2013)[1]. They found that average the main contributor of cost efficiency for Islamic domestic and foreign banks in Malaysia is allocated efficiency. Sufian (2007) found the domestic Islamic banks were more efficient compared to the foreign Islamic banks [2]. Even though, the development of Islamic bank in Malaysia show the outstanding growth but the demand for Islamic banking products and services are less than conventional bank. Thus it is important to analyze the performance of Islamic banking system in Malaysia market in order to encourage more investors' especially Muslim investors to invest in *shariah*-compliant shares.

Therefore, the main objective of this study is to forecast the performance of share price for Islamic Bank in Malaysia. This study chooses Bank Islam Malaysia Berhad (BIMB) because BIMB is the first Islamic bank in Malaysia. This research gives a new insight to investors and practitioners regarding the dynamic behavior of investment portfolio.

II. LITERATURE REVIEW

Stock price prediction is an important topic in finance and economics which has spurred the interest of researchers over the years to develop better predictive models (Adebiyi, et al, 2014)[3]. There are many methods used in prediction analysis. One of the famous methods is ARIMA model. ARIMA also known as Box-Jenkins method is a process of set an activity for identifying, estimating and diagnosing using time series data.

Various studies on ARIMA model are used by researchers to forecast the future value. The available literature such as the predictability of the Amman Stock Exchange using ARIMA Model by Al-Shiab (2014)[4], real estate market by Stevenson (2007)[5], currency by Balli and Elsamadisy (2012)[6] the construction industry and

economy by Lam and Oshodi (2016)[7] and housing price by Jadevicius and Huston (2015[8]).

Abu Bakar and Rosbi (2017)[9] analyzing the currency exchange rate between Malaysian Ringgit and United State Dollar and found that the ARIMA (1, 1, 1) is suitable for clustering the data between January 2010 until April 2017. While Nochai and Nochai (2006) [10] found the ARIMA Model for forecasting farm price of oil palm is ARIMA (2,1,0).

III. RESEARCH METHODOLOGY

This paper forecast the performance of share price for Islamic Bank in Malaysia. The method implemented in this study is autoregressive integrated moving average (ARIMA).

3.1 Data selection

Bank Islam Malaysia Berhad (BIMB) is the first institution that offers Islamic Banking in Malaysia. Therefore, the objective this study is to evaluate the performance of the share price for BIMB. The performance of the share price is selected from January 2010 until June 2017 (90 observations).

3.2 Forecasting statistical method

This study forecast the performance of share price using the statistical procedure as shown in Fig. 1. The forecasting process is start with the identification of the data model using autoregressive integrated moving average (ARIMA).

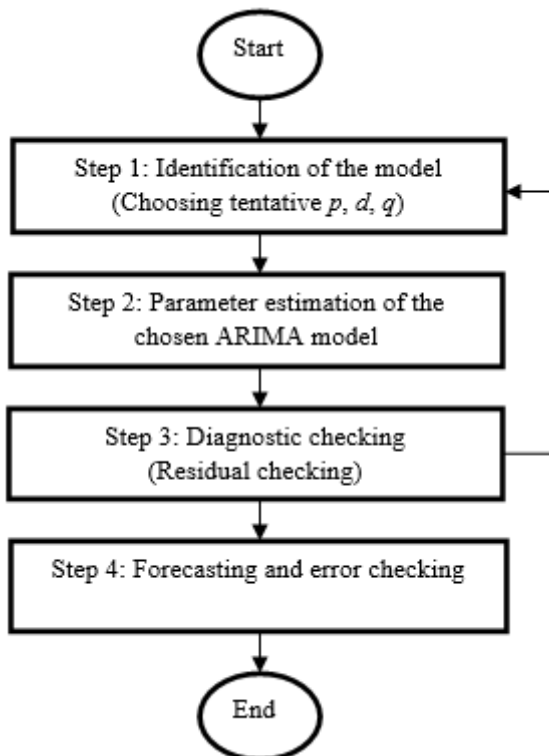


Fig. 1: Statistical forecasting procedure

Then, this research need to develop estimation of the parameter for chosen ARIMA model. In validating the model, diagnostics checking need to be developed. The residual is the difference between the observed value and the estimated value of the quantity of interest (sample mean). The residual should be uncorrelated, zero mean and zero variance. Then, forecasting and error checking stage can be performed.

3.3 Mathematical procedure of autoregressive integrated moving average (ARIMA)

In statistics, autoregressive integrated moving average (ARIMA) procedure provides the identification, parameter estimation, and forecasting of autoregressive integrated moving average model.

The AR part of ARIMA indicates that the evolving variable of interest is regressed on its own lagged values. The MA part indicates that the regression error is actually a linear combination of error terms whose values occurred contemporaneously and at various times in the past. The I (integrated) indicates that the data values have been replaced with the difference between their values and the previous values. The purpose of each of these features is to make the model fit the data as well as possible.

The autoregressive integrated moving average ARIMA (p, d, q) model is represented by Eq. (1).

$$\left(1 - \sum_{i=1}^p \phi_i L^i\right) (1-L)^d X_t = \delta + \left(1 + \sum_{i=1}^q \theta_i L^i\right) \varepsilon_t \quad (1)$$

where L is the lag operator, ϕ_i are the parameters of the autoregressive part of the model, θ_i are the parameters of the moving average part and ε_t are error terms. The error terms ε_t are generally assumed to be independent, identically distributed variables sampled from a normal distribution with zero mean

ARIMA models are generally denoted ARIMA (p, d, q) where parameters p, d, and q are non-negative integers, p is the order (number of time lags) of the autoregressive model, d is the degree of differencing (the number of times the data have had past values subtracted), and q is the order of the moving-average model.

In this study, the degree of differencing is set to one. The purpose of this step is to confirm the stationarity of the data. Therefore Eq. (1) can be represented as below:

$$\Delta X_t = \delta + \varepsilon_t + \sum_{i=1}^q \theta_i \varepsilon_{t-i} + \sum_{i=1}^p \phi_i \Delta X_{t-i} \quad (2)$$

3.3 Autocorrelation function(ACF) statistical method

Autocorrelation, also known as serial correlation, is the correlation of a signal with a delayed copy of itself as a function of delay.

The autocorrelation of a random process is the Pearson correlation between values of the process at different

times, as a function of the two times or of the time lag. Let X is set as a stochastic process, and t is any point in time (t may be an integer for a discrete-time process or a real number for a continuous-time process). Then X_t is the value (or realization) produced by a given run of the process at time t . Consider the process has mean μ_t and variance σ_t^2 at time t , for each t . Then the definition of the autocorrelation between times s and t is described in below equation:

$$R(s, t) = \frac{E[(X_t - \mu_t)(X_s - \mu_s)]}{\sigma_t \sigma_s} \quad (3)$$

If X_t is a stationary process, then the mean μ and the variance σ^2 are time-independent, and further the autocorrelation depends only on the lag between t and s : the correlation depends only on the time-distance between the pair of values but not on their position in time. This further implies that the autocorrelation can be expressed as a function of the time-lag, and that this would be an even function of the lag $\tau = s - t$. This gives the more familiar form in Equation (4).

$$R(\tau) = \frac{E[(X_t - \mu)(X_{t+\tau} - \mu)]}{\sigma^2} \quad (4)$$

3.4 Partial autocorrelation function (PACF) statistical method

Partial correlation is a measure of the strength and direction of a linear relationship between two continuous variables whilst controlling for the effect of one or more other continuous variables (also known as 'covariates' or 'control' variables).

Formally, the partial correlation between X and Y given a set of n controlling variables $\mathbf{Z} = \{Z_1, Z_2, \dots, Z_n\}$, written $\rho_{XY \cdot \mathbf{Z}}$, is the correlation between the residuals R_X and R_Y resulting from the linear regression of X with \mathbf{Z} and of Y with \mathbf{Z} , respectively. The first-order partial correlation (i.e. when $n=1$) is the difference between a correlation and the product of the removable correlations divided by the product of the coefficients of alienation of the removable correlations.

Partial autocorrelation function is described in below Equation (5).

$$\hat{\rho}_{XY \cdot \mathbf{Z}} = \frac{N \sum_{i=1}^N r_{X,i} r_{Y,i} - \sum_{i=1}^N r_{X,i} \sum_{i=1}^N r_{Y,i}}{\sqrt{N \sum_{i=1}^N r_{X,i}^2 - \left(\sum_{i=1}^N r_{X,i} \right)^2} \sqrt{N \sum_{i=1}^N r_{Y,i}^2 - \left(\sum_{i=1}^N r_{Y,i} \right)^2}}$$

IV. RESULT AND DISCUSSION

This section described the findings of stationary process, ARIMA model estimation process, residual diagnostics process and forecasting process.

4.1 Dynamic behavior analysis of share price

This study involved the monthly data of share price for Bank Islam Malaysia Berhad (BIMB). The selected data is collected from January 2010 until June 2017. This analysis involved 90 observations. Figure 1 shows the share price dynamic movement for Bank Islam Malaysia Berhad (BIMB). The maximum value of share price is MYR 4.622 in October 2013. The minimum value of share price is MYR 1.161 in February 2010.

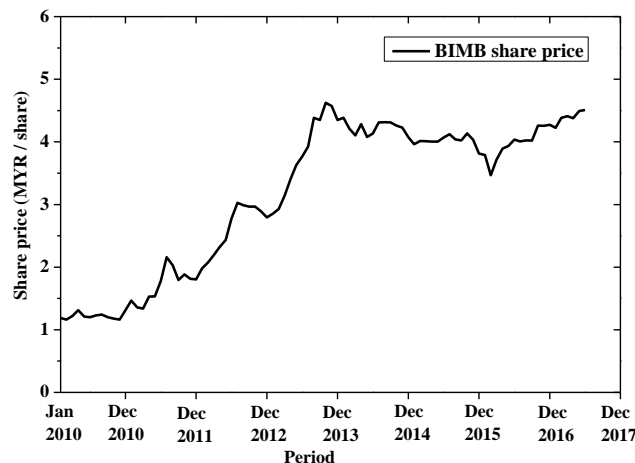


Fig. 2: Share price dynamic movement of BIMB

Next, this study performed the autocorrelation and partial correlation. Figure 2 shows the result of autocorrelation and partial correlation of share price. From Fig. 2, there is slow decay of autocorrelation number. Therefore, the data of share price is a non-stationary data. Statistical non-stationary is defined as statistical properties such as mean, variance are not constant over time.

Sample: 2010M01 2017M12 Included observations: 90						
	Autocorrelation	Partial Correlation	AC	PAC	Q-Stat	Prob
1	0.970	0.970	87.571	0.000		
2	0.937	-0.073	170.18	0.000		
3	0.904	-0.10	247.95	0.000		
4	0.868	-0.065	320.54	0.000		
5	0.832	-0.017	388.02	0.000		
6	0.798	0.007	450.78	0.000		
7	0.762	-0.042	508.75	0.000		
8	0.728	0.002	562.22	0.000		
9	0.693	-0.026	611.33	0.000		
10	0.660	0.014	656.45	0.000		
11	0.627	-0.036	697.65	0.000		
12	0.593	-0.030	734.96	0.000		
13	0.557	-0.053	768.32	0.000		
14	0.517	-0.090	797.46	0.000		
15	0.475	-0.054	822.37	0.000		

Fig. 3: Autocorrelation and partial correlation analysis

4.2 Stationary transformation of share price

Next, share price is needed to be transforming to be a stationary in order to apply ARIMA model. Figure 3 shows the data of share price with first difference. Figure 3 shows the mean and variance is constant over time. Mean value for the first difference of share price is

0.0373. Meanwhile, standard deviation for first difference of share price is 0.13967.

Figure 4 shows the histogram for first difference of share price. The result shows the distribution of the data is follow normal distribution. This finding is validated with statistical normality test namely Shapiro-Wilk test as shown in Table 1. The findings in Table 1 shows the probabilities is 0.265 which is larger than 0.05. Therefore, the distribution of first difference of share price is not significantly different from normal distribution. Therefore, first difference of share price is stationary data.

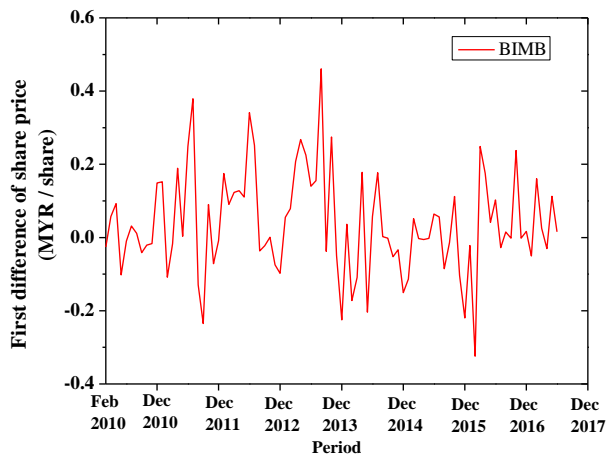


Fig. 4: First difference of share price

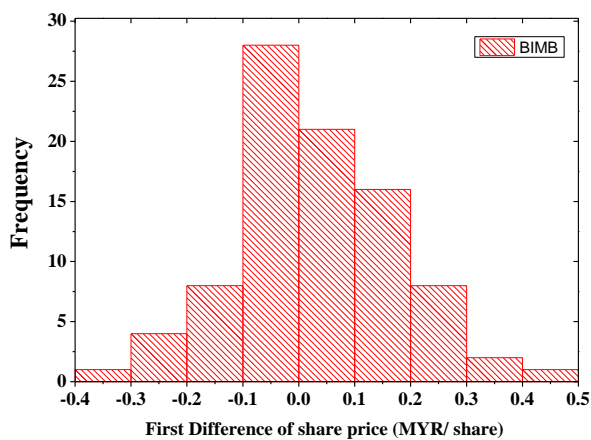


Fig. 5: Histogram for first difference of share price

Table 1: Statistical normality test

	Shapiro-Wilk		
	Statistic	df	Sig.
D_share_price	.982	89	.265

4.3 Autoregressive integrated moving average (ARIMA) model estimation

This section describes the selection of appropriate ARIMA model for modeling the data. Figure 5 shows the autocorrelation and partial correlation analysis for first difference of share price. From the analysis, there are two

model of ARIMA that developed from this analysis which are ARIMA(3,1,3) and ARIMA(3,1,4).

Then, this study performed reliability test for ARIMA(3,1,3) and ARIMA(3,1,4). Table 2 shows the R-squared value and Akaike info criterion (AIC) for each of the ARIMA model. From this result, ARIMA (3,1,4) show larger value of R-squared and lower absolute value of Akaike info criterion (AIC). Residual diagnostics result is described in Fig. 6. Result shows there is no significant residual. This indicates the residuals is white noise for ARIMA(3,1,4). Therefore, ARIMA (3,1,4) is reliable data modeling for share price of BIMB.

Figure 7 shows the estimation of parameters for ARIMA (3,1,4). The equation for ARIMA (3,1,4) defined as Equation (6).

$$\Delta y_t = c + \phi_1 \Delta y_{t-1} + \phi_2 \Delta y_{t-2} + \phi_3 \Delta y_{t-3} + \theta_1 \varepsilon_{t-1} + \theta_2 \varepsilon_{t-2} + \theta_3 \varepsilon_{t-3} + \theta_4 \varepsilon_{t-4} + \varepsilon_t$$

$$\Delta y_t = 0.037152 + (-0.598733) \Delta y_{t-1} + (-0.710547) \Delta y_{t-2} + (-0.490745) \Delta y_{t-3} + (0.781313) \varepsilon_{t-1} + (0.888097) \varepsilon_{t-2} + (0.883007) \varepsilon_{t-3} + (0.079593) \varepsilon_{t-4} + 0.016326$$

Sample: 2010M01 2017M12 Included observations: 89						
Autocorrelation	Partial Correlation	AC	PAC	Q-Stat	Prob	
1		1	0.161	0.161	2.3862	0.122
2		0.067	0.042	2.8058	0.246	
3		0.217	0.205	7.2364	0.065	
4		-0.155	-0.237	9.5362	0.049	
5		-0.072	-0.026	10.038	0.074	
6		0.021	0.006	10.083	0.121	
7		-0.127	-0.047	11.667	0.112	
8		-0.117	-0.114	13.042	0.110	
9		-0.045	-0.032	13.248	0.152	
10		-0.043	0.026	13.435	0.200	

Fig. 6: Autocorrelation and partial correlation analysis

Table 2: Statistical normality test

ARIMA (p,d,q)	R-squared	Akaike info criterion (AIC)
(3,1,3)	0.1503	-1.0766
(3,1,4)	0.1537	-1.0553

Sample: 2010M01 2017M06 Included observations: 89 Q-statistic probabilities adjusted for 7 ARMA terms						
Autocorrelation	Partial Correlation	AC	PAC	Q-Stat	Prob	
1		0.005	0.005	0.0019		
2		0.029	0.029	0.0827		
3		0.062	0.061	0.4391		
4		-0.026	-0.028	0.5055		
5		-0.028	-0.032	0.5826		
6		-0.005	-0.007	0.5851		
7		-0.148	-0.144	2.7615		
8		-0.045	-0.042	2.9616	0.085	
9		-0.003	0.004	2.9628	0.227	
10		-0.076	-0.059	3.5618	0.313	
11		0.108	0.110	4.7790	0.311	
12		0.176	0.178	8.0411	0.154	
13		0.178	0.192	11.408	0.077	
14		0.047	0.015	11.649	0.113	
15		0.081	0.046	12.368	0.136	

Fig. 7: Autocorrelation and partial correlation analysis

Variable	Coefficient	Std. Error	t-Statistic	Prob.
C	0.037152	0.019448	1.910326	0.0597
AR(1)	-0.598733	0.541031	-1.106653	0.2718
AR(2)	-0.710547	0.143177	-4.962715	0.0000
AR(3)	-0.490745	0.381166	-1.287483	0.2016
MA(1)	0.781313	0.536539	1.456210	0.1492
MA(2)	0.888097	0.256829	3.457926	0.0009
MA(3)	0.883007	0.442127	1.997180	0.0492
MA(4)	0.079593	0.302026	0.263530	0.7928
SIGMASQ	0.016326	0.002318	7.043308	0.0000
R-squared	0.153652	Mean dependent var		0.037305
Adjusted R-squared	0.069018	S.D. dependent var		0.139673
S.E. of regression	0.134767	Akaike info criterion		-1.055355

Fig. 8: Autocorrelation and partial correlation analysis

4.4 Forecasting error diagnostics (ex-post data range)

In this section, this research using ARIMA (3,1,4) for evaluating the reliability of forecasting. The period involved in this diagnostics is starting from January 2017 until June 2017 as stated in Table 3.

Table 3 shows the error of forecasting that calculated from the differences between actual data and forecast data. The mean absolute percentage error (MAPE) is 0.85%. This value is small and it indicates ARIMA (3,1,4) is a reliable forecasting model .

Figure 8 shows the value of actual data, forecast value including forecasting range of two standard errors.

Table 3: Forecasting error diagnostics

Period	Actual data	Forecast data	Error	Error (%)
Jan. 2017	4.223	4.343	-0.120	-2.8
Feb. 2017	4.384	4.366	+0.018	+0.4
March 2017	4.409	4.411	-0.002	0.0
April 2017	4.379	4.439	-0.060	-1.4
May 2017	4.492	4.483	+0.009	+0.2
June 2017	4.507	4.518	-0.011	-0.3

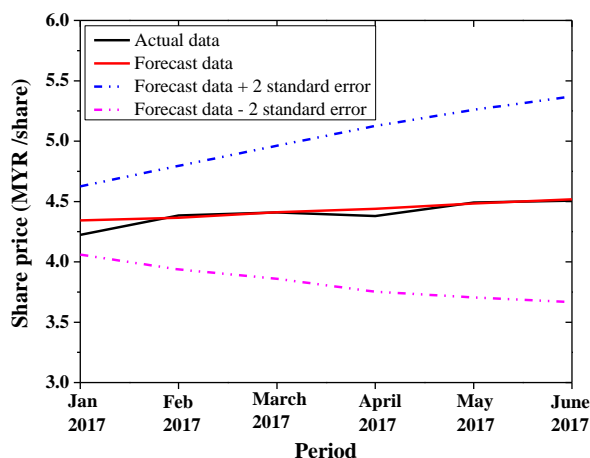


Fig. 8: Forecasting diagnostics region (ex-post data)

4.5 Forecasting error diagnostics (ex-ante data range)

This section is the main objective of this research paper. The objective is to forecast the share price performance of Islamic Bank namely Bank Islam Malaysia Berhad (BIMB).

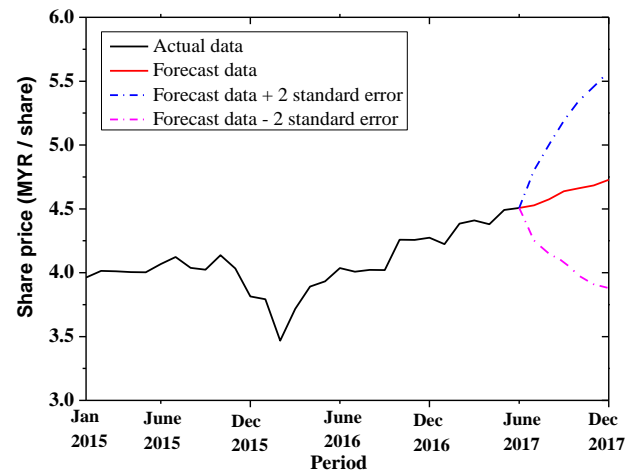


Fig. 9: Forecasting region (ex-ante data range)

Figure 9 shows the actual data value of share price including the forecast value. The range of the forecast is starting from July 2017 until December 2017 (6 months period of forecasting). The value forecast share price in July 2017 is MYR 4.523. The final value in December 2017 is MYR 4.727.

V. CONCLUSION

The objective of this study is to develop reliable forecasting model to evaluate the performance of share price for Islamic Bank in Malaysia namely Bank Islam Malaysia Berhad (BIMB). The findings from this study will help investors to select a better portfolio for their investment decision in order to gain better profits. In addition, the findings of this study also will help economists to understand the future condition of economic scenario in Malaysia. The main findings from this study are:

- (i) This study involved the monthly data of share price for Bank Islam Malaysia Berhad (BIMB). The selected data is collected from January 2010 until June 2017. This analysis involved 90 observations. The maximum value of share price is MYR 4.622 in October 2013. The minimum value of share price is MYR 1.161 in February 2010.
- (ii) This study performed reliability test for ARIMA(3,1,3) and ARIMA(3,1,4). From this study, ARIMA (3,1,4) show larger value of R-squared and lower absolute value of Akaike info criterion (AIC). Residual diagnostics result shows there is no significant residual. This indicates the residuals is white noise for ARIMA (3,1,4). Therefore, ARIMA

- (3,1,4) is reliable data modeling for share price of BIMB.
- (iii) This research using ARIMA (3,1,4) for evaluating the reliability of forecasting. This study calculated the error of forecasting from the differences between actual data and forecast data. The mean absolute percentage error (MAPE) is 0.85%. This value is relatively small and it indicates ARIMA (3,1,4) is a reliable forecasting model .
- (iv) The value of forecast share price using ARIMA (3,1,4) in July 2017 is MYR 4.523. The final value in December 2017 is MYR 4.727.

The future stage of this research can be extending to find the determinants that contribute to the dynamic behavior of share price.

(ARIMA) model for Islamic Country Currency: An Econometrics method for Islamic Financial Engineering, The International Journal of Engineering and Science, 6 (6) 22-31

- [10] Nochai R. and Nochai, T. (2006), ARIMA model for forecasting oil palm price, Proceedings of the 2nd IMT-GT Regional Conference on Mathematics, Statistics and Application, Penang, Malaysia, 13-15.

REFERENCES

- [1] Ab-Rahim, R, Kadri, N. and Ismail, F. (2013), Efficiency performance of Malaysian Islamic banks, MPRA Paper No. 46238
- [2] Sufian, F. (2007) ,The efficiency of Islamic banking industry in Malaysia: Foreign vs domestic banks, Humanomics, Vol. 23 Issue: 3, pp.174-192
- [3] Adebisi A. A, Adewumi, A. O. and Ayo, C.K. (2014), Stock Price Prediction Using the ARIMA Model, UKSim-AMSS 16th International Conference on Computer Modelling and Simulation, pp. 105-111
- [4] Al-Shiab, M. (2006), The Predictability of the Amman Stock Exchange using the Univariate Autoregressive Integrated Moving Average (ARIMA) Model, Journal of Economic and Administrative Sciences, Vol. 22 Issue: 2, pp.17-35
- [5] Stevenson, S. (2007), A comparison of the forecasting ability of ARIMA models, Journal of Property, Investment & Finance, Vol. 25 Issue: 3, pp.223-240
- [6] Balli, F. and Elsamadisy, E.M. (2012) , Modelling the currency in circulation for the State of Qatar, International Journal of Islamic and Middle Eastern Finance and Management, Vol. 5 Issue: 4, pp. 321-339
- [7] Lam, K.C. and Oshodi, O.S. (2016), Forecasting construction output: a comparison of artificial neural network and Box-Jenkins model, Engineering, Construction and Architectural Management, Vol. 23 Issue: 3, pp. 302-322
- [8] Jadevicius, A. and Huston, S. (2015), ARIMA modelling of Lithuanian house price index, International Journal of Housing Markets and Analysis, Vol. 8 Issue: 1, pp.135-147
- [9] Abu Bakar, N and Rosbi, S. (2017), Data Clustering using Autoregressive Integrated Moving Average

Characterization of α -Amylase Produced by the Endophytic Strain of *Penicillium digitatum* in Solid State Fermentation (SSF) and Submerged Fermentation (SmF)

Sideney Becker Onofre^{1,2}, Ivan Carlos Bertoldo^{1,2}, Dirceu Abatti², Amarildo Antonio Tessaro¹, Douglas Refosco²

¹ Universidade Comunitária da Região de Chapecó - UNOCHAPECÓ - Centro de Ciências Exatas e Ambientais - CEA - Programa de Pós-graduação em Tecnologia e Gestão da Inovação - PPGTI - Av. Senador Atílio Fontana, 591-E EFAPI - 89809-000 - Chapecó - Santa Catarina - Brazil. E-mail: beckerside@unochapeco.edu.br.

² União de Ensino do Sudoeste do Paraná - UNISEP - Av. União da Vitória, 14 - Bairro Miniguauçu - 85605-040 - Francisco Beltrão - Paraná - Brazil.

Abstract— α -Amylases are enzymes responsible for breaking the α -1.4 bond in polysaccharides with three or more glucose units, occupying the second place in the most widely employed enzymes in industry in the world. The objective of this study was to compare the yields of α -amylase produced by the endophytic fungus, *Penicillium digitatum*, strain D1-FB, isolated from *Baccharis dracunculifolia* D.C. (Asteraceae), through the solid state fermentation (SSM) and submerged fermentation (SmF) processes, in addition to characterizing the produced enzyme. The two fermentations were conducted for 120 hours, taking samples every 24 hours to obtain the peaks of production. The enzymes were characterized according to their optimal pH and temperature for performance and stability regarding the incubation in the presence of ions, variations in pH and temperature. The maximum yield of the enzyme was observed with SSF, using rice bran as substrate after 72 hours of fermentation, with 1,625 U/mL. The α -amylase had an optimal pH at 6.5 and optimal temperature at 45°C. All the ions resulted in a decrease in the activity of α -amylase in the concentration of 5mM. The enzyme proved to be quite stable in a pH range of 6.0 to 7.5 and up to the temperature of 37°C, but it presented great drops in activity with temperatures above 45°C and in the presence of ions at the concentration of 5 mM.

Keywords— *Penicillium digitatum*, α -amylase, starch, enzymes, endophytics.

I. INTRODUCTION

Starch is a polymer consisting of glucose molecules joined by α -1.4 and α -1.6 bonds. Two polysaccharides

comprise the structure of starch: amylose and amylopectin (Figures 1A and 1B). The first (1A) is a linear molecule containing more than 6000 glucose units connected by glycosidic α -1.4 bonds, and the second (1B), very similar to glycogen (Myers *et al.*, 2000), is highly branched, containing α -1.4 bonds between the of glucose monomers, and α -1.6 in the branching points at each 24-30 glucose residue (Brena *et al.*, 1996).

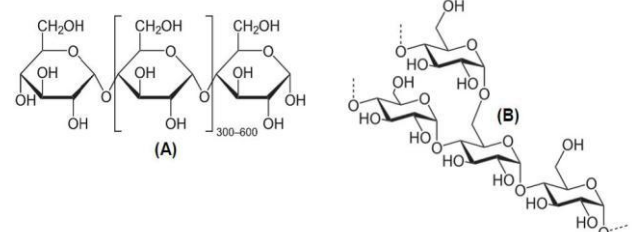


Fig 1: (A) Amylose Molecule. (B) Amylopectin Molecule. Corradini *et al.*, (2005).

Amylases are responsible for the hydrolysis of the starch molecule and are widely distributed in nature. Starch is found mainly in seeds of cereals, such as corn, barley, wheat and rice, and in tubers or roots, such as potatoes and manioc, with the size and shape of the grains being specific for the different cereals (Moraes, 2004). According to Gupta (2003), amylases are divided into two groups, endo-amylases catalyze hydrolyses within the starch molecule in various points of the chain simultaneously. This action causes the formation of dextrans and small polymers composed of glucose units of various lengths, breaking the glycosidic α -1.4 bonds present on the inside of the amylose or amylopectin chains. α -Amylase is the most well-known endo-amylase.

The exo-amylases known as amiloglicosidasas or glicoamilases, hydrolyze glycosidic α -1,4 and α -1,6 bonds (Lorentz, 2005; Onofre *et al.*, 2011). Amylases are applied in the most varied industrial sectors that require the hydrolysis of starch, being mainly used in the food industry for the preparation of beers, jellies and to obtain free glucose for the most varied applications (Michelin, 2005).

In addition to the food industry, these enzymes can be used in the formulation of detergents and in the paper, pharmaceutical, fermentation and textiles industries (Oliveira *et al.*, 2007).

There are two processes for the production of microbial enzymes: solid state fermentation (FES) and submerged fermentation (SmF). SmF is traditionally used for the production of enzymes because it provides a better control of some important process parameters, such as pH and cell growth, in addition to facilitating the recovery of extracellular enzymes and the determination of biomass (Fernandes, 2006).

One of the main characteristics of solid-state fermentation is the use of substrates with low water activity, in which the conditions for growth are similar to the fungi's natural habitat. This facilitates their growth on the solid substrate and the production of large quantities of enzymes (Paris *et al.*, 2008; Rocha, 2010).

The vast majority of microorganisms used in the solid-state fermentation are filamentous fungi (Silva, 2002). The reduced amount of water in the substrate greatly restricts the number of micro-organisms that are capable of adapting to this process, but fungi prove to be quite tolerant to this environment (Pandey *et al.*, 2005).

The objective of this study was to compare the production of α -amylase produced by the endophytic fungus, *Penicillium digitatum*, strain D1-FB, isolated from *Baccharis dracunculifolia* D.C. (Asteraceae), through the solid state fermentation (SSM) and submerged fermentation (SmF) processes, in addition to characterizing the produced enzyme.

II. MATERIALS AND METHODS

2.1 MICRO-ORGANISM STUDIED

For the realization of this work the endophytic fungus *Penicillium digitatum*, strain D1-FB, was used, isolated from *Baccharis dracunculifolia* D.C. (Asteraceae) maintained in the mycology collection of the Microbiology Laboratory of the Universidade Paranaense - UNIPAR - Campus Francisco Beltrão - Paraná - Brasil.

2.2 FERMENTATION PROCESS FOR THE PRODUCTION OF α -AMYLASES

2.2.1 Preparation of the Inoculum

After growing the fungus on PDA for 7 days, the cells were suspended in a phosphate 100mM buffer, pH 7.0, and subjected to stirring in order to obtain a homogeneous solution. The cell concentration was determined by counting in a Neubauer chamber (Germano, 2000).

2.2.2 Preparation of the Fermentation Media

Two different fermentation processes for the production of amylase were tested: solid state fermentation (SSF) and submerged fermentation (SmF). The substrate of choice for SSF was rice bran. Each Erlenmeyer flask of 125 mL received 10 g of rice bran (Fa), with the production of the enzyme in pure bran (Fa) being compared with bran supplemented with 20% of manioc starch (Fm).

The moisture content of the media was guaranteed by a phosphate buffer 100 mM, pH 6.5, in the proportion of 65% for the medium containing pure bran, and of around 90% for the medium supplemented with manioc starch. In SmF, the medium was composed of 50 g.L⁻¹ of manioc starch, 0.2 g.L⁻¹ of MgSO₄ and 0.2 g.L⁻¹ of ZnSO₄.7H₂O, solubilized in a phosphate buffer 100 mM, pH 6.5. Two different sources of nitrogen were tested, one organic (urea) and the other inorganic (NaNO₂) at 2.5g.L⁻¹.

The fermentation was conducted in Erlenmeyer flasks of 125 mL containing the medium at 20% of its maximum capacity. 10⁸ spores were inoculated in all media. The flasks were incubated in a Shaker at 28°C and 150 rpm. Samples were taken every 24 hours for 4 days for the evaluation of enzyme yields (Onofre *et al.*, 2012).

2.2.3 Recovery of the Enzyme from the Fermented Media

For the recovery of the enzyme from the solid fermented medium, 5 mL of NaCl 1% solution was added for each gram of solid substrate and maintained under stirring for 1 hour at 100 rpm. For the liquid medium, a solution of NaCl 1% was added until the volume reached 50 mL. After this process, the suspension was filtered to obtain the crude extract, and then centrifuged at 2000 rpm for 8 minutes, discarding the precipitate.

2.3 ENZYMATIC ASSAY

The activity of α -amylase was determined by measuring the levels of reducing sugars in solution as a result of the action of the α -amylase on the starch. The activity was determined in samples in triplicate by quantifying the reducing sugars (glucose) with the Miller (1959) and Fernandes *et al.*, (2007) method. A mixture containing 0.5 mL of enzymatic extract; 0.5 mL of a starch 0.5% solution in a Tris-HCl buffer 0.05M pH 8.5, and 0.2 mL of the same buffer was incubated at 90°C for 10 minutes. After this period, 1.0 mL of the Miller reagent (3,5-Dinitrosalicylic acid) was added to the reaction.

The mixture was placed in boiling water for 10 minutes, then cooled in an ice bath for 5 minutes and 4.8 mL of distilled water was added. The developed color was measured with a SHIMADZU UV-mini 1240 spectrophotometer, using a wavelength of 540nm. The same procedure was performed with the control, except that the miller reagent (3,5-Dinitrosalicylic acid) was added together with the enzyme to the starch 0.5% solution, and this mixture was placed in boiling water as described above.

The content of reducing sugars was determined through a glucose curve. One unit of enzyme activity (U) was defined as the amount of enzyme required to produce 1 μ mol of reducing sugar per minute per mL from the soluble starch under the test conditions (Onofre *et al.*, 2011; Onofre *et al.*, 2012).

2.4 CHARACTERIZATION OF THE α -AMYLASE

2.4.1 Optimal pH for Enzymatic Activity

For the assessment of the influence of pH on enzyme activity, the enzymatic assay was conducted according to item 2.3, while varying the addition of buffer solution: pH 5.0 - 6.0 (acetate buffer), 6.5 - 7.5 (phosphate buffer), 8.0 - 8.5 (Tris-HCl buffer) (Thys, 2004).

2.4.2 Optimal Temperature for Enzymatic Activity

For the assessment of the influence of temperature on enzyme activity, the enzymatic assay was conducted according to item 2.3, while only varying the incubation temperature: 10, 20, 30, 37, 45 and 65°C (Silva, 2002).

2.4.3 Influence of Ions on Enzymatic Activity

For the assessment of the influence of ions on enzyme activity the enzyme was incubated for 10 min at room temperature with the ions CaCl₂, BaCl₂, HgCl₂, FeCl₃ and MgCl₂ at concentrations of 1 and 5 mM, performing the enzymatic assay after this procedure (Giongo, 2006).

2.4.4 Thermal Stability of α -Amylase

The thermal stability of the amylase was tested by incubating the enzyme for 30 minutes at the temperatures of: 10, 20, 30, 37, 45 and 65°C, performing the enzymatic assay after this procedure as described by Rasiah and Rehm, (2009).

2.4.5 Stability of α -Amylase at Different pH Values

The stability of α -amylase at different pH values was tested by incubating the enzyme for 30 minutes in the following buffer solutions (100 mM): pH 5.0 - 6.0 (acetate buffer), 6.5 - 7.5 (phosphate buffer), 8.0 - 8.5 (Tris-HCl buffer), performing the enzymatic assay after this procedure as described by Thys, (2004).

III. RESULTS AND DISCUSSION

Through the analysis of the fermentation processes, one can observe that the endophytic strain of *P. digitatum*, isolated from *Baccharis dracunculifolia* D.C. (Asteraceae) had better results in the solid medium when compared with fermentation in the liquid medium, yielding 1625 U/mL through solid state fermentation in the medium containing only rice bran, while in submerged fermentation these values didn't exceed 712 U/mL in the medium containing inorganic nitrogen (Liq/Ino).

By comparing the data obtained in this study with those found by Spier (2005) working with *Penicillium* sp., one can see that he obtained similar results as those of this study, since he observed a production of 1690 U/mL of fungal amylases in SSF, with yields surpassing double the activity achieved in SmF. This same behavior was observed by Hu *et al.*, (2013), who found that the fungus *Penicillium* sp. in a semi-solid medium had better results than in submerged fermentation and in a medium supplemented with an inorganic fraction (NaNO₂) of nitrogen. In Figure 2 the enzyme yield data (in total units) in the different media over the course of 120 hours at 24-hour intervals, is presented.

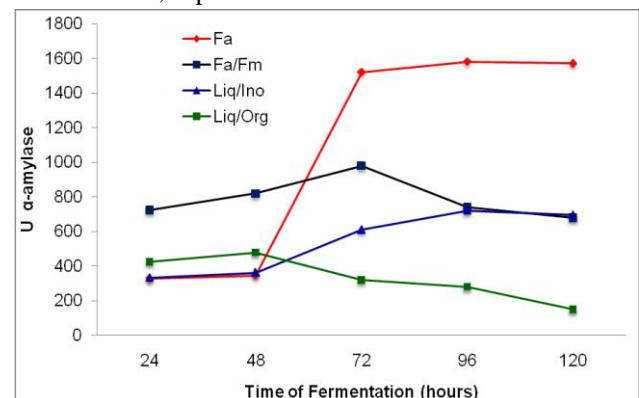


Fig. 2: Yield of α -amylase as a function of time in solid media containing only rice bran (Fa) and supplemented with manioc starch (Fa/Fm), and in liquid medium with the organic nitrogen source urea (Liq/Org) and the inorganic source NaNO₂ (On/Innovation).

SSF has been described as an excellent option for the growth of the filamentous fungi. In general, fungi have a good ability to grow on solid substrates, which explains their good adaptation to SSF. And for this reason, they have been widely used in this process, mainly to obtain enzymes (Silva, 2002; Lei *et al.*, 2014).

One of the main characteristics of SSF is the use of substrates with low water activity, in which the conditions for growth are similar to the natural habitat of fungi, which facilitates their growth on the solid substrate and the yield of large quantities of enzymes. The organic matter present in this material is used as a source of

energy for growth, and the carbon is used for the synthesis of cellular biomass and of the products of the microbial metabolism (Mitchell and Lonsane, 1992; Hattori *et al.*, 2013; Dris *et al.*, 2014).

It should be noted, however, that the SSF technology should not be seen as a technique that replaces submerged fermentation. In fact, each technique has its own potential and particularities. However, there is a consensus about the need for ongoing research on the factors related to SSF in order to take advantage of the full potential of this technology (Pandey *et al.*, 2001).

According to Del Bianchi *et al.*, (2001) and Pandey (2002), the control of certain variables is necessary to obtain products with constant and uniform characteristics. One can therefore state that the observation of these factors, and the correct handling in relation to each one of them, will certainly bring about better results in the solid state fermentation process. Environmental conditions, such as temperature, pH, water activity, oxygen level and the concentration of nutrients and products, significantly affect cell growth and product formation.

When the liquid fermentation media are compared, the fungus can be observed to have adapted better to the inorganic source of nitrogen, showing a maximum yield of 712 U/mL, while in the medium containing organic nitrogen the peak yield of total amylases was 438 U/mL.

According to Gupta *et al.*, (2003), organic nitrogen sources are preferred for the production of α -amylase by bacteria. On the other hand, various inorganic salts, such as ammonium sulfate, sodium nitrate and ammonium nitrate, have been reported in improved yields of α -amylase by fungi.

Both the solid media had good enzyme yields: 1625 U/mL in the medium containing rice bran, and 932 U/mL in the medium containing rice bran supplemented with manioc starch.

One would expect that the medium supplemented by starch would have higher enzyme yields, since the presence of starch should induce the production of amylolytic enzymes, but this was not the behavior observed. This fact may have occurred due to the presence of starch, which gelatinized after heat treatment (sterilization), making the medium more compact. As such, this made aeration of the solid medium harder. Spier (2005) reported this same limitation with the use of starch in submerged cultivation, noting that enzyme activity decreased with the increase of the concentration of starch in the medium.

3.1 CHARACTERIZATION OF THE ENZYME

3.1.1 Optimal pH for Enzymatic Activity

The α -amylase produced by SSF in the medium containing rice bran were used in the tests for

characterization of the enzyme. Figures 3 and 4 show the activity of the enzyme as a function of pH and temperature, respectively.

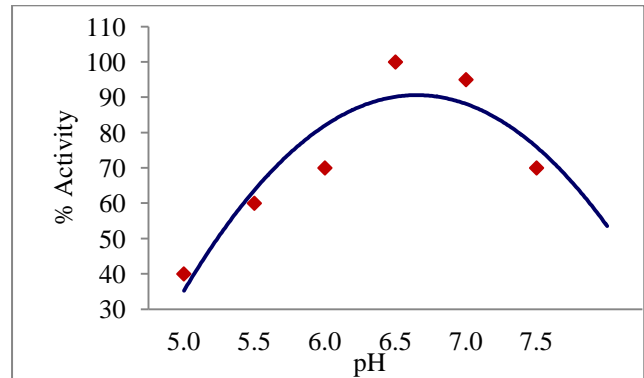


Fig. 3: Curve representing the optimal pH for α -amylase activity.

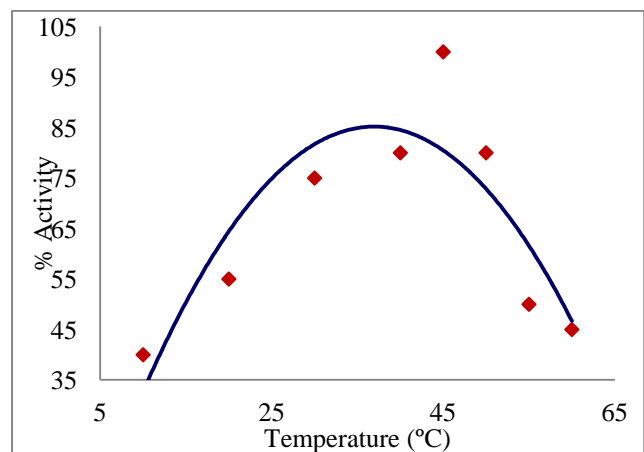


Fig. 4: Curve representing the optimal temperature for α -amylase activity.

The enzyme showed optimal pH at 6.5, while maintaining 96% of its activity at pH 7.0, characterizing it as a neutral α -amylase. This data is consistent with Figueira *et al.*, (2000) and Oliveira *et al.*, (2010) who produced amylases with the fungi *Fusarium moniliforme* and *Aspergillus flavus*, obtaining optimal pH values close to 6.9, demonstrating the trend for the production of slightly neutral amylases by filamentous fungi. Spier (2005), on the other hand, obtained a higher yield of amylolytic enzymes with an initial pH equal to 4.0 when working with *Aspergillus niger*, which shows that each species of fungus may have a different behavior in specific pH.

According to Soccol (1992), Onofre *et al.*, (2011); Onofre *et al.*, (2012), the growth capacity of fungi is limited in extreme conditions of acidity and alkalinity. This characteristic is of extreme importance in fermentation processes since they show that under these conditions the vast majority of the bacteria responsible for the contamination of fermentation processes are inhibited.

The optimal temperature was 45°C, with the enzyme being completely inactivated at the temperature of 65°C. Spier (2005) obtained similar results to those in this study for a fungal amylase, reporting optimal pH at 6.0 and optimal temperature between 45-55°C. This behavior is also in agreement with Kundu *et al.*, (1973) and Ueno *et al.*, (1987) cited by Pandey *et al.*, (2005), who reported that optimal yields of α -amylase were obtained at temperatures between 30 and 37°C.

3.1.2 Influence of Ions on Enzymatic Activity

Metal ions have a variety of functions in proteins. These ions may be directly involved in the catalytic process during the enzymatic reaction, or they may participate in electron transfer or redox reactions (Najafi *et al.*, 2005). The stabilization of some enzymes can be induced, mainly, by such divalent ions as Ca^{2+} , Mn^{2+} , Zn^{2+} e Mg^{2+} . If used in low concentrations, these ions can stabilize the tertiary structure of the protein, promoting the formation of cross-links that provide a greater stability to it (Tomazic, 1991). Figure 5 shows the behavior of α -amylase regarding the incubation with some ions.

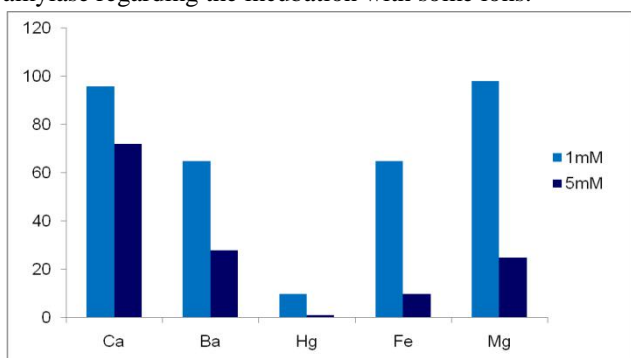


Fig. 5: Influence of ions on enzyme activity at the concentrations of 1 and 5mM.

All the ions tested at concentrations of 1 and 5 mM were associated with a drop in activity of the enzyme of at least 14 %, with the ions Hg^{2+} , at both concentrations, and Fe^{3+} , at the concentration of 5 mM, leading to the complete loss of enzyme activity.

The change in activity per ion is a very particular characteristic of each enzyme. Some enzymes may require divalent ions for their activation or as a cofactor, commonly Ca^{2+} , Mg^{2+} , Zn^{2+} e Mn^{2+} , increasing their activity. However, some ions may generate a drastic drop in activity, such as Hg^{2+} , Fe^{3+} , and may lead to total inhibition (Giongo, 2006).

It should be noted that high concentrations of ions can have an inhibitory effect. Some studies also show that the stability of α -amylase is compromised in the presence of small quantities of these ions (Yang and Liu, 2004; Bernhardtsson *et al.*, 2005; Hashim *et al.*, 2005).

3.1.3 Thermal Stability of α -Amylase and at Different pH Values

pH is one of the most important factors that affect fermentation processes, since it can change the chemicals of the culture medium, ionize polar molecules, affect enzymatic reactions and the post-translation processes of enzymes.

The pH of the culture medium can influence microbial growth, and induce the expression of genes that result in changes in phenotypes, such as changes in morphology, physiology or the expression of enzymes. The limitation of growth has been associated with a reduction in the production and/or activity of extracellular enzymes (Madigan *et al.*, 2004). Figures 6 and 7 shows the stability of the enzyme regarding the incubation at different pH values and temperatures, respectively.

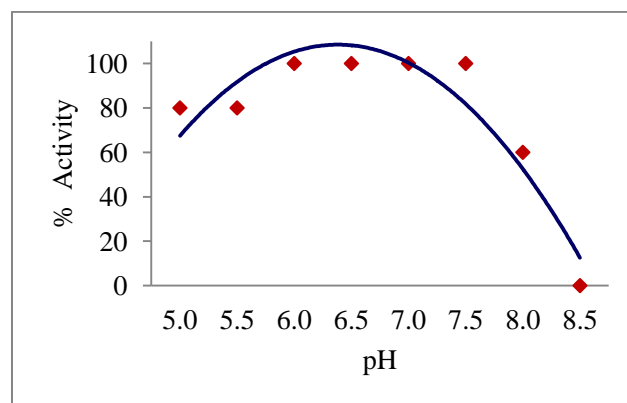


Fig. 6: Stability of α -Amylase regarding incubation at Different pH Values.

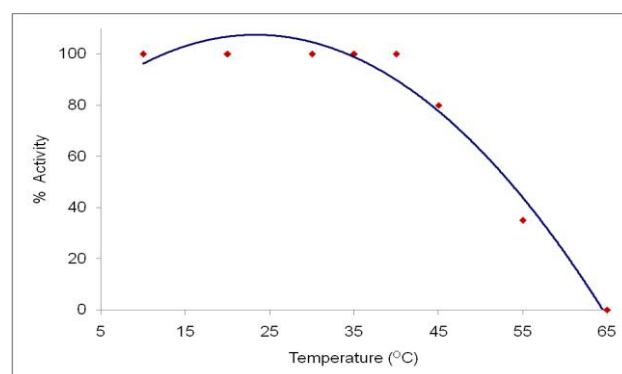


Fig. 7: Stability of α -amylase regarding different incubation temperatures.

In the more extreme pH values tested, α -amylase underwent a reduction in enzyme activity of at least 24%, with it being completely inhibited at pH 8.5. In the 6.0 - 7.5 pH range, the enzyme proved to be quite stable, maintaining at least 95% of its activity, with this being the recommended pH range for the application of the enzyme.

Thermal resistance is considered one of the most important criteria for the industrial application of the enzyme, given that most processes require the use of high temperatures (Ray and Nanda, 1996). The use of high temperatures for the activity of these enzymes, however, depends on the stability limit of the protein, since it will have a range within which its structure is maintained.

Outside of this range, denaturation would occur, resulting in a loss of activity. An increase in the use of the α -amylase enzyme in biotechnology has occurred due to its extensive range of working conditions, including high temperatures, extreme pH, and the presence of surfactants and organic solvents (Tanaka and Hoshino, 2002).

When the enzyme was incubated at temperatures of 10 to 37°C, it preserved its full activity. When a temperature of 45°C was employed, the enzyme suffered a decline in residual activity, although this has been its optimal temperature of operation, indicating that the produced α -amylase should be applied at temperatures below 45°C to maintain its activity for a longer period of time.

Rasiah and Rehm (2009) obtained amylase which proved quite stable at 85°C. Figueira *et al.*, (2000) produced amylases with the fungi *Fusarium moniliforme* and *Aspergillus flavus*, obtaining thermal stability close to 20°C. Fungal Amylases are more sensitive to the elevation of temperature, tending to suffer a drastic drop in activity at temperatures above 50°C (Spier, 2005).

Understanding the thermo-stability of enzymes will promote their addition to products that need to go through some form of heat treatment during their processing, while preventing inactivation or with the intentional inactivation of the enzyme when the expected result of its catalytic activity has been obtained.

IV. CONCLUSION

With the results obtained, it is possible to conclude that the production of α -amylase through solid state fermentation (SSF) was more efficient than the production of the enzyme through submerged fermentation (SmF), obtaining more than twice the activity found in SmF with SSF, with values of 1625 and 712 U/mL for SSF and SmF, respectively.

At 120 hours of solid state fermentation using rice bran as substrate, 1625 U/mL was obtained, demonstrating the excellent α -amylase secretion ability of the D1-FB strain of the endophytic fungus, *Penicillium digitatum*, isolated from *Baccharis dracunculifolia* D.C. (Asteraceae).

The enzyme characterization tests revealed an optimal pH at 6.5 and an optimal temperature at 45°C. The α -amylase produced was stable in the neutral pH range, but it showed great drops in activity with temperatures above 45°C and in the presence of ions at a concentration of 5 mM.

These results allow for the conclusion that the produced α -amylase may be a new enzyme alternative for application in industries that require the saccharification of starch.

CONFLICTS OF INTEREST

The authors declare there are no ethical, publishing or financial conflicts of interest regarding the data of this study.

REFERENCES

- [1] Bernhardsdotter ECMJ, Nig JD, Garriott OK, Pusey ML (2000). Enzymic properties of an alkaline chelator-resistant α -amylase from an alkaliphilic *Bacillus* sp. isolate L1711. *Process Biochem.* 40: 2401–2408.
- [2] Brena BM, Pazos C, Franco-Fraguas L, Batista-Vieira F (1999). Chromatographic methods for amylases. *Journal of Chromatography*, 684: 217-237.
- [3] Corradini E, Lotti C, Medeiros ES, Carvalho AJF, Curvelo AAS, Mattoso LHC (2005). Estudo comparativo de amidos termoplásticos derivados do milho com diferentes teores de amilose. *Polímeros*, 15: 268-273.
- [4] Del Bianchi VL, Moraes IO, Capalbo DMF (2001). Fermentação em estado sólido. In: Lima, U.A. et al. (Coord.). *Biotecnologia Industrial: Engenharia Bioquímica*. 1. Ed., v. 3. São Paulo: Edgard Blucher. 13:247-276.
- [5] Driss D, Zouari-Ellouzi S, Chaari F, Kallel F, Ghazala I, Bouaziz F, Ghorbel R, Chaabouni SE. (2014). Production and *in vitro* evaluation of xylooligosaccharides generated from corncobs using immobilized *Penicillium occitanis* xylanase. *Journal of Molecular Catalysis B: Enzymatic*. 102:146-153.
- [6] Fernandes LP, Ulhoa CJ, Asquieri ER, Monteiro VN (2007). Produção de amilases pelo fungo *Macrophomina phaseolina*. *Revista Eletrônica de Farmácia*. 4(1): 43-51.
- [7] Fernandes MLM (2006). Produção de lipases por fermentação no estado sólido e sua utilização em biocatálise. (2006). 130f. Dissertação (Doutorado em Química) - Setor de Ciências Exatas - Universidade Federal do Paraná. Curitiba, Brasil.
- [8] Figueira ELZ, Sá MC, Ida EI, Hirooka EY (2000). Produção e caracterização de amilases de *Fusarium moniliforme* e *Aspergillus flavus*. *B.CEPPA*. 18(1):13-26.
- [9] Germano S (2000). Desenvolvimento de bioprocessos para produção, caracterização e purificação de proteases de *Penicillium* sp. por fermentação no estado sólido. 2000. 142f. Tese

- (Doutorado em Processos Biotecnológicos) - Setor de Tecnologia - Universidade Federal do Paraná. Curitiba, Paraná, Brasil.
- [10] Giongo JL 2006. Caracterização e aplicação de proteases produzidas por linhagens de *Bacillus* sp. (2006). 95f. Dissertação (Mestrado em Microbiologia Agrícola e do Ambiente) – Faculdade de Agronomia – Universidade Federal do Rio Grande do Sul. Porto Alegre, Rio Grande do Sul, Brasil.
- [11] Gupta R, Gigras P, Mohapatra H, Goswami VK, Chauhan B (2003). Microbial α -amylases: a biotechnological perspective. *Process Biochemistry*. 38(11): 1599-1616.
- [12] Hashim SO, Delgado OD, Martínez MA, Kaul RH, Francis JM, Mattiasson B (2005). Alkaline active maltohexaose-forming α -amylase from *Bacillus halodurans* LBK 34. *Enzyme and Microbial Technology*. 36: 139-146.
- [13] Hattori T, Kato Y, Uno S, Usui T (2001). Mode of action of a β -(1 \rightarrow 6)-glucanase from *Penicillium multicolor*. *Carbohydrate Research*. 366:6-16. 25.
- [14] Hu Y, Liu G, Li Z, Qin Y, Qu Y, Song X (2013) G protein-cAMP signaling pathway mediated by PGA3 plays different roles in regulating the expressions of amylases and cellulases in *Penicillium decumbens*. *Fungal Genetics and Biology*. 58(59): 62–70.
- [15] Lei Y, Liu G, Li Z, Gao L, Qin Y, Qu Y (2014). Functional characterization of protein kinase CK2 regulatory subunits regulating *Penicillium oxalicum* asexual development and hydrolytic enzyme production. *Fungal Genetics and Biology*, 66: 44-53.
- [16] Lorentz RH (2005). Seleção de isolados de *Paenibacillus* spp com atividade enzimática e antimicrobiana. 2005. 103f. Dissertação (Mestrado em Microbiologia Agrícola e do Ambiente) – Faculdade de Agronomia – Universidade Federal do Rio Grande do Sul. Porto Alegre, Rio Grande do Sul, Brasil.
- [17] Madigan MT, Martinko JM, Parker J (2004). *Microbiologia de Brock*. 10. ed. São Paulo: Person Education. 517p.
- [18] Michelin M (2005). Estudo da glucoamilase e da α -amilase produzidas pelo fungo *Paecilomyces variotii*: purificação, caracterização bioquímica e relações filogenéticas. 2005. 160f. Dissertação (Mestrado em Ciências) – Departamento de Biologia – Universidade de São Paulo, Ribeirão Preto, Brasil.
- [19] Miller GL (1959). Use of dinitrosalicylic acid reagent for determination of reducing sugar. *Washington*, 31(3): 426-428.
- [20] Mitchell DA, Lonsane BK (1992). Definition, characterization and economic evaluation. In *Solid Substrate Cultivation*, Elsevier, London.
- [21] Moraes LMP (2004). Amilases. In: Said, S.; Pietro, R. *Enzimas como agentes Biotecnológicos*. Ribeirão Preto: Legis Summa. p.123-128.
- [22] Myers AM, Morell MK, James MG, Ball SG (2000). Recent progress toward understanding biosynthesis of the amylopectin crystal. *Plant Physiology*. 122:989-997.
- [23] Najafi MF, Deobagkar D, Deobagkar D (2005). Purification and characterization of an extracellular α -amylase from *Bacillus subtilis* AX20. *Protein Expr. and Purif.* 41:349-354.
- [24] Oliveira AN, Flor NS, Oliveira LA (2010). Influência do pH e temperatura sobre a atividade amilolítica de rizóbios isolados de solos da Amazônia. *Acta Amazonica*. 40(2):401-404.
- [25] Oliveira AN, Oliveira LA, Andrade JS, Chagas-Junior AF (2007). Produção de amilase por rizóbios, usando farinha de pupunha como substrato. *Ciência e Tecnologia de Alimentos*. 27(1): 61-66.
- [26] Onofre SB, Groff SA, Sartori A, Bertolini J, Kagimura FY, Rotta D, Mazzali L, Steilmann P (2011). Amylolytic Enzymes Produced by the Fungus *Colletotrichum gloeosporioides* in Rice Semi-Solid Fermentation. *Journal of Yeast and Fungal Research*. 2: 28-32.
- [27] Onofre SB, Groff SA, Sartori A, Bertolini J, Kagimura FY, Rotta D, Mazzali L, Steilmann P (2012). Production of α -Amylase and Amyloglucosidase by the Fungus *Cylindrocladium* sp. in Semi-Solid State Fermentation. *Journal of Microbiology Research*. 2: 123-126.
- [28] Pandey A (2002). Solid state fermentation. *Biochemical. Engineering Journal*, 3636:1-4.
- [29] Pandey A, Soccol CR, Rodrigues-Leon JA, Nigam P (2001). Solid state fermentation in biotechnology. Nova Deli, Asiotech. p.221, 2001.
- [30] Pandey A, Webb C, Soccol CR, Larroche C (2005). *Enzyme Technology*. 1º ed. New Delhi: Asiotech Publishers, Inc, p. 760.
- [31] Paris LD (2008). Produção de enzimas fúngicas por fermentação em estado sólido das sojas orgânica, transgênica e convencional. 115p., (2008). Dissertação de Mestrado. Programa de Pós-graduação em Engenharia Química, Centro de Ciências Exatas, Universidade Estadual do Oeste do Paraná (Unioeste), Toledo, Paraná, Brasil.
- [32] Rasiah IA, Rehm BHA (2009). One-step production of immobilized α -amylase in recombinant *Escherichia coli*. *Applied and Environmental Microbiology*. 75(7): 2012-2016.

- [33] Ray RR, Nanda G (1996). Microbial β -amylases: Biosynthesis, characteristics, and industrial applications. *Critical Reviews in Microbiology*. 22: 181-199.
- [34] Rocha CP (2010). Otimização da Produção de Enzimas por *Aspergillus niger* em Fermentação em Estado Sólido. 136p. Dissertação de Mestrado. Programa de pós-graduação em Engenharia Química, Universidade Federal de Uberlândia, Faculdade de Engenharia Química, Uberlândia, Brasil.
- [35] Silva ARZ (2002). Desenvolvimento de bioprocessos para a produção de fitase por *Aspergillus niger* em fermentação no estado sólido utilizando subprodutos agrícolas para aplicação como aditivo na alimentação de aves e suínos. 2002. 96f. Dissertação (Mestrado em Tecnologia de Alimentos) – Setor de Tecnologia – Universidade Federal do Paraná. Curitiba, Brasil.
- [36] Soccol CR (1992). Physiologie et Métabolisme de *Rhizopus* em Culture Solide et Submergée em Relation Avec la Dégradation d'Amidon et la Production d'Acide L(+) Lactique. 218p. Thèse de Doctorat. Mention Génie enzymatique, Bioconversion et Microbiologie, Université de Technologie de Compiègne. Compiègne-France.
- [37] Spier MR (2005). Produção de enzimas amilolíticas fúngicas α -amilase e amiloglicosidase por fermentação no estado sólido. 2005. 178f. Dissertação (Mestrado em Tecnologia de Alimentos) – Setor de Tecnologia – Universidade Federal do Paraná. Curitiba, Brasil.
- [38] Tanaka A, Hoshino E 2002. Thermodynamic and activation parameters for the hydrolysis of amylose with *Bacillus* α -amylases in a diluted anionic surfactant solution. *Journal of Bioscience and Bioengineering*. 93:485-490.
- [39] Thys RCS 2004. Produção, caracterização, purificação e aplicação de uma protease produzida pelo microrganismo *Microbacterium* sp. *kr10*. 2004. 114f. Dissertação (Mestrado em Microbiologia Agrícola e do Ambiente) – Faculdade de Agronomia – Universidade Federal do Rio Grande do Sul. Porto Alegre, Brasil.
- [40] Tomazic SJ (1991). Protein stabilization. In: *Biocatalysts for industry*. Topic in Applied chemistry. Ed. Plenum Press, New York and London. 330p.
- [41] Yang CH, Liu WH (2014). Purification and properties of a maltotriose producing α -amylase from *Thermobifida fusca*. *Enzyme and Microbial Technology* 35: 254–260.